Aspects of Vibrational Band Contours

by Ellis Brooke Gill, B.Sc.

A Thesis

presented to the Faculty of Science

of the University of London

in Candidature for

the Degree of

Doctor of Philosophy

The Bourne Laboratory,
Royal Holloway College,
(University of London),
Egham Hill,
Egham,
Surrey,
TW20 0EX.

May, 1976

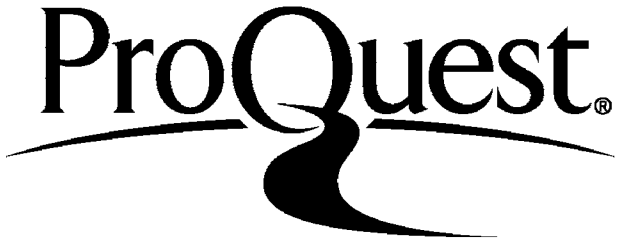

To my wife

and

my parents

ACKNOWLEDGEMENTS

I wish to express my sincere gratitude to Dr. D. Steele for his advice and guidance throughout the course of this work.

I also wish to thank my parents and parents-in-law for all their help and encouragement.

Thanks are also due to Mrs E.I. Kearsey for the typing of this thesis.

The receipt of a studentship from the Science Research Council is acknowledged with gratitude.

Finally I wish to thank my wife for her technical assistance in the preparation of this thesis - and for more than a little patience.

CONTENTS

PART 2

List of Figures

List of Tables

Abstract

An infra-red study was made of the molecular complex of hexafluorobenzene (HFB) in benzene solutions. Interactions between HFB and benzene lead to a frequency shift and a broadening of the band arising from the out of plane C-F bending vibration (a_{2u} species). It is deduced that the intermolecular interactions are short lived, stochastic, are not simple polar interactions, and that the resulting forces are directed perpendicular to the ring plane.

The band contours of the vibrational Raman band of chlorine in benzene/tetrachloromethane solution mixtures have been studied. Band fitting analysis of the complexed chlorine band using two Lorentzians, each with their isotopic sub bands, produced good simulations of the observed spectra. The consistency of the relative intensities suggests that they arise from complexes of the same stoichiometry. It is concluded that chlorine forms a 1:2 complex with benzene, with an equilibrium constant ${}^{2}K = .095\ dm^{6}mol^{-2}$. Entropy calculations imply that there is a large molecular ordering compatible with the idea of specific structure of the complex.

The vibrational Raman band of liquid chlorine was studied to shifts of 130 cm^{-1} from the band centre. The second moment of the anisotropic component is about 15% above the theoretical value. Good exponential decays of the second order orientational correlation function are observed from $t > 0.2$ ps. The resulting relaxation times are well reproduced by a microviscosity equation. The results are in reasonable accord with n.m.r. relaxation times.

Absolute intensity measurements have been made on the fundamental vibrations of methyl iodide, by integrating the optical density over the absorption band. Exact band fitting of the theoretical spectra to the experimental spectra was not possible, no explanation can be offered. The intensity measurements were analysed in terms of the dipole moment derivatives with respect to symmetry coordinates, using three formulations of the vibrational angular momentum correction. Gribov's formulation is considered superior to the earlier Crawford hypothetical isotope method. Barrow and Crawford also derived a formulation similar to Gribov's.

Chapter 1 INTRODUCTION

In this thesis we shall consider various aspects of the information available from infra-red and Raman band contours. In part one we shall show how these band contours, as well as the direction and specificity of frequency shifts of these bands, can provide information about the interactions of the absorbing molecules with their environment. Thus in Chapter 2 we present much of the basic theory necessary for an understanding of the studies in Chapters 3 to 5.

In Chapter 3 we shall show how a complete analysis of a band profile can be used to give some insight about the molecular relaxation processes which occur in the liquid phase. An overall band profile is usually determined by a combination of vibrational and rotational mechanisms, each of which is affected by the inter-molecular forces operative in the system. Gordon[12] has cast the theory in a form more favourable to experimental exploitation. It will be shown how studies of the band contour of the a_{2u} C-F bending vibration of HFB, in various benzene-cyclohexane solvent mixtures, can enable a determination of the decay rates of the correlation functions; and hence the different molecular interactions involved.

In Chapter 4 we shall consider the Raman spectra of chlorine, in the benzene-tetrachloromethane solvent system. It has long been considered that, in Raman and infra-red spectra, it should be possible to observe bands due to complexed and uncomplexed molecules, whatever the strength. It has been suggested that, if the estimates of complex lifetime for weak complexes were correct, then it could

be that low frequency vibrations (such as the halogen-halogen stretching frequency) may give rise only to averaged absorption bands[33]. There have been a number of attempts to observe "complex" and "free" ν(X-X) bands using Raman spectroscopy[73-75]. In early work Klaeboe and Rosen et al observed two Raman bands in the ν(Br-Br) and ν(I-I) regions for some aromatic donors, but not for benzene. More recently Jao[72] has considered the ν(Cl-Cl) region, and concluded that a charge transfer effect could be the main factor in the large intensification of the Raman band. We further extended the work of Jao by considering in detail, the contours of the ν(Cl-Cl) band in order to determine the actual extent and nature of the complexed species.

Recently the theory of molecular reorientations has been directly related to Raman scattering experiments[6]. As an extension of the study in Chapter 4, the Raman spectrum of liquid chlorine is discussed in Chapter 5. It is known that one of the more important model independent quantities to be obtained in studies of molecular reorientations is the reorientational correlation time τ. Values of τ have been extracted from our Raman studies of liquid chlorine. An estimation of the second and fourth moments is also carried out.

In part 2 of this thesis we shall discuss the absolute gas phase intensities of methyl iodide. Information concerning the geometry and mechanical properties of the molecule can be found from measurements of the infra-red absorption bands arising from atomic vibrations. A study of the number and frequency of those absorption bands, combined with a sufficiently well developed theory of small

vibrations can lead to determinations of the type of chemical bonding, and the internal and intermolecular interactions.

The intensities of the spectral bands reflect the structural details of the molecules' electron cloud. The properties of the cloud are characterised by the dipole moments of the molecular groups and bonds, and by the derivatives of these moments with respect to the displacement of the molecule from its equilibrium configuration. Thus infra-red band intensities can be used for calculating the dipole moments and their derivatives.

Despite the high sensitivity of the intensity method little work has generally been done in this field. The basic difficulty being that molecular structure is only studied indirectly using infra-red. The intensities bear a complex relation to the molecular structure and thus special care has to be used in determining the parameters involved in formulating the interpretations.

It is a well known fact that intensity is related to the magnitude and frequency of the alteration of the spatial dipole moment vector of the molecule, resulting from the vibration. In the interpretation of the infra-red absorption intensities of fundamental vibration bands, it is desired to break down the overall change of electric dipole moment with change in the normal coordinate $(\partial \rho / \partial Q)$ into contributions arising from individual bonds within the molecule.

Thus we have made a relatively detailed study of the gas phase infra-red absorption intensities of the fundamentals of methyl iodide. The methyl halides form a simple series of closely related compounds in which one may hope to observe trends in chemical and physical properties. For this reason they have been widely studied, and their infra-red spectra are well known. However the only measurements

of the gas phase infra-red intensities were made twenty years ago, initially by Barrow and McKean[161], and then more accurately by Dickson, Mills and Crawford[116]. We remeasured the gas phase intensities of the fundamentals of methyl iodide (CH_3I) in order to; (a) compare the results with those of Dickson et al; (b) compare the observed and calculated band contours; and (c) compare three methods of determining the relations between intensities and molecular parameters. The three methods considered, have a different formulation of the vibrational angular momentum correction.

In Chapter 6 we shall state briefly the infra-red absorption intensity theory, and also list the force constants for methyl iodide. In Chapter 7 we consider the band contour analysis of the fundamentals. Finally in Chapter 8 we shall discuss the molecular parameters, obtainable from the dipole moment derivatives, in terms of three formulations. The first of these formulations which will be studied is that of Dickson, Mills and Crawford. These authors used Crawford's[164] hypothetical isotope method to determine a vibrational angular momentum correction. The corrected dipole moment derivatives (with respect to the symmetry coordinates) $\partial p/\partial S$ were related to the molecular parameters based on the bond moment hypothesis. However it is well known that the bond moment hypothesis does not hold very well in several cases[115,162,175,176].

The second method is that by Gribov[162], who formed a single equation to consider the contributions to the dipole moment derivatives arising not only from angular reorientations (due to angular deformations), but also from vibrational angular momentum.

The third treatment studied is due to Barrow and Crawford[170] who derived a formulation similar to Gribov's, but never published the details. McKean[171] has summarised this treatment. It is less general than that of Dickson et al, to which it is equivalent, but has the merit of being based solely upon the S_j^n vectors of the Wilson GF method[119].

PART ONE

Chapter 2 GENERAL THEORY

2.1 Calculation of the Infrared Intensity data for Molecular Dynamics Studies

Given[1] that the attenuation of the intensity of a monochromatic beam of frequency ν is proportional to the light flux, or intensity, of the radiation of that frequency, and to the number of absorbing centres (= c.l where c is the concentration of the sample and l is the path length of the cell) then

$$dI(\nu) = \epsilon(\nu)\ I(\nu)\,c\,dl$$

on integrating and solving for $\epsilon(\nu)$ (the absorption coefficient) we have

$$\epsilon(\nu) = \frac{1}{cl} \ln \frac{I_o(\nu)}{I(\nu)} \qquad 2.1$$

where $I(\nu)$ and $I_o(\nu)$ are the intensities of the transmitted and incident radiation with respect to the frequency ν. The value of $\epsilon(\nu)/\nu$ is equivalent to $\Gamma(\nu)$ for the infrared correlation function defined in section 2.5.2. For this thesis $I_o(\nu)$ is taken as the baseline transmittance. The values of $I_o(\nu)$ and $I(\nu)$ are taken for every point from the spectra, the distance between each point being $\Delta\nu$, an arbitrary frequency interval. The correlation functions in section 2.5 are all calculated with respect to the band origin, which in this instance has been defined as the maximum of the absorbance curve.

All spectra were corrected for the distortion due to finite slit widths, by the method proposed by Hill and Steele.[2] The observed and true intensities $I(\nu)$ and $I_T(\nu)$ respectively, are related to the spectral slit width s and the second derivative of $I(\nu)$ with respect to the frequency, evaluated at ν, by

$$I_T(\nu) = I(\nu) - \frac{s^2 d^2 I(\nu)}{12\, d\nu^2} + \text{higher terms} \qquad 2.2$$

The higher terms are negligible if $2s < \Delta\nu_{\frac{1}{2}}$, which is true for the studies reported in this thesis. This method has an advantage over full spectral deconvolution in that it can be applied even when absorption does not decrease to zero at the spectral limits, and also that it is simple and rapid to apply. Corrections due to refractive index were considered to be so low as to be negligible.

2.2 The Raman Effect[3,4]

The Raman effect is concerned with the dipole moment π which is induced in the molecule by the electric field of the incident light. As a molecule consists of positively charged nuclei in a cloud of negative electrons, it is electrically polarizable; and therefore an applied electric field ϵ will induce in it a dipole moment π, thus we have

$$\pi = \alpha E \qquad 2.3$$

where α is the electric polarizability of the molecule. α is not generally a simple scalar quantity as the direction of vector π differs from vector E. In terms of components we have

$$\begin{aligned} \pi_x &= \alpha_{xx}E_x + \alpha_{xy}E_y + \alpha_{xz}E_z \\ \pi_y &= \alpha_{yx}E_x + \alpha_{yy}E_y + \alpha_{yz}E_z \\ \pi_z &= \alpha_{zx}E_x + \alpha_{zy}E_y + \alpha_{zz}E_z \end{aligned} \qquad 2.4$$

where α_{ij} are the components of the polarizability α.

The electric polarisability α will, in general, be a function of the normal coordinates Q_k, and it can be expanded as a Taylor series with respect to these coordinates. Neglecting all but the first power we have,

$$\alpha = \alpha_o + \sum\left\{\left(\partial\alpha/\partial Q_k\right)_o Q_k\right\} \qquad 2.5$$

where α_o is the polarizability tensor in the equilibrium configuration;

and $(\partial \alpha/\partial Q_k)_o$ is the derived polarizability for the Kth normal mode, it is usually denoted by α'.

In Raman spectroscopy the electric field is applied by irradiating the molecule with monochromatic light of frequency ν_o which usually lies in the visible region so that no absorption by the molecule can occur. Combining 2.3 and 2.5 we have

$$\pi = \alpha E = \alpha_o E + \sum_k \left\{ (\partial \alpha/\partial Q_k)_o \, Q_k \right\} E \qquad 2.6$$

The first term on the right is concerned with Rayleigh radiation at the frequency ν_o; and the second term gives the Raman radiation, where the scattering is at the frequencies $(\nu_o - \nu_R)$ (Stokes line) and $(\nu_o + \nu_R)$ (anti-Stokes line), ν_R is the Raman frequency shift.

From this, the condition that a particular normal frequency shall be active in Raman scattering is that

$$(\partial \alpha_{ij}/\partial Q_k)_o \neq 0 \qquad 2.7$$

for at least one of the components (i or j = x, y or z) of α. This is a restricted selection rule.

2.3 Raman intensities and the depolarization ratio

To explain the relative intensity of corresponding Stokes and anti-Stokes lines in Raman spectra, it is necessary to invoke the quantum theory of Raman scattering. In this case the transition moment arising from the induced dipole moment π is given by

$$\int \psi^{(n)} \pi \, \psi^{(m)} \, d\tau = E \int \psi^{(n)} \alpha \, \psi^{(m)} d\tau$$
$$= E \alpha_o \int \psi^{(n)} \psi^{(m)} \, d\tau + E \sum \left\{ (\partial \alpha/\partial Q_k)_o \int \psi^{(n)} Q_k \psi^{(m)} d\tau \right\}$$

Rayleigh scattering — Raman scattering

2.8

From this it is deduced that for an active vibrational mode Raman scattering involves transitions in which Δv_k is ± 1, v being the vibrational quantum number.

The anti-Stokes/Stokes intensity ratio is given by

$$I_{\text{anti-Stokes}}/I_{\text{Stokes}} = \left(\frac{\nu_{\text{anti-Stokes}}}{\nu_{\text{Stokes}}}\right)^4 \exp\left(-h\nu_R/kT\right)$$

$$= \left(\frac{\nu_o + \nu_R}{\nu_o - \nu_R}\right)^4 \exp\left(\frac{-h\nu_R}{kT}\right) \qquad 2.9$$

Calculation of the scattering coefficient for molecules in gases or liquids requires the use of the mean value $\bar{\alpha}'$, and of the anisotropy γ', of the change of polarizability by a normal vibration, where

$$\bar{\alpha}' = 1/3(\alpha'_{xx} + \alpha'_{yy} + \alpha'_{zz}) \qquad 2.10$$

$$\gamma' = \tfrac{1}{2}\left\{(\alpha'_{xx} - \alpha'_{yy})^2 + (\alpha'_{yy} - \alpha'_{zz})^2 + (\alpha'_{zz} - \alpha'_{xx})^2 + 6(\alpha'^2_{xy} + \alpha'^2_{yz} + \alpha'^2_{zx})\right\} \qquad 2.11$$

Here α'_{rr} is the derivative of $(\partial \alpha_{rr}/\partial Q)_o$.

In the Raman experiment in which light is vertically polarized, the analysis of the spectra requires a quantitative separation of the areas of the bands due to t he separate species. The quantities usually measured are $I_{y(xx)z}$ (in the Porto nomenclature[5]), the intensity associated with the vertical component of the field of the scattered light, and $I_{y(xy)z}$ the intensity associated with the component that is perpendicular to the incident polarization and the scattering plane. $I_{y(xx)z}$ and $I_{y(xy)z}$ are called the polarized and depolarized components of the scattered light. The component $I_{y(xx)z}$ contains contributions due to the isotropic and anisotropic scattering[6]. As the band widths

of these components are governed by different relaxation processes it is simplest to transform the measured $I_{y(xy)z}$ and $I_{y(xx)z}$ Raman spectra into isotropic and anisotropic components, and to refer all discussions to these transformed spectra. This is readily done using the well known relationships.

$$I_{y(xx)z} = \text{constant} \left\{45(\bar{\alpha}')^2 + 4(\gamma')^2\right\} \qquad (\nu_o \mp \nu_R)^4 \qquad 2.12a$$

$$I_{y(xy)z} = \text{constant}\ 3(\gamma')^2\ (\nu_o \mp \nu_R)^4 \qquad 2.12b$$

The upper signs relate to the Stokes frequencies and the lower to the anti-Stokes. Thus defining the isotropic and aniso tropic spectra in terms of $I_{y(xx)z}$ and $I_{y(xy)z}$ we have

$$I_{iso} = I_{y(xx)z} - 4/3\ I_{y(xy)z}$$

$$I_{aniso} = I_{y(xy)z}$$

For a totally symmetric vibration of a symmetric top molecule I_{iso} is a power spectrum associated with the vibrational relaxation and I_{aniso} is a convolution of the vibrational spectrum with a power spectrum associated with rotational relaxation.[7]

For our experiment, when the incident light is plane polarized and the observation is perpendicular to the incident electric vector, the degree of depolarization[3] is given by the quotient $I_{y(xy)z}/I_{y(xx)z}$, such that

$$\rho_\perp = \frac{I_{y(xy)z}}{I_{y(xx)z}} = \frac{3(\gamma')^2}{45(\bar{\alpha}')^2 + 4(\gamma')^2} \qquad 2.13$$

For all but fully symmetric vibrations $\bar{\alpha}' = 0$ and therefore $\rho = 3/4$. This value may also be approached for fully symmetric vibrations if $\bar{\alpha}' \ll \gamma'$ so that

$$3/4 \geqslant \rho_\perp \geqslant 0$$

The measurement of the depolarization ratio for Raman bands in fluid systems is a valuable means of determining the symmetry for Raman active modes. To this extent they provide a useful quantitative measure of relative polarizations of selective bands with the ultimate calculations of the separate entities in the dipole correlation functions.

2.4 The Fourier Transform

Electromagnetic radiation is sinusoidal and is expressed, for example, by amplitude = $A\sin(2\pi\nu t)$. An absorption spectrum is a measure of the intensity of a given waveform which is proportional to the amplitude squared and is plotted against frequency. The Fourier transform is used to convert this frequency spectrum into a time spectrum.

The conditions for a Fourier transform of a function, of angular frequency $\omega = 2\pi\nu$, $f(\omega)$ to exist are

(a) that the integral of $f(\omega)$ from $-\infty$ to $+\infty$ exists, and

(b) any discontinuities in $f(\omega)$ are finite.

The Fourier transform has the reciprocal property that the original $f(\omega)$ can be regenerated from the complete transformed spectrum by an inverse Fourier transform (see 2.14).

There are three mathematical distributions commonly encountered in spectroscopy, these are the Lorentzian function, the Gaussian function, and the exponential decay function. The Fourier transform of a Lorentzian function is an exponential decay function and vice versa, and the Fourier transform of a Gaussian function is a Gaussian function. Derivation of these Fourier transforms is given in 8 .

Mathematically the Fourier transform is given by

$$F(t) = \int_{-\infty}^{\infty} f(\omega) \exp(-i\omega t) \qquad 2.14a$$

and the inverse transform is

$$f(\omega) = \tfrac{1}{2}\pi \int_{-\infty}^{\infty} F(t) \exp(i\omega t) dt \qquad 2.14b$$

The exponential of the integral can be written as

$$\exp(-i\omega t) = \cos(\omega t) - i\sin(\omega t) \qquad 2.15$$

For further information of Fourier transforms a good reference is 9 .

2.5 Correlation Functions

2.5.1 Introduction

An absorption band is characterized by three parameters, its frequency, its intensity and its band contour[10]. The latter parameter provides a source of molecular information,which had been neglected until ten years ago, due to the use of the Schrödinger picture where attention was focussed on the energy levels of the system, rather than on its time development. For this approach the transition frequency and band intensity are both well defined molecular parameters, but the band contour is determined by entirely separate considerations, such as Doppler broadening and collisional interactions. There could also be so many transitions that interpretation is difficult, or the lines may blend together to form a continuous band. This is usually the case in dense gases, liquids, solutions and many solids. The assignment of individual lines is impossible. The intensity distribution, determined by all the many molecular wavefunctions of the system, is essentially impossible to calculate. Also there is no classical analogy of a single quantum state, so that even for systems which are described reasonably well by classical mechanics the Schrödinger picture does not allow any classical correspondence to be exploited.

However the Heisenberg picture of quantum mechanics provides a powerful interpretative tool for spectra of complicated systems. By focussing attention on the time development, interpretation of the unresolved lines is possible, and the interpretation is easily visible in terms of molecular motion in the system. Also, a classical correspondence exists which may be exploited for systems which approach classical behaviour. Thus the Heisenberg picture of spectroscopy shows that the Fourier transform of the spectral intensity with respect to the frequency shift from the band centre leads to the autocorrelation function of the transition moment [11]. This relationship of band contours to time dependent correlation functions describes how the fluctuation in the value of some dynamical property of the system persists until it is averaged out by microscopic molecular motion. Mathematically the autocorrelation function C(t) of a quantity A is given by the ensemble average

$$C(t) = \langle A(0) . A(t) \rangle_0 \qquad 2.16$$

where A can be any dynamical function of the variables of the system, such as the momentum of a certain atom. The time dependence of A is that produced by the natural molecular motion of the system, convoluted in some instances by the molecular relaxation of the property A (for example, by exchange of vibrational energy between molecules). The average $\langle \rangle_0$ is over an ensemble of systems at reference time zero [10-12].

If the system is ergodic then C(t) will approach zero as the time $t \longrightarrow \infty$. The shape of vibration-rotation bands in infrared absorption and Raman scattering experiments on linear and symmetric top molecules [10] can be utilized to determine the autocorrelation functions

$\langle U(0).U(t) \rangle$ and $\langle P_2(U(0).U(t) \rangle$

where U is a unit vector whose direction is parallel with any of the

three molecular axes (for a non linear case) and $P_2(x)$ is the Legendre polynomial of index 2 such that $P_2(x) = \frac{1}{2}(3x^2 - 1)$. These correlation functions measure the rate of reorientational motion of the molecules in a particular environment. The advantage vibrational spectroscopy possesses over techniques such as n.m.r., is essentially, that in both approaches we obtain a correlation time, but in the former case the shape of the correlation function is produced.

Thus Raman and infra-red spectroscopy are valuable techniques for determining information about the molecular forces and torques which determine the molecular motion and the nature of the motion itself.

2.5.2 The Infra-red correlation function

The dynamical property of the frequency spectrum which is used, is the transition dipole moment vector. The transition dipole moment vector is a simple molecular property influenced by the others in the system, so ideally we should use dilute solutions. Thus if the short time and long time behaviour of the system are different, the two are isolated in the autocorrelation function. However in the frequency spectrum the intensity at a particular frequency includes contributions from the entire time development of the autocorrelation function. The way in which the autocorrelation function is related to the frequency spectrum has been set out by Gordon[12] and Steele[1]. We shall merely quote the results in this thesis.

The transition dipole moment at a time t can be given as

$$\langle \psi' | \mu | \psi' \rangle = m(t)\ u(t) \qquad 2.17$$

where $m(t)$ is the transition dipole operator and $u(t)$ is a unit vector defining the direction of the moment. From equation 2.17 the infra-red spectrum, normalized to unit area, for a particular band, can be

related to a correlation function by[10-12]

$$\frac{\langle m(t)\ u(t).m(o)u(o)\rangle}{m(o)^2} =$$

$$\frac{\int \Gamma(\nu) \exp[i2\pi(\nu - \nu_o)t]\,d\nu}{\int \Gamma(\nu)\,d\nu} = C_1(t) \qquad 2.18$$

ν_o is the frequency of the band centre, $\Gamma(\nu)$ is $\left(\ln(I_o/I)_\nu\right)/\nu$ where $(I_o/I)_\nu$ is the inverse fractional transmission at a frequency ν; the integrations are over the whole band. Using a normalized spectrum largely eliminates dielectric effects on the local field due to the radiation, though corrections can be and have been applied where they are likely to be significant.

If $m(t)$ is independent of time, and if the motions of the different molecules are uncorrelated then the Fourier transform of the absorption intensity simplifies to the autocorrelation function of the unit vector defining the direction of the transition moment

$$\langle U_i(0).U_i(t)\rangle = \frac{\int \Gamma(\nu) \exp[i2\pi(\nu - \nu_o)t]\,d\nu}{\int \Gamma(\nu)\,d\nu} = C_{1R}(t) \qquad 2.19$$

Until recently it had been assumed that $C_1(t)$ was governed solely by the reorientation of the transition dipole with time. However, as for the Raman case (explained in the next section), it is now clear that non-reorientational broadening mechanisms contribute significantly to $C_1(t)$.

Amongst the most prominent non-reorientational broadening mechanisms is vibrational relaxation (or more generally isotropic relaxation). This vibrational relaxation is said to result from hard collisions which involve energy transfer and deexcitation. This

collisional deexcitation limits the lifetime of the excited vibrational state[13], inducing broadening in the observed spectral line. We believe that we have an induced vibrational relaxation for the a_{2u} mode of hexafluorobenzene (HFB) in the benzene-cyclohexane solvent system; we will study this system in Chapter 3. A second non-reorientational mechanism, is collision induced broadening. This can arise from long range electrostatic dipole-induced dipole interactions, as well as skeletal deformation[14,15]. Translational diffusion and an inhomogeneous solvent shift account for other non-reorientational mechanisms.

Goldberg and Pershan[16] note that if non-reorientational mechanisms are independent of rotational relaxation then $C_1(t)$ can be expressed as the simple product of the rotational and vibrational contributions. Thus:

$$C_1(t) = C_{1V}(t)\ C_{1R}(t) \qquad 2.20$$

The stochastic behaviour of the intermolecular interactions in this case leads to the result that, at times which are long compared with the average time between collisions, both $C_{1V}(t)$ and $C_{1R}(t)$ show an exponential decay with time. This is shown to be the situation for the a_{2u} band of hexafluorobenzene (HFB) in the C_6H_6-C_6H_{12} solvent system.

If on the other hand there is a significant coupling between translations and vibrations, a non exponential decay of C(t) results. An example of this behaviour is probably shown by the out of plane CH bending modes of benzene in polar solvents[17]. The increase in rate of decay of $C_1(t)$ for these vibrations over the corresponding values in cyclohexane is a Lorentzian function in t.

2.5.3 Raman Correlation Function

Bratos[6] showed that the Raman relaxation function $C_2(t)$ is given by

$$C_2(t) = A\, C_{iso}(t) + B\, C_{aniso}(t) \qquad 2.21$$

where A and B are coefficients which depend on the geometry of the scattering arrangement. $C_{iso}(t)$ represents the scattering associated with the isotropic component of the polarizability tensor and describes the relaxation of the vibrational energy. $C_{aniso}(t)$ is associated with the anisotropic part of the tensor and describes the relaxation of both the vibrational and rotational energy.

Thus the profile of the isotropic scattering can be described by the correlation function $C_v(t)$. Such that

$$C_v(t) = \int_{-\infty}^{\infty} \lambda^4\, I_{iso}(\nu) \exp[i2\pi(\nu_o+\nu)t]\, d\nu \qquad 2.22$$

and similarly for the perpendicular component associated with the anisotropic part of the tensor; if the rotational and vibrational relaxation mechanisms are not correlated the product correlation function $C_v(t)\, C_R(t)$ is

$$C_v(t)C_R(t) = \int_{-\infty}^{\infty} \lambda^4\, I_{aniso}(\nu) \exp[i2\pi(\nu_o+\nu)t]\, d\nu \qquad 2.23$$

Assuming cylindrical symmetry and 90^o scattering, the Fourier transforms of the isotropic and anisotropic components are equal to the correlation functions of the polarizability tensor[18]

$$C_{iso} = \langle \alpha(0).\alpha(t) \rangle \qquad 2.24$$

and

$$C_{aniso} = \langle \gamma(0)\, \gamma(t).P_2\{U(0).U(t)\} \rangle \qquad 2.25$$

where $P_2(x)$ is the second Legendre polynomial, and U is a unit vector along a fixed axis. If γ were time independent, then equation 2.25 degenerates to Gordon's result[12], for which molecular

reorientation is assumed to be the only broadening mechanism. This is not generally true as non-reorientational mechanisms can compete with rotational line broadening mechanisms.[19,20] These other broadening mechanisms are noted briefly in the previous section.

In order to obtain reorientational correlation functions from the anisotropic Raman spectrum, the additional broadening mechanisms must first be accounted for. An approximate scheme is utilized to accomplish the separation[6,19,21]. Assuming the non-reorientational broadening is statistically independent of the reorientation contribution and that these mechanisms contribute equally to the isotropic and anisotropic spectra, we can write

$$C_{iso}(t) = \frac{\langle \alpha(0) . \alpha(t) \rangle}{\langle \alpha(0) \rangle^2} = C_V \qquad 2.26$$

and

$$C_{aniso}(t) = \langle \gamma(0)\ \gamma(t) \rangle \langle P_2 \{ U(0) . U(t) \} \rangle$$

$$= C_V C_R \qquad 2.27$$

where C_{iso} and C_{aniso} are the normalized total correlation functions. C_R and C_V are the rotational and non-reorientational correlation functions respectively. C_R can therefore be obtained from the quotient C_{aniso}/C_{iso}[16].

The main reason for Fourier analysis of a band shape is so that we may consider separately the short and long-time motion of the molecular system. At short times, only a few molecules will have received hard collisions; most will be rotating fairly freely. The correlation function will be a superposition of periodic functions. Later on, most molecules will have undergone a number of hard collisions and will be approaching random orientation in an exponential way.

Gordon[10] showed that the behaviour of a correlation function at short times is best displayed by considering a power series in time. The coefficients in this time series are identified as analytic functions of the inertial constants and of the intermolecular torques.

For instance the time series in the classical limit for an infra-red band of a linear molecule begins:

$$\langle U(0).U(t)\rangle = 1-(kT/I)t^2 + [1/3(kT/I)^2 + (24I^2)^{-1}\langle(\dot{OV})^2\rangle]t^4 + \text{higher insignificant terms} \quad 2.28$$

where k is the Boltzmann's constant, T is the temperature, I is the moment of inertia and $\langle(\dot{OV})^2\rangle$ is the mean-square torque on a molecule due to other molecules.

Our main interest however has been in determining the coefficients (identified as frequency moments) for the Raman spectrum of chlorine. We shall consider this in Chapter 5.

The short term behaviour of the Raman correlation function is

$$\tfrac{1}{2}\langle 3[U(0).U(t)]^2 - 1\rangle = 1-\left(\frac{3kT}{I}\right)t^2 + \text{higher terms} \quad 2.29$$

The main point to notice from the above equation, is that the second moments (initial curvatures) of these correlation functions depend only on the temperature of the system and the moment of inertia.

At long times the molecular trajectories become very complex, and it has been found[10] that the reorientation process can be simulated by a stochastic process, such that the correlation functions should approach exponential decay. Various stochastic models will be discussed in section 2.5.6 . The intermediate time regime involves complicated paths for the motion and has eluded a simple dynamical description.

2.5.4 The Free Rotor Correlation Function

In the picosecond time domain of molecular motion the correlation function decays principally by inertial symmetry and intermolecular factors. To provide a fuller interpretation of the motion of the system a theoretical classical model was derived by Steele[22].

For our infra-red analysis of hexafluorobenzene in benzene-cyclohexane solvent mixtures, a simple free rotor was used of the form

$$C_1(t) = 1-2(kT/\hbar)\, Bt^2 + \text{insignificant terms in } (kT/hc)^n \quad n \geqslant 2. \qquad 2.30$$

For our work on the Raman spectra of liquid chlorine a marginally more complex form of free rotor equation was used. The orientational correlation function of an ideal gas of rough spheres (no collisons) is given by[23]

$$C_2(t) = \left\langle \frac{1}{5} \sum_{m=-2}^{2} e^{im\omega t} \right\rangle \qquad 2.31$$

where ω is the rotational speed of a sphere. Explicit evaluation gives

$$C_2(t) = \frac{1}{5} \sum_{m=-2}^{2} (1 - m^2\tau^2)e^{-m^2\tau^2/2} \qquad 2.32$$

where τ is the reduced time, such that

$$\tau = \left(\frac{kT}{I}\right)^{\frac{1}{2}} t \qquad 2.33$$

where I is the moment of inertia of the particle and T is the temperature.

2.5.5 Relaxation Times

In addition to the correlation functions themselves, we are interested in the relaxation times obtainable from them. The relaxation time τ for an exponentially decaying correlation function, due to stochastic behaviour on the Lorentz model, is defined by

$$C_l(t) = A\exp(-t/\tau_l) \quad l = 1,2 \qquad 2.34$$

For infra-red l = 1, and Raman l = 2.

Assuming the spectra to be Lorentzian, the relaxation time is simply related to the half width at half height (HWHH) of the spectrum

$$\tau = (2\pi\bar{c}\bar{\nu})^{-1} \qquad 2.35$$

where $\bar{c}$ is the speed of light and $\bar{\nu}$ is the HWHH in wave numbers. For this case a logarithmic plot of $C_l(t)$ should directly reveal the reciprocal relaxation time β as the slope of the resulting straight line. Another possible definition which is often used is

$$\tau_l = \int_0^\infty C_l(t)\,dt \qquad l = 1,2 \qquad 2.36$$

The reciprocal relaxation time τ_l^{-1} has been the subject of many papers[18,24]. It can be regarded as resulting from a combination of a collision induced vibrational relaxation and a random reorientation or rotational diffusion process; so we may write

$$\tau_l^{-1} \equiv \beta = \beta_v + \beta_r \qquad 2.37$$

where β_v is associated with the vibrational relaxation and β_r with the rotational diffusion. We shall use this relationship in Chapter 3.

2.5.6 Models for Molecular Motion

Once the experimental rotational correlation functions and relaxation times have been obtained the results can be compared to predictions of various molecular rotation theories.

For molecular reorientation studies[19] three approaches have been particularly useful[25]. In the first of these, for sufficiently small times the molecular rotation in fluids is described classically as free rotation. The molecules undergo frequent intermolecular collisions of short duration, and their angular momenta are randomised by the intermolecular torques associated with the collisions. In the situation where the time between collisions is short compared to the mean free rotational period, then the motion is well described by rotational diffusion. The second model pictures a fluid as a pseudo solid. A molecule undergoes solid like torsional oscillations in a potential well formed by the other molecules. The third approach is based on the collision-broadening theory of Van Vleck-Weisskoff; here the molecule reorients instantaneously and randomly upon collision.

The most generally used model is the rotational diffusion model developed by Debye[26] to describe relaxation phenomena. The rotational diffusion model is usually applicable to the situation where molecules undergo collisions in characteristic time for the experiments. For very small times the model is inapplicable since in this limit all motion tends to free motion.

Debye generalized the Stokes-Einstein relation,

$$D = kT/6\pi a\eta \qquad 2.38$$

(where D is the diffusion constant, a is the radius of a spherical diffusing particle and η is the viscosity) to the case of isotropic rotational motion of molecules.

The correlation functions obtained from this model are exponentials of the form

$$C_l = \langle P_l[U(0).U(t)] \rangle = \exp(-t/\tau_l) \qquad l = 1,2 \qquad 2.39$$

where the reciprocal relaxation times are given by

$$\beta = (\tau_l)^{-1} = l(l+1)D \qquad l = 1,2 \qquad 2.40$$

Thus this model predicts the quotient of $\tau_2/\tau_1 = 3$.

It has been reported[23] that the relaxation time τ_l associated with the motion of the symmetry axis of a symmetric top molecule can be calculated from simple hydrodynamic theory where

$$\tau_l = f \frac{4\pi a^3 \eta}{3kT} \qquad 2.41$$

f is an almost temperature independent empirical factor varying between zero and one, introduced to take into account the fact that, a molecule in a neat liquid cannot be represented accurately as a particle diffusing through a homogeneous fluid. McClung and Kivelson[27,28] discussed the meaning of f in terms of some specific hydrodynamic models. This Stokes-Einstein model assumes that the fluid adjacent to the large rotating particle "sticks" to the particle and rotates with it.

Although there is no particular reason why the reorientational correlation time, which depends upon rotational motion, should be a function of η (a translational property) it has been experimentally observed that this theory is applicable to small molecules in solution or in the pure liquid[29]. We shall use the rotational diffusion model in our investigation of the rotational motion of chlorine, in Chapter 5.

Gordon[30] has generalised the Debye model of rotational diffusion to allow molecular reorientation through angular jumps of arbitrary

size. This "J Diffusion" model assumes that collisions randomise the components and magnitude of the angular momentum at the end of a free rotation step. It also assumes that the rotation frequency in each step is spread over a Boltzmann distribution.

2.6 Interactions in Molecular Complexes

A General Survey

In this brief survey we have incorporated information on the ways in which the interactions in molecular complexes have been interpreted. Therefore this section is only designed to contribute to the understanding of the work presented in the next two Chapters.

In an attempt to explain the results of spectrophotometric studies of iodine with benzene[31], Mulliken introduced the "charge transfer" resonance theory[32]. This theory described the ground state electronic wave function Ψ_N of a donor-acceptor complex approximately, by a combination of two resonance structure functions Ψ_o and Ψ_1, such that

$$\Psi_N(D.A.) \simeq \underline{a}\Psi_o(D.A.) + \underline{b}\Psi_1(D^+\text{-}A^-) \qquad 2.42$$

no bond dative

Here $\underline{a}$ and $\underline{b}$ are the coefficients of the no bond and dative structures, respectively. In the ground state of a weak complex, $\underline{b}$ is expected to be less than 0.1 and $\underline{a}$ is approximately 1.0. The stability of the complex depends on the extent of the mixing between the wave functions of the no bond and dative structures.

If the ground state structure of a complex is given by Ψ_N then according to the "charge transfer" theory, there is an excited state Ψ_v which is called a charge transfer state given by

$$\Psi_N = -\underline{b}^*\Psi_o(D.A.) + \underline{a}^*\Psi_1(D^+\text{-}A^-) \qquad 2.43$$

The coefficients $\underline{b}^*$ and $\underline{a}^*$ are determined by the quantum theory

requirement that the excited state wave function be orthogonal to the ground state function $\int \psi_N^* \psi_v dz$. The electronic absorption frequency of the new band formed in the complex corresponds to the energy difference between the ground state (N) and the charge-transfer (V) of the complex.

Since Mulliken's original publication, large numbers of papers and reviews have appeared concerning the theoretical and experimental aspects of such systems[33,34]. The general conclusions from these publications are that the appearance of a charge-transfer band is no reason for the assumption of a molecular complex - likewise the absence of a charge transfer band does not necessarily mean the absence of a charge transfer interaction, only that the binding energy has an origin other than charge transfer. The suggestion is made by many workers in the field, that the contribution of charge-transfer to the intermolecular binding energy has been overestimated in the past, and that classical electrostatic and polarization effects are of major importance in this respect. The various types of intermolecular force that can exist in the $\pi - \pi$ molecular complexes have been discussed by Dewar and Thompson[35]. They argued that charge transfer forces are a special case of London dispersion forces which result from electrostatic interactions caused by electron correlation. These forces are represented by the mixing of a ground state unperturbed wave function with that of an excited state. Dispersion forces result when the excited state is caused by the π electron distribution of one molecule being perturbed from its symmetrical, equilibrium distribution. Dewar[35] studied the charge transfer of 14 TCNE/aromatic complexes and found that there was little correlation between the derived values of the equilibrium constants and the wavelength of the charge transfer band. This finding showed that the charge transfer forces played little part in the binding

energy of the $\pi - \pi$ complexes. A similar conclusion was suggested by Le Fevre[36] regarding the origin of the dipole moments of $\pi - \pi$ complexes. Models were used to compute the contributions of the dipole moments of such complexes caused by electrostatic and polarization effects and it was found that more than half of the experimental dipole moment could be accounted for in this way.

Hanna[37] studied the bonding in 'classical' charge transfer complexes of the type halogen/aromatic hydrocarbon by applying a perturbation treatment. This approach was particularly useful for the study of intermolecular forces in the region of small orbital overlap. Hanna also investigated the effect of electrostatic contributions and found that the most important contribution to the ground state properties was caused by an interaction resulting from the π-quadrupole moment of the hydrocarbon inducing a dipole in the halogen molecule. This quadrupole induced dipole interaction was found to account for 30 to 80% of the important ground state properties, such as the dipole moment, equilibrium constant, enthalpy of the complex form and certain magnetic properties. These properties had hitherto been assumed to arise from charge transfer forces.

Hanna and his associates[38] also attempted to interpret the change in the infra-red intensity of halogens in benzene as a purely electrostatic effect. They estimated an induced dipole for chlorine in a complex arising from the interaction of the field, along the sixfold z axis of the benzene molecule with the polarizable halogen molecule.

$$\mu_i = \tfrac{1}{2}\alpha''[\epsilon_1 + \epsilon_2] \qquad 2.44$$

Here α'' is the polarizability of the halogen parallel to its axis (in the z direction), ϵ_1 is the field from the benzene at the nearest halogen atom (X), and ϵ_2 is the field at the halogen atom (Y) further

away from the benzene. Taking the derivative of equation 2.44 with respect to the internal coordinate R_1 of the halogen

$$\frac{\partial \mu_i}{\partial R_1} = \frac{1}{2} \frac{\partial \alpha''}{\partial R_1} (\epsilon_1 + \epsilon_2)$$

$$- \frac{1}{4} \alpha'' \left[\left(\frac{\partial \epsilon}{\partial z} \right)_{z=z_2} - \left(\frac{\partial \epsilon}{\partial z} \right)_{z=z_1} \right]$$

From this it was determined that the intensity enhancement of the halogen stretching mode and its associated red shift were almost wholly explained by these effects. The dipole moment, induced in the halogen by the benzene π-quadrupole moment, changes as the halogen vibrates so that the halogen mode becomes infra-red active.

Chapter 3 THE HEXAFLUOROBENZENE - BENZENE SYSTEM

3.1 Introduction

This chapter gives an account of some infra-red spectroscopic studies of the hexafluorobenzene (HFB)-benzene-cyclohexane system. We shall show that concentration dependence and magnitudes of the frequency shifts and of the Fourier transforms of the absorption band contours, as well as symmetry considerations can be used to determine the nature of the intermolecular interactions within the system.

Equations for the infra-red correlation function, used in this chapter, have been quoted in the previous chapter.

3.2 General Survey

3.2.1 Nature of the Interaction

Patrick and Prosser[39] discovered that when benzene was mixed with an equimolar quantity of HFB, a solid of the two components formed. The solid/liquid phase diagram for benzene-HFB was studied in some detail. It was established that although the melting points of HFB and benzene are very similar (just above $5^{\circ}C$), the equimolar congruently melting compound had a melting point of $23.7^{\circ}C$. It was inferred that the HFB and benzene formed a 1:1'complex'. The occurence of the solid compound, in this system, composed of two simple non-polar substances, was taken as strong evidence that the intermolecular interactions were unusual. It was suggested that the enhanced stability of the compound was due to charge transfer complexing, although there appeared to be no spectroscopic evidence of this in liquid mixtures. For instance Baur et al[40] found that the dipole moment of the postulated complex was less than 0.1 Debye (where $1D = 3.335 \times 10^{-20} C\ m$). This value is small compared to

those reported for undoubted charge transfer complexes in which dipole moments are generally of the order of 1.0 Debye. Therefore it was assumed that the formation of a compound was, in the main, attributable to entirely different effects.

The measurement of various thermodynamic excess functions of binary liquid systems, containing aromatic fluorocarbons at reduced temperatures, has been the subject of research by Fenby and Scott[41]. The sign and magnitude of the principle excess functions gives a good indication of the relative strengths of the like and unlike interactions occurring in binary mixtures. Large positive excess free energies, enthalpies, entropies and volumes, and negative excess heat capacities indicate weak unlike interactions. Negative values for excess free energies, enthalpies, entropies and volumes, and positive excess heat capacities are normally characteristic of systems with strong unlike interactions. These excess functions measured by Fenby and Scott show a large negative excess enthalpy, for HFB of $-433\ J\ mol^{-1}$ and a positive excess volume of $+\ .801\ cm^3 mol^{-1}$. It was considered that there was some evidence of complex formation. Ferri[42], using Hanna's calculations [37], considered that the interactions in these mixtures of aromatic hydrocarbons with aromatic fluorocarbons were due to electrostatic interactions rather than charge transfer.

Powell, Swinton and Young[43] applied the statistical theory of Rowlinson and Sutton to measurements of gas-liquid critical temperatures of the HFB-benzene system, and deduced that there was an angle dependent force. However, they were of the opinion that the interaction is short-lived and could probably be explained without invoking specific covalent bonding forces. The thermodynamic measurements made by Powell and Swinton[44] tended to support a model which indicated complex formation in solution, but that the interaction was relatively weak.

There is also evidence for specific association of benzene and HFB in the vapour, from second virial coeffients[45].

Bauer et al[46] made measurements of the orientational relaxation times of the components of the mixture HFB with benzene, by depolarised Rayleigh scattering. In this mixture they noticed strong "static" and dynamic cross correlation terms which affected the individual reorientation times. They concluded that there was no significant contribution to the Rayleigh scattering spectra, from a long lived complex in the mixture.

Ferri[42] studied the correlation functions of the HFB-benzene system, and concluded that the system was unlikely to form anything more than a 'sticky' interaction when the molecules were aligned in certain (time averaged) preferential orientations.

3.2.2 Nature of the Structure

Ledaal[47] attempted to find, a possible common structure for the geometry of collision complexes, and the main factors which appeared to determine this geometry. He studied a large number of polar solute/solvent collision complexes. He deduced that there was a common model in all cases, in which the dipole axis of the polar solute molecule is located along the sixfold symmetry axis of a benzene solvent nucleus. The factors determining the collision complex geometry were found to be the attraction between the electrophilic positive end of the local solute dipole and the nucleophilic π electron system of the benzene nucleus. However HFB is not polar, therefore it would not necessarily orientate itself in this way.

Le Fevre et al.[48] noted a strong static correlation between benzene and HFB using the Cotton-Mouton effect. The molar Cotton-Mouton constants of several non polar and axially symmetric solutes were measured in both benzene and tetrachloromethane. Differences between

the Cotton-Mouton constants of the same solute in these two solvents were attributed to angular correlations between the solute and the benzene molecules. The positive signs of these correlation functions for HFB revealed a net tendency for the molecular plane of HFB and its nearest benzene neighbours to adopt parallel orientations. Using the observation made by Barrett and Steele, that the in plane β_H modes of HFB are not affected in benzene solution whereas the γ_H modes are, we shall show in section 3.5 that we favour the parallel orientation as well.

3.3 Experimental

3.3.1 Chemicals

Spectroscopic quality benzene and cyclohexane from B.D.H. Chemicals Ltd. and Puriss respectively, were used for this investigation. The benzene and cyclohexane were stored over molecular sieves. No further purification was considered necessary.

Hexafluorobenzene (HFB) was a spectroscopically pure sample from Bristol Organics Ltd. Again no further purification was considered necessary.

3.3.2 Equipment and Conditions

Our infra-red spectra were recorded on a Perkin Elmer 325 double beam spectrometer, at a resolution of about 2.0 cm^{-1}, in the region of the a_{2u} mode of the hexafluorobenzene.

A Perkin Elmer comb attenuator was inserted into the reference beam to adjust the baseline for practical purposes. In all cases one metre of chart paper was equivalent to a scan of 60 cm^{-1}. The spectral slit width was observed at the beginning, middle and termination of each scan. The beam balance was checked before a

series of scans, since the beams should be of equal energy prior to insertion of the cells into the sample and reference beams. In all cases the optimum conditions for operation of the spectrometer were utilized. The slit program, gain, pen speed, response, scanning speed and suppression were selected to produce the best quality spectra. The transmission linearity of the PE 325 was verified as being within 0.5% by the use of calibrated choppers.

A number of mixtures of benzene and cyclohexane were made up by weight, covering the range from pure benzene to pure cyclohexane. The ratios of the various benzene:cyclohexane solutions were 1:0, 3:1, 3:2, 1:2, 1:3, 1:5, 1:10, 1:15, 1:30 and 0:1. Several spectra were run for each solution. Good agreement was obtained from the different runs on frequencies and band widths. All measurements were made at an HFB concentration of 0.08 mol dm^{-3}.

Perkin Elmer cells were used with caesium iodide plates; a lead spacer of .02 dm thickness was used to obtain the desired intensity. Care was taken to keep the CsI windows dry at all times. All the spectral measurements were carried out at a cell temperature of 30°C. The measurements on all solutions were repeated at cell temperatures of 5°C and 55°C using the Perkin Elmer variable temperature cell and a RIIC-Beckmann temperature controller Tem 1. A cardice-acetone mixture was used to cool the cell. Data were processed on a CDC 6600 computer, using program VANSA listed in appendix 1.

3.3.3 The a_{2u} vibration

It should be noted that some authors have assigned the a_{2u} mode to the band of hexafluorobenzene at 315 cm^{-1}, and the lowest e_{1u} mode to the band near 210 cm^{-1} [49,24]. However in this work it has been assumed that the band of hexafluorobenzene near 210 cm^{-1} arises from the

a_{2u} vibration. This is based on the assignments made by Steele and Whiffen[50], which were given some support by the band contours measured in the vapour phase[51]. More recently a comprehensive study[52,53] of the out of plane and in plane vibrations and force fields of all fluoro substituted benzenes gives confirmation of the assignments used in this work.

In the a_{2u} vibration for HFB the fluorine atoms move out of the plane of the carbon skeleton, and the original sp^2 hybrid orbitals around the carbon tend towards a non-planar sp^3 valence state, thereby producing an increased electron density on the opposite side of the ring. Steele and Wheatley[51] observed differences between the effective bond dipoles as derived from intensity measurements of the in plane and out of plane fundamentals of HFB. They suggested that the change in hybridization produces an electronic hybridization moment due to the displacement of the π charge in a direction opposite to that of the movement of the fluorine atoms out of the plane of the ring.

Support for this suggestion came from Jalsovsky and Orville-Thomas[54] who calculated bond moment constants from the infra-red band intensities of benzene, and compared these with the theoretical bond moment constants. This theoretical was established by the CNDO method, taking into account the dipole moment contribution of the hy brid orbitals.

3.4 Experimental Results

The initial significant observation was that no e_{1u} band of HFB was affected in any way by change of solvent; whereas the a_{2u} umbrella mode experiences both an increase in the wavenumber of its band centre of 5 cm^{-1} in going from cyclohexane to benzene solution and also a drastic change in band controur (see **Figure** 1). The bond contour

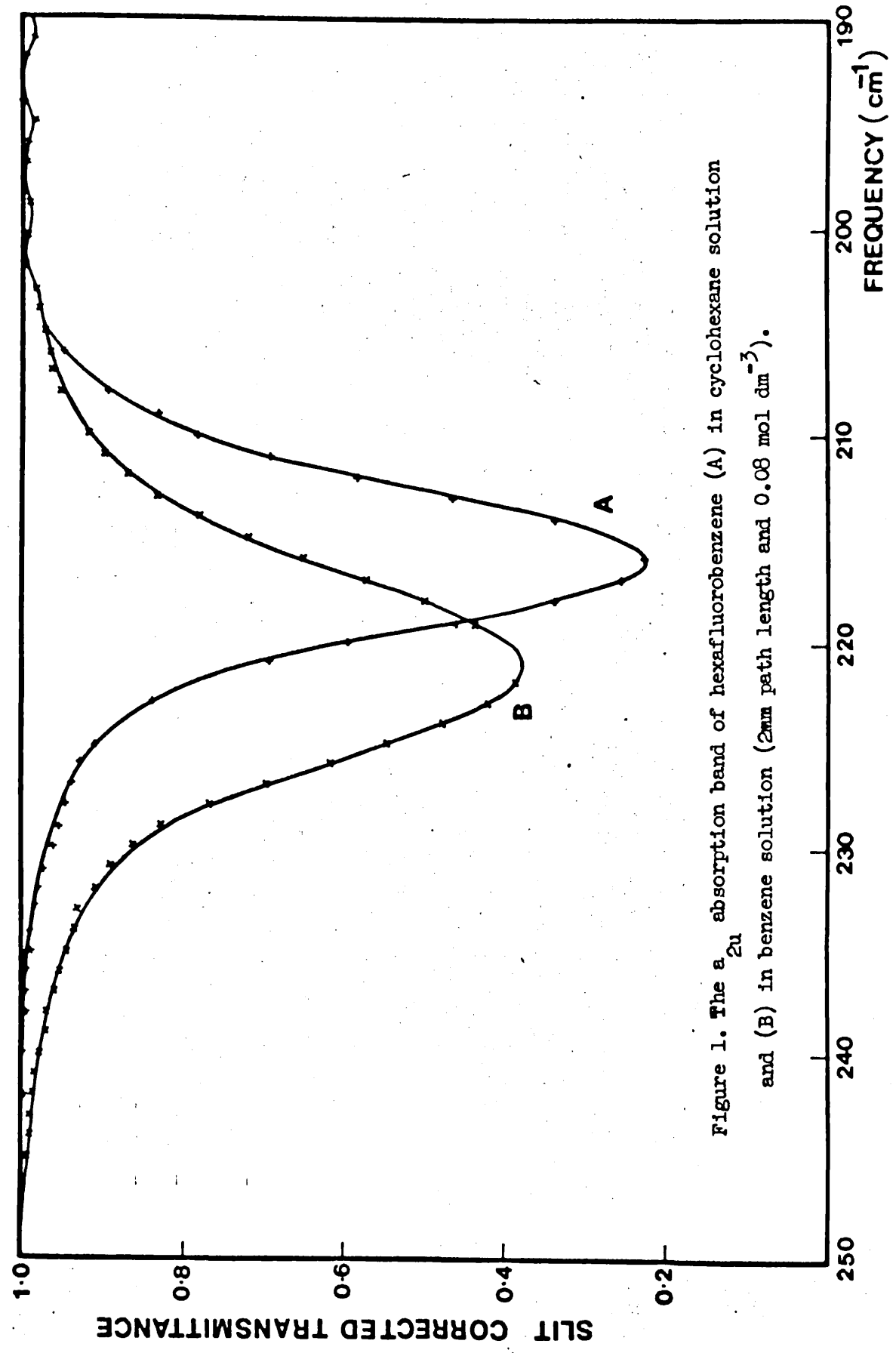

Figure 1. The a_{2u} absorption band of hexafluorobenzene (A) in cyclohexane solution and (B) in benzene solution (2mm path length and 0.08 mol dm^{-3}).

remains reasonably symmetric in all solutions.

Interferometric studies by Barrett[55] showed a 30% increase in the intensity of the band in going from cyclohexane to benzene solution. However no such increase of intensity was observed using the PE 325 up to a 1:1 mixture of cyclohexane to benzene. A small increase of 10% occurred in going to HFB in pure benzene.

Program Vansa was used to correct the observed I_o and I for slit width distortion (see section 2.1), and then to perform a Fourier transform of each band. The complex transformation, given by equation 2.18 was used to yield lnC(t) against t graphs. No account had to be taken of the effects of different isotopes as fluorine has no second isotope. The procedure was simplified further by assuming that any shift of band centre, due to the ^{13}C content, was of no account as the effect was small and would not vary between the different solutions.

Comparison of the lnC(t) curves for the solutions, with that of a free rotor (see equation 2.30) showed that the simple free rotor plot lay above all those of the solutions. In figure 3 it was observed that up to .5 picosecond the lnC(t) plot of the cyclohexane solution lies about 20% below that expected for a free rotor. This initial discrepancy is possibly due to the experimental difficulties in measuring the intensities of the wings. For the benzene solution the whole curve lies well below that for cyclohexane solution.

At longer times (greater than .5 ps) the lnC(t) against t plots gave a linear relationship in all cases, some of these plots are given in figure 2.. The gradient of the linear section of each graph gives β the reciprocal relaxation time (see Chapter 2.5.5). In order to determine the nature of the interaction, the experimentally

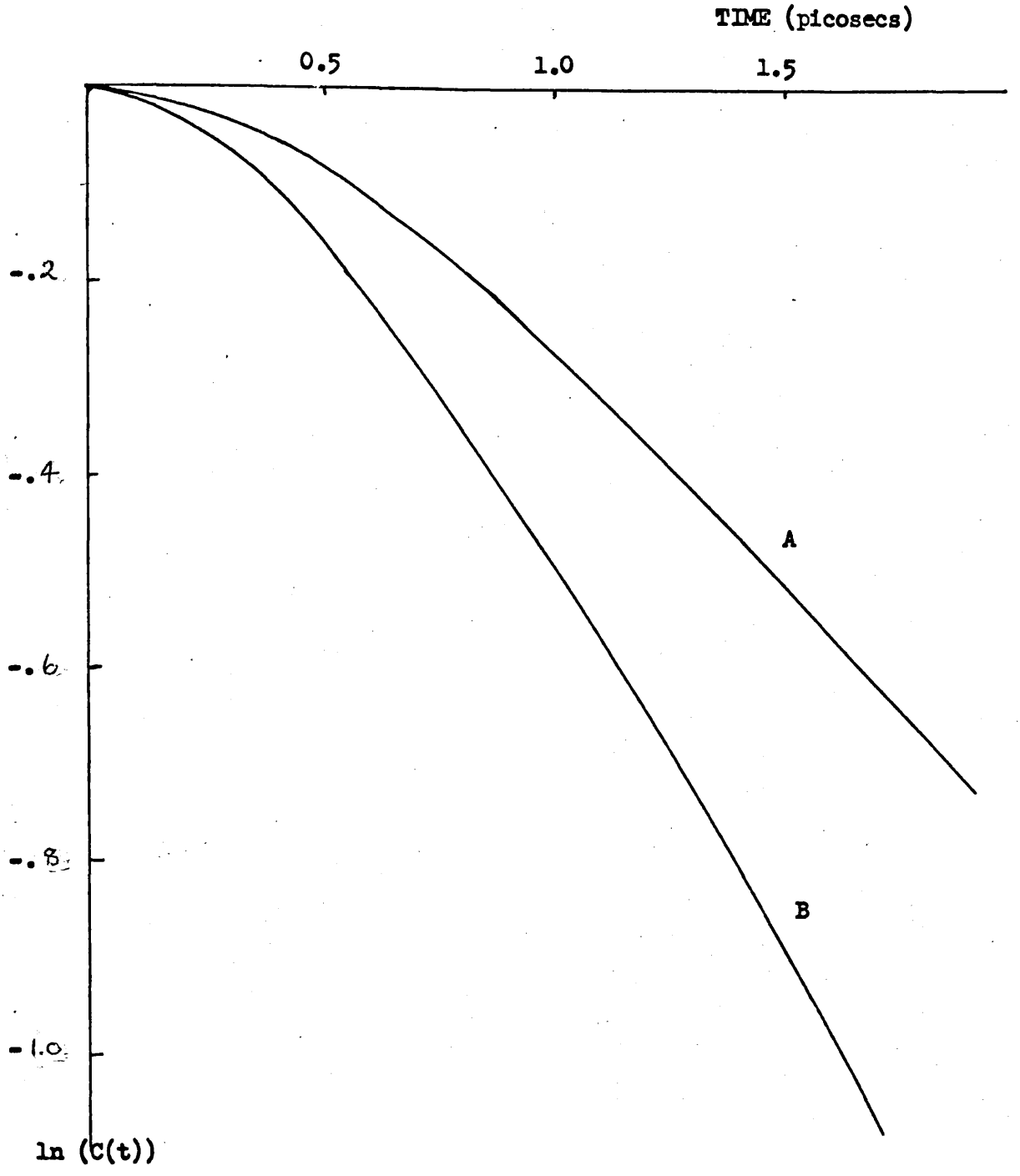

Figure 2. The ln C(t) against time plot for the a_{2u} vibration of hexafluorobenzene in benzene solution (B) and in cyclohexane solution (A).

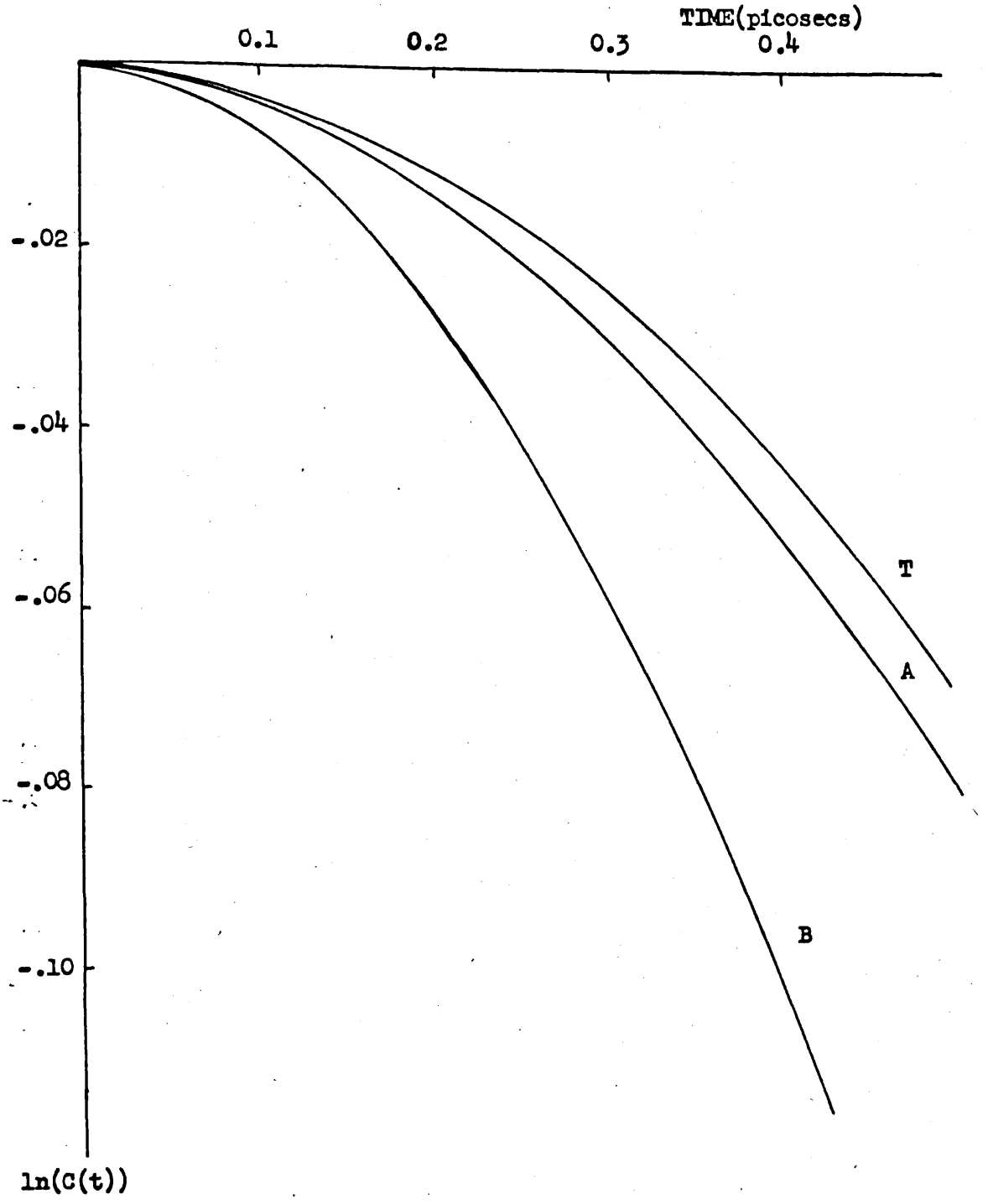

Figure 3. An expansion of that part of fig.2 referring to the short time behaviour ($< 0.5 \times 10^{-12}$ s). T is the free rotor curve.

obtained β is plotted against benzene concentration. The resultant graph is that given by A in figure 4. The graph appears to be linear up to the asymptotic value of β which occurs at about 35% benzene. After this point the value of β changes only slightly, up to pure benzene. Further information will be derived from a graph of β against the observed frequency shift ($\Delta\nu$) of the a_{2u} mode, see figure 5. These shifts are considerable, being up to 5 cm^{-1} in 210 cm^{-1}. The relevance of these graphs will be discussed in the next section.

Some studies of the temperature dependence were made. Spectra for the different solutions were run at a series of temperatures from 5°C to 55°C, however the results were of low accuracy due to experimental difficulties. We can only generalise on the results obtained. The two principle observations were that (a) there is very little alteration of band width due to the temperature change, and (b) there is a small frequency shift of .03 $cm^{-1}{}^{o}C^{-1}$.

3.5 Discussion

3.5.1 Types of broadening mechanisms considered

It was considered that the change of band contour could be accounted for by an interaction arising from long lived complexing of the $\pi-\pi$ type. In this picture the benzene and HFB are seen as interacting on collision, in such a way as to perturb the orbitals which are symmetric with respect to the C_6H_6 axis.

In figure 1 the 5 cm^{-1} move in band centre is of the order of one half height band width, therefore it is unlikely that the broadening mechanism is one in which there is an overlapping of bands due to molecules in different long lived states of aggregation.

We deduce that a long lived complex should exist for longer

Figure 4. A plot of the reciprocal relaxation time ($\beta = \beta_v + \beta_r$) against concentration of benzene. The concentration of hexafluorobenzene is 0.08mol dm^{-3} in cyclohexane+benzene mixtures, curve (A). Curve (B) is as expected for a property arising from a HFB+benzene complex with an equilibrium constant of 0.68$dm^3 mol^{-1}$ and assumes $\beta(0) = 0.545 ps^{-1}$ and $\beta(max) = 1.445 ps^{-1}$.

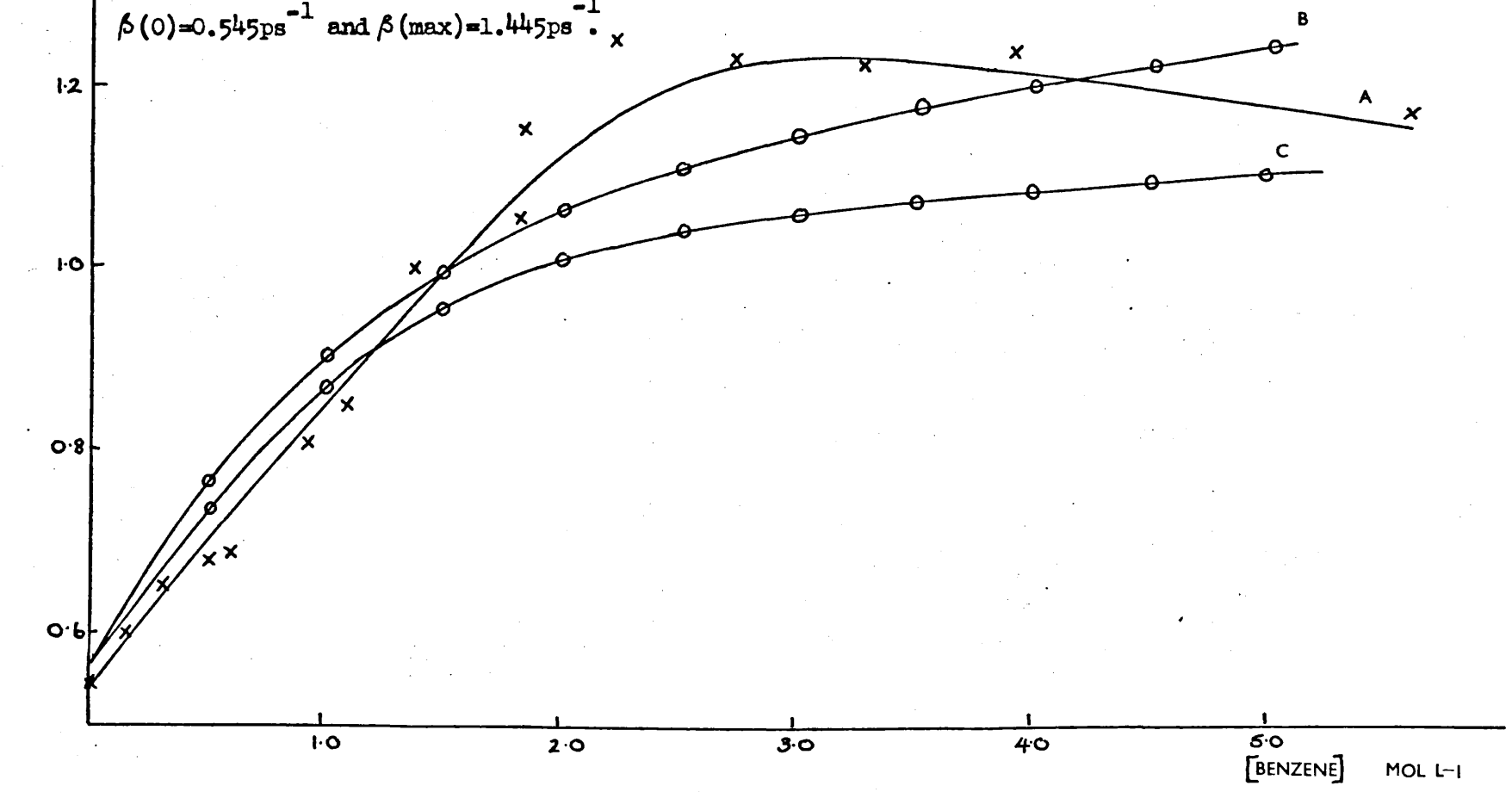

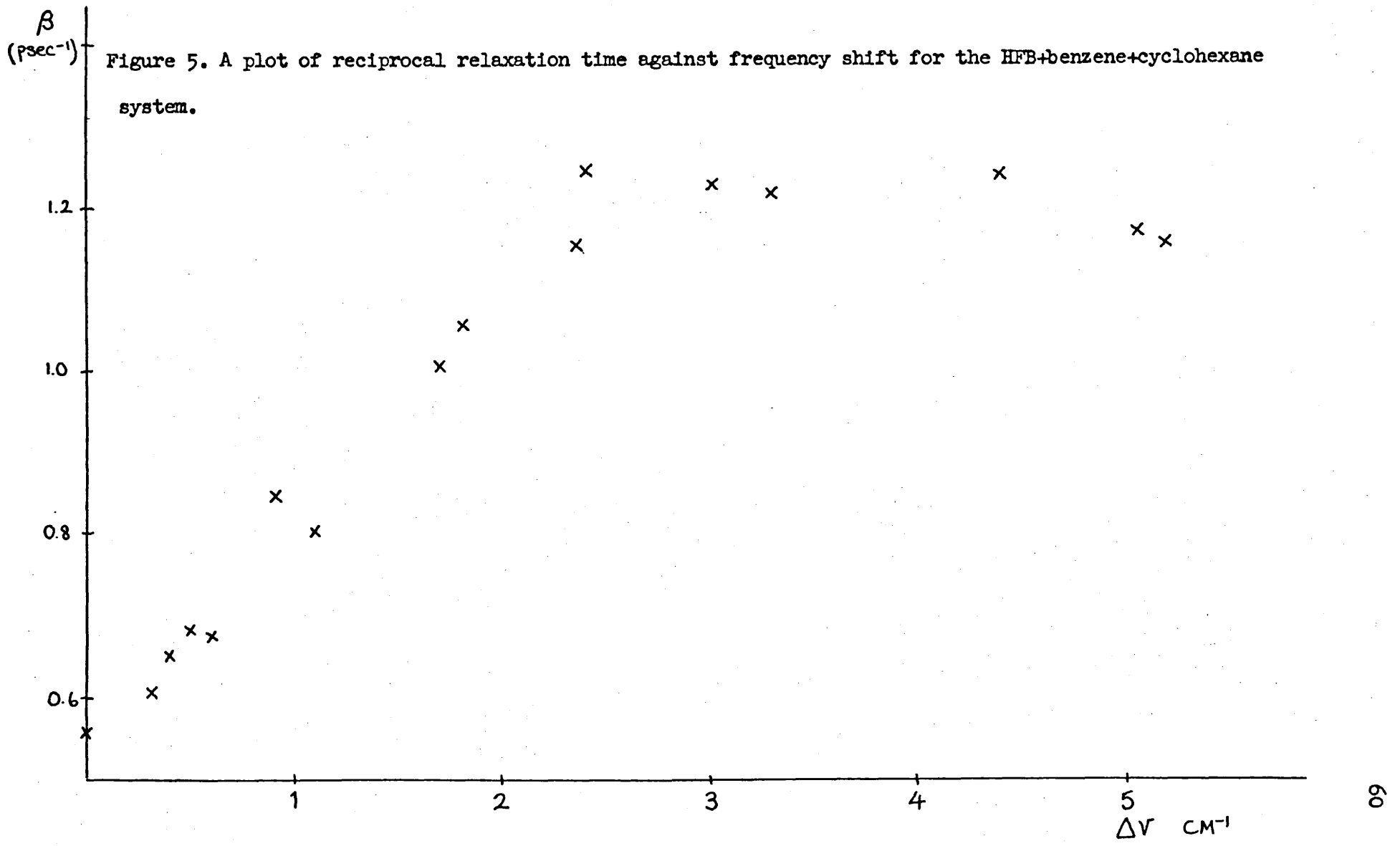

Figure 5. A plot of reciprocal relaxation time against frequency shift for the HFB+benzene+cyclohexane system.

than the reciprocal of the radial frequency separation between the two bands in the two pure solvents (where τ would be about 1×10^{-12} sec). However from figures 2 and 3 we deduce that the benzene-HFB complex is much shorter lived.

Two alternative mechanisms are considered to be causing the broadening; either exchange broadening or vibrational relaxation. If the a_{2u} vibration of the HFB molecules is sensitive to the surrounding solvation sheath, and if the exchange time of the environment is within a scale of the order of the reciprocal of the radial frequency difference between the transition frequencies in the two environments ($\tau_e \approx 1/\Delta\omega$), then exchange broadening occurs. If the exchange time is very slow ($\tau_e \gg 1/\Delta\omega$) then the bands from different solvated species will appear; whereas if the exchange time can be increased significantly ($\tau_e \ll 1/\Delta\omega$) then coalescence to a single sharp band occurs.

The second broadening mechanism is induced vibrational relaxation of the a_{2u} vibration. As with the exchange broadening mechanism the relaxation may be due to solvation exchange; however the principle difference is that, for this relaxation an increase in the exchange rate does not lead to a narrowing of the band.

From figure 4 the observed reduc tion of β at high benzene concentrations is possibly due to exchange narrowing. This would be in accord with the continuing increase in $\Delta\nu$ observed in figure 5. However from our limited temperature data we failed to see a change in band widths on varying the temperature by 50°C. We would have expected the exchange rate to vary significantly over this temperature, if only as a result of variation in molecular velocities. Thus the mechanism of kinetic exchange broadening would seem to be less likely than a vibrational relaxation mechanism, because for kinetic exchange

there should be a distinct narrowing of the a_{2u} band, of HFB in C_6H_6 solution, on increase of temperature.

Although our data is not convincing enough to distinguish between the two broadening processes, we shall discuss the experimentally observed phenomena in terms of the vibrational relaxation mechanism.

3.5.2 The short and long time behaviour

The initial curvatures of the $\ln C(t)$ curves of the a_{2u} band of HFB in different benzene/cyclohexane mixtures are much greater than expected for a free rotor, thus no adequate explanation of the short time behaviour can be advanced. Extrapolation backwards of the longer time behaviour suggests a relaxation in addition to that arising from free rotation, peculiar to short times. Since our general interpretation indicates that association is short lived, the short time behaviour ought to represent free movement of the HFB in cavity fields.

Two deductions can be made from the good linear relationship of the $\ln C(t)$ graphs at long times. First, they indicate that experimental errors in the measured intensities within 30 cm^{-1} of the band centre are very small, as far as the correlation functions are concerned. Secondly we see that all the relaxation processes involved at these times are random. Coupling between translations and vibrations would lead to a Lorentzian contribution to $C(t)$[56]. If we further assume that the Fourier transform of the intensity leads to a reciprocal relaxation time β (see Chapter 2.5), then following Favelukes et al[57] and Yarwood[58], we can write

$$C(t) = \text{constant} + C(0)\exp[-\beta v + \beta r] \qquad 3.1$$

where βv and βr are the reciprocal relaxation times for vibration and rotation respectively. If βv was proportional to the extent of complexing and βr was constant, then we could further assume that if

the reciprocal relaxation time $(\beta)_{cyc}$ for HFB in cyclohexane solution is unaltered by addition of benzene then

$$\beta_{cyc} \equiv \beta(0) = \beta r \qquad 3.2$$

Using this relationship we can achieve an extraction of βv for the various solutions, Plotting βv $(+\beta r)$ against concentration of benzene yields the calculated curves B and C in figure 4. The method of calculation is described in the next section. All $(\beta v + \beta r)$ values were derived by a least squares fitting of some 50 points in the linear portions of the $\ln C(t)$ against t graphs.

3.5.3 The equilibrium constant

The shape of graph (A) in figure 4, obtained experimentally, was taken to suggest a bimolecular collision reaction. For this reaction we endeavoured to find an approximate value for the equilibrium constant (K) and thence a calculated curve to fit to graph (A).

The equilibrium constant for the interaction of two unlike species A and B to form a complex C is given by

$$K_a = \frac{a_C}{a_B\, a_A} = K_c\, K_\gamma$$

$$\text{where} \quad K_c = \frac{C_C}{C_B\, C_A} \qquad 3.3$$

$$\text{and} \quad K_\gamma = \frac{\gamma_C}{\gamma_B\, \gamma_A}$$

The symbols, a, C and γ represent activity, concentration and activity coefficient, respectively. If complexes are studied entirely in solution, then it can be assumed that K_γ is unity. Thus equilibrium constants are based on equation 3.3 and are written as

$$K_C = \frac{C_C}{(C_B^o - C_C)(C_A^o - C_C)} \qquad 3.4a$$

where C_B^o and C_A^o are the initial concentrations of A and B.

Therefore for HFB complexing with benzene we can write

$$K = \frac{[\text{complexed HFB}]}{[\text{free HFB}][\text{Benzene}]_A} \qquad 3.4b$$

where $[\text{Benzene}]_A = [\text{Benzene}]_{\text{initial}} - [\text{HFB complexed}]$. The square brackets denote "concentration of".

To simplify the calculation of K, we assumed that this second order equilibrium was given by the concentrations of the reactants at half complexing

$$\text{Thus} \qquad K = \frac{[HFB]_{\frac{1}{2}}}{[HFB]_{\frac{1}{2}}([B]-[HFB]_{\frac{1}{2}})} = \frac{1}{[B]-[HFB]_{\frac{1}{2}}} \qquad 3.5$$

Initially we take a value for $\frac{1}{2}$ complexing as the mid point of the linear portion of the graph in figure 4. If $\beta_{max} = 1.24\ ps^{-1}$ and $\beta(0) = .545\ ps^{-1}$ then $\beta_{\frac{1}{2}} = .893\ ps^{-1}$; therefore $[B]_{\frac{1}{2}} = 1.17\ mol\ dm^{-3}$. From our experimental data $[HFB]_{initial} = .079\ mol\ dm^{-3}$. The calculated value of $K \simeq .88\ dm^3 mol^{-1}$. Using this value of K we can now work backwards to obtain the theoretical curve C. As can be seen this is a rather bad fit to the experimental. By a process of trial and error we obtained the better fit of curve B. The assumed values for this curve are $\beta_{max} = 1.445\ ps^{-1}$, $\beta(0) = .545\ ps^{-1}$, $\beta_{\frac{1}{2}} = .995\ ps^{-1}$, $[B]_{\frac{1}{2}} = 1.56\ mol\ dm^{-3}$ and therefore $K = .68\ dm^3 mol^{-1}$.

It is probably unrealistic to expect to be able to separate βr and βv as we have done, because we cannot necessarily explain the behaviour in terms of solvent cage effects alone. When the asymptotic value of β is reached at 35% concentration, we suggest that the HFB molecules are embedded in a cage of benzene molecules. It follows that well before this point relaxation and pairing is going to be enhanced above and beyond the expectations for a simple bimolecular reaction.

As we have already noted figure 5 shows a plot of β against $\Delta\nu$, where $\Delta\nu$ is the frequency shift for the HFB-benzene-cyclohexane system. A behaviour similar to that in figure 4 is observed. Up to 35% benzene concentration there is a linear relationship between $\Delta\nu$ and β; at which point there is a sharp change in gradient. $\Delta\nu$ continues to increase up to 100% benzene solvent, while β changes only very slightly. Our explanation of this graph is that at 35% benzene concentration each of the HFB molecules have been embedded in a benzene cage. The continued increase in $\Delta\nu$ up to 100% benzene is due to some other competing interaction. We consider that this interaction is between the non-associated benzene molecules and the complexed species. The presence of the free benzene molecules causes an increase in the restoring force of the γ_H vibration of the benzene molecules in the complex. The continued increase in $\Delta\nu$ up to 100% benzene is in accord with the thermodynamic evidence that the association energy between HFB and benzene is very small.

3.5.4 Model for the Interaction and the mechanism of Vibrational relaxation

First we shall consider the electrostatic model devised by Lalau[59]. Lalau observed that the out of plane γ_H vibrations of aromatic systems were shifted towards higher frequencies, with increasing polarity of the solvent. He considered a H-atom of the solute, at a distance r from the terminal atom O of any polar bond.

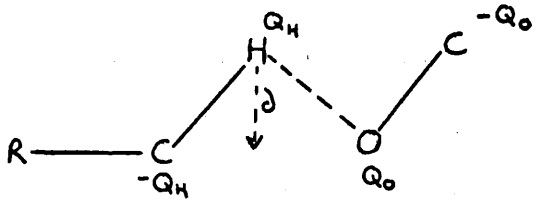

Fig. 6 Schematic representation of the interaction of the γ_{CH} vibration with a neighbouring dipole

In Figure 6 R is the remainder of the benzene molecule lying in a plane perpendicular to ∂; where ∂ is the deviation of H from its equilibrium position. If Q_H and Q_O are the excess charges at H and O respectively. The component $F\partial$ along ∂ is

$$F\partial = \frac{Q_H Q_O}{r^2} \frac{\partial}{r} \qquad 3.6$$

This implies that there is a corresponding force constant h where

$$h = \frac{Q_H Q_O}{r^3} \qquad 3.7$$

For the unperturbed γ_{CH} mode the corresponding frequency ν_o is determined by

$$4\pi^2 \nu_o^2 = \frac{h(m_H + m_C)}{m_H m_C} \qquad 3.8$$

where h is the force constant of the particular motion of the H atom; while m_H and m_C are the atomic masses. Similarly the electrostatic interaction with the polar solvent gives a new force constant $(\Delta h + h)$, so that the new frequency ν is given by

$$4\pi^2 \nu^2 = (\Delta h + h) \frac{m_C + m_H}{m_C m_H} \qquad 3.9$$

Thence the relative frequency shift is found from

$$\frac{\Delta \nu}{\nu_o} = \frac{\Delta h}{2h} \qquad 3.10$$

Lalau observed good agreement between observed and calculated shifts for acetone + benzene and acetonitrile + benzene systems. However for HFB + benzene this model does not work. Using the accepted values for the CH and CF bond dipoles, of .3D and .6D [51,60], and r is about 2.3Å, then the extra dipolar resotoring force is 0.10 Nm^{-1}, whereas the actual force constant for the movement of a fluorine out of the plane of the ring is 20 Nm^{-1}. Thus this

electrostatic model implies a .25% shift, i.e. 0.5 cm^{-1}, which is far too small. In this configuration, where the interacting bonds are collinear, it might also be supposed that the in plane β_H vibrations would be affected equally. However as we have already noted in section 3.2.2 no shifts or band broadenings have been observed for the in plane modes.

A more favourable configuration would be one in which the dipoles are opposed thus

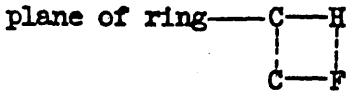

However modification of the restoring forces due to the electrostatic interaction is much reduced. In this configuration, during the γ_H vibration one pair of interacting poles will approach while the other recedes.

Thus these electrostatic interactions do not provide an adequate explanation of the observed phenomena. It would seem from the observable data that the frequency shifts arise from $\pi-\pi$ interactions which modify the restoring forces. From figures 4 and 5 we can now suggest that after the HFB molecules have reached their maximum relaxation rate at 35% benzene concentration, the continued increase in the number of benzene molecules in the environment will lead to further increases in the restoring force.

While it is easy to visualise the manner in which interactions (charge transfer for example, see section 2.6) can lead to an increase in the γ restoring force, the mechanism of vibrational relaxation is less obvious. We noted in section 3.3.3 that it has been suggested that for the a_{2u} mode of both HFB and benzene, there is an electronic

rehybridisation moment, resulting from movement of the F or H atoms out of the plane of the ring[51 54 60]. It follows that the $\pi - \pi$ interactions are necessarily modified to some extent by the γ type motions. In this respect it is notable that the vibrational quantum ($hc\nu$) has a value close to that of kT ($\sim 410 \times 10^{-14}$ ergs); where T is the room temperature. It could well be that in a dissociation process the vibrational quantum has a significant probability of being degraded to thermal energy. Obviously as kT and $hc\nu$ are of the same magnitude, this process could be considered as likely.

As we have already shown from the data in figure 4, if the dissociation of a molecular pair involving a vibrationally excited HFB molecule led to vibrational relaxation, then we deduced the equilibrium constant for the complex formation to be 0.88 dm^3mol^{-1}. The way in which the system relaxes is also related to the rate constants for the processes involved in the equilibrium. If we take the reciprocal lifetime of the complex as the asymptotic value of βv, then it can be seen that the dissociation rate constant is around $0.7 \times 10^{12} s^{-1}$. This implies that the bimolecular association rate is about 0.5×10^{12} $dm^3mol^{-1}s^{-1}$. This value is about 50 times larger than predicted for a dissocation controlled reaction, using the Smouluchowski-Debye treatment[61] where

$$K_{DC} = f \frac{8RT}{3000\eta} \quad dm^3mol^{-1}s^{-1}$$

where f, the efficiency factor, is unity. η is the viscosity. (Generally f is greater than unity for unlike charges and less unity for like charges).

Thus we conclude that cage effects could explain the enhancement of the bimolecular association rate. In view of the extremely short lifetime of the HFB complex a very high rate of interaction may occur within a benzene cage.

Chapter 4 RAMAN STUDIES OF THE CHLORINE-BENZENE SYSTEM

4.1 Introduction

Despite the large number of studies[33,34,62] made during the past 25 years on the halogen-benzene systems, there is still a great deal of controversy on the nature of the interaction.

The first careful ultraviolet study of the complex of chlorine with benzene was made by Andrews and Keefer[63]. The complex formed an additional band at 278 nm which was absent for the spectra of either component. Using the Benesi-Hildebrand method[31] they gave the equilibrium constant (^1K) as 0.033 dm^3mol^{-1} with a maximum absorb tivity $\epsilon_{max.}$ for the complex at 280 nm of 909.0 dm^2mol^{-1}. For the iodine complex the values were .17 dm^3mol^{-1}, and $\epsilon_{max.}$ 1500.0 dm^2mol^{-1}. Therefore the complex of chlorine with benzene is weaker than that for iodine with benzene. This is in agreement with the expected Lewis acid strengths of chlorine and iodine. Mulliken[32] attempted to explain these results in terms of the charge transfer theory - see Chapter 2.6.

Infra-red spectral studies allowed a more direct investigation of the ground electronic state structure. The observations have generally been classified into three groups; (a) modifications to the donor (benzene) spectrum; (b) modifications to the acceptor (halogen) spectrum, and (c) the appearance of new bands.

The first infra-red study of the chlorine-benzene system was made by Collin and D'Or[64,65]. A new weak and relatively broad absorption band was observed near 526 cm^{-1} for solutions of chlorine dissolved in benzene. The Raman shift of chlorine ($^{35}Cl_2$) in carbon tetrachloride was known to be[66] at 548 cm^{-1}. More quantitative studies of the infra-red spectrum were carried out by Person[67,68]; who found that for chlorine in a 3.6M solution of benzene, the integrated intensity is 153×10^3 $cm^{-1}mol^{-1}$.

An attempt was made by Friedrich and Person[69] to interpret the changes in vibrational frequency of the halogen-halogen stretching vibration, when the halogen molecule (an $\underline{a}\sigma$ acceptor) complexes with benzene (a $\underline{b}\pi$ donor), in terms of charge transfer theory (see Chapter 2.6). They postulated that a relationship existed between the vibrational frequency shift ($\Delta\nu$) and $\underline{b}$ the coefficient of the dative wavefunction; such that

$$F_{1N} = (\underline{b}^2 + \underline{ab}\ S_{o1}) \simeq \frac{\Delta K}{K_o} = 2\Delta\nu/\nu_o \qquad 4.1$$

where F_{1N} is the weight of the dative structure in Ψ_N (the ground state structure), S_{o1} is the overlap integral of two resonance structure functions, K is the force constant and ν_o is the vibrational wave number of the isolated molecule, while ΔK is a change (K_o-K) in the complex. Agreement was found to be qualitatively good for the calculated and observed values of the intensity.

Hanna et al[38] argued that the observed effects and the small equilibrium constants are of the order expected simply from collisional perturbations and electrostatic association. Hanna's[37] electrostatic theory (see Chapter 2.6) has been used to determine the values of the intensity. While agreement was relatively good between the calculated and observed values the parameters used were apparently not easy to determine. Some support for Hanna's view may be derived from the PVT studies of the gaseous benzene-iodine system by Atack and Rice[70]. These authors detected only a small pressure decrease which could be attributed to molecular association, and from the very small enthalpy and entropy of the reaction derived from this, they concluded that for the gaseous system the association was only through the weak Van der Waal's forces.

However in the original formulation of the electrostatic 'collision induced' infra-red absorption[71], the absorption was predicted to be due to (a) an atomic distortion effect, and (b) a quadrupole distortion effect. It has been concluded[72] that, for the benzene-halogen 'complex', Hanna had only considered the latter effect, which results from the interaction between one polarizable molecule and the electric field generated by the quadrupole moment of the other molecule. In line with the correct collision induced infra-red absorption theory[71], the estimated induced infra-red absorption intensity for chlorine in benzene should be obtained as an appropriate statistical average overall intermolecular orientations.

With the advent of the modern laser Raman spectrometer, studies of the Raman spectra were expected to supplement and extend the earlier infra-red studies. The Raman spectra of halogens are complicated by the absorption of the exciting light. Despite this Klaeboe[73] made a Raman spectroscopic study of iodine in benzene solution. He observed only one Raman band in the iodine solution, and did not see a Raman shift for the uncomplexed iodine. It had been expected that two Raman bands might be observed in such a study, one corresponding to the uncomplexed halogen and the other to the complexed species.

More recently Rosen, Shen and Stenman[74 75] made a more systematic study of the Raman spectra of iodine with benzene in n-hexane solution. They observed a uniform shift of the wavenumber of the band maximum of the iodine, as the solvent varied from pure benzene to n-hexane with no appreciable change in half band width. They concluded that the reason for not resolving two Raman peaks, one for the complexed iodine and one for the uncomplexed iodine, was the weakness of the charge transfer interaction between iodine and benzene, so that iodine could interact with more than one donor.

As can be seen from these initial studies there was a considerable conflict in the interpretation of the interactions involved. T.C. Jao[72] reinvestigated the chlorine-benzene system with a view to understanding better the interpretations of the spectroscopic phenomena. He repeated the study of the ultraviolet spectrum, at different chlorine concentrations and obtained an equilibrium constant of 0.025 ± 0.015 dm^3mol^{-1} based on the equation

$$C_6H_6 + Cl_2 \leftrightharpoons C_6H_6Cl_2$$

Jao remeasured the infra-red intensity of the complex of chlorine with benzene; and also studied the infra-red absorption spectrum of chlorine in tetrachloromethane (which is not expected to form a charge transfer complex with chlorine), in order to compare it with the spectrum of chlorine in benzene. It was concluded that, for infra-red absorption, a vibronic charge transfer effect could be the main factor in the large intensification. For these absorption spectra an equilibrium constant of .03 dm^3mol^{-1} was calculated; this value was seen to be in good agreement with the value previously quoted for the electronic spectrum.

In spite of this earlier work, it was decided that a careful study of the Raman spectrum of chlorine in benzene and tetrachloromethane mixtures, for several reasons. As Jao[72] noted, chlorine is more transparent to visible light than bromine or iodine. Therefore there should be fewer complications due to photochemical reactions caused by exciting light, or in general from absorption of the exciting line (or of the scattered Raman radiation) in the chlorine solutions. Also chlorine is expected to be a slightly weaker electron acceptor than either bromine or iodine, so it was expected that the

detection of two Raman bands in these solutions would suggest that they had also been present in the solutions of the stronger acceptors (bromine and iodine) in benzene.

4.2 Experimental Equipment and Chemicals

Chlorine gas (99.5%), bromine liquid and iodine solid from B.D.H. Chemicals Ltd., were used for this investigation. The solvents, benzene and tetrachloromethane were spectroscopic grade from B.D.H. Chemicals Ltd., and were used without further purification.

For this study a Coderg Raman spectrophotometer (type PHO) with double monochromator was used with the D.C. detection mode. A tunable Kr-Ar mixture laser (Coherent Radiation Ltd., U.S.A.) was the exciting line source. The line at 647.1 nm was used for most of the studies. A typical laser output power was around 100 mw. Some measurements, on the bromine-benzene and iodine-benzene systems, were made with the 676.4 nm line, however there was a reduction of the laser output power to about 50 mw. The lines at shorter wavelength were not suitable for this work because of a photochemical reaction. For most of the measurements a resolution of 0.6 cm^{-1} to 1.5 cm^{-1} was achieved.

All spectra were corrected for the distortion due to finite slit widths using the relationship previously stated in equation 2.2 .

For depolarization studies it is also necessary to correct for the different transmission efficiencies of the spectrometer for light polarized with its electric vector parallel to the grating rulings and for light with perpendicular polarization. The Jobin-Yvon gratings in our system are particularly bad for this effect in that the transmission efficiency for parallel radiation is only about 20% at the best, relative to that for perpendicularly polarized radiation. The $\lambda/4$

plate after the analyser cannot cope efficiently with such a severe spectral distortion. Hence we corrected all polarization data by calibration using the known depolarization of the tetrachloromethane ϵ band at 218 cm^{-1}.

The laser and recorder were allowed to warm up for an hour before use in order to stabilize the system. The spectrometer was kept on all the time. Whilst the laser power output was stabilizing the chlorine solutions were prepared (this will be discussed in the next section).

The sample cell was made from a grease free stopcock (Glass Precision Engineering, England) by sealing off one end and connecting it to an appropriate joint, adaptable to the vacuum line on the other (open) end. The volume of the cell was about .01 dm^3.

In order to measure the Raman spectrum of chlorine in tetrachloromethane/benzene mixtures at lower temperatures, a thermostatic cooling system Churchill Instrument Co., variable heat model (+ 30°C to -30°C), was employed with ethylene glycol (70% v/v in water) as chiller.

A sample cell, for the variable temperature studies, was constructed by modifying the one described above (see figure 7a), so that the chilled glycol could be circulated around the cell, leaving the irradiated section of the sample tube clear of the coolant. The cell and cooling jacket were enclosed in a vacuum. The actual temperature near the light path was monitored constantly using a Cr/Al thermocouple. The whole system was well lagged with cotton wool, and the fluctuation of the sample temperature was minimized to ± 1°C.

For our work on pure chlorine liquid, the chlorine was distilled into an evacuated sample tube at liquid nitrogen temperature. The

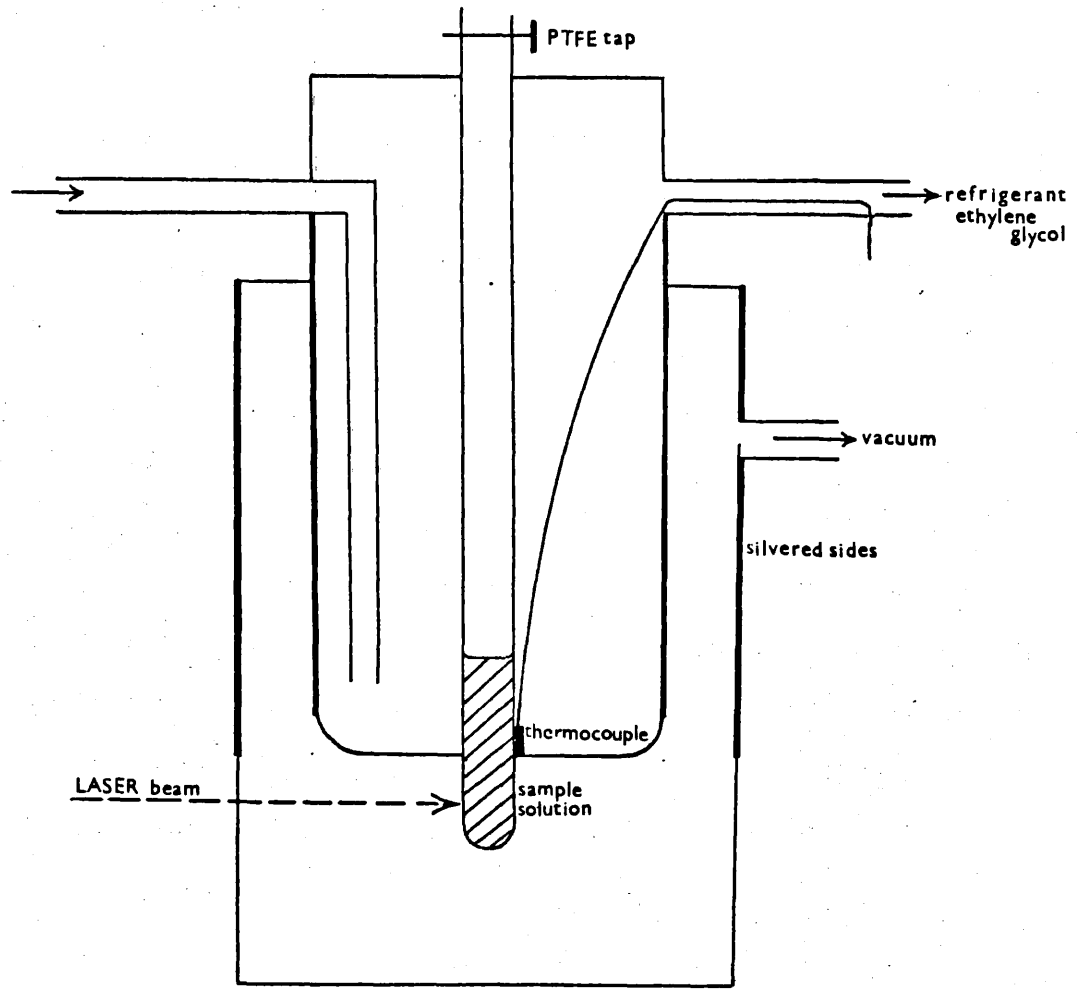

Figure 7a. Variable Temperature Cell used for the chlorine in benzene/tetrachloromethane solutions.

tube was then sealed off. This sealed sample cell had an internal diameter of .6 cm and was approximately 5 cm long; the cell was half filled with the chlorine. This sample was used for all measurements; the sample cell was stored in a cardice-acetone mixture, when not in use.

It was required to measure the spectra of chlorine at a range of its liquid temperatures, $-103.5^{\circ}C$ to $-34.5^{\circ}C$. The Coderg variable temperature apparatus was used in conjunction with a RIIC-Beckman Tem 1 temperature controller. Cold nitrogen gas, drawn from liquid nitrogen was used as the coolant.

4.3 Experimental Procedure

4.3.1 The Chlorine-Benzene-Tetrachloromethane solutions

The instability of the chlorine in benzene solution makes it desirable to work at low chlorine concentrations of about .4M and to scan the spectrum quite rapidly. The spectral scan rate, for all solutions was 2.5 cm^{-1} per minute or 70 minutes to measure a complete Raman spectrum from 470 cm^{-1} to 640 cm^{-1}.

Before studying the Raman spectrum of chlorine solutions we investigated the solvent background, in the region where the Raman band of chlorine would appear. The Raman shift for chlorine appears between the two bands, ν_1 of tetrachloromethane at 461 cm^{-1}, on the low frequency side, and ν_{18} of benzene at 606 cm^{-1} on the high frequency side. These solvent bands overlap to a small extent. This overlap results in the loss of some of the spectral information from the wings of the chlorine band. For all the spectra we had to approximate the extent of the wings by continued extrapolation to the baseline.

The chlorine solutions were prepared by first distilling .003 dm^3 of the solvent into a 1.0 cm diameter glass sample tube at liquid nitrogen temperature. After evacuating the line and cell of all air, a PTFE stopcock on top of the sample cell was closed. Chlorine was introduced into the vacuum line to a pressure of about 5×10^2 Pa, and the stopcock was opened so that chlorine could condense on the top of the solvent. When the closed cell warmed up the chlorine dissolved completely in the solvent, to form the solution to be studied. Because of the well known photochemical reaction between chlorine and benzene, occurring in daylight or under fluorescent lights it was necessary to keep the room as dark as possible throughout all stages of the experiment.

As the chlorine solution was in a sealed tube under vacuum it was not possible to determine the concentration of chlorine, before obtaining the Raman spectrum. Tests on the consistency of the chlorine concentration were made on solutions that would not be used for running spectra. To obtain the initial concentration, a saturated potassium iodide solution was introduced into the sample cell. The iodine released by the reaction with chlorine was titrated with standard aqueous thiosulphate. By improving the experimental expertise it was possible to assure that there was an initial chlorine concentration of about .4M. The concentrations of the chlorine solutions, after the spectra had been recorded, were determined by the same procedure, to make sure that the Raman spectrum observed for the chlorine solution was really due to the chlorine molecule, and not to any compound formed between chlorine and the solvent. After titration with the thiosulphate solution the organic layer was removed by ether extraction. Following this treatment the spectrum of the organic solution was taken,

in order to see if any absorption by the photochemical products was present. Within experimental error there is no observable Raman band due to photochemical products in the spectral region of the complexed chlorine, and therefore any small amounts of the product formed should not interfere with the band shape studies.

Jao[72] found that when a benzene solution of chlorine, which has been exposed to light, is evaporated, a white residue is left. The residue was dissolved in tetrachloromethane and the n.m.r. spectrum observed; the residue was found to be mainly hexachlorocyclohexane ($C_6H_6Cl_6$).

4.3.2 Bromine and Iodine in benzene solutions

We attempted to extend the studies on chlorine solutions, to iodine and bromine solutions. As for chlorine the acceptor molecules iodine and bromine have broad electronic absorption bands in the region 4000 - 5000nm when dissolved in inert solvents. Therefore only the longer wavelength Raman excitation is feasible.

Bromine has a relatively high solubility in most solvents. Absorption of the 647.1nm line is less prominent than others to lower wavelength. Thus it would appear that the bromine complexes would be easy to study and that fairly high halogen concentrations could be employed. However Klaeboe[73] found that bromine was so reactive that oxidation and substitution reactions occurred very easily in the mixed solutions. These reactions were accompanied by precipitations and in less obvious circumstances by new Raman bands assigned to various new species. These were formed by irreversible reactions and not by complex formation.

The tendency for reactions can be diminished by (a) reducing the concentration of bromine to below 0.6M, (b) keeping daylight away from the samples during preparation, and (c) using the 676.4nm line, which gives the samples considerably longer lifetimes than the 647.1nm line.

An inert solvent such as n-hexane or tetrachloromethane would have been useful to dissolve the complexes. However they have strong Raman bands in the low frequency region, and were therefore not suitable for our band contour studies of bromine and iodine in benzene.

Holzer, Murphy and Bernstein[76] studied the resonance Raman spectra of the halogen gases. They listed frequencies, depolarization ratios and relative scattering cross sections for the fundamentals of bromine and iodine. These values were used to obtain initial parameters for the band fitting procedures.

The resolution used was 1.0 cm^{-1}, and the actual halogen concentrations used were .5M for bromine and .06M for iodine. Despite the low bromine concentration used the radiation from the laser catalysed the photochemical reaction to such an extent that the maximum time to scan a spectral range of 100 cm^{-1} was typically ten minutes. As these spectra were run so rapidly it was not possible to obtain a true representation of the band shape.

For the iodine in benzene spectrum, the loss in scattered intensity arising from the increased energy of absorption did not allow a good quality spectrum to be obtained.

4.4 Results

4.4.1 General Details

In Figure 7b are shown sample Raman spectra of the chlorine band near 530 cm^{-1} for four solutions of chlorine in (a) pure

Figure 7b. Raman spectra of the Cl-Cl stretch band in CCl_4:benzene mixtures. All measurements were for the parallel component ($I_{y(xx)z}$), and at room temperature.

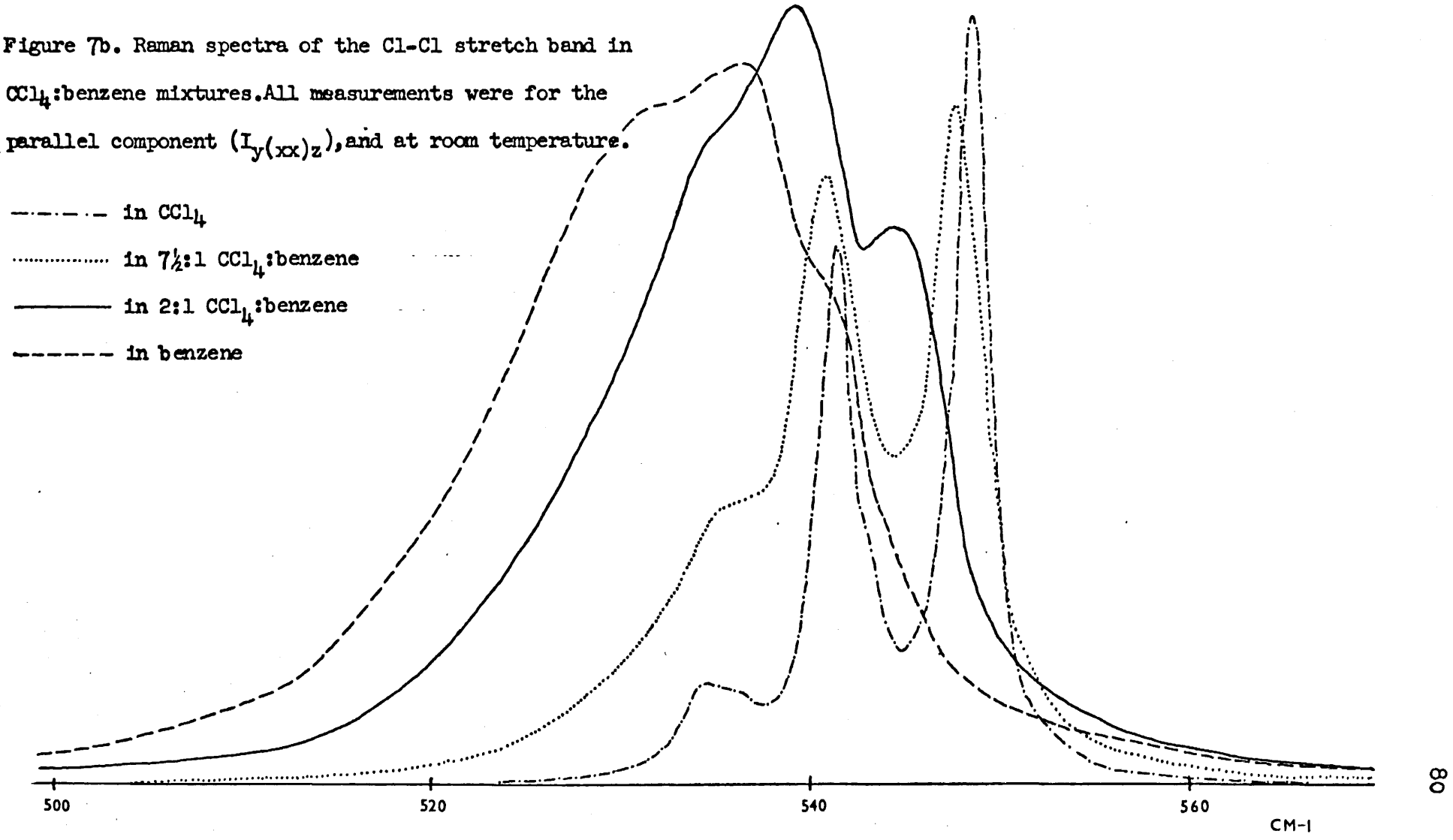

tetrachloromethane, (b) a 1:7½ C_6H_6:CCl_4 mixture, (c) a 1:2 C_6H_6:CCl_4 mixture, and (d) pure benzene. All concentration ratios quoted are by weight. 1:1, 1:3 and 1:6 C_6H_6:CCl_4 mixtures were also studied. The concentrations of the benzene and tetrachloromethane were accurately determined. The bands of CCl_4 at 762/791 cm^{-1} and benzene at 606 cm^{-1} were used as internal references in the experiment. The Raman spectra of these bands were run immediately after a chlorine solution spectrum, so that fluctuations in the laser power and room temperature were taken into account. If the solvent band areas are accurately determined with respect to each other, then by comparing the relative band shapes from different runs the above fluctuations can be eliminated. Thus we can obtain a measure of true chlorine band intensity relative to the CCl_4 762/791 cm^{-1} fermi resonance pair.

The spectra measured were the components $I_{y(xx)z}$, $I_{y(xy)z}$ and $I_{y(xx+xy)z}$ (see section 2.2). The analysis of these spectra requires a quantitative separation of the areas of the bands due to the separate species. As the band widths of these components are governed by different relaxation processes, the measured $I_{y(xx)z}$ and $I_{y(xy)z}$ Raman spectra are transformed into the isotropic $(\bar{\alpha}')^2$ and anisotropic $(\gamma')^2$ components (see figure 8b). All discussions refer to these transformed spectra.

4.4.2 The Chlorine in Tetrachloromethane spectra

The chlorine in CCl_4 solution is considered first, as the spectrum obtained has the simplest composition. The structure of the chlorine band in CCl_4 solution is due to the presence of the three isotopically related molecules $^{35}Cl_2$, $^{35}Cl^{37}Cl$, and $^{37}Cl_2$ in the concentration ratio 1.00:0.67:0.11 plus a set of corresponding hot bands shifted by 5.5 cm^{-1} to lower frequencies. This structure has been noted

Figure 8a. The Raman spectrum of the Cl-Cl stretch of chlorine in CCl_4, for parallel polarisation ($I_{y(xx)z}$).

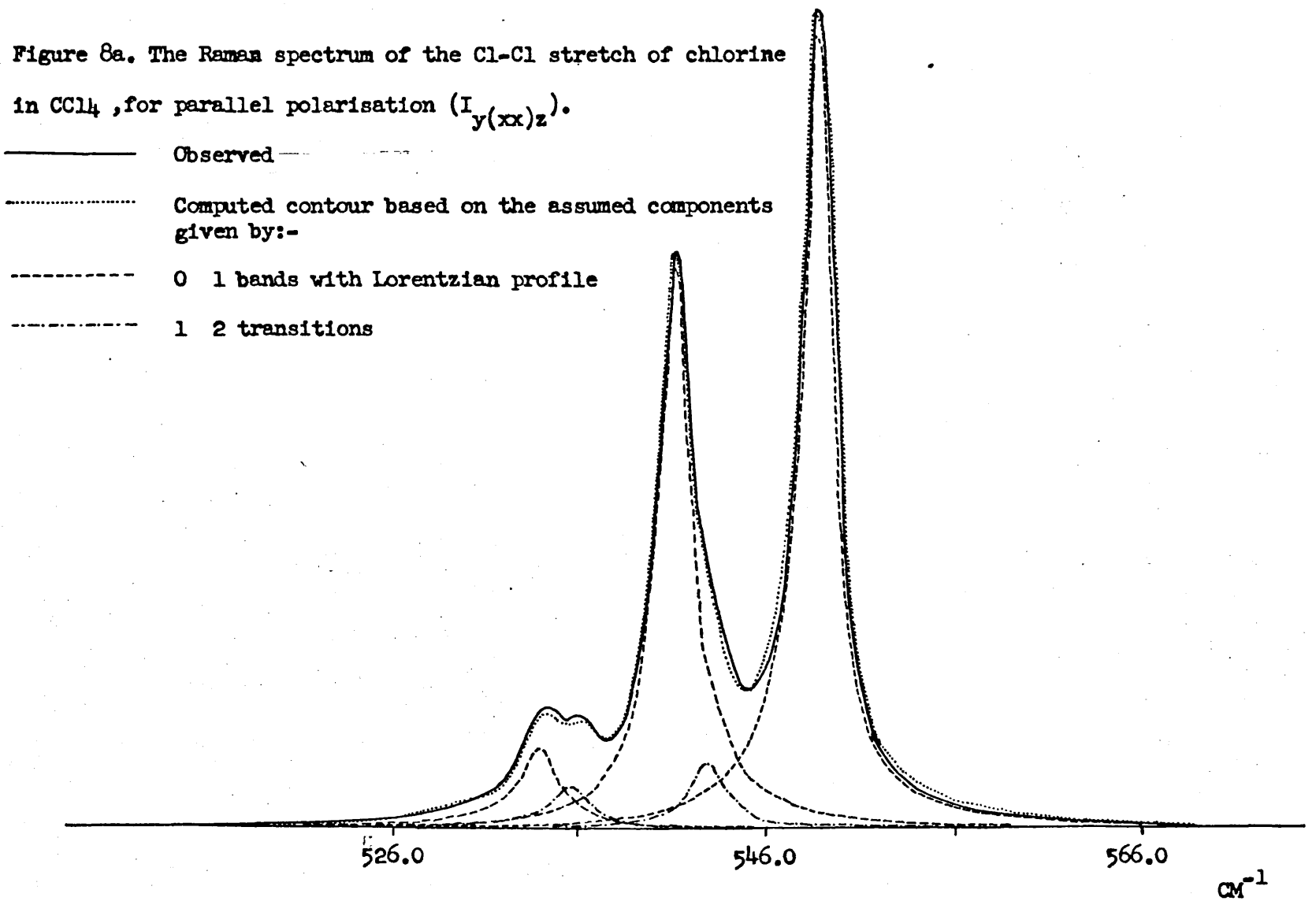

Figure 8b. The Raman spectrum of the Cl-Cl stretch of chlorine in CCl_4. The relative profiles of the $(\bar{\alpha}')^2$ and $(\gamma')^2$ components.

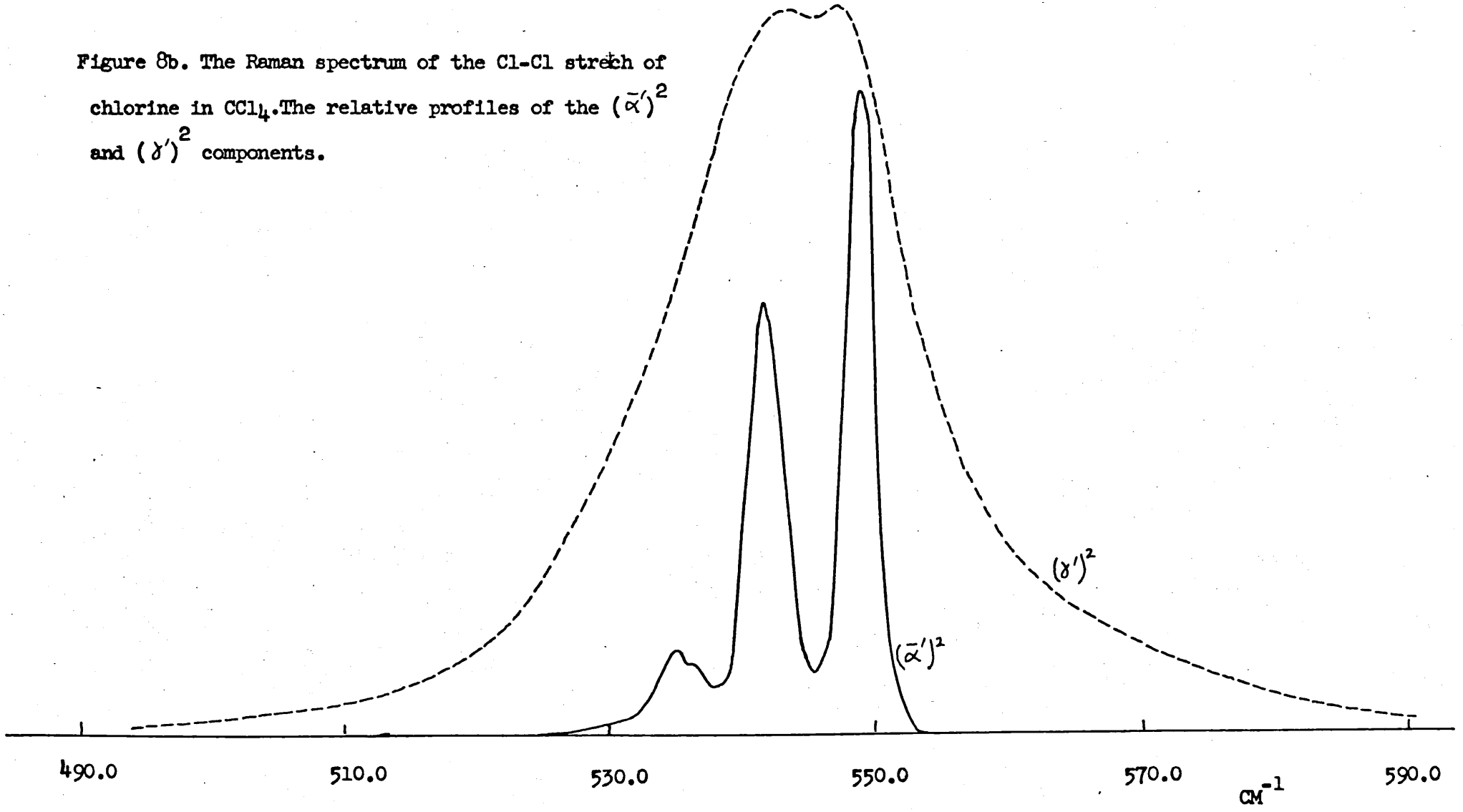

for liquid chlorine by earlier investigators[77,78]. In figure 8a we see a comparison between the observed spectrum and a computer simulated spectrum calculated on the assumptions that,

1) The components are Lorentzian in shape; the equation is given by

$$\text{intensity} = K_{INT} \frac{\Delta\nu_{\frac{1}{2}}}{(\nu - \nu_o)^2 + (\frac{\Delta\nu_{\frac{1}{2}}}{2})^2} \qquad 4.2$$

where K_{INT} is a constant for each isotope, ν_o is the frequency ν of the band centre of each isotope or hot band; $\Delta\nu_{\frac{1}{2}}$ is the half height band width.

2) The intensity ratios are based on the known isotope abundances and on a Boltzmann distribution between the $v = 0$ and $v = 1$ states.

The anharmonicity assumed is that of gaseous chlorine[79,80]. The parameters are given in Table 1. It can be seen that the isotopic and hot band maxima of chlorine are the same, within experimental error, as those from liquid chlorine obtained by Stammreich and Forneris[78]. As we expected this suggests there is little or no complexing of chlorine in tetrachloromethane. For benzene/tetrachloromethane mixtures the isotopic components show structure due to the uncomplexed chlorine, superimposed on some less structured absorption centred at lower frequencies. Even a visual comparison with the anisotropic component shows that there is a considerable frequency shift between the maxima of $(\bar{\alpha}')^2$ and $(\gamma')^2$ for the complexed chlorine. These components are shown in figures 9-14 for all the solutions excluding chlorine in tetrachloromethane.

4.4.3 Band Contour Analysis of the chlorine spectra in C_6H_6/CCl_4 solutions

Initially we attempt, by a trial and error method, to remove the contribution of the free (or CCl_4 solvated) chlorine bands from the

total band contour. In order to do this the following constraints were used.

(i) The relative intensities of the three isotopically related systems were constrained to their theoretical values.

(ii) The contribution of the anisotropy of the free Cl_2 was neglected since it was assumed that its contribution to the intensity was very small.

(iii) The frequency of the band centres of the $^{35}Cl_2$, $^{35}Cl^{37}Cl$, $^{37}Cl_2$ components were varied independently to some extent, but the results re mained in accord with expectations based on the Redlich-Teller[81] sum rule and the known anharmonicity of the chlorine vibration.

(iv) The half height band widths of the three components were taken as equal, but allowed to vary from the chlorine in CCl_4 values.

As can be seen from Table 2A the band widths and band centres of the free chlorine show a steady change with benzene concentration.

When the contri bution of the unassociated chlorine is removed from the total contour there is a difference of about 4 cm^{-1} in the $(\bar{\alpha}')^2$ and $(\gamma')^2$ maxima. From Table 2D it it seen that the contribution of the unassociated chlorine is very small in the benzene solution. Figures 14a and 14b show that the $(\bar{\alpha}')^2$ maximum is near 537 cm^{-1} whereas that of the $(\gamma')^2$ is at 530 cm^{-1}. These large differences in the band centres suggested that two bands with different depolarization ratios were present. The structure of the isotropic bands also indicated that the isot opic structure existed. It was found that for all solutions we could reproduce the $(\bar{\alpha}')^2$ and $(\gamma')^2$ band contours to within experimental uncertainty by superimposing two sets of three isotopic and three hot bands.

Table 1 Lorentzian Function Parameters for the Isotopic and Hot bands of Chlorine in Tetrachloromethane

Transition	Intensity ratio calc.[a]	Intensity ratio this work[b]	Half-band width (cm^{-1})[c]	Band Maxima this work[c]	Band Maxima calc.[d]	Ref. 78
$0 \rightarrow 1$ $^{35}Cl_2$	100	100	2.5	549.0	549.0	548.4
$0 \rightarrow 1$ $^{35}Cl^{37}Cl$	67	67	2.5	541.5	541.5	540.9
$0 \rightarrow 1$ $^{37}Cl_2$	11	11	2.5	534.0	534.0	533.4
$1 \rightarrow 2$ $^{35}Cl_2$	7	9	2.5	543.4	543.7[e]	543.1
$1 \rightarrow 2$ $^{35}Cl^{37}Cl$	5	6	2.5	535.9	536.0	535.7
$1 \rightarrow 2$ $^{37}Cl_2$	0.7	1	2.5	528.4	528.5	528.2

Notes on Table 1

a) Relative populations calculated with respect to the isotopic molecule $^{35}Cl_2$ from the isotopic abundance ratios; for the hot bands, the population of the v = 1 level of $^{35}Cl_2$ relative to the v = 0 level is $e^{-hc(549)/k(298)}$.

b) Relative intensities used in the computer simulated spectrum to fit the observed spectrum shown in fig. 8a.

c) Values obtained from forcing the computer simulated spectrum to fit the observed spectrum in fig. 8a.

d) Frequencies calculated from ν_o for $^{35}Cl_2$, using the isotope product rule: $\nu_i = \sqrt{\mu_i/\mu_o}\ \nu_o$, where μ_i is the reduced mass of the isotopic molecule and μ_o is the reduced mass of $^{35}Cl_2$.

e) $\nu_{1 \rightarrow 2} = \nu_{0 \rightarrow 1} - 2\chi_e\omega_e$; with $\chi_e\omega_e = 2.65\ cm^{-1}$ for $^{35}Cl_2$ and $2.75\ cm^{-1}$ for $^{35}Cl^{37}Cl$ from the gas phase (Ref. 80).

Fig.9 The Raman spectra of the Cl-Cl stretch of chlorine in a 1:7½ benzene:tetrachloromethane mixture, and a comparison of overall contour with predicted, assuming Lorentzian profiles.

(a) isotropic component $(\bar{\alpha}')^2$

(b) anisotropic component $(\gamma')^2$

..... observed profile

_____ total calculated profile

-..-..-.. unassociated Cl_2 component

- - - - - high frequency associated components

-.-.-.-.- low frequency associated components

Fig.10 As for figure 9 but for a 1:6 benzene:tetrachloromethane mixture

Fig.11 As for figure 9 but for a 1:3 benzene:tetrachloromethane mixture.

Fig.12 As for figure 9 but for a 1:2 benzene:tetrachloromethane mixture.

Fig.13 As for figure 9 but for a 1:1 benzene:tetrachloromethane mixture.

Fig.14 As for figure 9 but for benzene as solvent.

Figure 9a

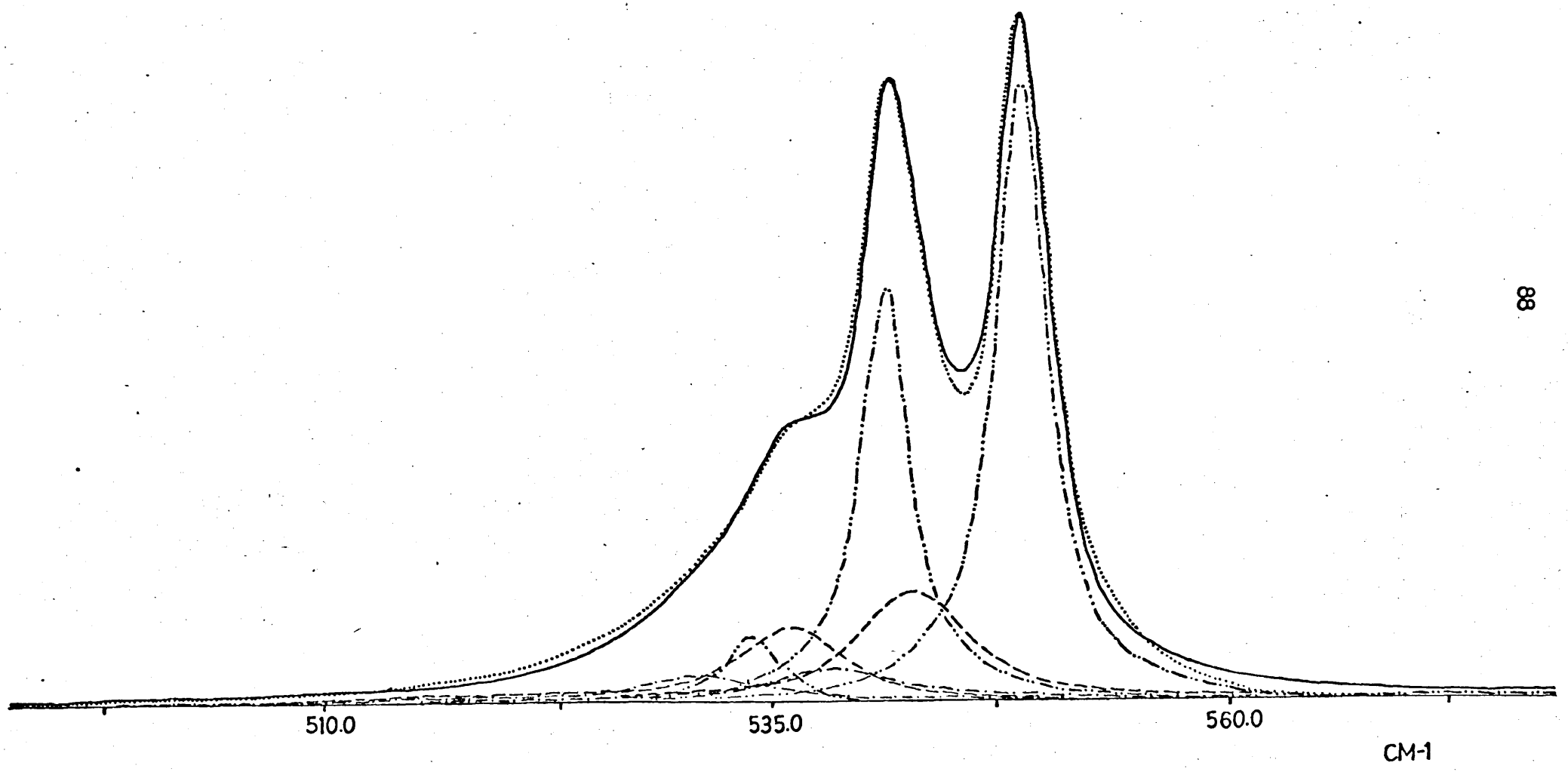

Figure 9b

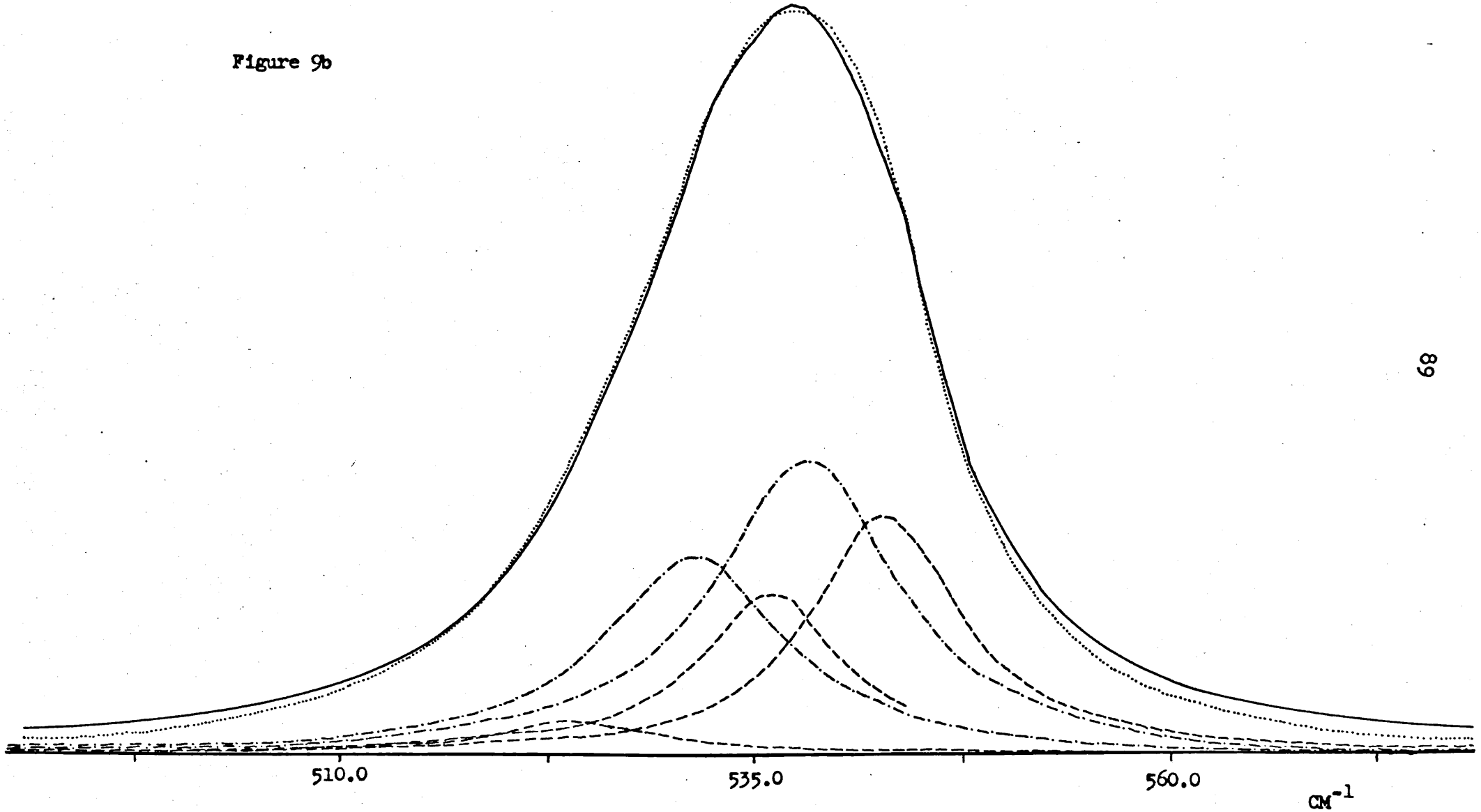

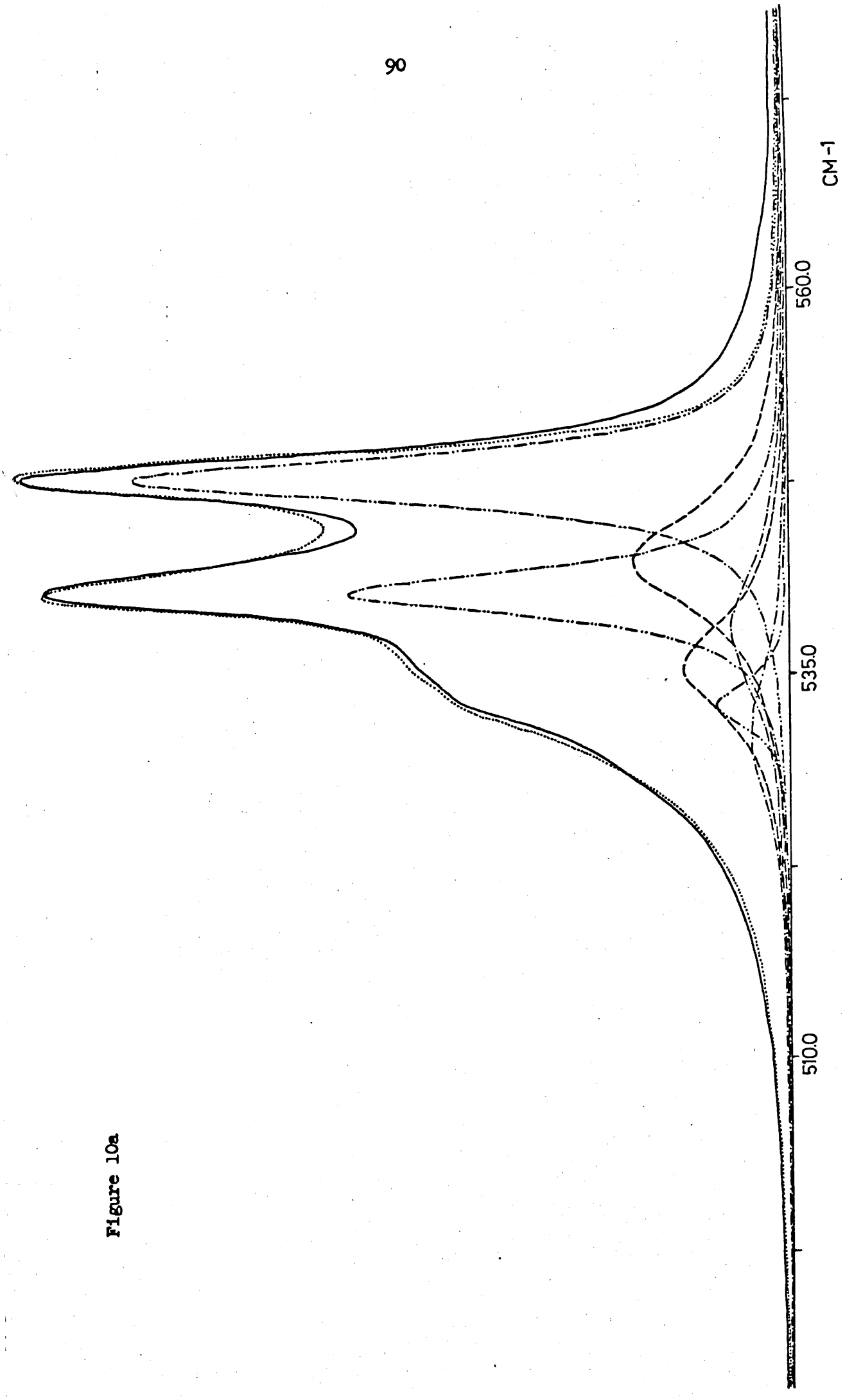

Figure 10a

Figure 10b

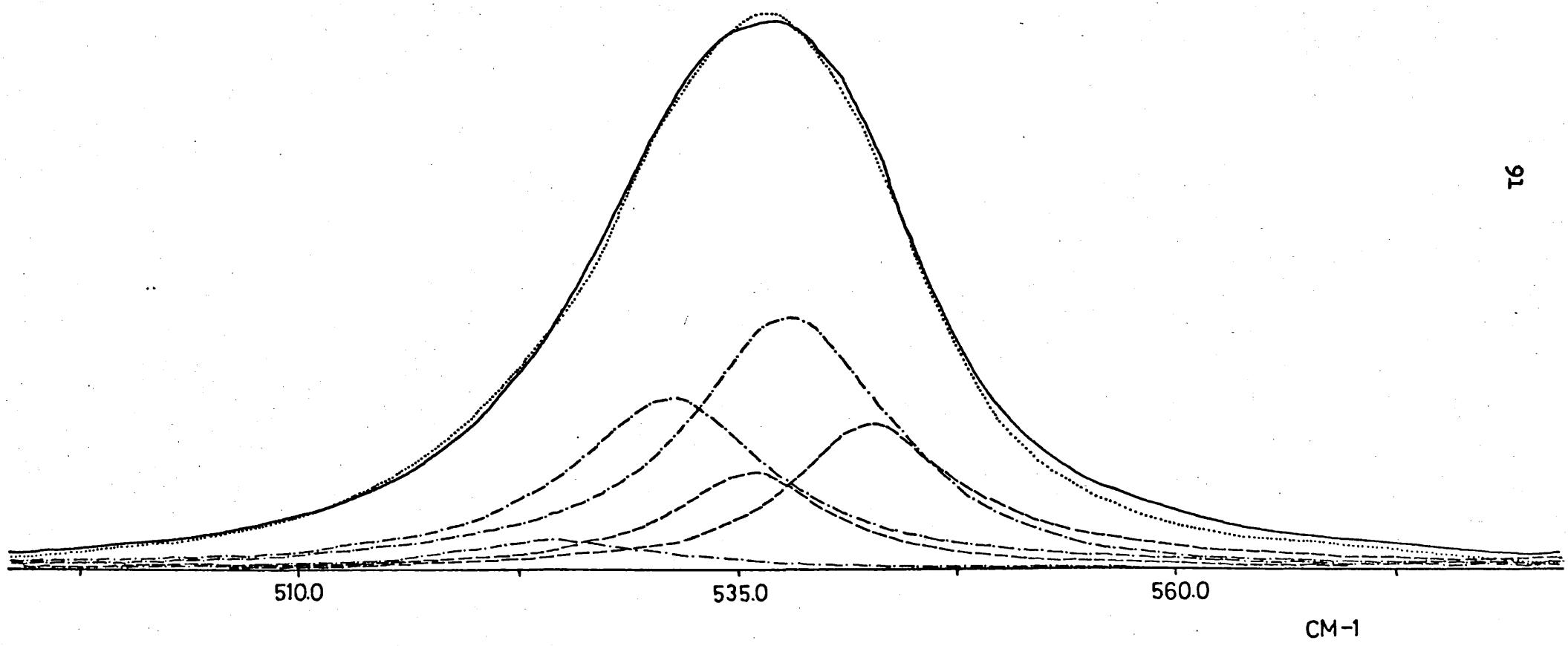

Figure 11a

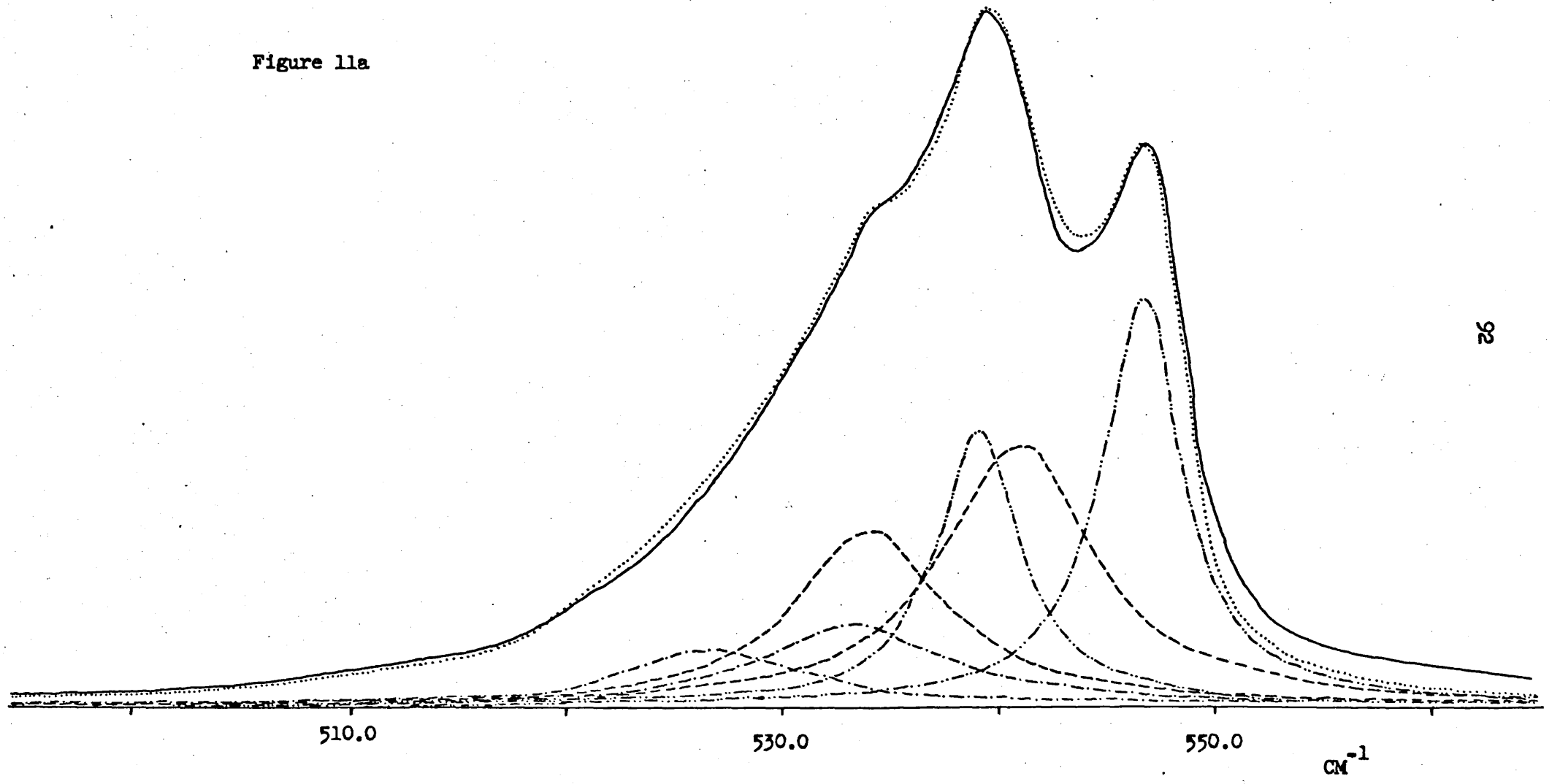

Figure 11b

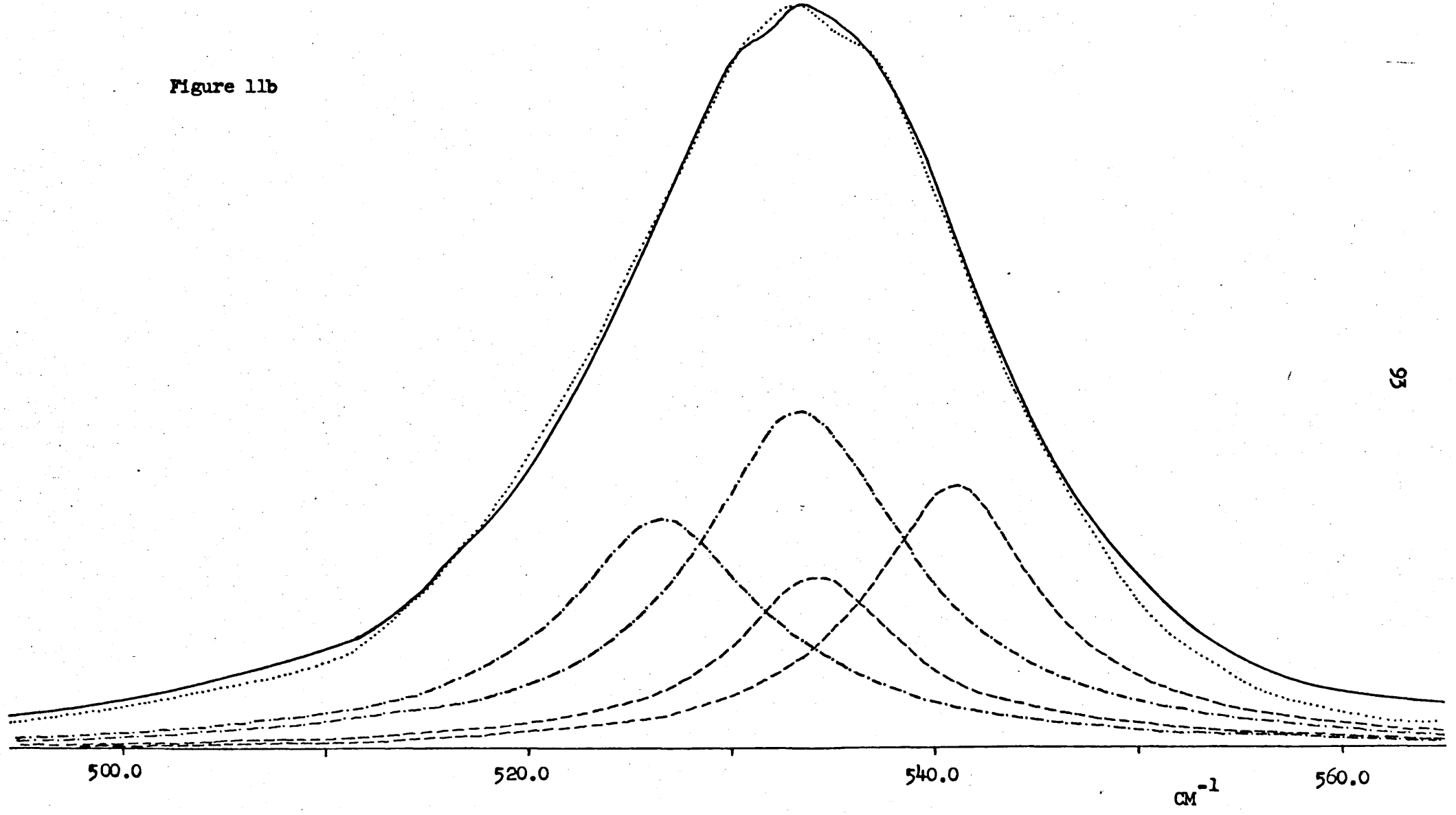

Figure 12a

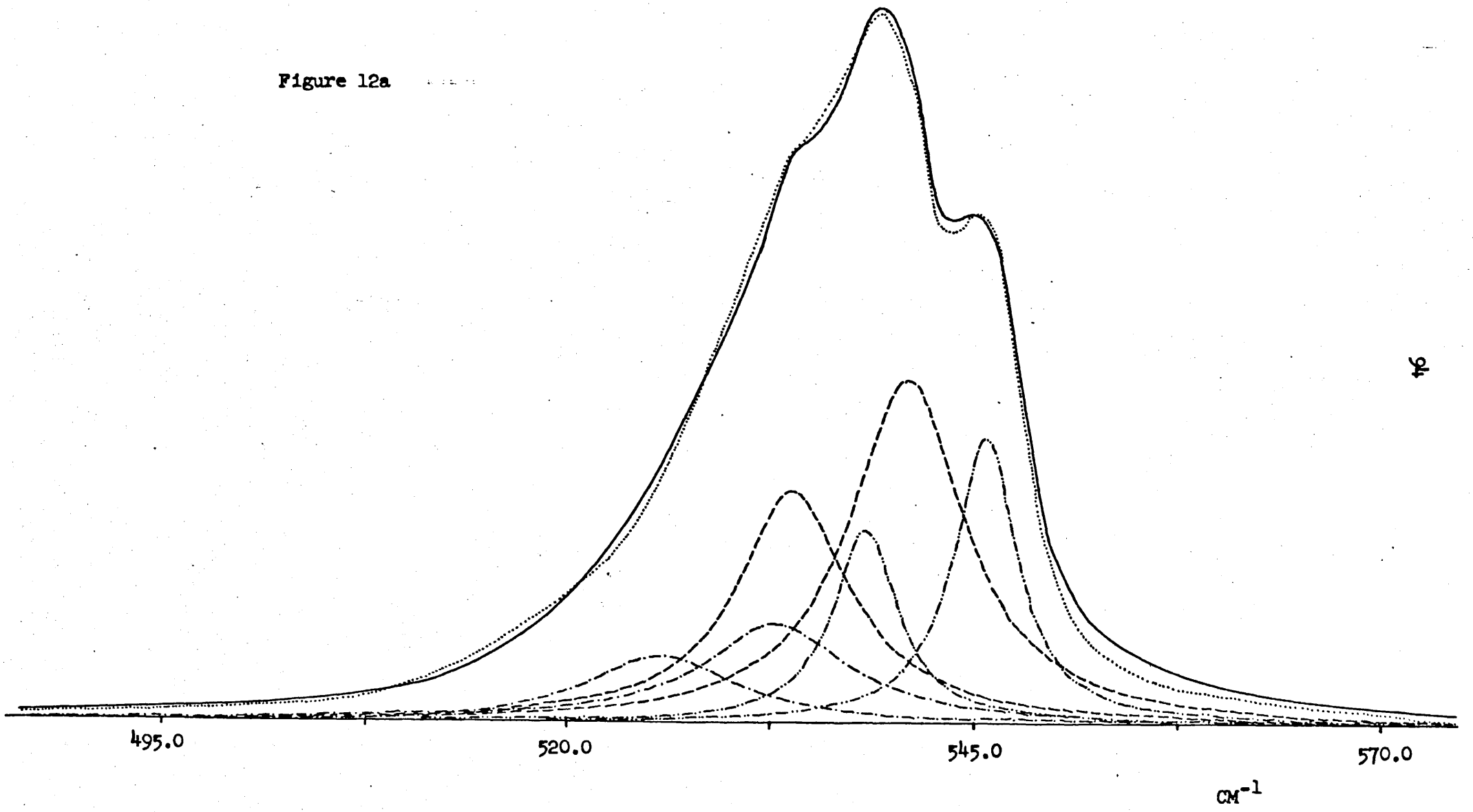

Figure 12b

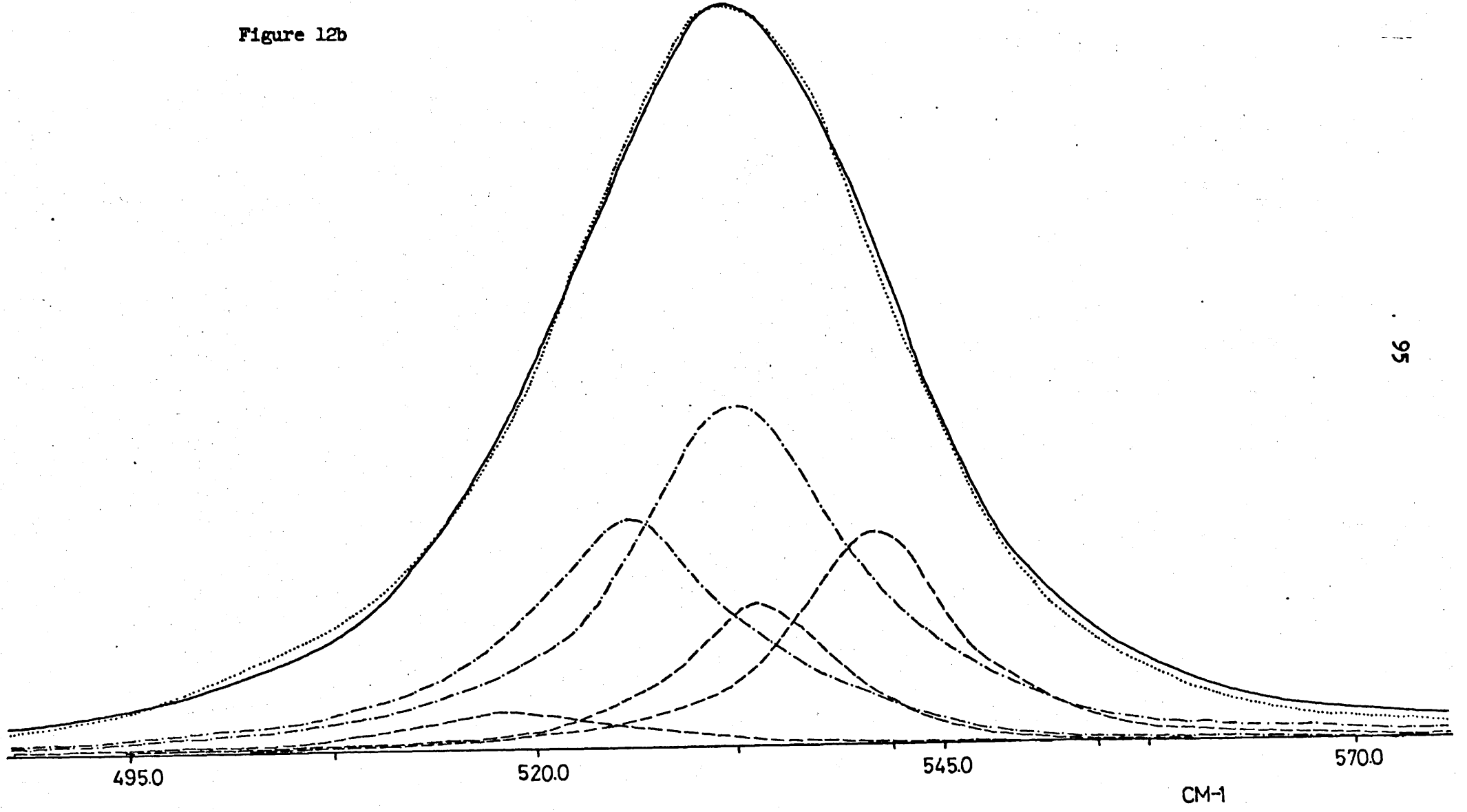

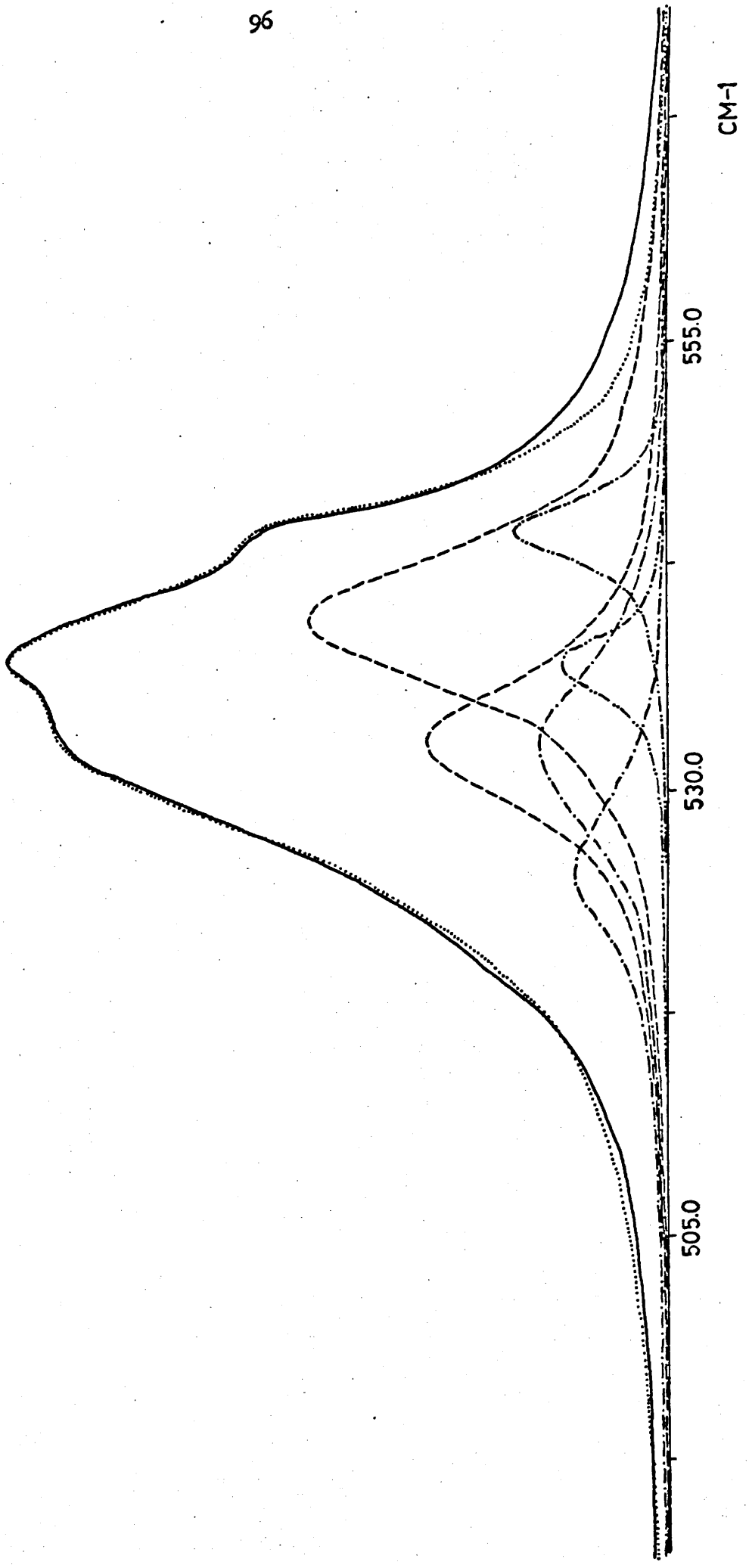

Figure 13a

Figure 13b

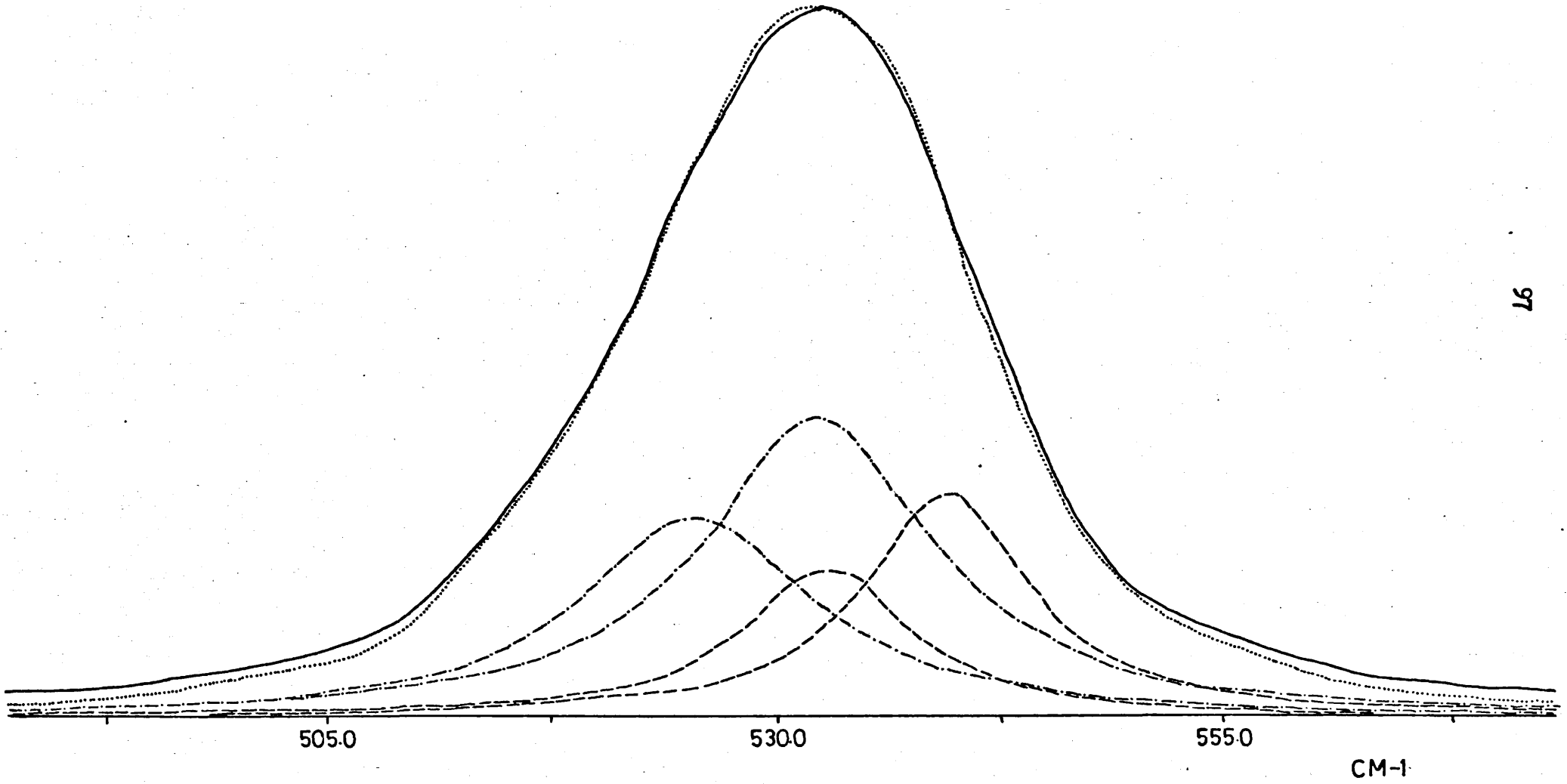

Figure 14a

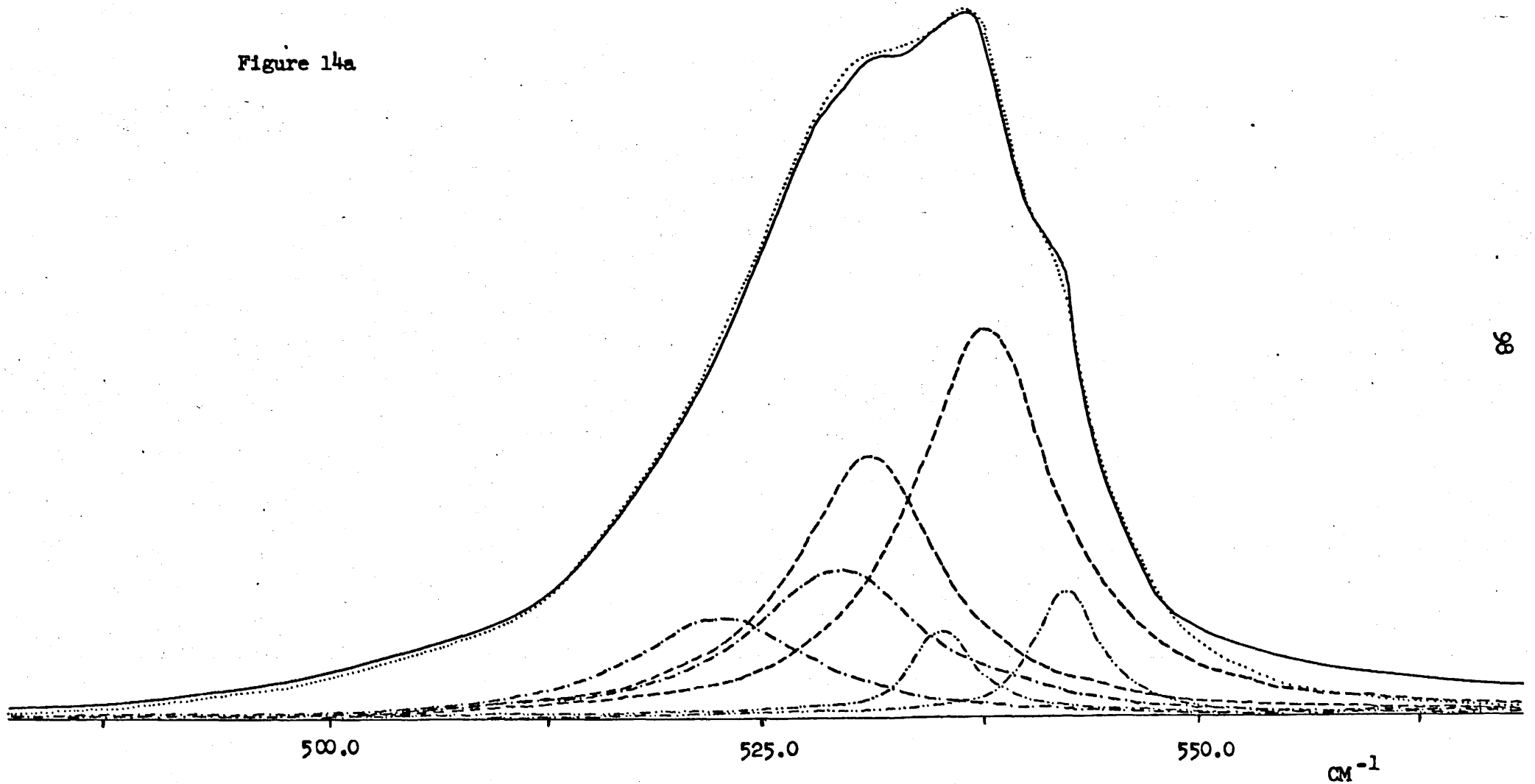

Figure 14b

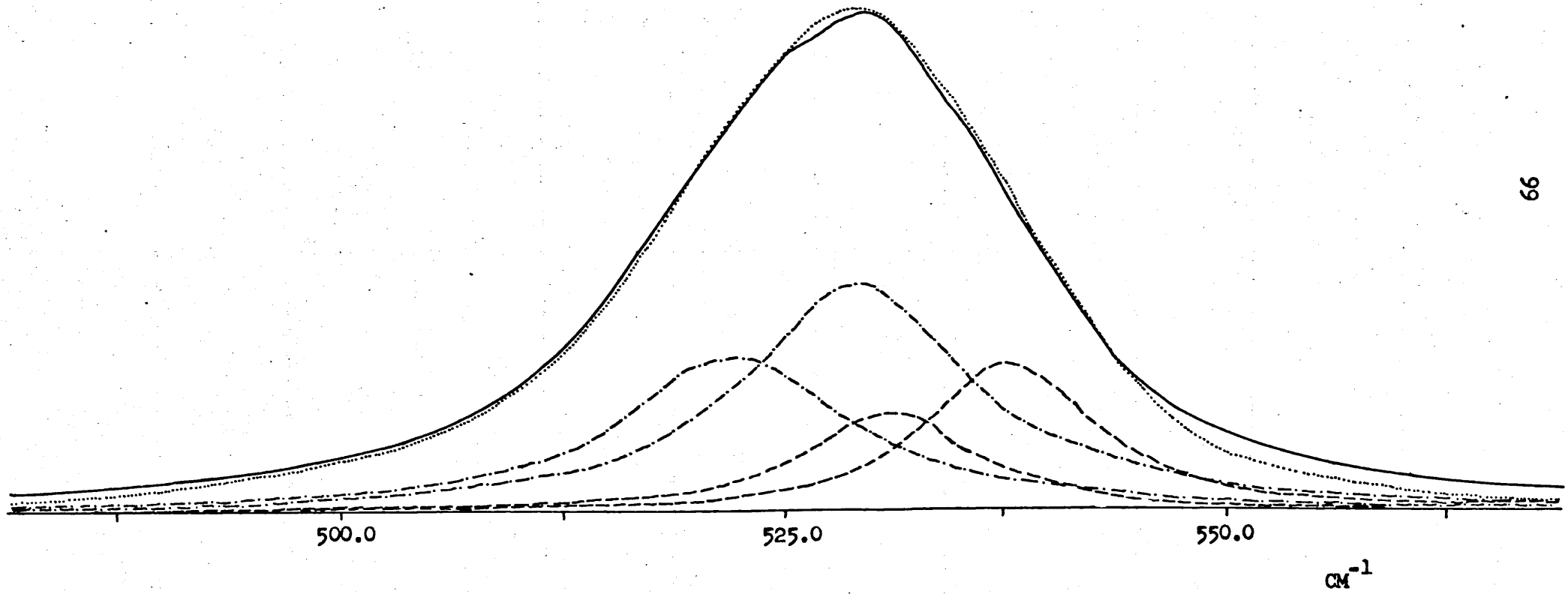

Table 2A A listing of the optimum parameters for the Lorentzian bands used in simulating the band profiles: The uncomplexed species

Solution CCl_4:C_6H_6	0⟶1 transition $\nu_o(cm^{-1})$		1⟶2 transition $\nu_o(cm^{-1})$	$\Delta\nu_{\frac{1}{2}}(\bar{\alpha}')^2$	$\Delta\nu_{\frac{1}{2}}(\gamma')^2$
1:0	$^{35}Cl_2$	549.0	543.4	2.5	?
	$^{35}Cl^{37}Cl$	541.5	535.9		
	$^{37}Cl_2$	534.0	528.4		
$7\frac{1}{2}$:1		548.3	543.0	3.5	?
		540.8	535.5		
		533.3	528.0		
6:1		547.4	542.2	3.6	?
		540.0	534.7		
		532.5	527.2		
3:1		546.1	540.8	4.6	?
		538.6	533.3		
		531.1	525.8		
2:1		544.9	539.7	4.8	?
		537.4	532.4		
		530.0	525.0		
1:1		543.8	538.5	5.1	?
		536.3	531.0		
		528.8	523.5		
0:1		541.6	536.3	5.3	?
		534.3	529.0		
		527.0	521.7		

Table 2B The 1st complex species

Solution $CCl_4:C_6H_6$	$0 \rightarrow 1$ transition $\nu_o(cm^{-1})$		$1 \rightarrow 2$ transition $\nu_o(cm^{-1})$	$\Delta\nu_{\frac{1}{2}}(\bar{\alpha}')^2$	$\Delta\nu_{\frac{1}{2}}(\gamma')^2$
$7\frac{1}{2}:1$	$^{35}Cl_2$	542.2	536.9	7.8	11.2
	$^{35}Cl^{37}Cl$	535.2	529.9		
	$^{37}Cl_2$	528.2	522.9		
6:1		542.0	536.7	8.2	11.2
		535.0	529.7		
		528.0	522.7		
3:1		540.4	535.1	8.4	11.0
		533.6	528.3		
		526.8	521.5		
2:1		540.2	534.9	8.6	11.2
		533.2	527.9		
		526.2	520.9		
1:1		538.8	533.5	9.1	11.3
		532.0	526.7		
		525.2	519.9		
0:1		537.0	531.7	10.0	11.3
		530.2	524.9		
		523.4	518.1		

Table 2C The 2nd complex species

Solution $CCl_4:C_6H_6$	0⟶1 transition ν_o (cm^{-1})	1⟶2 transition ν_o(cm^{-1})	$\Delta\nu_{\frac{1}{2}}(\bar{\alpha}')^2$	$\Delta\nu_{\frac{1}{2}}(\gamma')^2$
$7\frac{1}{2}$:1	$^{35}Cl_2$ 537.5	532.2	10.0	13.8
	$^{35}Cl^{37}Cl$ 530.7	525.4		
	$^{37}Cl_2$ 523.9	518.6		
6:1	537.3	532.0	10.3	14.0
	530.5	525.2		
	523.7	518.4		
3:1	532.8	527.5	10.4	14.0
	526.0	520.7		
	519.2	513.9		
2:1	532.0	526.8	11.2	15.2
	525.2	520.0		
	518.4	513.2		
1:1	531.5	526.3	11.7	15.3
	524.7	519.5		
	517.9	512.7		
0:1	528.4	523.2	12.3	15.5
	521.6	516.4		
	514.8	509.6		

Table 2D The relative intensities at the maxima (for Tables 2A, B and C)

Solution CCl_4:C_6H_6	Relative intensities at maxima in the ratio uncomplexed: complex 1: complex 2	
	$(\bar{\alpha}')^2$	$(\gamma')^2$
1:0	-	-
$7\frac{1}{2}$:1	2.56:1.0:0.41	0.0:1.0:1.52
6:1	1.86:1.0:0.48	0.0:1.0:2.19
3:1	0.86:1.0:0.38	0.0:1.0:1.57
2:1	0.47:1.0:0.37	0.0:1.0:2.22
1:1	0.20:1.0:0.46	0.0:1.0:1.84
0:1	0.13:1.0:0.46	0.0:1.0:2.11

It appears that the agreement between the simulated and observed spectrum is not so good on the high frequency side. This could be because of the assumption of Lorentzian band contours, which gives too large a wing contribution and partly from the overlap of the observed spectrum of chlorine with the 610 cm^{-1} band of benzene. For each set of bands the constraints (i), (iii) and (iv), listed for the free chlorine band fitting, were used. The resultant optimum band parameters are listed in Tables 2A, B, C and D.

In the initial studies on the contour fitting procedures we tried to fit only one set of three bands representing the complexed component. However we found that after removing the unassociated component, it was possible to fit to the isotropic component but not the anisotropic component, or vice versa.

From the theory given in section 2.3, the total Raman intensity $I_{y(xx+xy)z}$ is given by

$$I_{y(xx)z} + I_{y(xy)z} = 45(\bar{\alpha}')^2 + 4(\gamma')^2 + 3(\gamma')^2$$

$$= 45(\bar{\alpha}')^2 + 7(\gamma')^2 \qquad 4.3$$

Having calculated $(\bar{\alpha}')^2$ and $(\gamma')^2$ by simulation, we multiplied them by 45 and 7 respectively in order to obtain the total calculated band contour. The comparisons between the calculated and experimental $I_{y(xx+xy)z}$ spectra, for the different solutions are given in figures 15-20. The band shapes of the five calculated components 45 $(\bar{\alpha}')^2$ uncomplexed, 45 $(\bar{\alpha}')^2$ complex 1, 45$(\bar{\alpha}')^2$complex 2, 7$(\gamma')^2$ complex 1 and 7 $(\gamma')^2$ complex 2, are shown.

In Table 2D it is rather disconcerting to observe that the ratio of the integrated intensities of the two sets of complexed bands remains relatively constant over the entire range of the mixed solvents studied. One is forced to conclude that both sets arise from the same species.

Figure 15. The Raman spectra of the Cl-Cl stretch of chlorine in a 1:7½ benzene:tetrachloromethane mixture .A comparison of the total band intensity $I_{y(xx+xy)z}$ from experiment,with that predicted assuming Lorentzian profiles.

-·-·-·-·-·- observed profile

———————— total calculated profile

..... unassociated Cl_2 component

– – – – – – the high and low frequency associated components obtained from the band contour analysis of the isotropic species $(\bar{\alpha}')^2$

-·-·-·-·- the high and low frequency associated components obtained from the band contour analysis of the anisotropic species $(\gamma')^2$

Figure 16. As for figure 15, but for a 1:6 benzene:tetrachloromethane mixture.

Figure 17. As for figure 15,but for a 1:3 benzene:tetrachloromethane mixture.

Figure 18. As for figure 15, but for a 1:2 benzene:tetrachloromethane mixture.

Figure 19. As for figure 15, but for a 1:1 benzene:tetrachloromethane mixture.

Figure 20. As for figure 15, but for benzene as solvent.

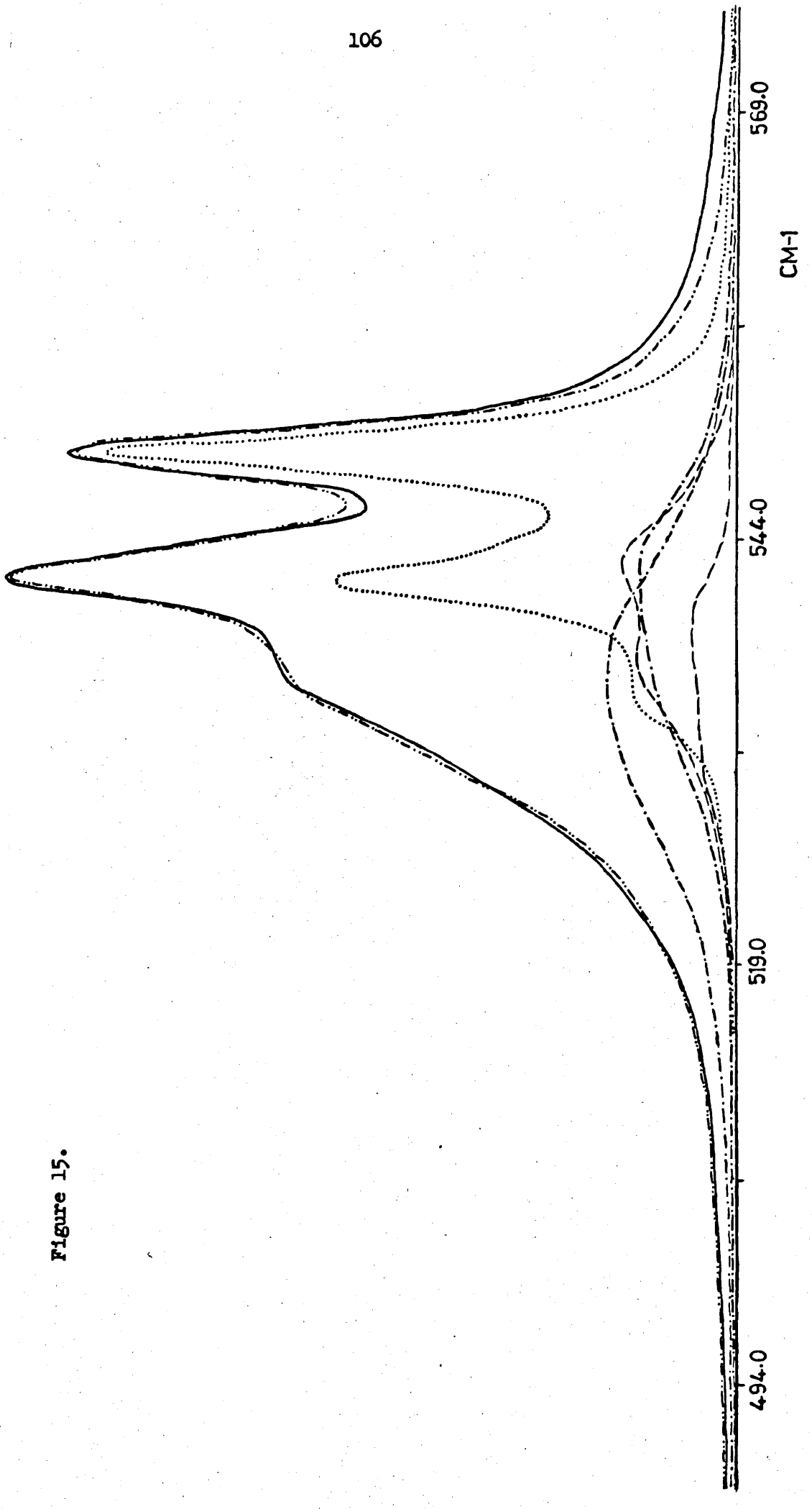

Figure 15.

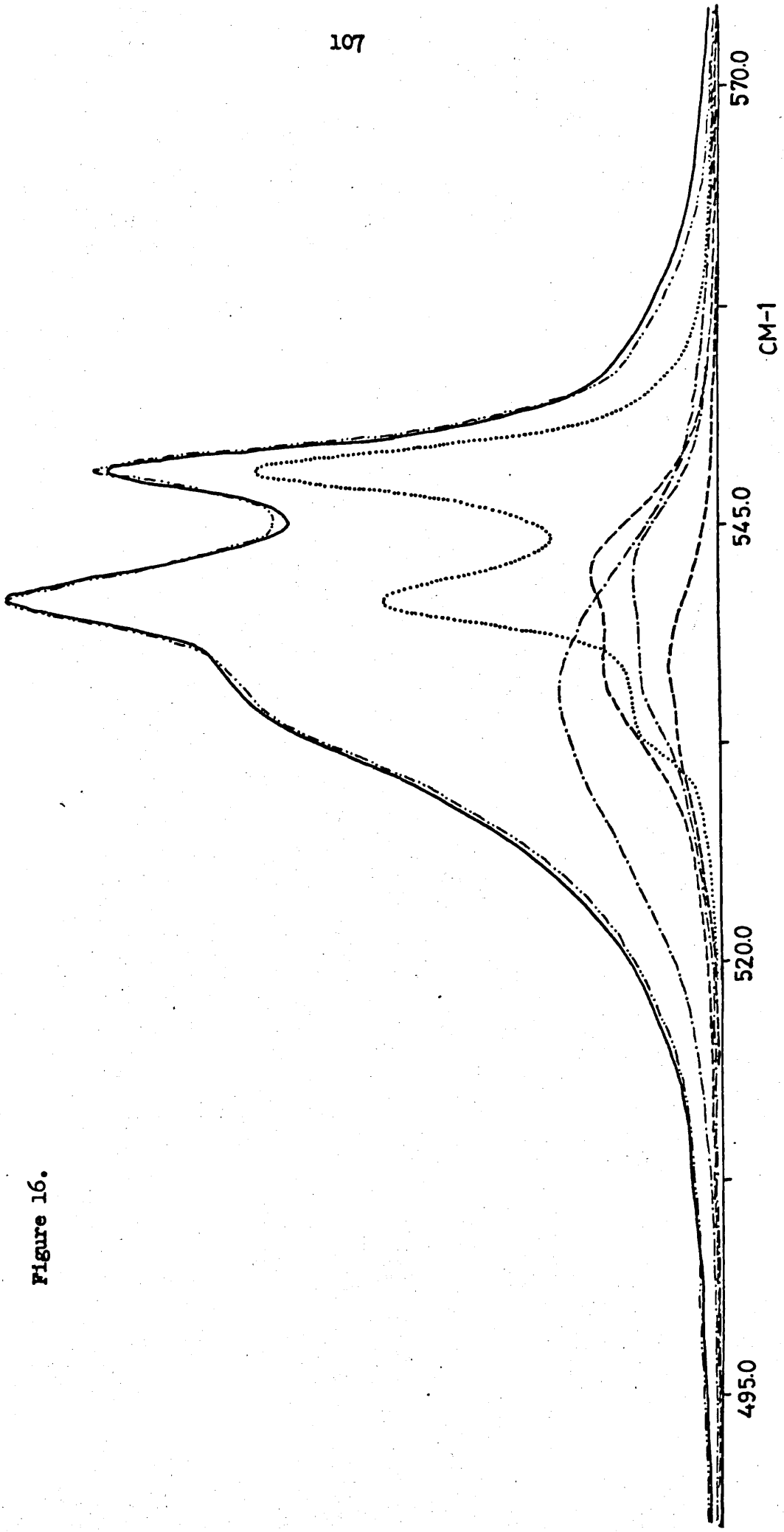

Figure 16.

Figure 17.

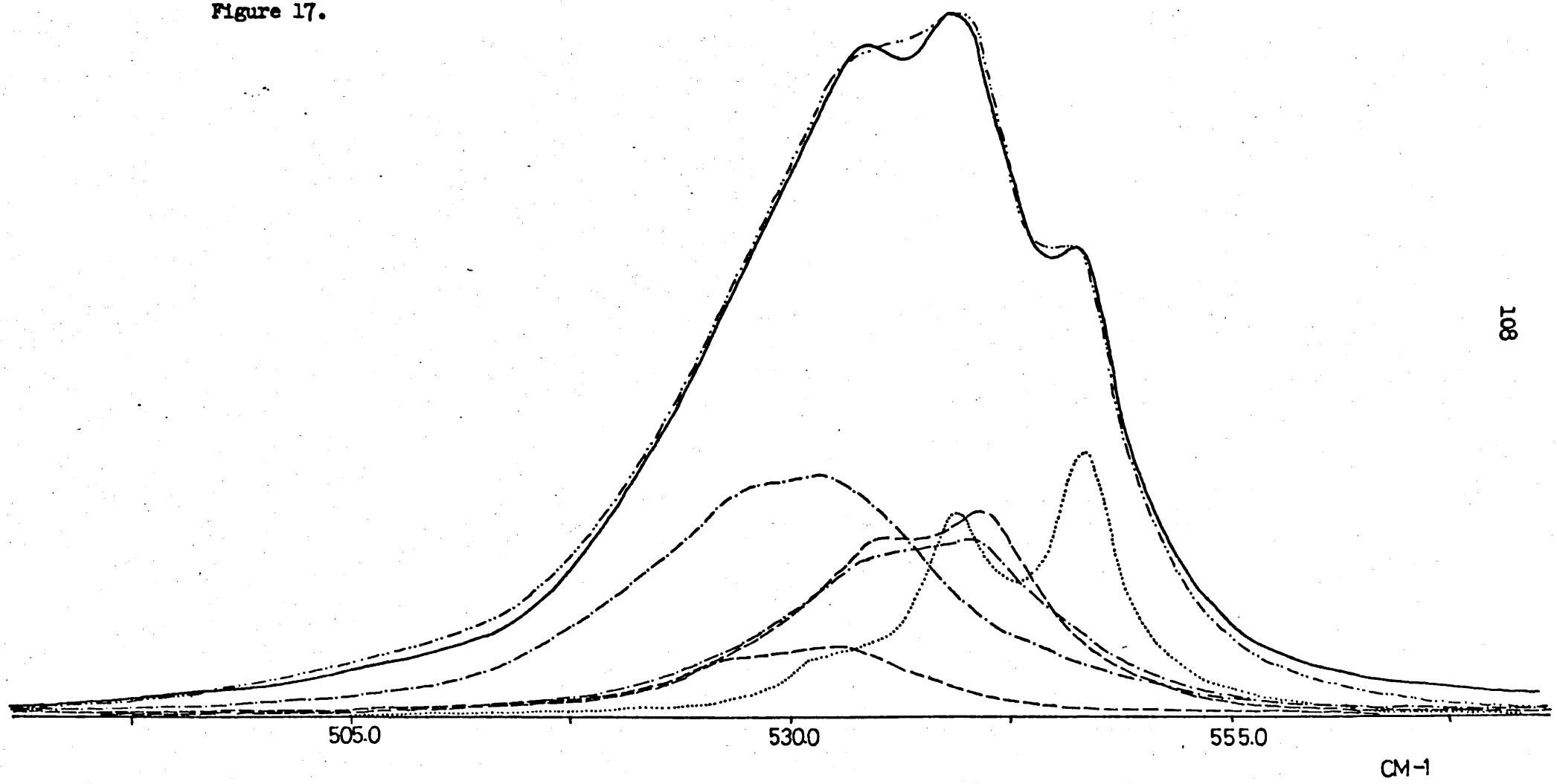

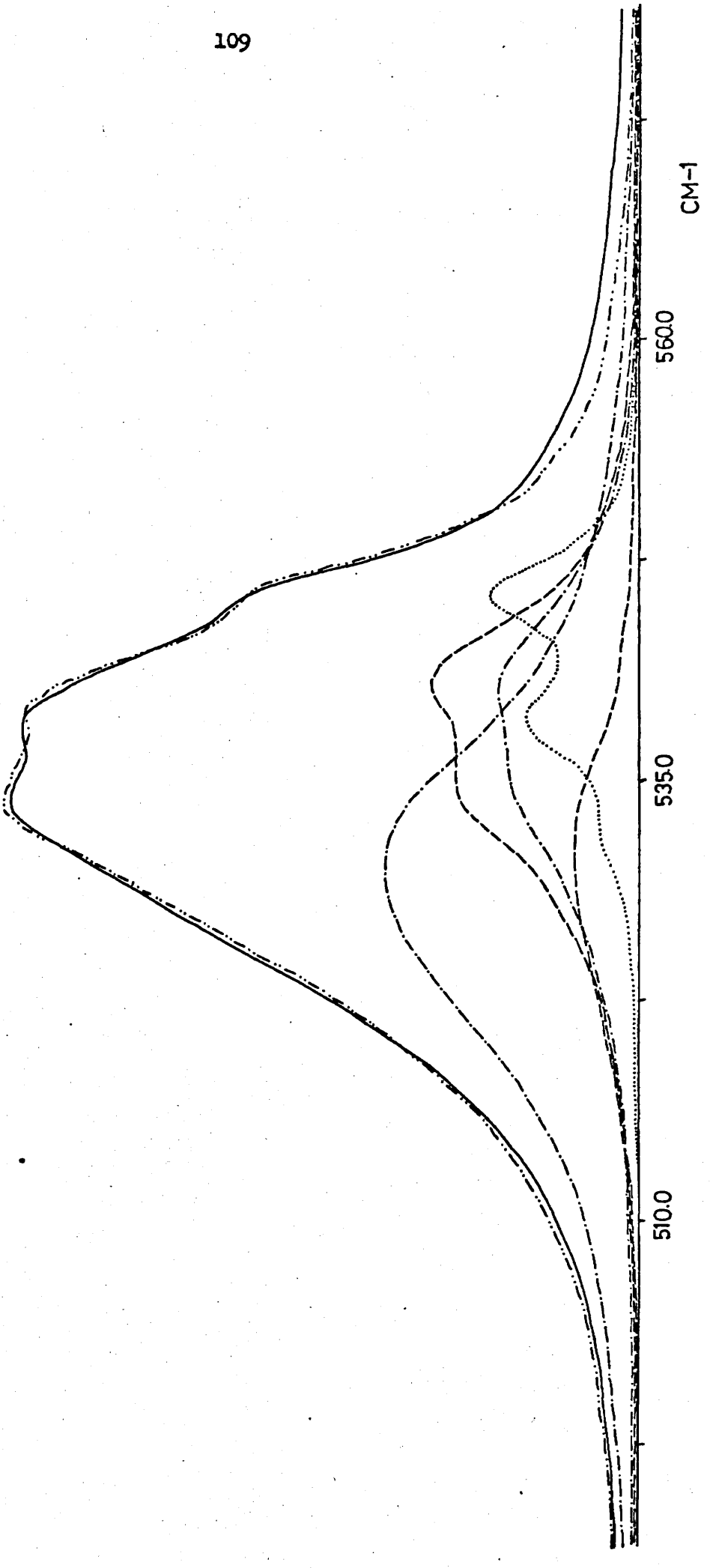

Figure 18.

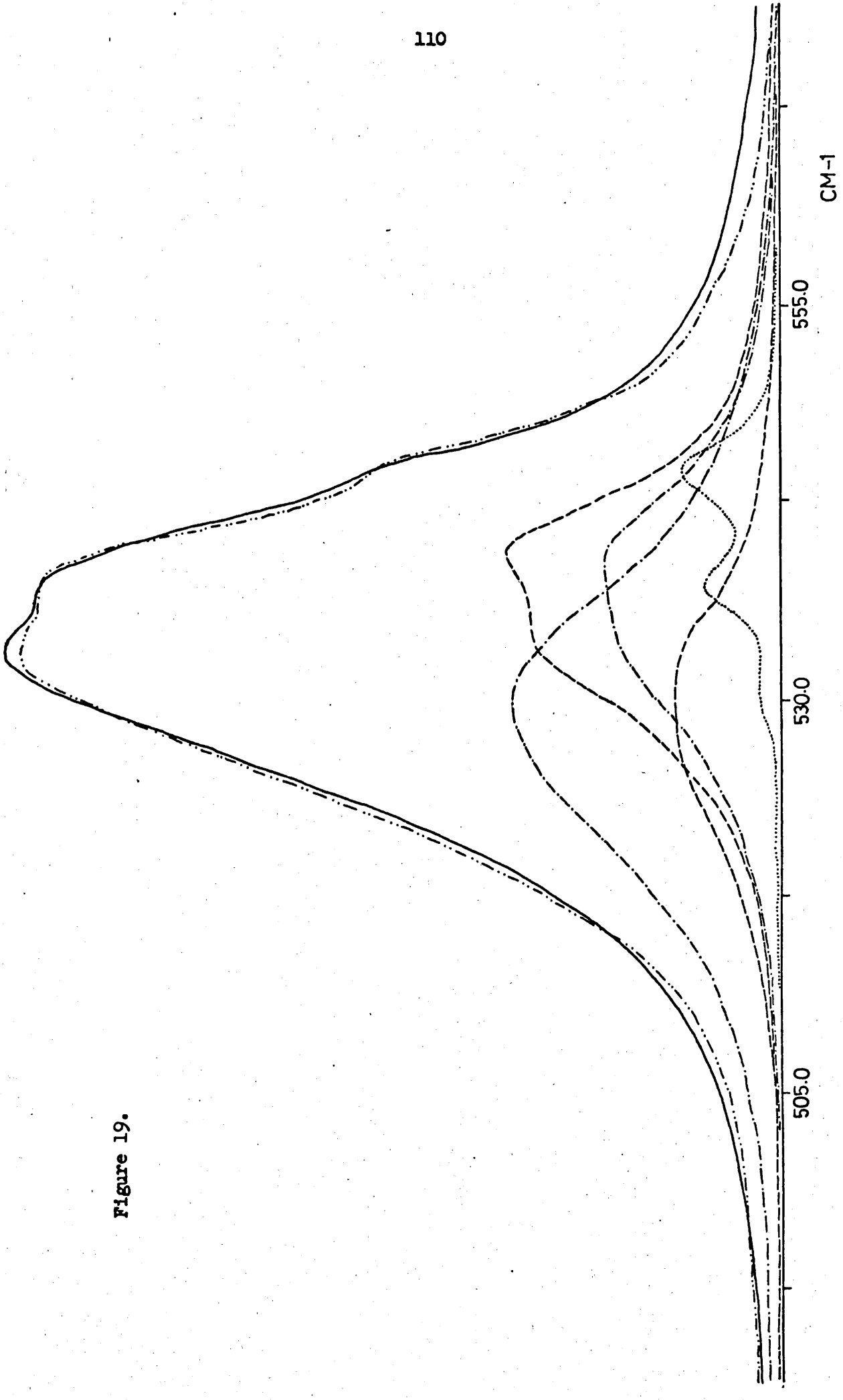

Figure 19.

Figure 20.

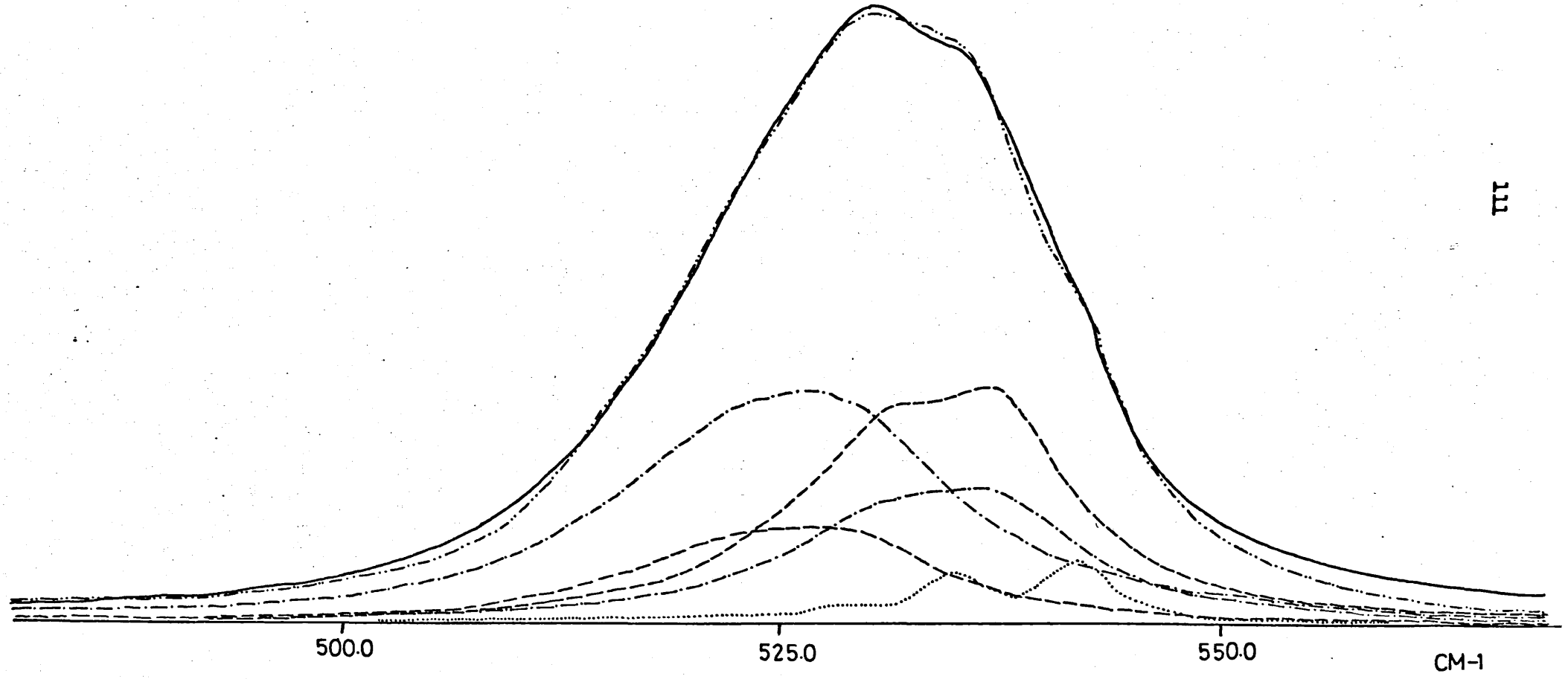

Table 3 The depolarization ratios for the two complexed chlorine bands

Solution	Depolarization ratio	
CCl_4:C_6H_6	Complex 1	Complex 2
7½:1	.487	.246
6:1	.481	.205
3:1	.480	.222
2:1	.451	.221
1:1	.441	.201
0:1	.435	.184

Table 3 shows the depolarization ratios of the two complexed bands. As one can see the bands have different depolarization ratios, as was expected. However, the ratios remain remarkably constant for all solutions, thus adding weight to our argument that we have two complexed bands of the same species. The depolarization ratio for chlorine in tetrachloromethane was calculated to be .065.

4.4.4 Calculation of the Equilibrium Constant

The total chlorine concentration C_T, at the termination of each experiment, was determined by the addition of iodine, and subsequent iodine titration. The experimental details were discussed in section 4.3

The scattering strength of the free chlorine, relative to the tetrachloromethane standard, was derived directly from the band area of the CCl_4 760/792 fermi resonance pair. In order to calculate the equilibrium constant the standard molar band strength, ϵ_f, must be determined. Defining the band areas of the CCl_4 standard and free

chlorine as A_s and A_f respectively; and the concentration of CCl_4 and free chlorine as C_s and C_f then

$$\epsilon_f = \frac{A_s}{C_s}\frac{C_f}{A_f} \qquad 4.4$$

Values of A_s and C_s are determined during the course of the experiment. The band area of free chlorine is determined from the calculated bands in figure 15. A similar procedure is used to determine the band areas of free chlorine in other solutions. In Table 4a the percentage contributions of the various species, to the total chlorine band area, are listed. The value ϵ_f is then used to derive the concentration of free chlorine in the mixed solvent solutions. It is assumed that the polarizability tensor of the free chlorine is unchanged in all the benzene-tetrachloromethane solutions. As changes in the refractive index of the solutions, with changing benzene concentration, should affect both bands equally, its effect should cancel.

Tetrachloromethane is being used as an internal standard, in the Raman band shape studies, because it is considered 'inert' with respect to its interaction with chlorine. However much evidence has accumulated in the literature to demonstrate that tetrachloromethane is not 'inert' with respect to benzene. It has been found that CCl_4 and benzene do associate in solution[82,83]. Bahnick and Person investigated the relative intensity changes of the Raman bands of CCl_4 and of the 1260 cm^{-1} band of cyclohexane, as benzene was added to the system. Evidence was presented to show that the cyclohexane band does not change in intensity as benzene or CCl_4 was added; apart from the change arising from refractive index variations. The Fermi

doublet at 760/790 cm^{-1} and 459 cm^{-1} band of CCl_4 both showed the same significant linear intensity increase, as the proportion of benzene is increased, in a cyclohexane-CCl_4-benzene mixture. For a solution containing a volume fraction of .35 benzene, the increase was taken to be 10%. Obviously we need to take this effect into account in interpreting the chlorine in CCl_4 and benzene data. Therefore the observed band areas of the tetrachloromethane reference band were adjusted by the appropriate correction factor, for each solution.

When the concentration of free chlorine is evaluated from equation 4.4, and then subtracted from the total chlorine concentration C_T, we are left with the concentration of associated chlorine. If our analysis is to be valid then the concentration of complexed species so deduced must be linearly related to the normalized area of the associated chlorine band. This was found to be the case, see figure 21. It was now possible to deduce the stoichiometry of the complex. A non-linear relationship between the ratio $\frac{[Cl_2]_{complex}}{[Cl_2]_{free}}$ and $[C_6H_6]$ shows that we are not dealing with a 1:1 complex, see figure 22. However a very good linear relationship was found for $[C_6H_6]^2$, see figure 23. Thus we have established that chlorine forms a 1:2 complex with benzene.

The equilibrium constant is given by

$$ {}^2K = \frac{[Cl_2]_{complex}}{[Cl_2]_{free}\,[C_6H_6]_A^2} \qquad 4.5 $$

where $[C_6H_6]_A = [C_6H_6]_{initial} - 2[Cl_2]_{complex}$.

The value of ${}^2K$ is given by the gradient of the graph in figure 23, such that ${}^2K = .095 \pm .01\ dm^6 mol^{-2}$ (at room temperature).

Table 4 (a) Percentage contributions, of the 3 species, to the total intensity $I_{y(xx+xy)z}$ of the Chlorine band in the CCl_4:C_6H_6 solutions

(All measurements at Room Temperature (25°C))

Solutions CCl_4:C_6H_6	Uncomplexed	Complex 1	Complex 2
0:1	4.4	46.3	49.3
1:1	5.9	46.8	47.3
2:1	11.0	41.8	47.2
3:1	17.9	41.9	40.2
6:1	32.8	31.6	35.6
$7\frac{1}{2}$:1	40.2	30.2	29.6

Table 4 (b) Percentage contributions to the total intensity ($I_{y(xx+xy)z}$) for 1:1, 1:2, 1:3 C_6H_6:CCl_4 solutions at −10°C and +30°C

Solutions CCl_4:C_6H_6	Temperature °C	Uncomplexed	Complex 1	Complex 2
1:1	−10.0	4.6	45.7	49.7
1:1	30.0	5.9	44.7	49.4
2:1	−10.0	6.2	44.5	49.3
2:1	30.0	10.6	44.0	45.4
3:1	−10.0	12.5	43.8	43.7
3:1	30.0	17.2	42.2	40.6

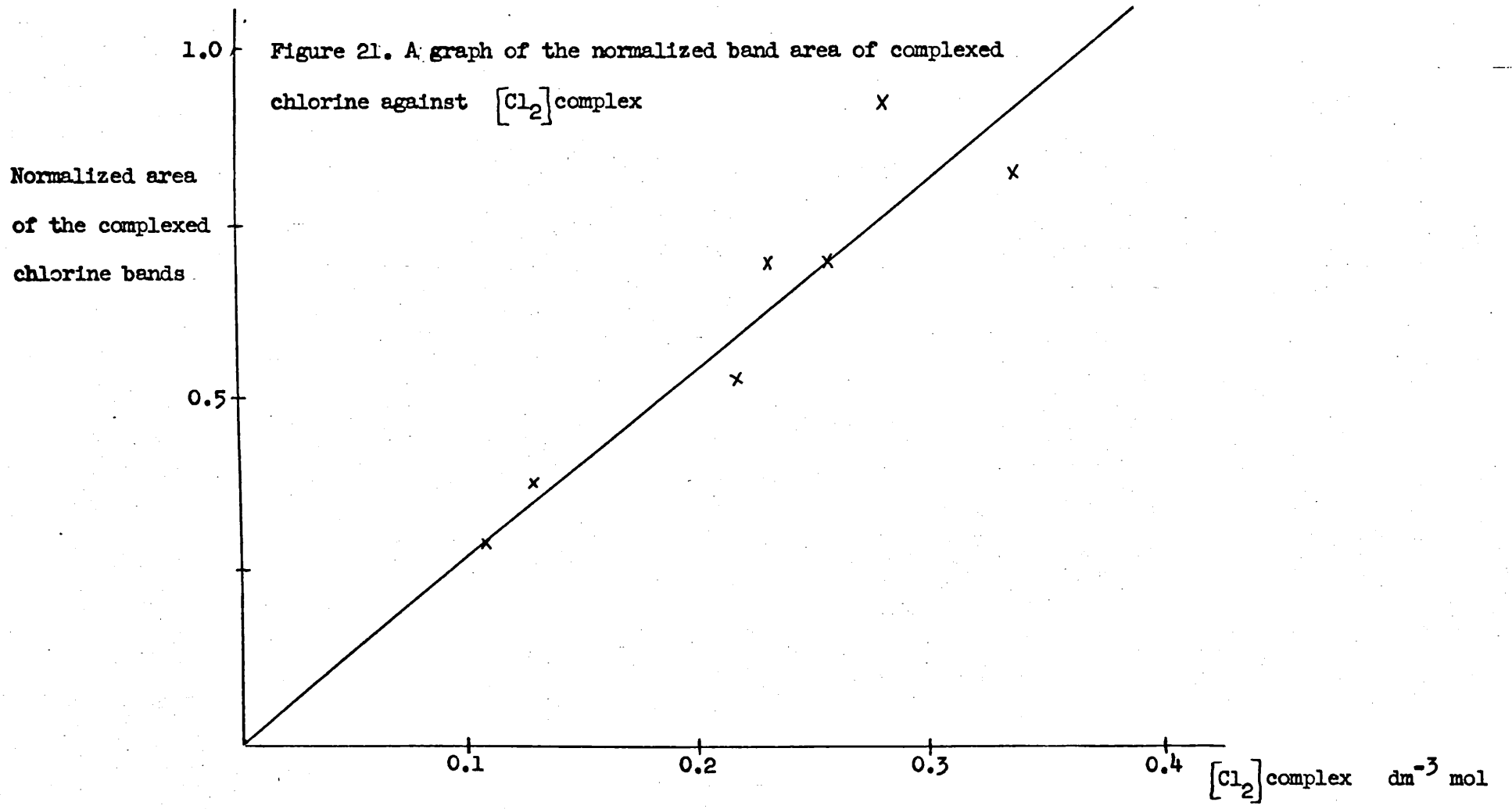

Figure 21. A graph of the normalized band area of complexed chlorine against $[Cl_2]$complex

Figure 22. A graph of $\left\{\frac{[Cl_2]\,\text{complex}}{[Cl_2]\,\text{free}}\right\}$ against $[C_6H_6]$, showing the non-linearity of the plot.

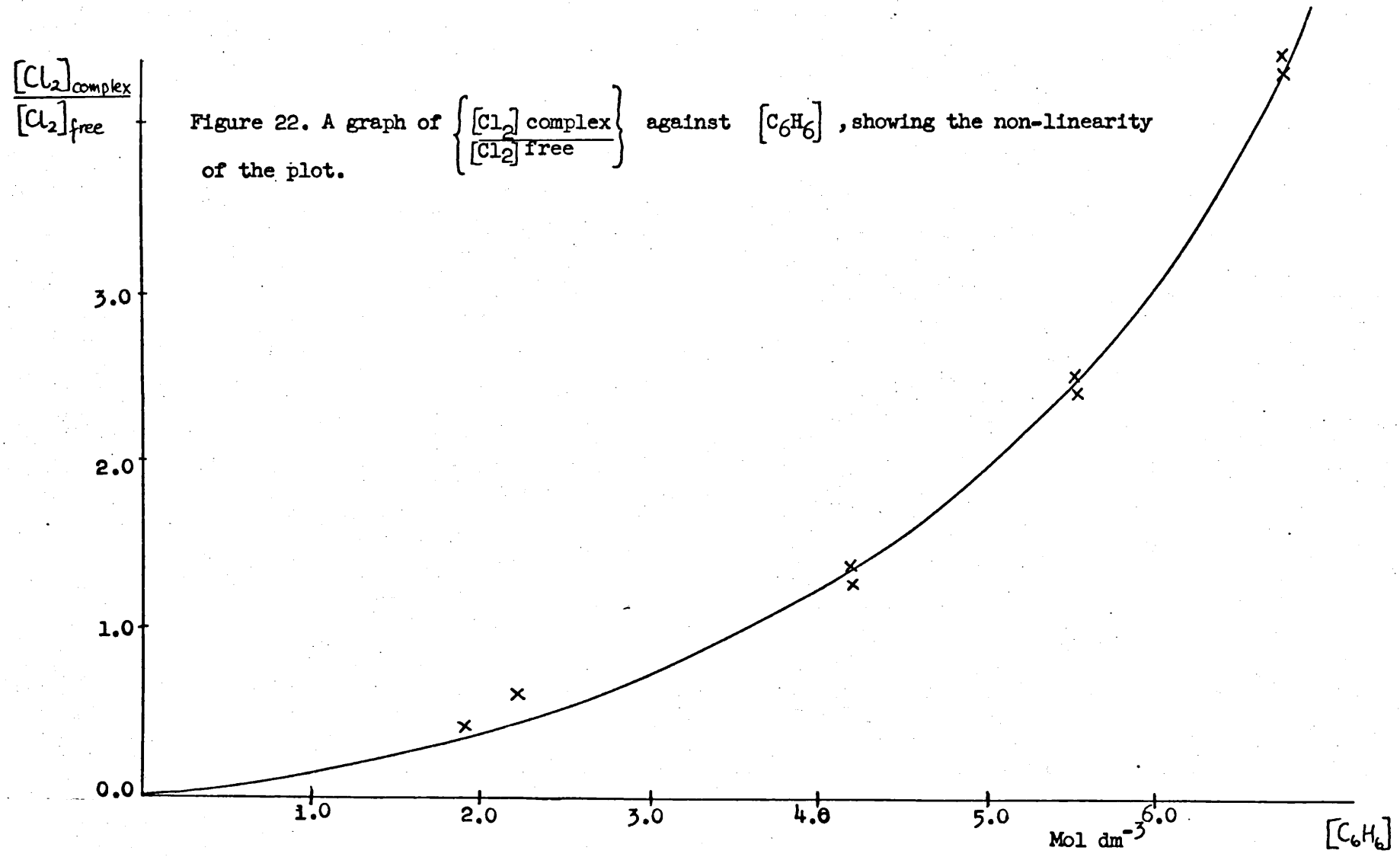

Figure 23. A graph of $\frac{[Cl_2]complex}{[Cl_2]free}$ against $[C_6H_6]_A^2$.

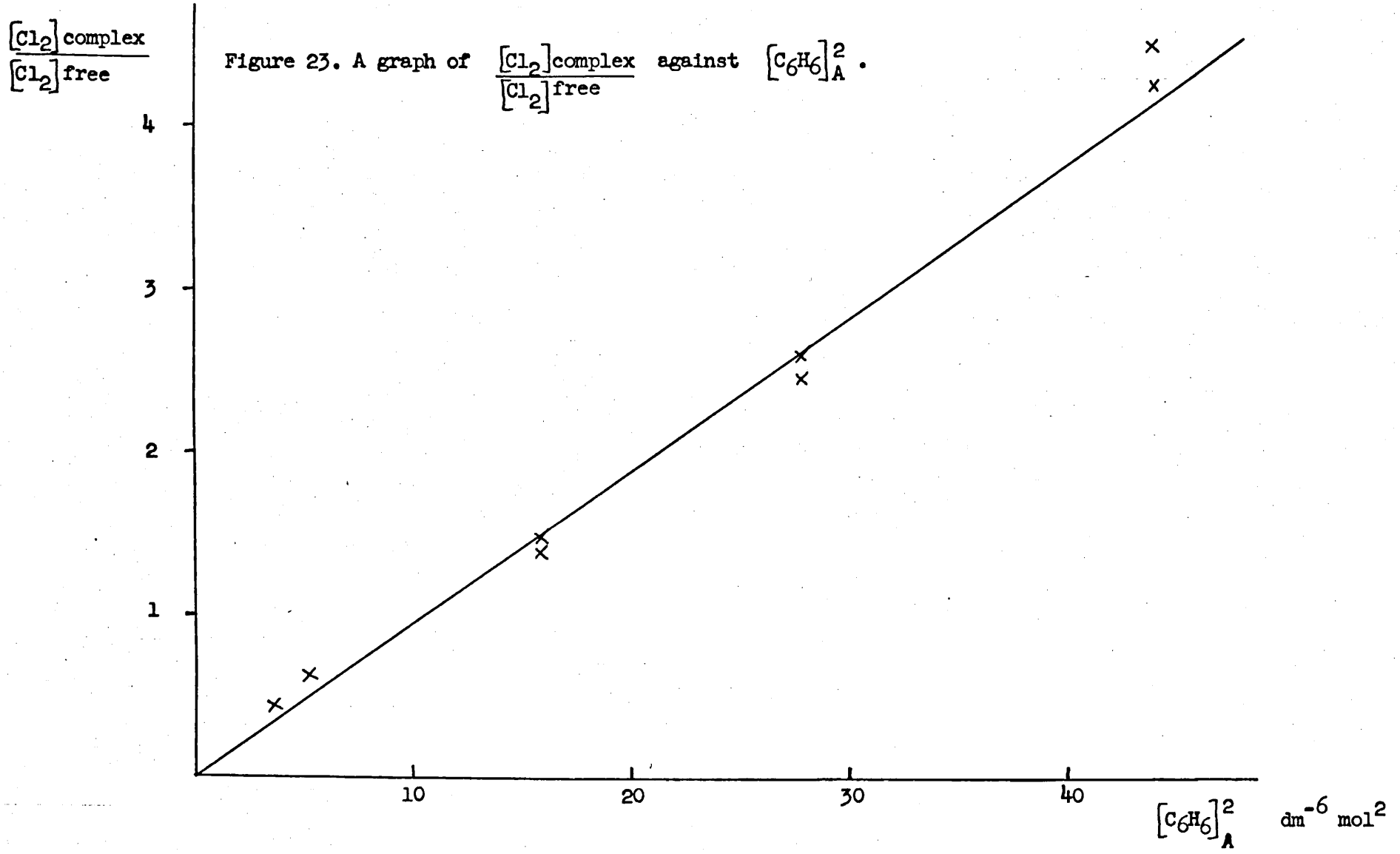

Figure 24. The temperature dependence of the isotropic Raman spectrum of chlorine in a 1:2 C_6H_6:CCl_4 solution.

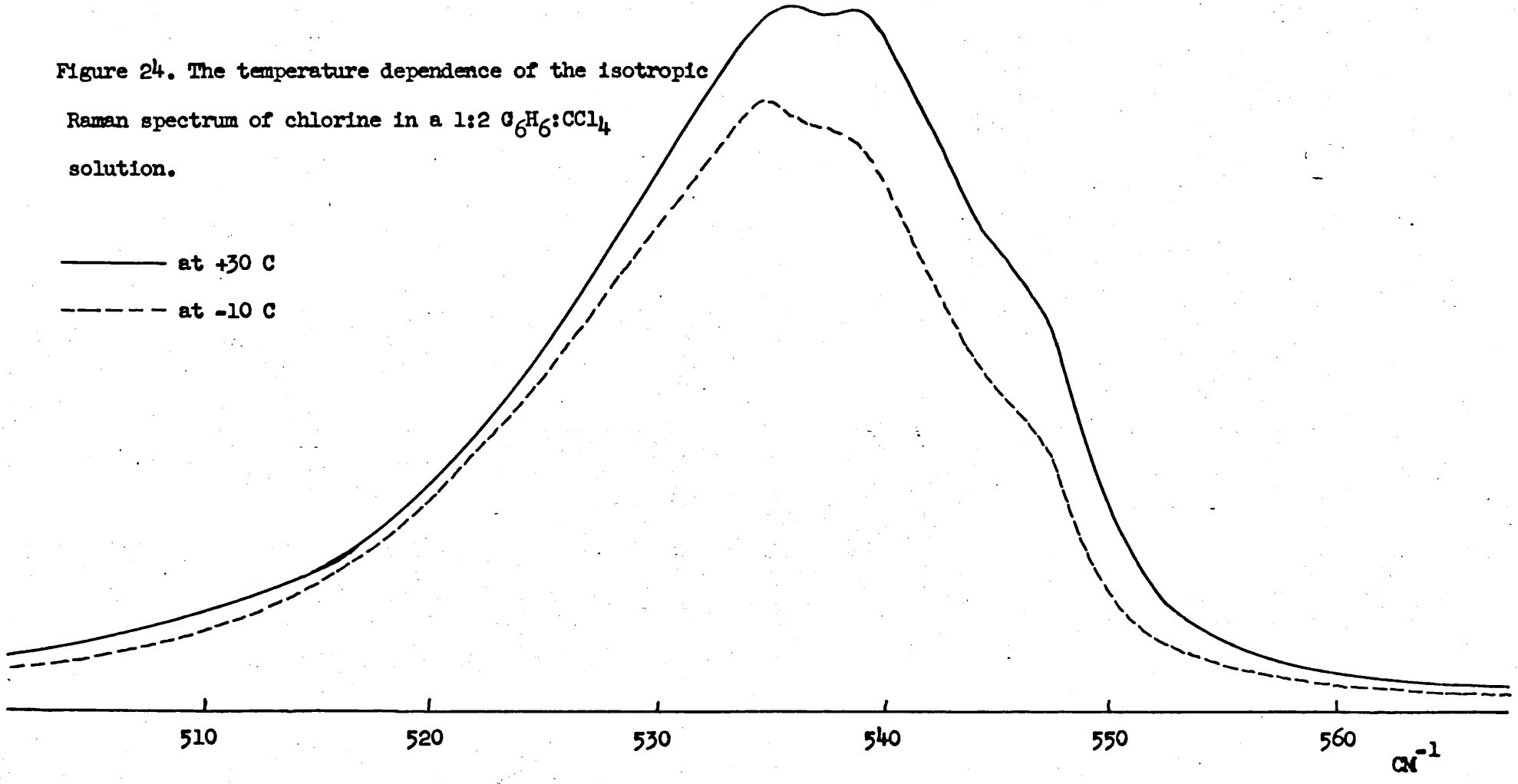

Figure 25. The Raman spectra of the Cl-Cl stretch of chlorine in a 1:1 benzene:tetrachloromethane mixture.A comparison of the observed band intensity ($I_{y(xx+xy)z}$) with that predicted assuming Lorentzian profiles.

(a) at -10°C

(b) at +30°C

..... observed profile

——— total calculated profile

—·—·—·— unassociated Cl_2 component

– – – – – high frequency associated component

—·—·—·— low frequency associated component

Figure 26. As for figure 25 but for a 1:2 benzene:tetrachloromethane mixture.

Figure 27. As for figure 25 but for a 1:3 benzene:tetrachloromethane mixture.

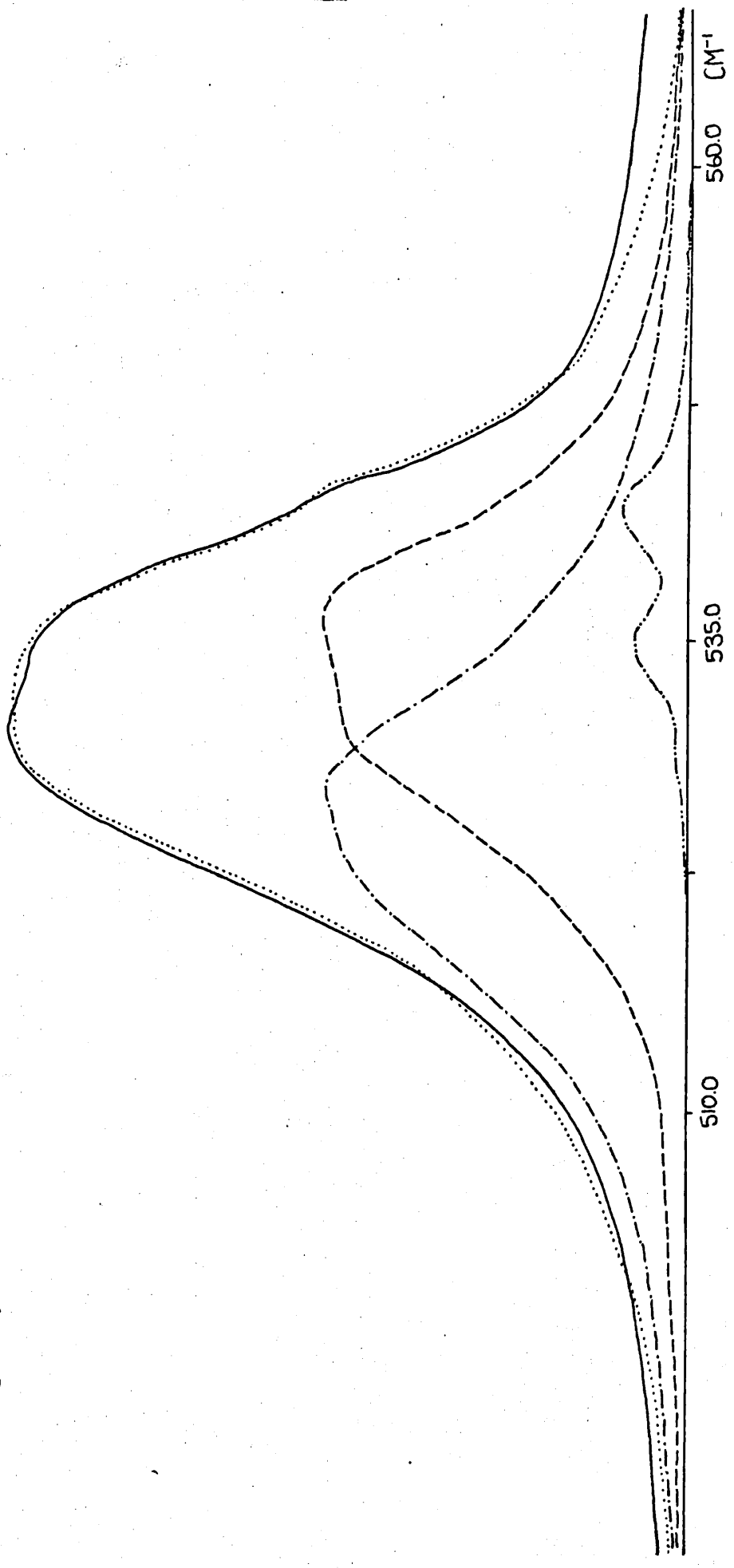

Figure 25a

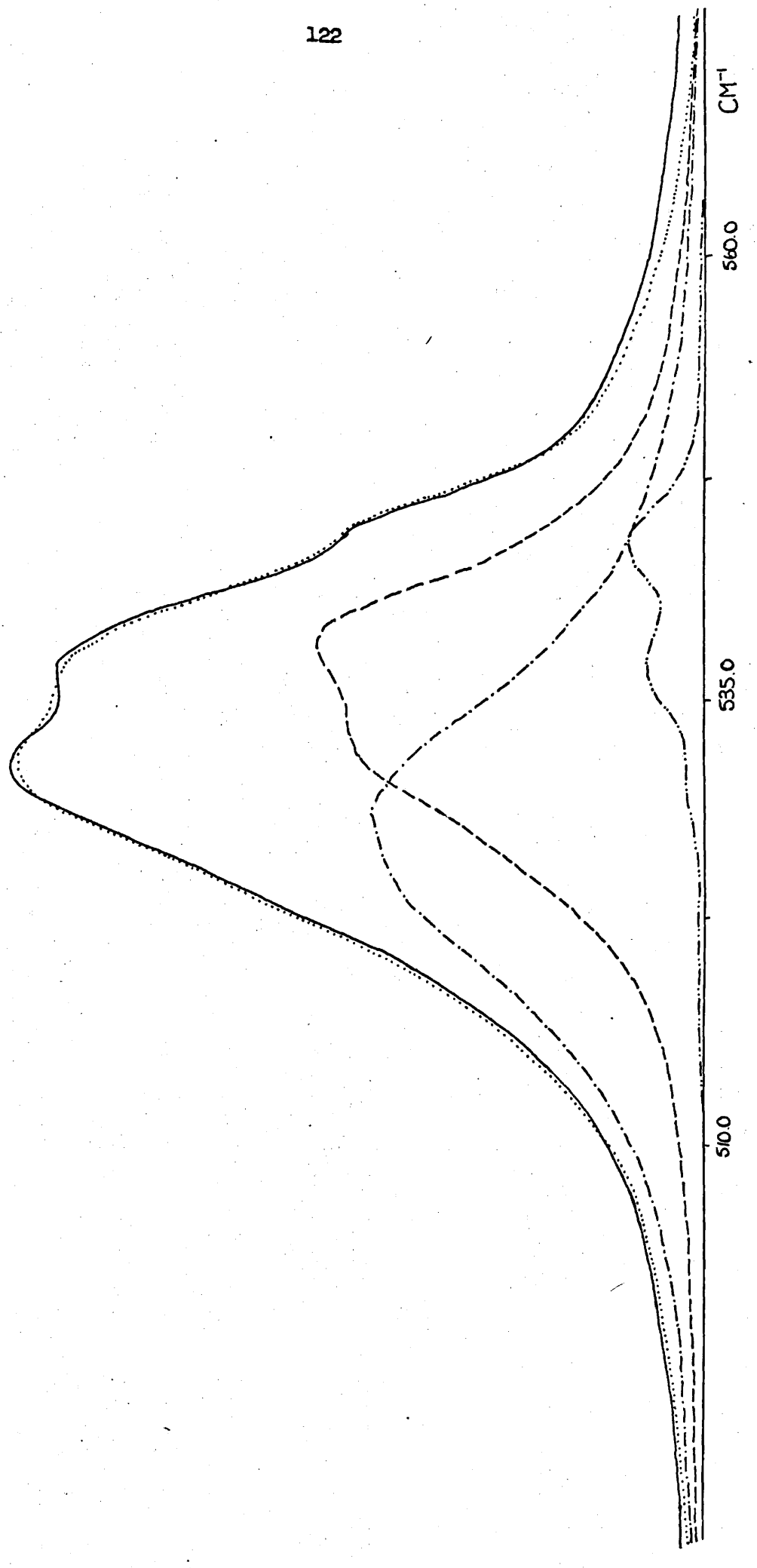

Figure 25b

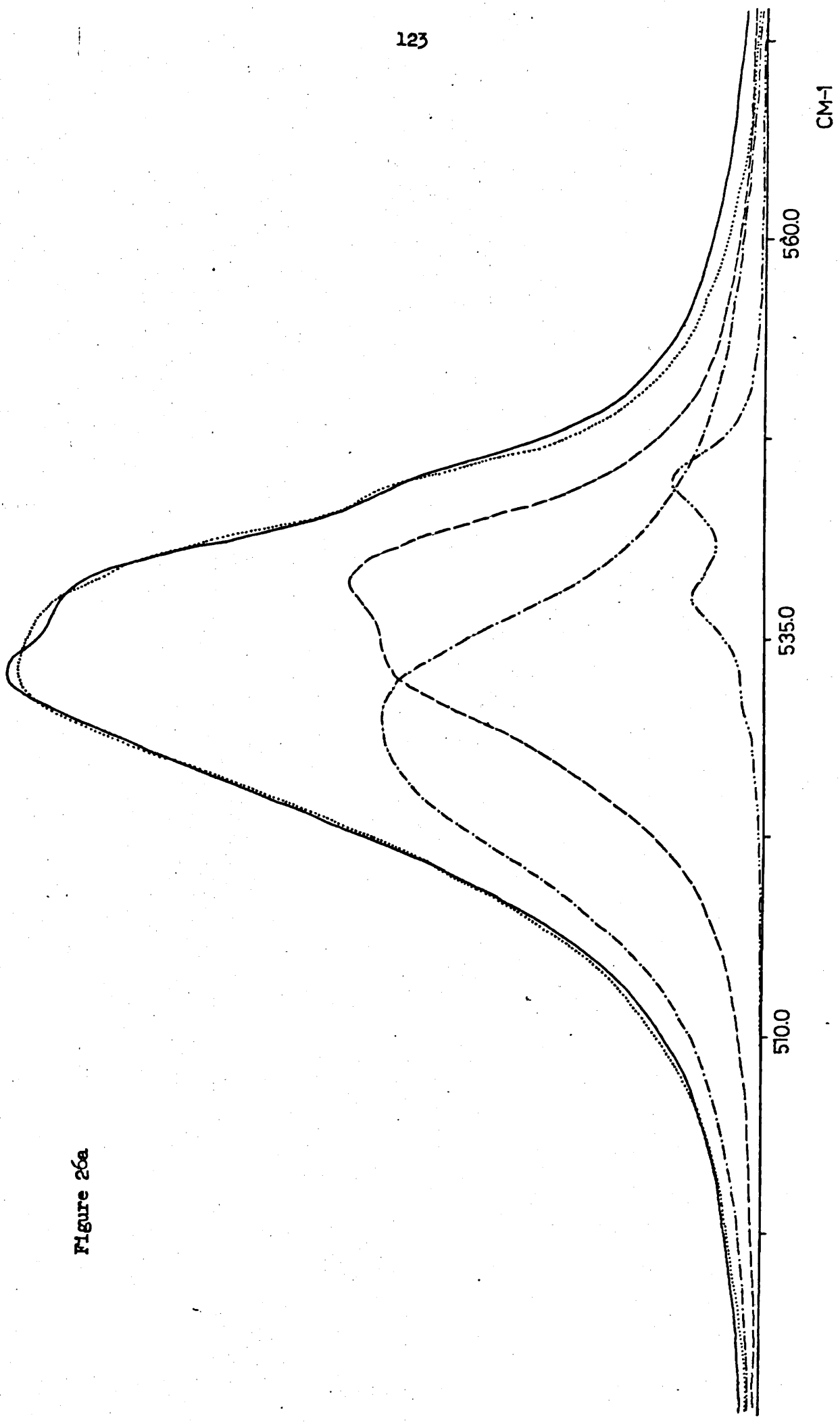

Figure 26a

Figure 26b

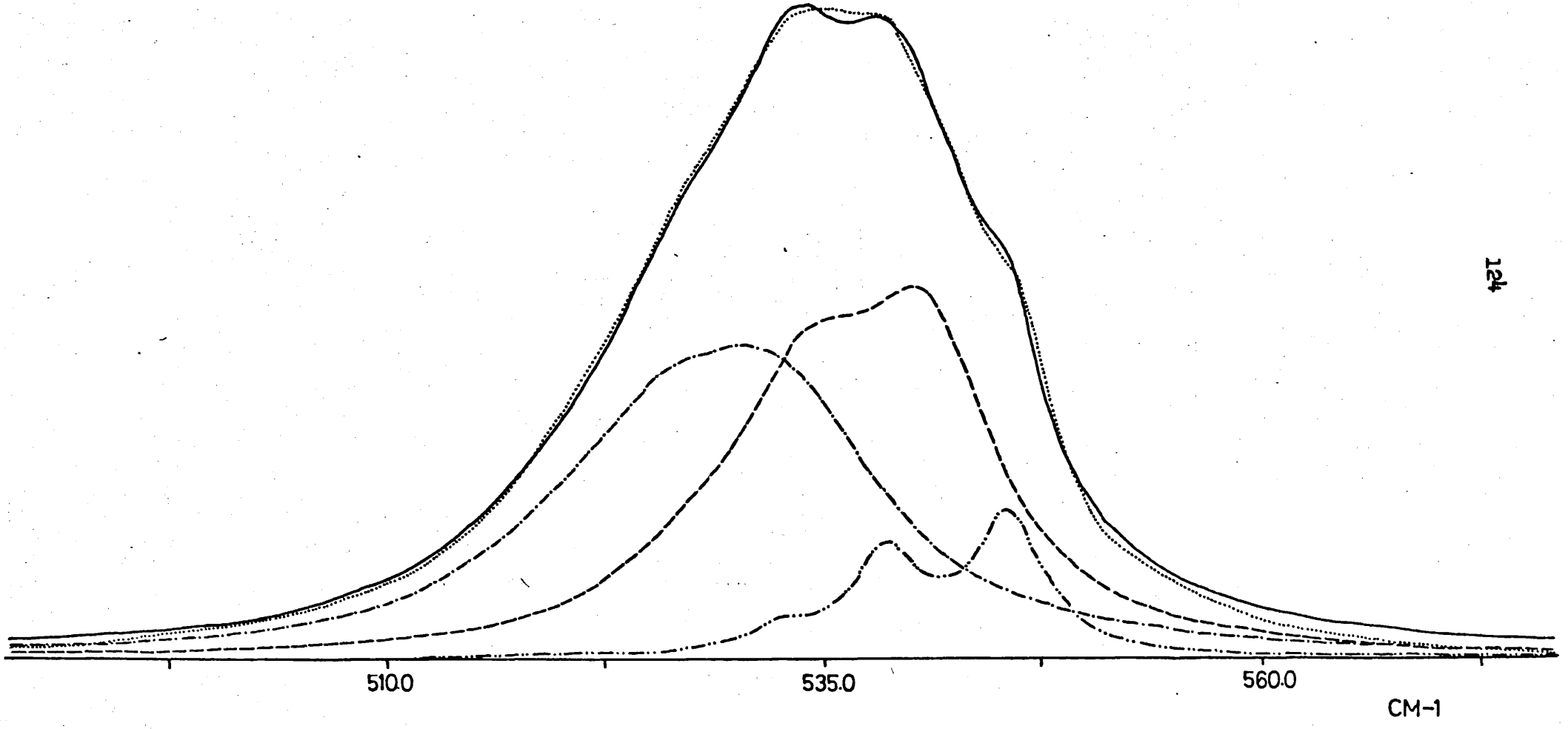

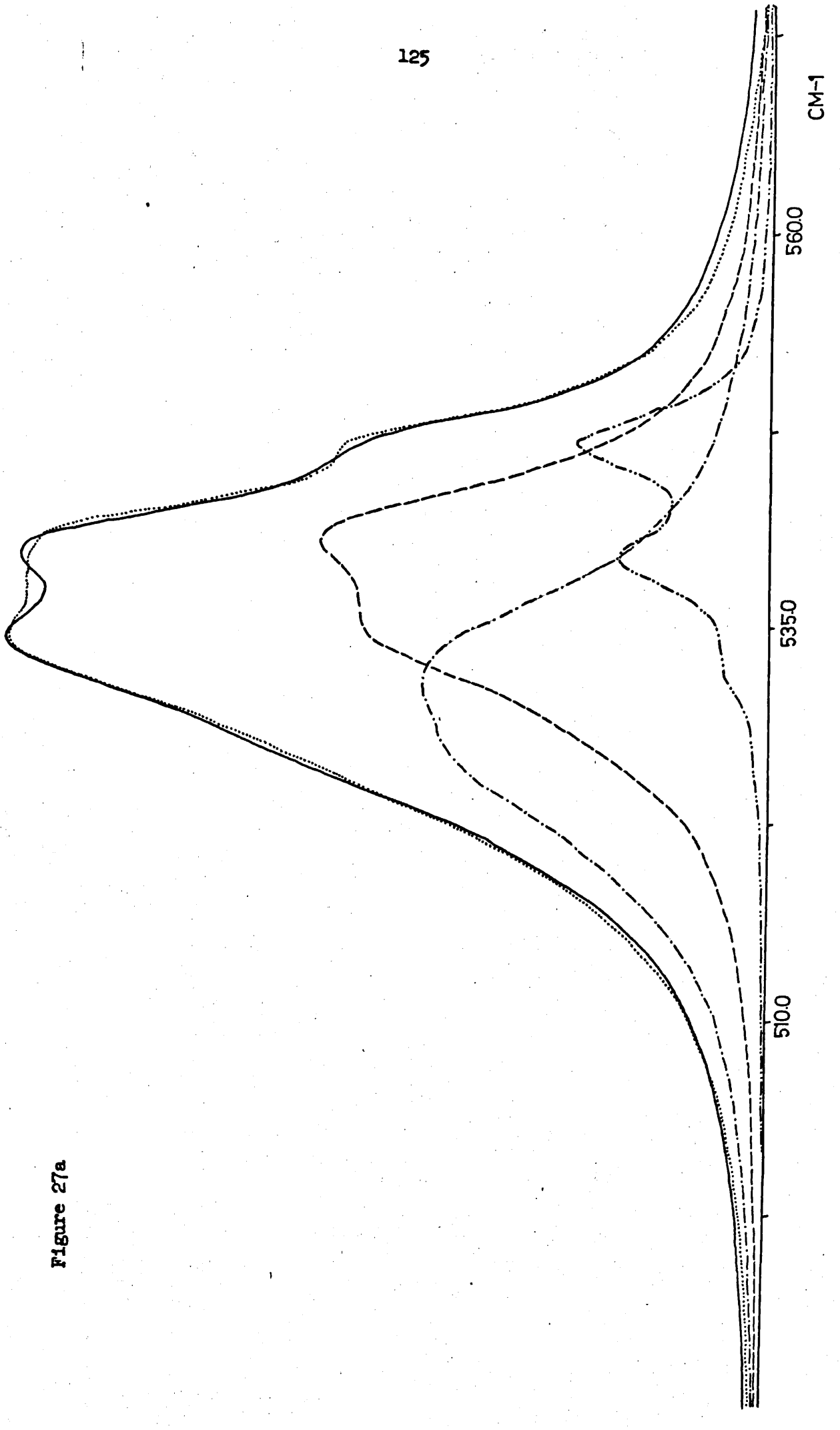

Figure 27a

Figure 27b

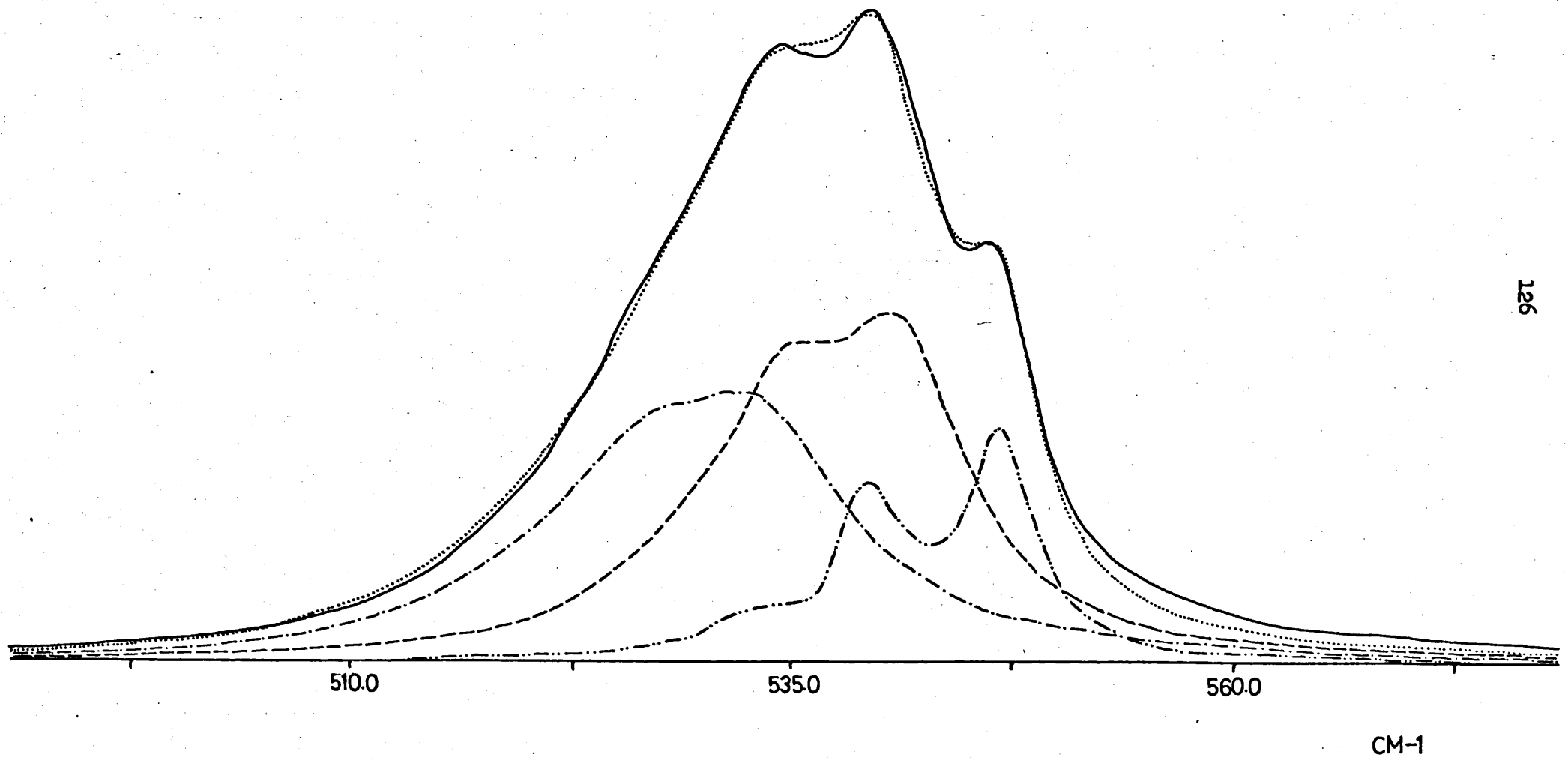

Solution CCl_4:C_6H_6	0 → 1 Transition			1 → 2 Transition			$\Delta\nu_{\frac{1}{2}}$		
	Uncomplexed	Complex 1	Complex 2	Uncomplexed	Complex 1	Complex 2	Uncomplexed	Complex 1	Complex 2
1:1 (-10°C)	542.0	537.4	528.9	536.7	532.1	523.5	5.2	10.1	14.3
	534.7	530.1	522.1	529.4	525.3	516.9			
	527.4	523.3	515.3	521.7	518.2	510.0			
1:1 (30°C)	544.2	539.2	531.9	538.9	533.9	526.9	5.1	10.1	14.5
	536.7	532.4	525.1	531.9	527.1	520.0			
	529.2	525.5	518.3	524.8	520.3	513.0			
2:1 (-10°C)	544.2	538.6	531.5	538.9	533.3	526.3	4.8	9.8	14.0
	536.7	531.7	524.7	531.4	526.4	519.5			
	529.2	524.8	517.9	523.9	519.5	512.7			
2:1 (30°C)	545.0	540.2	532.0	539.7	534.9	526.8	4.8	9.8	14.0
	527.7	533.2	525.2	532.4	527.9	520.0			
	530.4	526.2	518.4	525.0	520.9	513.2			
3:1 (-10°C)	546.0	540.1	532.4	540.7	534.8	527.2	4.65	9.0	12.0
	538.5	533.3	525.6	533.2	528.0	520.4			
	531.0	526.5	518.8	525.7	521.2	513.6			
3:1 (30°C)	546.1	540.4	532.8	540.8	535.1	527.5	4.60	9.0	12.5
	538.6	533.6	526.0	533.3	528.3	520.7			
	531.1	528.8	519.2	525.8	521.5	513.9			

Table 5 A listing of the optimum parameters for the Lorentzian bands used in simulating the band profiles: Temperature studies.

There is a strong temperature dependence of the ratio of intensities from the bands arising from associated chlorine with benzene, and with tetrachloromethane. An example of this behaviour is shown in figure 24. This shows the isotropic $I_{y(xx)z}$ Raman spectra of chlorine in a 2:1 CCl_4:C_6H_6 solution mixture at 30°C and -10°C. The intensity of the band near 547 cm^{-1} seems to decrease, whereas the intensity of the band at 535 cm^{-1} appears to increase. Table 4B shows the percentage contributions of each of the three species (uncomplexed, complexed 1, complexed 2) to the total band shape ($I_{y(xx+xy)z}$), for the solutions 1:1, 2:1 and 3:1 (CCl_4:C_6H_6). From Table 4B we can see that with decreasing temperature, the intensity of the uncomplexed species decreases and complexed species 2 increases. This confirms the observation of figure 24.

A simplified method of band fitting procedure was used to fit to the total band shape, at these different temperatures. We followed the same method as before, except that we assumed, from the start, that there were three species; each species was made up of three isotopes and three hot bands. The calculated fits to the chlorine bands (in 1:1, 2:1 and 3:1 CCl_4:C_6H_6 solutions), at the two temperatures are shown in figures 25-27. The calculated and observed band contours compare relatively well. The values of $\Delta\nu_{\frac{1}{2}}$ and the band centres, of the isot opes in each species are given in Table 5.

We have derived values for the enthalpy of formation of the 2:1 complex, from the three CCl_4/C_6H_6 mixtures at -10°C and +30°C. Initially we had to determine the free energy changes ΔG from the expression

$$\Delta G^{\circ} = -RT\ln^2 K \qquad 4.6$$

These values are shown in Table 6, along with values of ^2K.

Table 6 The equilibrium constants for the formation of $(C_6H_6)_2Cl_2$ at +30°C and at -10°C, and the derived free energy changes for three different solvent mixtures.

Solution CCl_4:C_6H_6	^2K (+30°C)	^2K (-10°C)	ΔG°(30°C) J mol^{-1}	ΔG°(-10°C) J mol^{-1}
1:1	.098	.102	5824	4974
2:1	.085	.121	6199	4604
3:1	.083	.096	6259	5104
			$\Delta G^\circ_{average}$ 6170	$\Delta G^\circ_{average}$ 4903

From Table 6 it would appear that there is a 20% increase in free energy, on increase of temperature, from -10°C to +30°C.
The uncertainties in ^2K probably arise from uncertainties in the determinations of the free and complexed chlorine at the various temperatures.

From the mean values of the free energy change the enthalpy and entropy change can be deduced, using the equation

$$\Delta G^\circ = \Delta H^\circ - T\Delta S^\circ \qquad 4.7$$

Thus the enthalpy is calculated to be -3.0 ± 1.0 kJ mol^{-1}, and the entropy change is -30 ± 5 J mol^{-1}K^{-1}.

4.4.5 Measurements of Bromine and Iodine in benzene

As explained in the previous section our studies of (a) bromine and (b) iodine in solution, were limited for (a) by the increase in photochemical reaction arising from the increased energy absorption, and for (b) by the loss in scattered intensity arising

from the same energy absorption. However, the spectra of bromine in benzene and iodine in benzene, were recorded, and the anisotropic and isotropic components are shown for each halogen in figures 28a and b. From these figures it was observed that for bromine and iodine in benzene there are differences in the frequencies of the intensity maxima for $(\bar{\alpha}')^2$ and $(\gamma')^2$, (just as there was for chlorine). For Cl_2, Br_2 and I_2 the frequency shifts are 4, 2 and 1 cm^{-1} respectively.

Initially an attempt was made to fit one set of isotopic bands to the bromine in benzene contour, using the isot opic intensity ratios quoted by Holzer et al[76] for gas phase Br_2. However we could not reproduce the experimental contour $(I_{y(xx+xy)z})$. When two sets of isotopic bands were used, keeping in mind the constraints listed earlier, a good calculated band contour was achieved. The parameters are listed in Table 7.

For iodine in benzene it was assumed that only one isotope contributed significantly to the band contour, ^{127}I. Again one set of bands did not provide a good fit, whereas a reasonable reproduction of the band contour was obtained using two sets of bands. It should be noted, that the fitting of two sets of bands is somewhat dubious due to (a) the weakness of the iodine band, and (b) the smallness of the frequency shift between $(\bar{\alpha}')^2$ and $(\bar{\gamma})^2$. We have tabulated some parameters, for fitting two sets of bands to the iodine spectrum, in Table 8.

As we did not study bromine or iodine in more 'inert' solvents such as tetrachloromethane we cannot discuss the nature of the two sets of bands used, for either halogen. We can merely conjecture that bromine and iodine behave in a similar fashion to chlorine.

Figure 28a. A comparison of $(\bar{\alpha}')^2$ and $(\gamma')^2$ for bromine in benzene. The intensity scale is in arbitrary units.

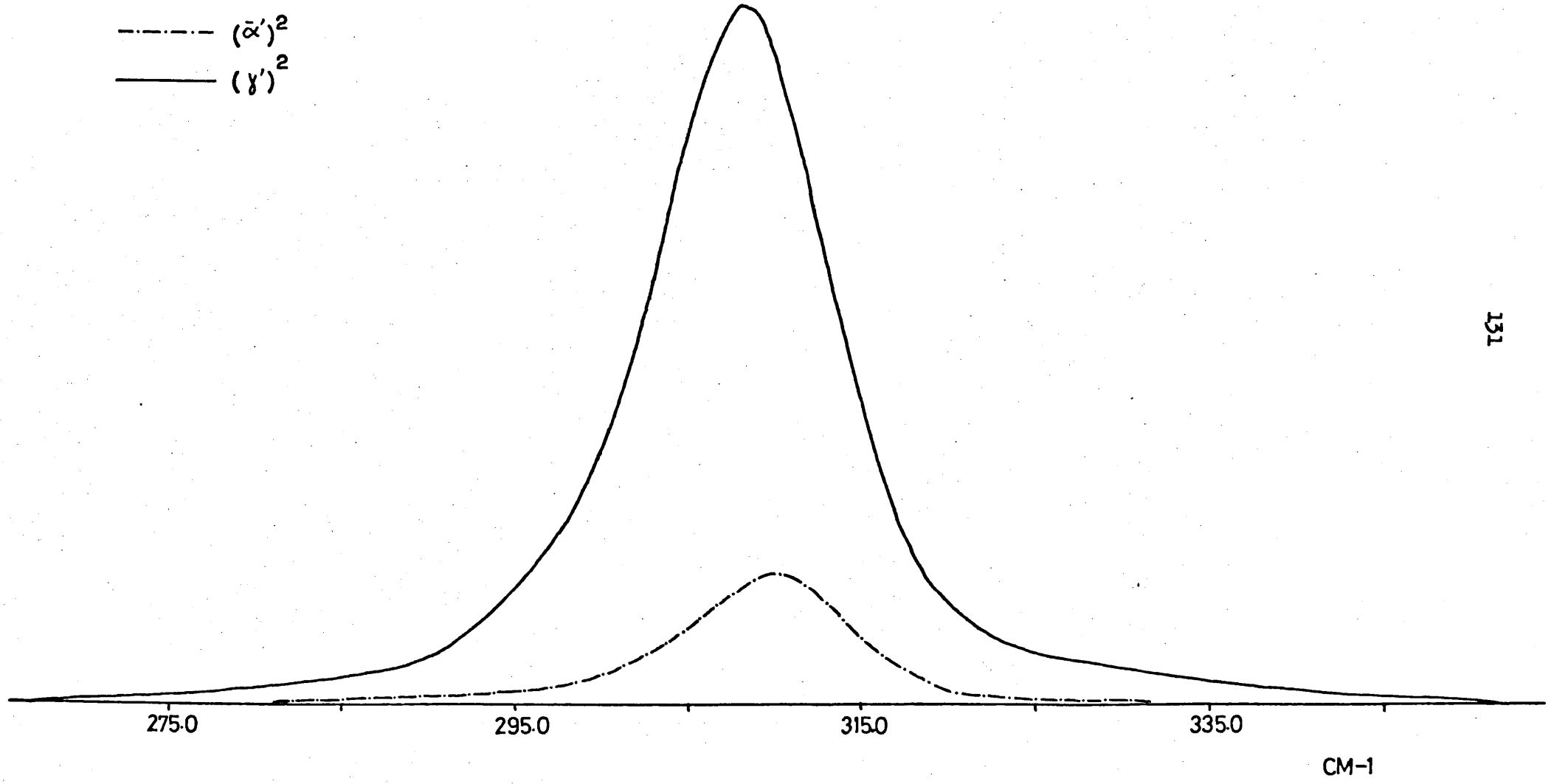

Figure 28b. A comparison of $(\bar{\alpha}')^2$ and $(\gamma')^2$ for iodine in benzene. The intensity is in arbitrary units.

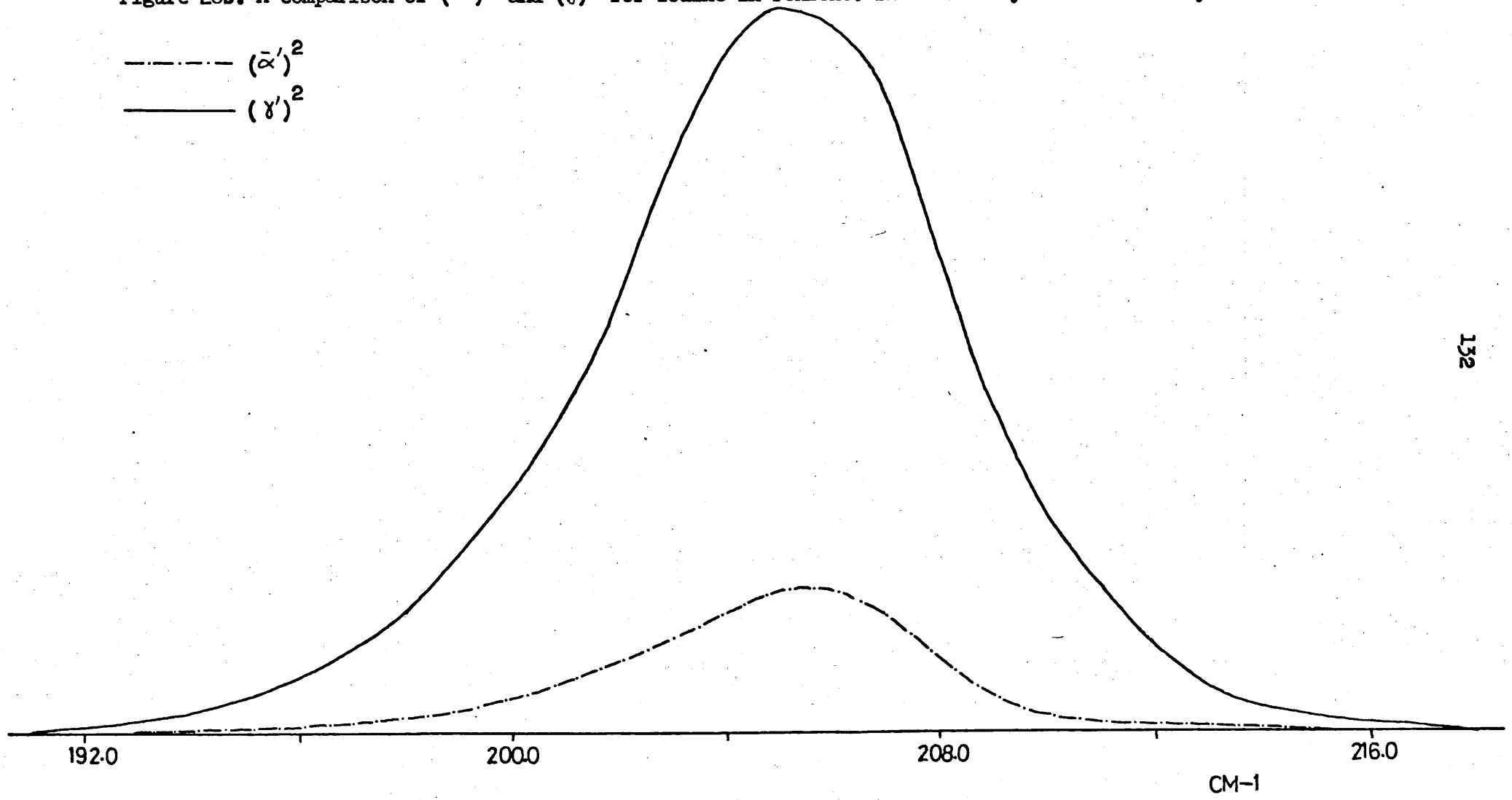

Table 7 Lorentzian function parameters of the isotopic and hot bands of Bromine in Benzene+

		hlf ht band width (cm^{-1})	Intensity ratio*	Band maxima
Complexed isotopic bands	$0 \rightarrow 1$ $^{79}Br_2$	9.5	50	308.85
	$0 \rightarrow 1$ $^{79}Br^{81}Br$	9.5	100	306.90
	$0 \rightarrow 1$ $^{81}Br_2$	9.5	50	305.00
Complexed first hot bands	$1 \rightarrow 2$ $^{79}Br_2$	9.5	11.3	306.65
	$1 \rightarrow 2$ $^{79}Br^{81}Br$	9.5	22.6	304.70
	$1 \rightarrow 2$ $^{81}Br_2$	9.5	11.3	302.80
Uncomplexed isotopic bands	$0 \rightarrow 1$ $^{79}Br_2$	8.0	41.8	312.25
	$0 \rightarrow 1$ $^{79}Br^{81}Br$	8.0	83.6	310.30
	$0 \rightarrow 1$ $^{81}Br_2$	8.0	41.8	308.40
Uncomplexed first hot bands	$1 \rightarrow 2$ $^{79}Br_2$	8.0	9.5	310.05
	$1 \rightarrow 2$ $^{79}Br^{81}Br$	8.0	18.9	308.10
	$1 \rightarrow 2$ $^{81}Br_2$	8.0	9.5	306.20

* Intensity ratio is calculated with respect to the isotopic band (complexed) $^{71}Br^{81}Br$ (see ref 76).

\+ These parameters are for fitting to the total ($I_{y(xx+xy)z}$) Raman band shape.

Table 8 Lorentzian function parameters of the isotopic and hot bands of Iodine in Benzene +

		half band width	Intensity Ratio*	Band Centre
Complexed isotopic band	$0 \rightarrow 1$ $^{127}I_2$	4.3	100	204.8
1st hot band	$1 \rightarrow 2$ $^{127}I_2$	4.3	37.1	203.4
2nd hot band	$2 \rightarrow 3$ $^{127}I_2$	4.3	13.8	201.97
Uncomplexed isotopic band	$0 \rightarrow 1$ $^{127}I_2$	2.3	75.1	206.9
1st hot band	$1 \rightarrow 2$ $^{127}I_2$	2.3	27.9	205.5
2nd hot band	$2 \rightarrow 3$ $^{127}I_2$	2.3	10.4	204.1

* Intensity ratio calculated w.r.t. the isotopic complexed band.

\+ These parameters are for fitting to the total $(I_{y(xx+xy)z})$ Raman band shape.

4.5 Discussion

4.5.1 Evidence for the 2:1 complex

From this current Raman study, the experimental results show that a 2:1 benzene:Cl_2 species is a major constituent of mixed benzene/CCl_4/Cl_2 systems. We failed entirely to detect a 1:1 component. However this is not surprising, because if we are to accept the magnitude of the 1:1 equilibrium constant, as given by Jao and Person[72], and the value of the 2:1 equilibrium constant as produced in this investigation, we see that the concentration of the 1:1 species is a minor component in the benzene concentrations used in this study. For instance, using the relationship

$$\frac{[Cl_2]_{complex}}{[Cl_2]_{free}} = [C_6H_6]'K \quad , \qquad 4.8$$

at a 3:1 CCl_4:benzene ratio the benzene concentration is 3.9 Ml^{-1}; and therefore the ratio of chlorine in a 1:1 species to free chlorine would be about 3.9 x .03 = .12. Thus provided that the Raman bands of the 1:1 species are not too different in contour and position from those of the 2:1 species, it is likely that we would fail to detect them in the experiments described in this communication.

At this point we must examine the compatibility of the results with other observations. Mulliken's[32] original suggestion, regarding the structure of the 1:1 benzene–iodine complex was of an arrangement (see figure 29a) in which the axis of the iodine molecule is parallel to

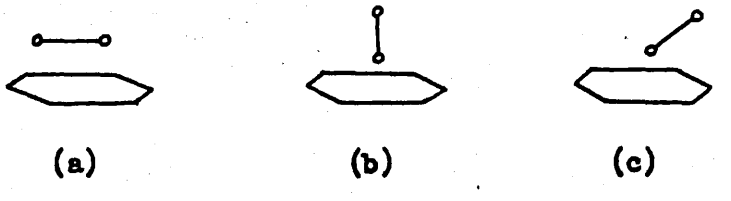

Fig. 29 Possible orientations of the 1:1 halogen-benzene complex.

the benzene ring. This view could not be substantiated by Collin and D'Or[65]. An oblique model[84] fig. 29 (c) was suggested in which one halogen atom was placed on the chief axis of the benzene molecule. However Ferguson[85] seemed to be strongly in favour of the axial model in which halogen atoms lie on the benzene's chief axis, which thus retains its six-fold symmetry (fig. 29 (b)).

Hassell and Stromme[86,87] carried out an x-ray crystallographic examination on single crystals of a 1:1 benzene-bromine, and a 1:1 benzene-chlorine compound. They found that the two benzene halogen compounds form isomorphous crystals belonging to the monoclinic system. Chains of alternating benzene and halogen molecules being parallel. The other notable feature was that the halogen molecules are equidistant from each of the two neighbouring benzene molecules in the chain, and they lie on centres of symmetry. Thus these crystals did not appear to be formed of one to one benzene-bromine complexes as units, but rather they are n-to-n infinite complexes. This form of structure was confirmed by infra-red studies by Person et al[88] on solid C_6H_6-Br_2. It is reasonable therefore to expect that our 2:1 species has the halogen oriented along the C_6 axes of the two benzene rings.

IR inactive

If the molecules lie on sites possessing a centre of symmetry then mutual exclusion exists and the halogen stretching mode is inactive. The observed weak absorption must therefore arise from the earlier proposed 1:1 structure formed either from the component stable species or from dissociation of the 2:1 complex.

Whilst we have been considering the perturbation of the ν(Cl-Cl) mode when dissolved in benzene, several studies have also been made on

the perturbations of the donor spectrum (benzene) by the halogen, these results are summarised in references 33 and 89. Two of the vibrations of the benzene molecule which are infra-red inactive give rise to bands when a halogen is added. These are the a_{1g} mode at 992 cm^{-1} and the e_{1g} mode at 850 cm^{-1}. Similarly, although all the Raman active modes have bands which show perturbations when a solvent is added, the a_{1g} and e_{1g} modes show specific enhancement when halogens are added. The appearance of these modes in the complex spectrum has been attributed to changes in ionisation potential and overlap integral[33] . Despite the fact that we have a centro-symmetric 2:1 complex these modes should still become active provided we take the ungerade combination.

Some of the most conclusive work on the benzene halogen complexes is that of Childs, Christian and Grundes[90-92] , using a constant activity method. This method was pioneered by Kortum et al[93,94] who calculated the equilibrium constants of iodine complexes in solution by measuring the increased solubility of iodine, in the solvent upon addition of a donor. The increased solubility was attributed to 1:1 complex formation; the equilibrium constant for this iodine benzene association was reported to be 0.3 $dm^3 mol^{-1}$ in cyclohexane solution. Childs used an extension of this solubility method based on maintaining constant activity of iodine through an equilibrium between tetramethyl ammonium polyiodide solids. As benzene is added to the hydrocarbon so the iodine concentration rises as a result of complex formation. Childs studied the change in iodine concentration in the benzene solution by monitoring the system at the isobestic point using electronic absorption spectroscopy. A plot of iodine concentration versus aromatic concentration gave a deviation from the

expected linear behaviour for 1:1 complexation. This was attributed to the formation of higher complexes, and it was found that a reasonable fit to the data, for the benzene-iodine complex, was obtained if the formation of a 2:1 as well as a 1:1 complex was assumed. For the methyl benzenes and pyridine it was found that the equilibrium constant for the 2:1 species (^2K) bore a simple statistical relation to the 1:1 equilibrium constant (^1K).

Thus $^2K \approx (^1K)^2/4$

The derivation of this relation involved the assumption that the acceptor has two sites, either of which is used to form a complex bond. In Childs' study these correspond to the two iodine atoms of the acceptor. These two sites were considered equivalent and independent. That is the formation of the 1:1 complex does not interfere with the subsequent formation of the 2:1 complex. Childs found that this procedure underestimated the observed value of ^2K by about a factor of 2, for the benzene-iodine complex. In a later note[92] the ^1K, as derived from the initial curvature, was corrected for change in the activity coefficients, by estimating these from solubility parameter theory[95]. The corrected equilibrium constants were very close to those obtained by spectroscopic methods. Data has not yet been published on the corrected ^2K. However it seems unlikely that the overall picture will change too drastically. This work on the benzene-iodine system is the only evidence that has previously been presented for the 2:1 species in solution, though the linear chain structure of the bromine-benzene solid complex implies that such multimolecule structures must exist. Certainly from a theoretical standpoint it is quite possible to have 2:1 complexes in this situation[96].

4.5.2 Entropy and Enthalpy changes

As mentioned earlier ^1K has been estimated from electronic and infra-red absorption studies[72] to be .03 $dm^3 mol^{-1}$. We see that our ^2K is far greater than can be explained on a simple statistical basis used by Childs. This implies an extra stabilization of the $a\sigma.b\pi$ orbitals through mutual interaction, or an extra entropy contribution.

The entropy change of -30 ± 5 J $mol^{-1}K^{-1}$ shows a large molecular ordering compatible with the idea of a specific structure of the molecular complex as opposed to a loose weakly directed association. If the entropy change is related to the molar volume by

$$-\Delta S = R \ln (V'_2 / V_2) \qquad 4.9$$

then an estimate of the reduction in the molar volume by a factor of 30 is obtained. It is extremely unlikely that complexation could lead to a very significant change in the translational free volume, and so most of the entropy change must be related to loss of rotational freedom in the complex. The enthalpy change of -3.0 (± 1) kJ mol^{-1} is small though in keeping with estimates of the enthalpy of formation of the 1:1 complexes[33]. Unfortunately no data exists as yet on ΔS and ΔH for the 2:1 iodine complex, though the tetramethyl ammonium iodide method ought to allow such data to be derived.

4.5.3 Frequency shift between the maxima of $(\bar{a}')^2$ and $(\gamma')^2$

Two interpretations have been considered here to explain the phenomenon of the frequency shift between the maxima of $(\bar{a}')^2$ and $(\gamma')^2$. These are:

a) There are two overlapping complexed bands with different depolarization ratios.

b) There is an inherent shift in the maxima of the isotropic and anisotropic components.

The experimental band contour fittings seem well satisfied by interpretation (a). Thus we have obtained good simulations of the observed spectra using two Lorentzians each with their isotopic sub-bands separated by 7 cm^{-1} and with average depolarization ratios of .46 and .21 (see Table 3). (The uncomplexed band has a depolarization ratio of .065). The consistency in the relative intensities (see Table 2D) suggests that they arise from complexes of the same stoichiometry, or that the basic assumption of two bands is incorrect. If there really are two complexed bands we can only speculate that there are two conformations of equal energy of formation. The crystal structure would suggest that one of these conformations has the chlorine situated along the C_6 axis i.e. perpendicular to the aromatic planes. The other conformation could have the chlorine parallel to the aromatic planes.

Concerning the second interpretation, Schwartz and Wang[97] recently discussed the effects of angular dependent forces on peak frequencies in the isotropic and anisotropic Raman scattering. According to their analysis the non-coincidence of the peak frequencies could be analysed by taking the first spectral moment of the spectral density function. If the polarized spectrum is due mainly to isotropic scattering (i.e. when the depolarization ratio of the band is small), then the difference in the first intensity moments for $(\bar{a}')^2$ and $(\bar{\gamma})^2$ is given by

$$\Delta = 6B + h^{-1} < (V^1 - V^o)\left((\gamma')^2 | <\gamma'>^2 - (\bar{\alpha}')^2 | <\bar{\alpha}'>^2\right) > \qquad 4.10$$

where B is the rotational constant, V^1 and V^o are the intermolecular interaction potentials for the ground and excited states. Given that B_e is about .24 cm^{-1}, we see that most of the shift has to be explained by the change in the intermolecular potential on vibrational excitation. This is not unreasonable. However, without further information as to the magnitude of the second term any further analysis cannot be other than highly speculative. In conclusion we maintain that the observed contours are not compatible with this idea, attractive as it may be. For example the anisotropic component of the Cl–Cl stretch of Cl_2 in benzene (figure 14b) is remarkably symmetric. In view of the isotopic shifts of the component bands, it is difficult to understand for a single set of bands. As can be seen from figure 14 (b) it is easily understood in terms of two sets of overlapping bands. The same is true for the other solutions and components, although it becomes less apparent as the tetrachloromethane concentration is increased.

Chapter 5 THE RAMAN SPECTRUM OF LIQUID CHLORINE

5.1 Introduction

Following our studies of the Cl_2:C_6H_6:CCl_4 system we considered observing the spectrum of liquid chlorine at different temperatures, in order to determine information on its molecular motion. In Chapter 2.5 we noted that the calculation of orientational correlation functions from infra-red and Raman spectra is a widely used method of deducing the nature of molecular motion in the liquid phase. There is however one problem in the application of the theory listed in 2.5.3, and that is that the theory only applies to single bands. Konynenburg and Steele listed the possible complications only two of which concern this study[14]. These are:

(a) If the molecules contain different isotopic species (as indeed liquid chlorine does), then the spectral band will actually be made up of several overlapping bands with different band centres. This can lead to considerably broader bands than would be obtained for a single species.

(b) A similar correction must be applied if an appreciable number of molecules are in excited vibrational levels. The hot bands that result are slightly displaced from the fundamental band by anharmonicity and again give rise to broadening that is unrelated to rotational motion.

Konynenburg and Steele showed that it is not difficult to eliminate the effects of broadening due to (a) and (b); the calculation is essentially the same in both cases and applies to any source of broadening where the band consists of a number of incompletely resolved peaks, all of the same band shape, centred at frequencies ω_j and having fractional intensity x_j. Then the intensity at frequency ω is

$$I(\omega) = \Sigma x_i I(\omega - \omega_j) \qquad 5.1$$

where ω and ω_j are measured relative to the apparent band centre. Konynenburg and Steele then formulated the determination of the apparent correlation functions in terms of the real Fourier transform. However as discussed by Hill et al[98] it is essential to take the modulus of the complex transformation when the spectral structure is sharp, as it is for Cl_2. Thus the apparent Raman reorientation correlation function $C'_{2R}(t)$ is

$$C'_{2R}(t) = C_{2R}(t) \sqrt{\left[\Sigma x_j(\cos \omega_j t, \; i \sin \omega_j t)\right]^2} \qquad 5.2$$

where it is assumed that the true rotational band shape is symmetrical and identical for each of the overlapping bands and gives rise to the true rotational correlation function $C_{2R}(t)$. In this manner the bands can be separated.

There are two principle objectives to this study. (a) To find a model for the molecular motion, and (b) to determine the second and fourth moments[99]. The second moment arises from three types of terms, (a) the fluctuation of the difference between the intermolecular potentials for the excited state and the ground state averaged in the initial external state; (b) rotational kinetic energy terms and (c) collision-induced terms. If the shift fluctuation effect is small and so are the collision induced terms, a measurement of M(2) is essentially of the average molecular rotational kinetic energy.

5.2 Results and Discussion

5.2.1 General Details.

The main problem encountered in running the spectra was in

Figure 30. The temperature dependence of the anisotropic component, $(\gamma')^2$, of the Raman spectrum of liquid chlorine.

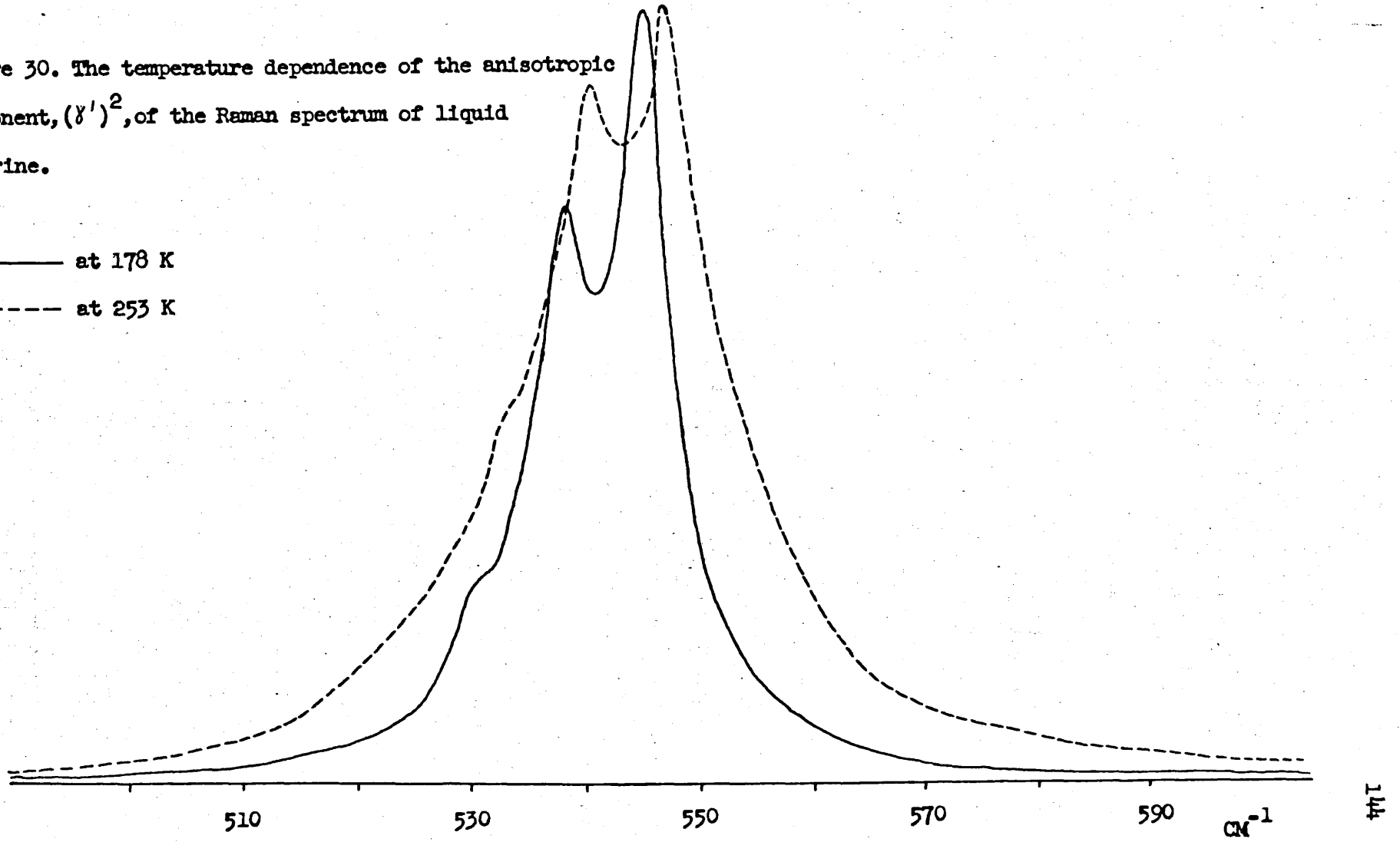

determining how much intensity was in the spectral wings. Eventually it was decided to record the spectrum up to 130 cm^{-1} either side of the chlorine band centre. Details of equipment and experimental procedure were listed in section 4.2.1. We processed our data on a CDC 6600 computer using a program developed by D. Steele and I.R. Hill. As in the previous Raman study the observed spectral intensities $I_{y(xx)z}$ and $I_{y(xy)z}$ were converted to the isotropic $(\alpha')^2$ and anisotropic components $(\gamma')^2$ (using the nomenclature of Woodward[4]).

5.2.2 The Correlation Functions

The anisotropic components of liquid chlorine at 178°K and 253°K are shown in figure 30. The half height band width of the anisotropic component is seen to broaden considerably with increase of temperature as would be expected in terms of a kinetic effect. There is also an observable shift between the maxima of $(\bar{\alpha}')^2$ and $(\gamma')^2$ with increase of temperature. At 178 K there is no observable shift in the maxima, however with increase of temperature there is a linear increase up to 2 cm^{-1} at 253 K (see figure 31).

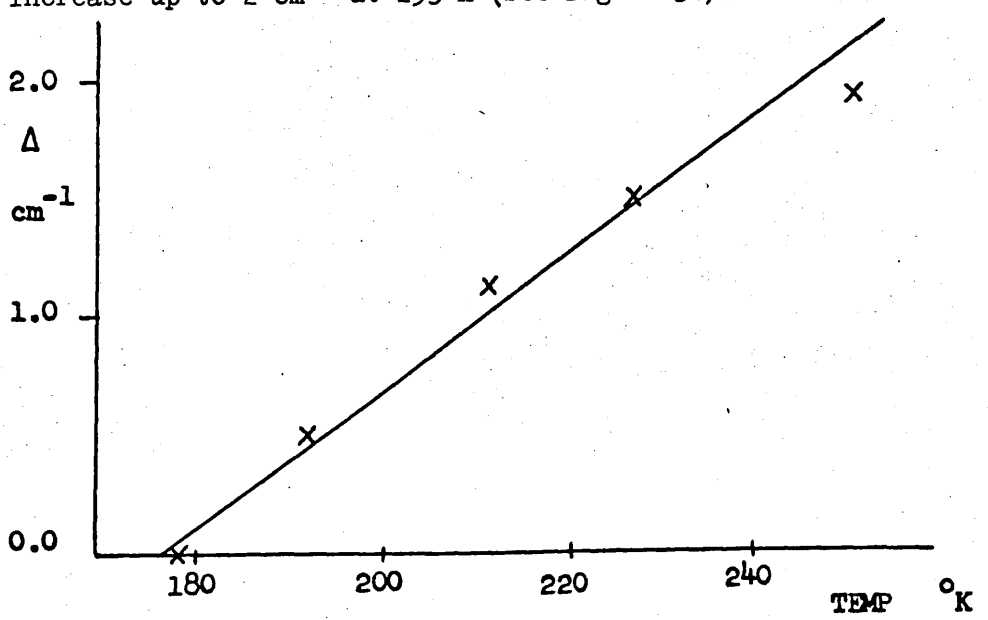

Figure 31 Graph of the shift (Δ) between the maxima of $(\alpha')^2$ and $(\gamma')^2$ against absolute temperature.

If we consider the difference in band maxima in terms of equation 4.10, developed by Wang and Schwartz[97], we see that the shift of 2 cm^{-1} at 253°K could be almost entirely explained by the 6B term. However as B is not considered to be affected by temperature, we see no reason for the shift to decrease to zero with decrease of temperature. Thus although the shift of the maxima appears to be reproducible we can find no satisfactory explanation.

The rotational correlation functions were determined at five temperatures over the interval 178°K to 253°K, which covers nearly the entire liquid range of chlorine. These functions were obtained by Fourier transformation of the Raman spectrum using the relations of section 2.53 and equation 5.2.

Figure 32 shows the ln $C_{2R}(t)$ against time plots for all the temperatures of liquid chlorine studied. At 253°K the liquid chlorine is 14°K above the temperature at which the pressure of the chlorine is 1 atmosphere, and the reorientation is seen to be rapid. The correlation function decreases to about 0.2 p.sec before exponential decay (given by the linear portion of the ln $C_{2R}(t)$ graph) is observed. From all the ln $C_{2R}(t)$ graphs in figure 32 we see that the decay of the orientational correlations is slowest in liquid chlorine at 178°K. We therefore deduce that the rotation is less hindered at the higher temperatures, as would be expected on purely kinetic grounds.

In figure 32 we also show the free rotor functions at 253°K and 178°K. At short times the free rotor correlation function is given by equation 2.3 1. We see that in general even at very short times the free rotor function lies well below the observed functions.

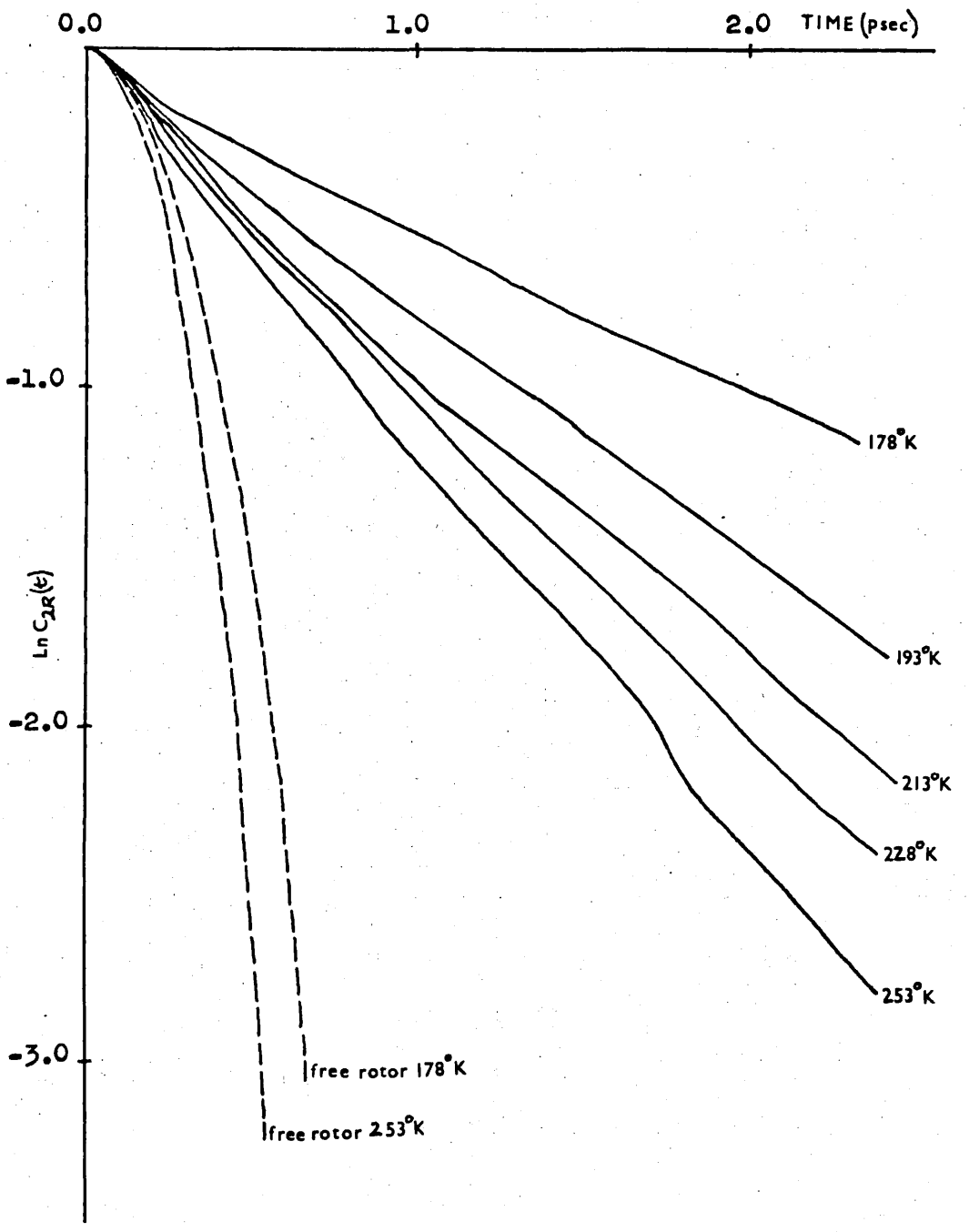

Figure 32. The temperature dependence of the ln $C_{2R}(t)$ against time plot, for the Cl-Cl stretch of liquid chlorine.

5.2.3 Rotational relaxation times

As discussed in section 2.5.6 the rotational diffusion model is often used to describe the rotational motion in the liquid state. When very small diffusive steps are used in the hydrodynamic model, then the correlation time associated with the motion of the symmetry axis of a symmetric top molecule can be calculated from

$$\tau = f\left(\frac{4\pi a^3 \eta}{3\ kT}\right) \qquad 5.3$$

Gierer and Wirtz[100] gave the microviscosity factor f in terms of, a, the radius of the molecular sphere in question, and a_L the radius of a molecule of the surrounding medium, such that

$$f = \left(\frac{6a_L}{a} + \frac{1}{(1 + (a_L/a))^3}\right)^{-1} \qquad 5.4$$

For a pure liquid $a_L = a$, and thus the equation 5.4 collapses to $1/6.125 = .163$.

Assuming the chlorine molecule to be a simple symmetric top with a molecular radius of 1.988×10^{-8} cm, then utilizing the viscosity values of liquid chlorine quoted in table 9 we can determine the relaxation times τ_2.

Before we discuss our results more fully we note that molecular orientation in liquid chlorine has been studied by other authors[101-103] using nuclear resonance techniques. The most recent work has been done by Obermyer and Jones[103] who determined the ^{35}Cl nuclear spin lattice relaxation times in liquid chlorine from the melting point at 173°K to the boiling point 243°K. They assumed that the molecular reorientation process was described in terms of a correlation function C(t), where C(t) was an exponential of the form $\exp(t/\tau_2)$. Also if

τ_2 is much less than the Lamor period (i.e. the resonance condition does not change) then the spin-lattice and spin-spin relaxation times, T_1 and T_2, are equal and are given for a nucleus with spin 3/2 by

$$T_1^{-1} = T_2^{-1} = \frac{1}{10} (e^2qQ/\hbar)^2 \tau_2 \qquad 5.5$$ (see reference 104)

where $(e^2qQ/\hbar)$ is the quadrupole coupling constant (in radial frequency) resulting from the nuclear electric quadrupole moment interacting with the electric field equation. The quadrupole coupling constant measured in solid chlorine was given as 109 MHz.

In figure 33 the values of τ_2, calculated from the spin lattice relaxation times, are graphed against temperature. These values obtained from n.m.r. are compared with our experimental values of τ_2, obtained as the reciprocals of the gradients of the linear portions of the $\ln C_{2R}(t)$ against time graphs (see figure 32). The solid line in figure 33 represents the theoretical values of τ_2, obtained for a hydrodynamic model. Table 9 gives the precise values of τ_2, for the hydrodynamic model and from our experiments.

For liquid chlorine the Raman scattering will measure an average reorientation time associated only with the tumbling motion given by[30]

$$\tau_{2_{RAMAN}} (6D_\perp)^{-1}$$

where $D_\perp$ is the diffusion constant for rotation of the symmetry axis. N.M.R., on the other hand, depending on the relative orientation of the molecular electric field gradient, should couple to a complicated combination of the tumbling and spinning motion. For n.m.r. it has been shown that the average reorientation time is given by[105-106]

$$\tau_{2_{nmr}} = 2K_2\left\{\frac{1}{4}(3\cos^2\theta - 1)^2/6D_\perp + [(3\sin^2\theta\cos^2\theta)/5D_\perp + D_{11})] + \frac{3}{4}\sin^4\theta/(2D_\perp + 4D_{11})\right]$$

where K_2 is a constant depending on the nuclear spins and the quadrupole

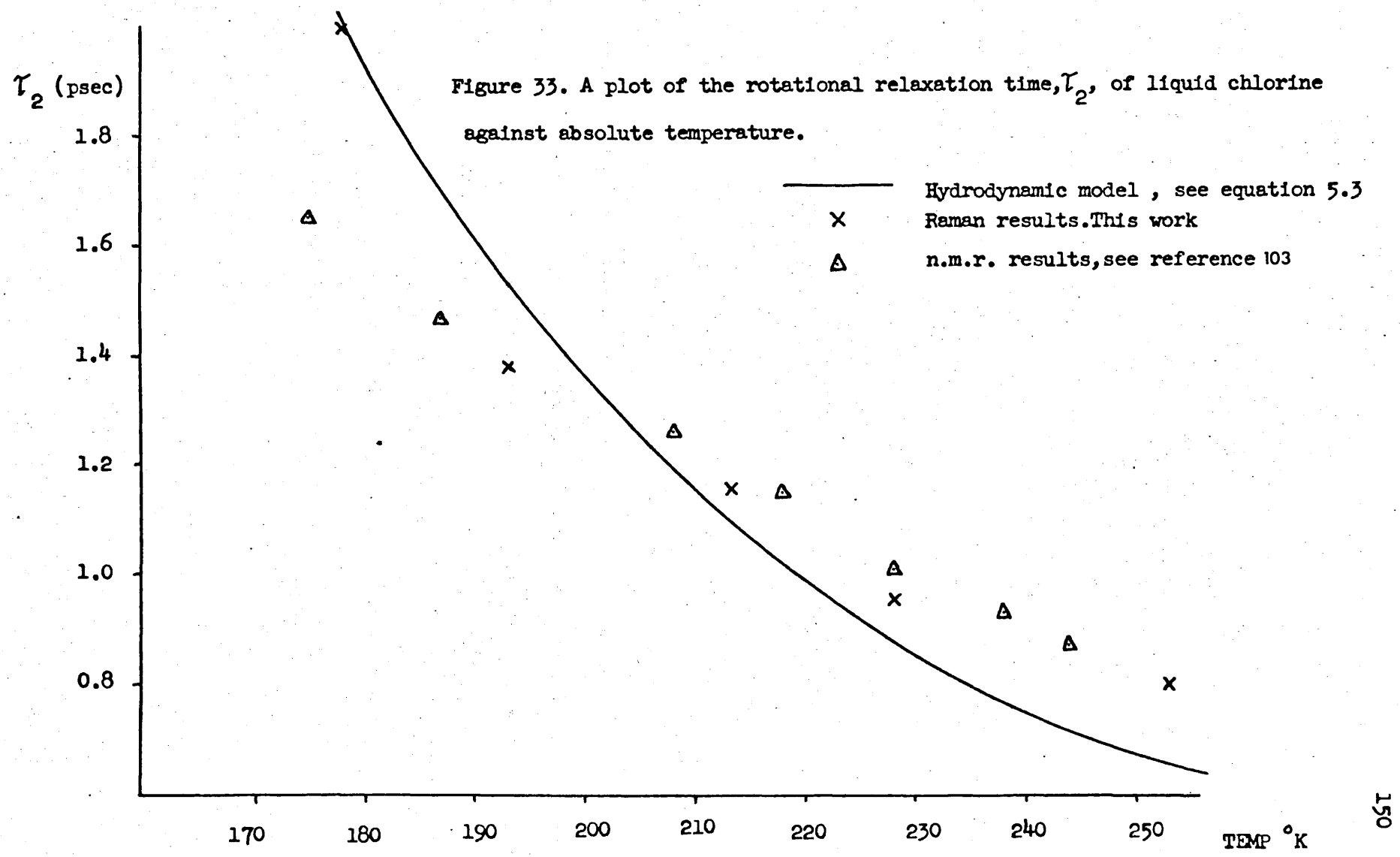

Figure 33. A plot of the rotational relaxation time, τ_2, of liquid chlorine against absolute temperature.

coupling constant. It has a value of $\frac{8}{15}$ (see reference105). Θ is the angle between the symmetry axis of the molecule, and the z axis of the molecular coordinate system which diagonalizes the field gradient tensor at the size of the nucleus of interest.

If the spinning motion is much faster than the tumbling motion then $D_{\parallel} >> D_{\perp}$, which implies that the second and third terms are negligible. However it should also be noted that for the linear Cl_2 molecule the angle Θ is zero, and thus the second and third terms are zero. This implies that

$$\tau_{2\,nmr} = 2\frac{8}{15}\left((1/4)(2)^2/6D_{\perp}\right)$$

$$\approx \frac{1}{6D_{\perp}} = \tau_{2\,RAMAN}$$

It would seem then, that the observed good agreement, between the values of τ_2 from the nmr and the Raman, is reasonable. From these independent measurements it is also apparent that the experimental values of τ_2 for liquid chlorine are very close to thos obtained from a hydrodynamic model.

Thus we conclude that at long times the Debye diffusion theory seems to explain well the molecular motion in liquid chlorine.

Table 9 The theoretical and observed rotational relaxation times τ_2, of liquid chlorine[a]

Temperature ^{o}K	τ_2 theoretical[b] p.sec.	τ_2 observed p.sec	viscosity η[c] cp
178	2.01	2.00	.92
193	1.54	1.38	.76
213	1.10	1.16	.61
228	.88	.95	.53
253	.65	.80	.43

(a) The liquid chlorine is under its own vapour pressure.

(b) τ_2 values calculated for a hydrodynamic model given by equation 5.3

(c) Using viscosity data from reference 107 . The equation of the viscosity temperature curve is given by $\eta_T = \eta_o /(1+AT + BT^2)$ where η_o, A and B are constants.

5.2.4 Spectral Moment Analysis of Liquid Chlorine

As we noted briefly in section 2.5.3 another type of information about intermolecular forces can be deduced from spectral moment calculations[99]. Using a relation between the second and fourth band moments it is possible to derive the mean square torque $\langle (\dot{\Omega}V)^2 \rangle$, acting on the scattering molecule. The second moment, which depends essentially on molecular parameters and temperature, gives an idea of the accuracy of the experiment if reorientation is the only relaxation process involved. In the classical approximation, and taking into account the vibration-rotation coupling, the second moment for absorption by linear molecules is given by[108].

$$M(2) = 4\ (kT/hc)B_1 + 8(kT/hc)B_1\Delta + 2(kT/hc)^2\Delta^2 \qquad 5.6$$

where $\Delta = (B_1 - B_o)/B_o$, B_o and B_1 being the rotational constants of the ground and first excited vibrational states respectively. To a first approximation M(2) simplifies to 4 (kT/hc)B.

The second moment of a Raman band of a linear molecule is equal to three times that for absorption; while the relationship between second and fourth moments for scattering is[109]

$$M(4) = 2.66\ M(2)^2 + 12B_o^2\ \langle (\dot{\Omega}V)^2 \rangle \qquad 5.7$$

The experimental Raman second moments can be calculated[7] from the anisotropic second moments and the vibrational second moments using the relationship

$$M_{rot} = M_{aniso}(2) - M_{vib}(2) \qquad 5.8$$

The vibrational second moment for liquid chlorine has a value of $10.6\ cm^{-2}$ at $178^{o}K$. This is about 2% of the total value of M(2). This would suggest that the vibrational second moment has little effect on the overall results of M(2) for liquid chlorine. Thus in this study we neglected its contribution.

As we noted in section 2.4 the Fourier transform has the reciprocal property that when a function is transformed, and the resulting function is retransformed, we finish up with the original function. If this procedure is applied to the anisotropic component of the polarizability $(\gamma')^2$, and if we correct the chlorine spectrum for isot opic and hotband distortion using Konynenburg and Steele's formulae (see equations 5.1 and 5.2), then we can obtain a single band from which we can obtain the second moment. The experimental normalized second moment is given by[7]

$$M(2) = \int_{band} \omega^2 I(\omega) d\omega \Big/ \int_{band} I(\omega) d\omega \qquad 5.9$$

Experimental values for M(2) and M(4) at different temperatures are given in table 10. The theoretical values are also listed. Values of the mean square torque are given based on the experimental values of M(2) and M(4), from $178^{o}K$ to $253^{o}K$.

The classical invariance of the second moment provides a convenient check on the completeness of the frequency range of an experimental band shape. If the second moment of the depolarized Raman band of chlorine had been far below its classical value then we might have suspected that measurements were not carried far enough into the 'wings' of the band, and the correlation function obtained by

Table 10 Raman band moment calculations and determination of the mean square torques for liquid chlorine

Temperature (°K)	Theoretical M(2) (cm^{-2})	Observed M(2) (cm^{-2})	Observed M(4) (10^6 cm^{-4})	$\langle(\omega v)^2\rangle$ † (10^4 cm^{-2})
178	347.3	443.0	2.409	266.0
193	387.5	510.4	2.464	249.9
213	427.6	551.6	2.830	285.2
228	457.7	588.6	2.835	270.0
253	507.8	627.7	3.004	276.0

† Using a value of B_o for $^{35}Cl_2$ of 0.243 (reference 79).

Fourier transformation in such a case would have been incorrect. However as we see in Table 10 the experimental value of M(2) is significantly larger than is expected. This could be due to two factors: (a) The background trace recorded for each of the spectra could have been incorrectly recorded. (b) There is an extra effect which is contributing excess intensity to the depolarized Raman spectrum. Gordon[10] assumed that the sole source of spectral broadening was molecular reorientation. Since then, however, it has become evident that molecular interactions and vibrational relaxation contribute to the spectra in addition to molecular reorientation. The existence of the excess intensity in the depolarized Raman bands has been interpreted in terms of a collision induced effect[110-114]. (In other words, strong molecular interactions are causing a fluctuating distortion of

the polarizability tensors). It has also been assumed that such effects must be separated.

Konynenburg and Steele[112] attempted a separation by examination of the experimental correlation function. Whilst Dardy et al[111] estimated a collision induced spectrum and removed it prior to Fourier transformation. The latter approach is used here.

Although no completely satisfactory method for eliminating the effects of the collision induced phenomena exists at the present time, a simple procedure that has been utilized in recent work[112-114] is to assume that the reorientational and collisional induced spectral intensities are additive

$$I(\Delta\nu)_{\text{total}} = I(\Delta\nu)_{\text{coll.}} + I_{OR}(\Delta\nu) \qquad 5.10$$

where $\Delta\nu$ is the frequency shift from the band centre. $I_{OR}(\Delta\nu)$ gives the shape of the band around the band centre; it approximates to a Lorentzian given by the equation

$$I_{OR}(\Delta\nu) = \frac{I(0)}{1 + (\tau_c \Delta\nu)^2} \quad \frac{\nu_{\frac{1}{2}}^2}{\nu_{\frac{1}{2}}^2 + 4(\Delta\nu)^2} \qquad 5.11$$

$I(0)$ is the intensity at the band cetre, $\nu_{\frac{1}{2}}$ is the half band width and τ_c is an adjustable parameter which should be close to the average time between molecular collisons.

$I_{coll}(\Delta\nu)$ is designed to fit to the wings of the band and is given by an exponential equation which we have taken from the theory[110,114]. It has the form

$$I_{coll}(\Delta\nu) = a(\Delta\nu)^q \frac{\exp(-|\Delta\nu|/p)}{(1 + \exp(\frac{-hc\,\Delta\nu}{kT})} \qquad 5.12$$

where a, p and q are constants whose values are determined partly from theory and partly by the fitting of data. In particular q is still the subject of controversy; in the wings, any value of q between 1 and 2 has been used to try to fit to the data. Currently no realistic theory exists for non-spherical molecules that is capable of predicting an accurate value of q, or for that matter that the spectral intensities are additive. For liquid chlorine we found that a value of q = 1.2 gave the best fit to most of the spectra. Values of a and p were selected so that $I_{coll}(\Delta\nu)$ gave a good fit to the data in the wings. One rather disturbing feature of this fitting procedure was that the Lorentzian component, $I_{OR}(\Delta\nu)$, did not appear to be damped towards high frequency shifts from the band centre.

On removal of the collision induced component from the observed band, the second moment was taken of the resulting band. These values of M(2), for the observed minus collision-induced spectra, are given in Table 11. Comparison of these values with the theoretical values of M(2) listed in Table 10, suggests that too much collision-induced component has been removed. It seems that at best this approach is acceptable only when the collision-induced term is small. However, if the collision-induced component is smaller than used in our fitting procedure, and if the Lorentzian component is undamped (as we found), then it is not possible to obtain a good fit to the wings any more. Thus until such time as we obtain more accurate measurements of the intensity in the far wings, we observe that it is by no means certain that there is a collision-induced contribution in the band contour. Finally we note that if a collision-induced contribution does occur, the results of Tables 10 and 11 suggest that its primary effect would be to increase M(4) and thereby to increase the intermolecular torques.

Table 11 Raman band moment calculations and determination of the mean square torques, for the observed spectra of liquid chlorine minus a collision-induced contribution.

Temperature ^{o}K	Observed-collisional $M(2)$ cm^{-2}	Observed-collisional $M(4)$ $(10^{6}\ cm^{-4})$	$\langle(\Omega V)^2\rangle$ $(10^{4}\ cm^{-2})$
178	206.60	.900	111.0
193	243.40	.954	112.4
213	264.85	.984	112.6
228	274.10	1.08	124.2
253	367.00	1.27	129.0

In conclusion we see from Table 10 that the values of the mean square torque (of about 270 x 10^{4} cm^{-2}) seem to be fairly independent of temperature.

Perchard et al[21] give a value of 53 x $10^{4}cm^{-2}$ for the mean square torque of liquid HCl. Thus our values for liquid Cl_2 are higher by a factor of five. This is probably due to the fact that in the chlorine molecule there are, obviously, two comparatively heavy atoms, whereas in the HCl molecule one atom is heavy and the other light.

As we have observed, the effects of the intermolecular forces are seen in the terms of order t^4. The hindering of rotation increases the coefficient of t^4 by an amount proportional to $\langle(\Omega V)^2\rangle$. Thus as the mean square torque of liquid chlorine is five times larger than that of HCl, and $C_{2R}(t)$ for HCl lies above that for free molecules, then we would expect the rotational correlation function for chlorine to lie above the curve for free molecules as well. This is indeed the case as was seen in figure 32.

PART TWO

Chapter 6 GENERAL THEORY OF ABSOLUTE INFRA-RED INTENSITIES

6.1 Absorption of radiation[115]

A complete understanding of the absolute intensities of infra-red absorption bands requires a close look at the mechanism by which electromagnetic radiation interacts with matter. In the presence of a radiation field, there is a probability that a molecule will exchange energy with the field and appear in a quantum state other than its original. This process gives rise to a spectral line of finite width and intensity at a particular frequency ν given by the Bohr frequency rule.

$$\nu_{n'',n'} = \nu_{n',n''} = \frac{(E' - E'')}{h} \qquad 6.1$$

where E refers to the energies of the n'', n' quantum states and h is Planck's constant. If $E'' < E'$, radiation is absorbed by the molecule, giving rise to an absorption spectrum, and if $E'' > E'$ radiation is emitted by the molecule giving rise to an emission spectrum.

The intensity of the resulting spectral line is determined by the probability of the transition which gives rise to the line. It can be shown that the probability of a randomly orientated molecule (for example in the gas) being promoted from a state n'' to a state n' is

$$\frac{8\pi^3}{3h^2} |\langle n'' | P | n' \rangle|^2 \rho(\nu_{n'',n'}) \qquad 6.2$$

where $\langle n'' | P | n' \rangle$ is the quantum mechanical matrix element of the dipole moment, and $\rho(\nu_{n'',n'})$ is the density of the radiation of the particular frequency matching the quantum jump. The probability of induced emission is given by the same expression with the primes reversed and thus the net absorption probability is given by

$$\frac{8\pi^3}{3h^2} \langle n'' | P | n' \rangle^2 \rho (\nu_{n'',n'})(N_{n''} - N_{n'}) \qquad 6.3$$

where N_n represents the number of molecules per unit volume in each state. Each such transition reduces the energy of the field by an amount $h\nu_{n'', n'}$ so that the net loss of energy for a differential element of absorbing length dl and of unit cross sectional area will be

$$-dI = (\nu_{n'',n'}) \frac{8\pi^3}{3h} \langle n'' | P | n' \rangle^2 \rho (\nu_{n'',n'})(N_{n''} - N_{n'}) \, dl \qquad 6.4$$

The radiation flux density is related to the radiation density by

$$I = \bar{c}\rho \qquad 6.5$$

where $\bar{c}$ is the velocity of light. Substitution for ρ followed by integration gives

$$\ln (I_o/I) = (\nu_{n'',n'}) \frac{8\pi^3}{3\,h\bar{c}} \langle n'' | P | n' \rangle^2 (N'' - N') \qquad 6.6$$

At equilibrium the populations of the states ψ'' and ψ' follow the Boltzmann distribution and thus

$$(N'' - N') = c N Q_v^{-1} [\exp(-E_{n''}/kT) - \exp(-E_{n'}/kT)] \qquad 6.7$$

where $Q_v = \sum_i \exp(-E_i/kT)$. N is Avogadro's number and c is the molar concentration.

In the case of any but the simplest polyatomic molecule it is not possible to determine an experimental quantity with 6.7. Rather the transition probabilities for all the rotational components must be summed and this quantity compared with the total integrated intensity of the vibrational transition. Thus we have

$$\Gamma_{n'',n'} = \frac{1}{cl} \int_{\text{band}} \ln (I_o/I) d\ln \nu \qquad 6.8a$$

$$= \frac{8\pi^3 N}{3hc} \langle n'' | p | n' \rangle^2 Q_v^{-1}$$

$$x\left[\exp(-E_{n''}/kT) - \exp(-E_{n'}/kT)\right] \qquad 6.8b$$

Equation 6.8 is applicable as it stands to a fundamental transition (i.e. from n'' as the ground vibrational state $v = 0$, to n', having vibrational quantum number $v = 1$).

Equation 6.7 is exact for a single transition between two levels n' and n''. However, such a transiton can seldom be studied in practice, for most spectral bands consist of a main band with a number of overlapping hot bands. In the case of a diatomic molecule for example, there are hot bands due to $2 \leftarrow 1$, $3 \leftarrow 2$ etc., which fall at about the same frequency as the $1 \leftarrow 0$ transition. Vibration bands of polyatomic molecules are even more complicated.

The experimental intensity is usually determined by integrating over a fundamental and all the associated hot bands, and for comparison with this quantity equation 6.7 should be summed over all the corresponding transitions. For a diatomic fundamental this yields the quantity,

$$\Gamma_{(obs)} = \frac{8\pi^3 N}{3hc} \sum_{v=0}^{\infty} \langle v | p | v+1 \rangle^2 Q_v^{-1}$$

$$x\left\{\exp\left[-\frac{v h\omega}{kT}\right] - \exp\left[-(v+1)\frac{h\omega}{kT}\right]\right\} \qquad 6.9$$

In the harmonic approximation

$$\langle v | p | v+1 \rangle^2 = \frac{h}{8\pi^2 \omega c} (v+1) \left(\frac{dp}{dQ}\right)^2 \qquad 6.10$$

(dp/dQ is the derivative of the dipole moment with respect to a normal coordinate Q, see section 6.2)

and hence,

$$\Gamma_{(obs)} = \frac{N\pi}{3\bar{c}^2\omega}\left(\frac{dp}{dQ}\right)^2 Q_v^{-1} \times \sum_{v=0}^{\infty} (v+1)\left\{\exp\left[-\frac{vh\omega}{kT}\right] - \exp\left[-(v+1)\frac{h\omega}{kT}\right]\right\} \quad 6.11$$

The summation in equation 6.11 may be carried out exactly to yield.

$$\Gamma_{(obs)} = \frac{N\pi}{3\bar{c}^2\omega}\left(\frac{dp}{dQ}\right)^2 \quad 6.12$$

When the vibration is degenerate the expression 6.12 applies to each of the components of the degeneracy so that it is necessary to introduce a degeneracy factor, g, into the equation

$$\Gamma_{(obs)} = \frac{N\pi g}{3c^2\omega}\left(\frac{dp}{dQ}\right)^2 \quad 6.13$$

6.2 Relationship of Intensity to the change of dipole moment[115]

The quantum mechanical matrix element of the dipole moment can be expressed as

$$\langle 0 | P | 1 \rangle = \int \psi_0^* \, p \, \psi_1 \, d\tau \quad 6.14$$

where ψ_0^* is the complex conjugate of the wavefunction for the ground state, ψ_1 is the wavefunction for the state $v = 1$, and $d\tau$ is the volume element of the space configuration. p is a vector quantity having components p^x, p^y, p^z which can be expressed

$p^x = \sum_i \epsilon_i x_i$, $p^y = \sum \epsilon_i y_i$ and $p^z = \sum \epsilon_i z_i$. Where ϵ_i is the charge on the ith particle, and x, y and z are the space fixed Cartesian coordinates. These components of p may be considered in terms of a Taylor series with respect to the normal coordinate Q_i.

Thus

$$p^{\xi} = p_o^{\xi} + \sum_{k=1}^{3N-6} \frac{\partial p^{\xi}}{\partial Q_k} Q_k + \text{higher order terms} \qquad 6.15$$

Where ξ stands for the Cartesian directions. It is common practice to consider only the constant and linear terms in equation 6.15, and so in the harmonic oscillator approximation, for a transition between the ground state and the first excited state of the ith normal mode

$$\langle 0 \mid p^{\xi} \mid 1 \rangle = \frac{\partial p^{\xi}}{\partial Q_k} \int \psi_o^{*} Q_k \psi_1 \, dQ_k \qquad 6.16$$

The integral involving the harmonic oscillator wavefunctions is expressed in explicit form by

$$\int \psi_o^{*} Q_k \psi_1 \, dQ_k = \left(\frac{h}{8\pi^2 \bar{c} \omega_i} \right)^{\frac{1}{2}}$$

hence

$$\langle 0 \mid p^{\xi} \mid 1 \rangle^2 = \frac{h}{8\pi^2 \omega_i \bar{c}} \left(\frac{\partial p^{\xi}}{\partial Q_k} \right)^2 \qquad 6.17$$

where ω_i is the harmonic frequency of the ith mode. Comparison of equation 6.17 with 6.10 shows that we then obtain the expression

$$\Gamma_i = \frac{N\pi g}{3\bar{c}^2 \omega_i} \left(\frac{\partial p}{\partial Q_i} \right)^2$$

where

$$\left(\frac{\partial p}{\partial Q_i} \right)^2 = \left(\frac{\partial p^x}{\partial Q_i} \right)^2 + \left(\frac{\partial p^y}{\partial Q_i} \right)^2 + \left(\frac{\partial p^z}{\partial Q_i} \right)^2 \qquad 6.18$$

For a molecule of fairly high symmetry, all except one of the components of the dipole derivative will vanish for vibrations of a particular symmetry class, provided that the axes are chosen to

coincide with the symmetry axes (i.e. the change in dipole moment will be oriented along a fixed direction in the molecule for all vibrations of that symmetry class). A molecule of lower symmetry may have two or three non-vanishing components of $\langle 0 \mid P \mid 1 \rangle$ in the same symmetry class. It should be remembered that the direction of $\partial p/\partial Q$ is completely arbitrary and there is no reason to expect the dipole moment slopes to be similarly oriented for all vibrations of the same symmetry.

It is rather more convenient for the purpose of calculation to consider the derivative of the dipole moment with respect to internal symmetry coordinates S, which are related to those with respect to normal coordinates by the transform

$$p_j = \partial p/\partial S_j = \sum_i (\partial p/\partial Q_i)(\partial Q_i/\partial S_j) \qquad 6.19$$

These normal coordinates are obtained from the analysis of the observed spectra and are ultimately a function of the molecule's vibrational force constants and geometry. These last two quantities we shall discuss in the following sections.

6.3 The symmetry coordinates

The CH_3I molecule has C_{3v} symmetry, and has three non degenerate type A_1 vibrations and three doubly degenerate type E vibrations. Since a non-linear molecule containing N atoms has 3N-6 vibrational degrees of freedom, 3N-6 coordinates are necessary to describe the vibrations of the molecule. To attain the simplification made possible by the use of group theory it is necessary that these 3N-6 coordinates be expressed in terms of symmetry coordinates, which are linear combinations of the internal coordinates. The internal

coordinates are the changes in bond distances and in interbond angles. It is convenient to construct the symmetry coordinates from equivalent internal coordinates only. Moreover the choice of linear combinations is not arbitrary, but must be made in such a way that the symmetry coordinate transforms according to the characters of the vibration type concerned. Also the symmetry coordinates must be normalized and orthogonal. As there are 3(5)-6, or nine, vibration frequencies, only nine symmetry coordinates are necessary. However for CH_3I there are ten internal coordinates, following the notation of Dickson et al,[116] these are R_{CI}, $r_1, r_2, r_3, r\alpha_{12}, r\alpha_{23}, r\alpha_{31}, r\beta_1, r\beta_2, r\beta_3$ (see figure 34). Hence one of these is not independent of the others. Instead of ignoring one of the internal coordinates, which would destroy the symmetry, ten symmetry coordinates are constructed and then one is considered as redundant, see Table 12.

From Table 12 we note that the redundancy in the symmetry coordinates S_{2a} and S_{2b} may be removed by the orthonormal transformation

$$S_r = Q.S_{2a} + PS_{2b} = 0$$

It should be noted that since each of the three E type vibrations is doubly degenerate, it is necessary to have two symmetry coordinates designated by the subscripts a and b for each of these vibrations.

All these symmetry coordinates are therefore of the form

$$S_j = \sum_k U_{jk} R_k \qquad 6.20a$$

where U_{jk} is the coefficient of the kth internal coordinate R_k, and the summation is taken over all of the equivalent internal coordinates. Equation 6.20a can be written more concisely in the matrix notation as

Figure 34 Geometry of Methyl Iodide

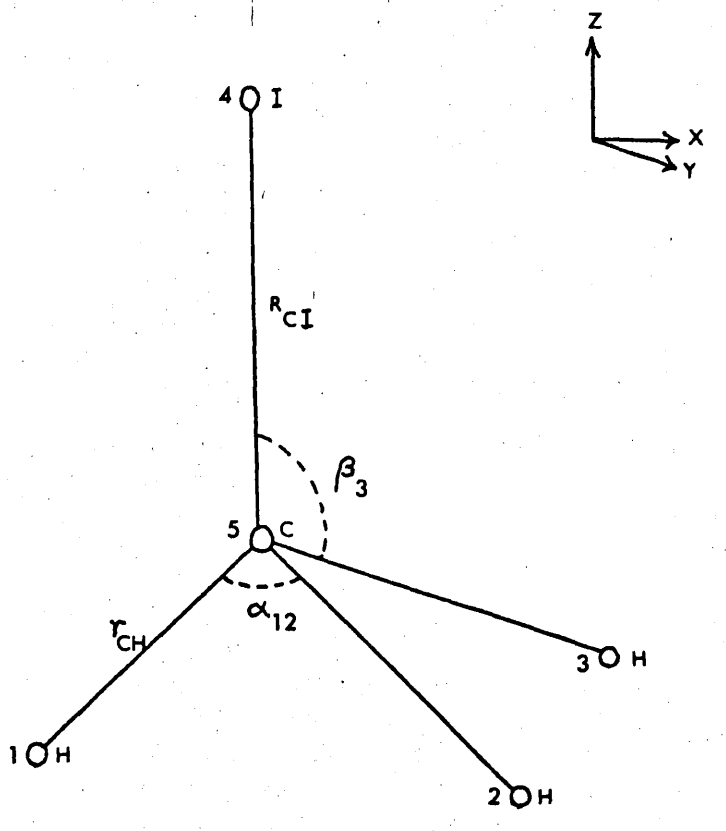

Notes: As more accurate values for the equilibrium rotational constants have been obtained, so different values for the molecular parameters have been presented. The equilibrium geometry originally used by Aldous and Mills[118] is quoted below, along with some more recent data by Duncan[120]. As one can see there is little difference between them.

	Duncan	Aldous and Mills
HCH = α	111.28333°	111.67°
HCI = β	107.59°	107.17°
r_{CH}	$1.085 \pm .003$ (°A)	1.095°A
R_{CI}	$2.133 \pm .002$ (°A)	2.139°A

All atomic masses are taken relative to ^{12}C

Thus $M_C = 12.00000$
$M_H = 1.00784$
$M_I = 126.90454$

Table 12 The symmetry coordinates used in this thesis, in terms of the internal coordinates,* for CH_3I.

	$1/N^2$	r_1	r_2	r_3	R_{CI}	$r\alpha_1$	$r\alpha_2$	$r\alpha_3$	$r\beta_1$	$r\beta_2$	$r\beta_3$
S_1	3	+1	+1	+1							
S_{2a}†	6					+1	+1	+1	−1	−1	−1
S_{2b}†	6					+1	+1	+1	+1	+1	+1
S_3	1				+1						
S_{4a}	6	+2	−1	−1							
S_{4b}	2		+1	−1							
S_{5a}	6					+2	−1	−1			
S_{5b}	2						+1	−1			
S_{6a}	6								+2	−1	−1
S_{6b}	2									+1	−1

* As defined by Aldous and Mills[117,118]. Their bending coordinates were defined as $r\alpha$ and $r\beta$.

† $S_2 = PS_{2a} - QS_{2b}$

$P = (1 + K)/(2 + 2K^2)^{\frac{1}{2}}$

$Q = (1 - K)/(2 + 2K^2)^{\frac{1}{2}}$

$K = -3 \sin\beta \cos\beta / \sin\alpha$

N = Normalization factor.

$$S = UR \qquad 6.20b$$

The condition for normalization of the jth symmetry coordinate is that $\sum_k (U_{jk})^2 = 1$.

6.4 The S_j^n vectors of Meister and Cleveland[119]

The S_j^n vectors of Meister and Cleveland are given by

$$S_j^n = \sum_k U_{jk} \, b_{kn} \qquad 6.21$$

(in matrix form S = UBX).

The b_{kn} vectors (of Woodward's notation[4]) can be expressed in terms of unit vectors e_k directed along the chemical bonds k.

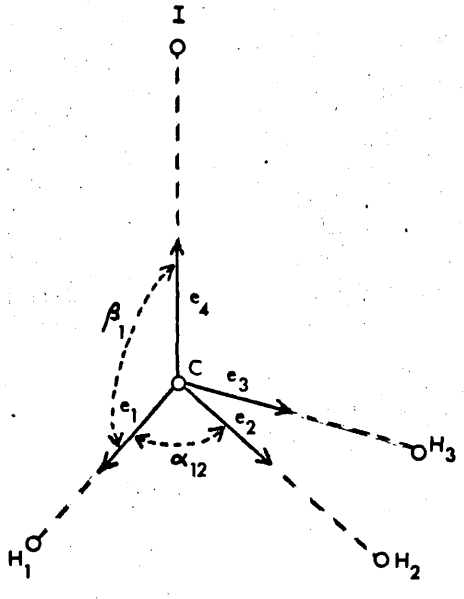

R_{CI} = CI bond length

r = CH bond length

Figure 35 The unit vectors along the bonds, and the interbond angles of CH_3I.

Using the unit vectors, bond distances and interbond angles indicated in figure 35, and assuming tetrahedral angles (i.e. $\alpha = \beta =$

$109^{\circ}\ 28'$), then the b_{kn} vectors are found to be:

For the H_1 atom

$$b_{r_1 H_1} = e_1$$

$$b_{r\alpha_{12}H_1} = \frac{-3}{4}\sqrt{2}\left(e_{1/3} + e_2\right) \quad .$$

$$b_{r\alpha_{31}H_1} = \frac{-3}{4}\sqrt{2}\left(e_{1/3} + e_3\right) \quad .$$

$$b_{r\beta_1 H_1} = \frac{-3}{4}\sqrt{2}\left(e_{1/3} + e_4\right) \quad .$$

where

$$b_{r\alpha_{23}H_1} = b_{r_2 H_1} = b_{r_3 H_1} = b_{RH_1} = b_{r\beta_2 H_1} = b_{r\beta_3 H_1} = 0$$

Expressions for the b_{kn} vectors of the other atoms can be obtained easily. Also, in terms of Cartesian coordinates, when X, Y and Z are unit distances along the x, y and z axes, the e vectors can be expressed as

$$e_1 = \frac{\sqrt{8}}{3}X - \frac{1}{3}Z$$

$$e_2 = -\frac{\sqrt{8}}{6}X \frac{-2}{\sqrt{6}}Y - \frac{1Z}{3}$$

$$e_3 = -\frac{\sqrt{8}X}{6} + \frac{2}{\sqrt{6}}Y - \frac{1Z}{3}$$

$$e_4 = Z$$

(for tetrahedral angles)

Using equation 6.21 above, the S_j^n vectors for the A_1 vibrations can now be expressed as, (using our symmetry coordinates defined in Table 12):

$$S_1^{H_1} = \frac{1}{\sqrt{3}} e_1$$

$$S_2^{H_1} = (-\frac{\sqrt{3}}{12})(e_1 + 3e_2 + 3e_3 - 3e_4)$$

$$S_3^{H_1} = 0$$

$$S_1^c = (-1/\sqrt{3})(e_1 + e_2 + e_3)$$

$$S_2^c = (\frac{7\sqrt{3}}{12} - \frac{\sqrt{3}}{4}\frac{r}{R})(e_1 + e_2 + e_3) - \left(\frac{\sqrt{3}}{4}\right)\left(3+\frac{r}{R}\right) e_4$$

$$S_3^c = -e_4$$

$$S_1^I = 0$$

$$S_2^I = \frac{r}{R} (e_4 + e_1 + e_2 + e_3)$$

$$S_3^I = e_4.$$

for the E vibrations

$$S_{4a}^{H_1} = (2/\sqrt{6})\, e_1 \qquad S_{4b}^{H_1} = 0$$

$$S_{5a}^{H_1} = (-\sqrt{3}/2)(e_1/3 + e_2/2 + e_3/2) \qquad S_{sb}^{H_1} = \frac{3}{4}(-e_2+e_3)$$

$$S_{6a}^{H_1} = (-\sqrt{3}/2)(e_1/3 + e_4) \qquad S_{6b}^{H_1} = 0$$

$$S_{4a}^c = \frac{1}{\sqrt{6}}(-2e_1 + e_2 + e_3) \qquad S_{4b}^c = \frac{1}{\sqrt{2}}(e_3 - e_2)$$

$$S^c_{5a} = \frac{1}{\sqrt{3}}(2e_1 - e_2 - e_3) \qquad S^c_{5b} = (e_2 - e_3)$$

$$S^c_{6a} = \frac{\sqrt{3}}{4}\left(\frac{r}{R} + \frac{1}{3}\right)(2e_1 - e_2 - e_3) \qquad S^c_{6b} = \frac{3}{4}\left(\frac{r}{R} + \frac{1}{3}\right)(e_2 - e_3)$$

$$S^I_{4a} = 0 \qquad S^I_{4b} = 0$$

$$S^I_{5a} = 0 \qquad S^I_{5b} = 0$$

$$S^I_{6a} = \frac{\sqrt{3}}{4}\frac{r}{R}(-2e_1 + e_2 + e_3) \qquad S^I_{6b} = \frac{3}{4}\frac{r}{R}(e_3 - e_2)$$

6.5 The L Matrix

In order to determine the L matrix, whose elements l_i are the amplitudes of motion of the various displacement cordinates in the ith vibration, it is necessary for us to consider very briefly the basic theory involved. The use of the L matrix will be shown in Chapter 8.

To obtain the equations from which the elements of the L matrix can be considered we must calculate the elements of a matrix F (related to the potential energy), and a matrix G related to the kinetic energy. If one assumes harmonic motion of a small amplitude for nuclei, the expression for potential energy V of the molecule can be written in the form

$$2V = \sum f_{ik} R_i R_k \qquad 6.22$$

where $f_{ik} = f_{ki}$ and i and k extend over all the internal coordinates. In matrix notation 6.22 becomes

$$2V = R^t F R \qquad 6.23$$

where F is a square matrix whose elements are the force constants f_{ik}. The superscript t stands for the transpose of the matrix.

Again in terms of the internal coordinates, the purely kinetic energy can be simply expressed by use of the matrix, G.

G is defined by

$$G = BM^{-1}B^{t} \qquad 6.24$$

Here B is the matrix which generates the 3N-6 internal coordinates from the 3N Cartesian coordinates X, in accordance with

$$R = BX \qquad 6.25$$

M^{-1} is the inverse diagonal matrix M representing the nuclear masses.

Thus a secular equation[121] expressed in terms of F, G and l_i, and of the form

$$|F - \lambda_i G^{-1}| l_i = 0 \qquad 6.26$$

can be used to solve the vibrational problem. The vertical lines indicate that the array is to be regarded as determinant.

Premultiplying by G we have

$$|GF - \lambda E| l_i = 0 \quad (\text{where } GG^{-1} = E \text{ the unit matrix}) \qquad 6.27$$

where $\lambda_i = 4\pi^2 \nu_i^2$. As 6.27 is the full expression of the vibrational problem we can have

$$GFl_i = \lambda_i E l_i \qquad 6.28$$

There is an equivalent expression for each λ_i. Combining all the eigenvector column matrices into one matrix L we have

$$GFL = L\Lambda \qquad 6.29$$

where Λ is a diagonal matrix with the elements $(\lambda_1 \ldots \lambda_i)$. If we take the force constant matrix for CH_3I from the literature, and express G in terms of 6.24, then using a method proposed by Steele[1] we can determine L.

Normally the vibrational problem in simple internal coordinates is factorised by use of the symmetry coordinates S_j. The coordinate transformation is given in 6.20; the corresponding symmetrised inverse kinetic energy and force constant matrices will be denoted by $\mathcal{G}$ and $\mathcal{F}$.

where $$\mathcal{G} = UGU^t$$

and $$\mathcal{F} = UFU^t$$

6.6 The Force Constants of Methyl Iodide

We have already shown that the vibration frequencies and the form of the 3N-6 normal vibrations of an N atomic molecule are characteristic of two features of the molecular structure.

i) The atomic masses and the geometrical distribution of the vibrational nucleii.

ii) The force field which tends to restore the molecule to its internal equilibrium configuration during any distortion.

In the interpretation of absolute infra-red intensity studies it is important to know the mode of vibration (i.e. the form of the normal coordinate, associated with each vibrational frequency). Unlike the vibrational frequencies the normal coordinate cannot be directly observed; in fact they can only be determined from a force constant calculation, since a knowledge of the normal coordinates implies a detailed knowledge of the force field. The force field of methyl iodide has been discussed by several authors, and we shall briefly note their results.

Aldous and Mills[118] have published force constants of the methyl iodide which were adjusted to fit the harmonic frequencies (determined by Dennison's[122] method, after correcting the observed vibrational frequencies for obvious resonance effects), the Coriolis coupling constants of the degenerate fundamentals, and the known centrifugal distortion constants. They included in their analysis data for the fully deuterated molecules in addition to those for the normal ones. We had originally intended to use these force constants to determine the L matrix. However the force constants have been revised by Russell et al[123], and more recently by Duncan, Allan and McKean[124].

Russell et al found that there was sufficient data to fix unambiguously a single family of symmetry force constants for CH_3I. Unfortunately they found that even with such a large number of observables, the force constants were not satisfyingly well determined. In particular for each of the methyl halides they found that $\mathcal{F}_{12}$, $\mathcal{F}_{13}$ and $\mathcal{F}_{46}$ had high dispersions using the General Harmonic Force Field. These are just the force constants constrained in the hybrid orbital force field (HOFF)[125]. Using the HOFF all the authors mentioned above found that the dispersions of the force constants turn out to be much lower.

A major computational difference between the investigations of Aldous and Mills, and Russell et al lies in the uncertainties associated with the harmonic frequency data and hence in their weighting factors. Aldous and Mills[118] assumed a 1 per cent uncertainty throughout, whereas Russell et al adopted a constant uncertainty of 20 cm^{-1} on all frequencies. Duncan et al[124] made use of ^{13}C frequency data in order to increase the precision with which the

parameters of the HOFF could be obtained. They also used improved frequency and Coriolis coupling data. We shall use the force constants calculated by Duncan et al. More recently Mallinson[126] has studied the Microwave spectrum of CH_2DI, and has redetermined the GHFF of CH_3I; however he did not consider the HOFF, which remains the best force field to use in this case.

In Table 13a we show the F matrix, and in 13b we give the relations between the symmetry force constants $\mathcal{F}_{ij}$ and the internal coordinate force constants. Values for $\mathcal{F}_{ij}$ are given in Table 14.

Table 13a The force constant matrix in terms of internal coordinates

The F matrix

	r_1	r_2	r_3	R_{CI}	$r\alpha_1$	$r\alpha_2$	$r\alpha_3$	$r\beta_1$	$r\beta_2$	$r\beta_3$
r_1	f_r	f'_{rr}	f'_{rr}	f_{Rr}	$f'_{r\alpha}$	$f_{r\alpha}$	$f_{r\alpha}$	$f'_{r\beta}$	$f_{r\beta}$	$f_{r\beta}$
r_2		f_r	f'_{rr}	f_{Rr}	$f_{r\alpha}$	$f'_{r\alpha}$	$f_{r\alpha}$	$f_{r\beta}$	$f'_{r\beta}$	$f_{r\beta}$
r_3			f_r	f_{Rr}	$f_{r\alpha}$	$f_{r\alpha}$	$f'_{r\alpha}$	$f_{r\beta}$	$f_{r\beta}$	$f'_{r\beta}$
R_{CI}				f_R	$f_{R\alpha}$	$f_{R\alpha}$	$f_{R\alpha}$	$f_{R\beta}$	$f_{R\beta}$	$f_{R\beta}$
$r\alpha_1$					f_α	$f'_{\alpha\alpha}$	$f'_{\alpha\alpha}$	$f'_{\alpha\beta}$	$f_{\alpha\beta}$	$f_{\alpha\beta}$
$r\alpha_2$						f_α	$f'_{\alpha\alpha}$	$f_{\alpha\beta}$	$f'_{\alpha\beta}$	$f_{\alpha\beta}$
$r\alpha_3$							f_α	$f_{\alpha\beta}$	$f_{\alpha\beta}$	$f'_{\alpha\beta}$
$r\beta_1$								f_β	$f'_{\beta\beta}$	$f'_{\beta\beta}$
$r\beta_2$									f_β	$f'_{\beta\beta}$
$r\beta_3$										f_β

Table 13b The relations between the symmetry force constants and the internal force constants F

$$\mathcal{F}_{11} = f_r + 2f'_{rr}$$

$$\mathcal{F}_{22} = \frac{(P-Q)^2}{2}\left(f_\alpha + 2f'_{\alpha\alpha}\right) + \frac{(P+Q)^2}{2}(f_\beta + 2f'_{\beta\beta}) + (P^2 - Q^2)(f'_{\alpha\beta} + 2f_{\alpha\beta})$$

$$\mathcal{F}_{33} = f_R \qquad \mathcal{F}_{13} = 3f_{Rr}$$

$$\mathcal{F}_{12} = \frac{(P-Q)}{2}(f'_{r\alpha} + 2f_{r\alpha}) - \frac{(P-Q)}{2}(f_{r\beta} + 2f'_{r\beta})$$

$$\mathcal{F}_{23} = \sqrt{3}\left[\frac{(P-Q)}{\sqrt{2}} f_{R\alpha} - \frac{(P-Q)}{\sqrt{2}} f_{R\beta}\right]$$

$$\mathcal{F}_{44} = f_r - f'_{rr} \qquad \mathcal{F}_{45} = f'_{r\alpha} - f_{r\alpha}$$

$$\mathcal{F}_{55} = f_\alpha - f'_{\alpha\alpha} \qquad \mathcal{F}_{46} = f_{r\beta} - f'_{r\beta}$$

$$\mathcal{F}_{66} = f_\beta - f'_{\beta\beta} \qquad \mathcal{F}_{56} = f'_{\alpha\beta} - f_{\alpha\beta}$$

P and Q are defined in Table 12.

Table 14 A comparison of the converged results of the Hybrid Orbital Force Field for methyl iodide, from references 118,123,124. The force constants are all in mdyn/Å and are for our scaled symmetry valence coordinates (see Table 12).

	Aldous and Mills[a] 118		Russell, Needham[b] and Overend 123		Duncan, Allan[c] and McKean 124	
	$\mathcal{F}$	$\sigma(\mathcal{F})$	$\mathcal{F}$	$\sigma(\mathcal{F})$	$\mathcal{F}$	$\sigma(\mathcal{F})$
$\mathcal{F}_{11}$	5.48	.05	5.482	.024	5.532	.031
$\mathcal{F}_{12}$	0	0	0	0	.092	.002
$\mathcal{F}_{22}$	.48	.004	.48	.008	.485	.002
$\mathcal{F}_{13}$	0	0	0	0	.026	.017
$\mathcal{F}_{23}$	-.351	.012	-.351	.05	-.38	.004
$\mathcal{F}_{33}$	2.337	.02	2.338	.052	2.39	.010
$\mathcal{F}_{44}$	5.61	.06	5.642	.019	5.453	.027
$\mathcal{F}_{45}$	-.157	.014	-.16	.011	-.131	.003
$\mathcal{F}_{46}$	.157	.014	.16	.011	.131	.003
$\mathcal{F}_{55}$	.472	.004	.47	.003	.448	.002
$\mathcal{F}_{56}$	-.026	.009	-.016	.008	-.011	.002
$\mathcal{F}_{66}$	.48	.004	.48	.006	.474	.002

(a) $\mathcal{F}_{12} = \mathcal{F}_{13} = 0; \mathcal{F}_{46} = -\mathcal{F}_{45}$ geometry: $r_e = 1.095$Å $R_{CI} = 2.139$Å

(b) $\mathcal{F}_{12} = \mathcal{F}_{13} = 0; \mathcal{F}_{46} = -\mathcal{F}_{45}$ geometry: $r_e = 1.085$Å $R_{CI} = 2.133$Å

(c) $\mathcal{F}_{12}/\sqrt{2} = -\mathcal{F}_{45} = \mathcal{F}_{46}$ geometry: $r_e = 1.085$Å $R_{CI} = 2.133$Å

The internal force constants are calculated from the symmetry force constants by direct substitution into the equations in Table 13b. The constraints used were $f_{R\beta} = f'_{r\beta} = f'_{\alpha\beta} = f'_{\beta\beta} = 0$.

Chapter 7 BAND CONTOUR ANALYSIS OF THE METHYL IODIDE FUNDAMENTALS

7.1 Symmetric Top Theory

In order to obtain the calculated infra-red spectrum of methyl iodide, we used the theory for symmetric top molecules. This has been considered in detail by Herzberg[127]. We shall note the equations used. Values for the rotational constants, coriolis coupling constants and frequencies were obtained from the literature and are listed in Table 15. The computer programs based on this theory were written by D. Steele and I.R. Hill. The programs are called ASPEC for parallel bands and ESPEC for perpendicular bands; and the details of the programs are given in reference 8.

7.1.1 Rotational Constants and Geometry

Symmetric top molecules have equal moments of inertia about two of the three axes of rotation. The third axis is the main axis of rotation and is called the z axis; the other two axes are the x and y axes. The symmetric top molecules fall into two categories.

a) The prolate symmetric top in which the moment of inertia about the z axis, I_z, is less than the moment of inertia about the x and y axes. Methyl iodide is such a molecule (see figure 34).

b) The oblate symmetric top in which $I_x = I_y < I_z$ (e.g. benzene).

The rotational constant about the axis i, B_i, is defined by

$$B_i = h/8\pi^2 I_i c \quad (cm^{-1}) \qquad 7.1$$

It is usual to label the rotational constant for the z axis of a prolate symmetric top, A and the rotational constant for the x and y axes B. It is quite straightforward to calculate the moment of

inertia and thus the rotational constants from molecular geometry. Using $I_i = m_j r_{ij}^2$ where m is the mass of atom j, and r is its distance from the axis i, passing through the centre of gravity. Then for CH_3I, $I_z = 5.3285 \times 10^{-47}$ Kg m^2 and $I_x = I_y = 108.09 \times 10^{-47}$ Kg m^2.

In a first approximation $B_{(v)}$ and $A_{(v)}$ are the average values of the rotational constants during a vibration which differ in general from the equilibrium values B_e and A_e. Where

$$B_{(v)} = B_e - \sum \alpha_i^B \left(v_i + \frac{d_i}{2}\right) \qquad 7.2a$$

$$A_{(v)} = A_e - \sum \alpha_i^A \left(v_i + \frac{d_i}{2}\right) \qquad 7.2b$$

α_i^B and α_i^A are vibration-rotation interaction constants. d_i is the degree of degeneracy of the vibration v_i.

Values of the rotation-vibration interaction constants, ground state constants and coriolis constants for the methyl iodide fundamentals have been discussed by a number of authors[128-150]. The values which have been used for computing the 'calculated' A_1 and E fundamental bands are listed in Table 15.

7.1.2 Vibration-Rotation Energy and Selection Rules

The total energy of vibration and rotation T, of a symmetric top molecule in a particular degenerate or non-degenerate vibrational state is given by

$$T = G_{(v)} + F_v(J,K)$$

where $G_{(v)}$ is the vibration term value, given to a first approximation by

$$G_{(v)} = \frac{(v + \frac{1}{2})(f/\mu)^{\frac{1}{2}}}{2\pi c} \quad cm^{-1} \qquad 7.3$$

Table 15 Rotation-vibration interaction constants, ground state constants, coriolis constants and frequencies used for calculating the CH_3I fundamentals. The figures in brackets are the references from which the constants are taken.

15A Rotation vibration interaction constants

α_1^A	$+0.0514\ cm^{-1}$	(138)	
α_2^A	-0.0222	(143)	
α_3^A	-0.0038	(148)	
α_4^A	$+0.0311$	(136)	
α_5^A	$+0.046$	(148)	
α_6^A	-0.0347	(143)	
α_1^B	$+0.00017$	(138)	
α_2^B	$+0.000849$	(135)(148)	*
α_3^B	$+0.001816$	(147)	
α_4^B	-0.000127	(145)	
α_5^B	$+0.000058$	(148)	*
α_6^B	$+0.000787$	(143)(135)	

* Not affected by interaction between ν_2 and ν_5.

15B Ground state rotational constants (in cm^{-1})

A_e	5.228 ± 0.001	(144)
B_e	0.25235 ± 0.00005	(144)
A_o	$5.1745 \pm .0006$	(150)
B_o	$0.250156 \pm .0000002$	(142)(145)
D_o^K	$1.23 \pm .22 \times 10^{-4}$	(150)

Table 15 (continued)

15C Coriolis constants

$$\xi_{44} = 0.0590 \quad (132)$$

$$\xi_{55} = -0.2444 \quad (148)$$

$$\xi_{66} = 0.210 \quad (143)$$

15D Frequencies (in cm^{-1})

	ν_1	ν_2	ν_3	ν_4	ν_5	ν_6
ν_o	2971.29	1250.75	533.21	3060.27	1435.1	882.6
Reference	(138)	(143)	(148)	(145)	(148)	(143)

where υ is the vibrational quantum number ($\upsilon = 0,1,2....$), f is the effective force constant, and μ the effective mass, for the vibration.

$F_{\upsilon}(J,K)$ is the rotational term which has two forms depending on whether the vibration is degenerate or non-degenerate. For symmetric top molecules a non-degenerate vibration (an A mode vibration) has a transition dipole directed along the z axis, and the resulting band is called a parallel band. Whereas a doubly degenerate vibration (E mode vibration) has a transition dipole directed along the x or y axes, and the resultant band is called a perpendicular band. J is the total angular momentum quantum number, and K is the quantum number determining the component of the angular momentum about the unique axis of the molecule. J takes integer values 0,1,2...; and K takes integer values of $0,\pm1,\pm2...\pm J$.

The selection rules for infra-red spectra are as follows. For a parallel band

$$\Delta K = 0 \quad \Delta J = 0,\pm1 \quad \text{if } K \neq 0 \qquad 7.4$$
$$\Delta K = 0 \quad \Delta J = \pm1 \quad \text{if } K = 0$$

And if the transition moment is perpendicular to the top axis

$$\Delta K = \pm1 \quad \Delta J = 0,\pm1 \qquad 7.5$$

7.1.3 Transitional Non-degenerate vibrational levels (|| bands)

The energy levels of the non-rigid symmetric top for a non-degenerate vibrational state are given by

$$F_{\upsilon}(J,K) = B_{(\upsilon)}J(J+1) + (A_{(\upsilon)}-B_{(\upsilon)})K^2 - D_J J^2(J+1)^2 - D_{JK}J(J+1)K^2 - D_K K^4 + \text{higher order terms} \qquad 7.6$$

The D terms are due to centrifugal distortion, and are generally exceedingly small compared with the ground state rotational constants A and B. Normally the higher order terms and the centrifugal terms are neglected.

From selection rule 7.4, for a particular value of K we obtain a sub-band with 3 simple branches P, Q and R. The complete parallel band is a superposition of a number of these sub-bands (the K = 0 sub-band has no Q branch). Due to the interaction between vibration and rotation there is a slight difference between B' and B'', and between A' and A'', (where these are the values of $B_{(v)}$ and $A_{(v)}$ in the upper and lower states).

From equation 7.6 and neglecting the D terms the formulae for the two branches R and P (of each sub-band) corresponding to $\Delta J = +1$ and -1 respectively are

$$\nu^R \equiv R(J) = \nu_o^{sub} + 2B' + (3B'-B'')J + (B' - B'')J^2 \qquad 7.7$$

$$\nu^P \equiv P(J) = \nu_o^{sub} - (B' + B'')J + (B' - B'')J^2 \qquad 7.8$$

and for $\Delta J = 0$

$$\nu^Q \equiv Q(J) = \nu_o^{sub} + (B' - B'')J + (B' - B'')J^2 \qquad 7.9$$

where for the sub-band origins (J = 0) we have

$$\nu_o^{sub} = \nu_o + [(A' - A'') - (B' - B'')]K^2 \qquad 7.10$$

Each band consists of a number of components J + 1 in the R branch and J in the P branch. However because of the restriction $J \geq K$ more and more lines will be missing from the beginning of the sub-band branches.

7.1.4 Degenerate vibrational levels ($\perp$ bands)

For a degenerate vibrational state the influence of the Coriolis force[1] is in general much larger than it is for the non-degenerate states. Since rotation about the top axis may occur, the Coriolis force can produce an interaction between the two components of a degenerate pair of vibrations.

The ν_6 vibration of methyl iodide (which is the in plane bending and rocking mode) is shown below.

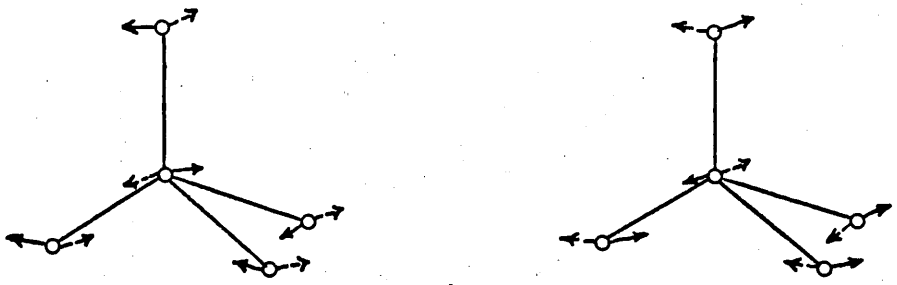

(a) (b)

It is known that when species (a) is coupled to species (b) and is rotating about the z axis, the Coriolis force produces a splitting of the degenerate vibrational levels into two levels. The separation increases with increasing rotation (K) about the z axis, although the splitting is zero for K = 0.

Thus the formula for the rotational energy levels of a degenerate vibrational state is given by

$$F_{(v)}(J,K) = B_{(v)}J(J+1)+\left(A_{(v)} - B_{(v)}\right)K^2 \mp 2A_{(v)}\zeta K \qquad 7.11$$

Higher order coupling terms and centrifugal distortion terms are neglected. The negative sign preceding the third term on the right hand side of 7.11 applies if the vibrational angular momentum has the same direction as the rotational angular momentum (+ℓ state), and the positive sign applies in the opposite case. For transitions between a lower non-degenerate state and an excited doubly degenerate state, the selection rules are given in equation 7.5.

The expression for the Q branch frequencies when a degenerate upper state is present, is:

$$\nu^{Q} = \nu_0 + [A'(1-2\xi)-B'] \pm 2\,[A'(1-\xi)-B']K$$
$$+[(A'-B')-(A''-B'')]K^2 + (B'-B'')J(J+1) \qquad 7.12$$

where the frequencies of the sub-band centres corresponding to the case when J = 0, are obviously given by

$$\nu_o^{sub} = \nu_o + (A'(1-2\xi)-B'] \pm 2[A'(1-\xi)-B']K$$
$$+[(A'-B') - (A''-B'')]K^2 \qquad 7.13$$

The upper sign applies to $\Delta K = +1$ and the lower sign for $\Delta K = -1$.

The P and R branch transitions of the sub-bands of a perpendicular band are given by a formula very similar to that for parallel type bands

$$\nu^{P,R} = \nu_o^{sub} + (B'+B'')m + (B'-B'')m^2 \qquad 7.14$$

where $m = J + 1$ for the R branch

and $m = -J$ for the P branch.

7.1.5 Line intensities

The rigorous formulae for the line intensities in the bands of symmetric top molecules were first given on the basis of the quantum theory by Honl and London[151], and were later derived on the basis of wave mechanics by Dennison[152], Reiche and Rademaker[153].

The absorption coefficient $\alpha(\nu)$ at a frequency ν, arising from a given rovibrational transition of energy $h\nu$ is given by[154]

$$\alpha(\nu) = CA_{J,K} \quad \nu_{J,K}\, g_{J,K} \exp[-F_{J,K}(hc/kT)]\,|\langle \psi' | \mu | \psi'' \rangle|^2\, S(\nu, \nu_{J,K}) \qquad 7.15$$

Where g_{JK} and F_{JK} are the statistical weight and the rotational term value for the lower state; $\langle \psi' | \mu | \psi'' \rangle$ is the transition integral for the vibration. C is a normalization constant independent of K and J, but depending on the vibrational transition. The $S(\nu, \nu_{JK})$ is a line shape function satisfying the normalization condition

$$\int_0^\infty S(\nu, \nu_{JK}) = 1$$

A_{JK} is a term whose value depends on the rotational quantum numbers J and K and also on the selection rules for the transition, and takes the values below for the indicated transitions.

parallel transitions

$$J,|K| \longrightarrow J+1,|K| \qquad (2-\delta_{K,0})\frac{(J+K+1)(J-K-1)}{(J+1)} \qquad 7.16a$$

$$J,|K| \longrightarrow J,|K| \qquad (2-\delta_{K,0})\frac{(2J+1)K^2}{J(J+1)} \qquad 7.16b$$

$$J,|K| \longrightarrow J-1,|K| \qquad (2-\delta_{K,0})\frac{(J+K)(J-K)}{J} \qquad 7.16c$$

perpendicular transitions

$$J,|K| \longrightarrow J+1,|K| \pm 1 \qquad \frac{(J \pm K+1)(J \pm K+2)}{(J+1)} \qquad 7.17a$$

$$J,|K| \longrightarrow J,|K| \pm 1 \qquad \frac{(2J+1)(J \mp K)(J \pm K+1)}{J(J+1)} \qquad 7.17b$$

$$J,|K| \longrightarrow J-1,|K| \pm 1 \qquad \frac{(J \mp K)(J \mp K-1)}{J} \qquad 7.17c$$

J and K refer to the lower state; and $\partial_{K,0}$ is the Kronecker delta.

7.1.6 Spin weighting $g_{J,K}$

For the CH_3I molecule which has a 3-fold axis (point group C_{3v}), in the ground state the levels with K = 0,3,6.... have a larger weight factor due to spin than those with K = 1,2,4,5... . Thus we observe an alternation of the type strong,weak,weak,strong.... .

For the general case in which the spin of the three identical nuclei is I, Dennison[155] has shown that the weight factors due to spin in a C_{3v} molecule are

for K divisible by 3 (including zero)

$$1/3(2I+1)(4I^2+4I+3) \qquad 7.18a$$

for K not divisible by 3

$$1/3(2I+1)(4I^2+4I) \qquad 7.18b$$

The population N_{JK} of the various levels in thermal equilibrium is given by

$$N_{JK} \simeq g_{JK} \exp[-(A-B)K^2(hc/kT)] \qquad 7.19$$

7.2 Experimental Procedure

Methyl iodide (Koch Light) was fractionally distilled at atmospheric pressure, and then thoroughly dried by standing for several hours over phosphorus pentoxide (P_2O_5). The methyl iodide was stored over copper in a sealed flask, in the dark.

The spectrometer used was the same P.E. 325 used for our molecular motion studies. Although the optical path of the spectrometer is automatically flushed with dry CO_2-free air, we found it necessary to keep dishes of P_2O_5 in the enclosed sample chamber to remove extraneous water vapour.

A small amount of methyl iodide sample was introduced into a previously dried vacuum line. The sample was degassed several times, and then stored in a reservoir until required. For each spectrum the sample was transferred to an evacuated 1.0 dm gas cell. The cell was contained in a brass holder; KBr windows were used for all measurements. Care was taken to place the cell in precisely the same position for each spectrum. The cell was thoroughly checked for leakage. Tests were made to detect concentration errors caused by adsorption of the sample on the cell walls; the results were negative.

For each band at least six different pressures of CH_3I vapour were used, ranging from 6.4×10^3 Pa to 38.2×10^3 Pa. The pressures were measured on a mercury manometer. In order to determine the molar concentration we also required to know the initial temperature of the cell. The ν_4 band was found to be rather weak so rather than using the 1.0 dm cell we used a multiple reflection cell of path length 37.5 dm.

In the field of gas intensities, errors can sometimes be reduced by broadening the individual rotation-vibration absorption lines. If a band shows a strong Q branch arising from vibrational transitions with no change of quantum number the sides of the Q branch will be very steep, and it may be necessary to use large pressures to broaden the band contour sufficiently to eliminate any appreciable error. Therefore, in this study, the spectra of ν_2, ν_3 and ν_6 bands were also run at atmospheric pressure. Air was gradually bled into the cell until atmospheric pressure was reached. No difference in the spectra at the low pressures or atmospheric pressure, was observed. Looking at Table 16 we see that our values for the integrated intensities are very much the same as Dickson et al's, despite the fact that we used no pressure broadening and Dickson used a broadening pressure of 8.27×10^6 Pa.

Penner and Weber[156] suggested a relatively simple and important test to ensure that adequate pressures were used, namely that the Beer's Law plot must be a straight line through the origin with the experimental points randomly scattered. On plotting $\ln(I_o/I)$ against concentration we did indeed obtain relatively good straight lines for all the bands. This check was carried out on the Q branches of the bands.

For our study we used resolutions of between .24 and .77 cm^{-1}. Resolutions of this order produce errors in studies of the gas phase, and methods have been described by which the errors can be minimised[157-158]. The most accurate method to have used, would have been the curve of growth method[115]. However our spectral resolution was not good enough to obtain the completely resolved rotation-vibration lines required for this method to be applied.

The technique used in this study, was one in which the integrated intensity is graphed against concentration, and the plot extrapolated to zero concentration. This leads to the true integrated intensity if (1) the incident intensity I_o does not vary over the slit width (this is easy to ensure provided that care is taken to remove the atmospheric water vapour and CO_2 from the absorbing path, as we have done), and (2) the fluctuations in the slit corrected (see section 2.1) transmitted intensity I are not large over the frequency range transmitted by the slit. The second condition is not possible to fulfil as there will always be rapid fluctuations in I even though the individual lines are not properly resolved. However, we approximate that the true integrated intensity is that at zero concentration.

Using the theory of section 7.1 and the data of Table 15 it was possible to obtain calculated A and E band spectra. The problem of band separation, and the determination of values for the observed band areas of the fundamentals will be discussed in section 7.3.2.

7.3 Band Contour Analysis

7.3.1 X-Y Coriolis Interactions

As already explained Coriolis interactions between vibrational levels not degenerate cause rather minor perturbations to the vibration-rotation spectra of small molecules accounted for in contributions to the dependence of the rotational constants on the vibrational energy level. They are known as second order Coriolis interactions, since they appear as off diagonal perturbation terms in the usual form of the Hamiltonian matrix. However when interacting

levels are nearly accidentally degenerate such second order perturbations become more important than many first order effects; they produce major complications in the observed spectrum, which can no longer be interpreted by the usual perturbation theory approach.

DiLauro and Mills[159] considered the interactions in symmetric top molecules due to rotation about the X and Y axes, and applied their theory to A_1-E Coriolis interactions. We shall merely quote the equations for the Hamiltonian and the rovibrational line strengths.

Considering the matrix representing H in the vibration rotation basis functions, denoted $|v_r, v_s^{l_s}; J,k\rangle$, the important selection rules for interaction between the first excited vibrational levels in Q_r (A_1 species) and Q_{S1}, Q_{S2} (E species) are $\Delta k = \Delta l_s = \pm 1$.

For each J value the Hamiltonian factorises into a number of (3 x 3) blocks, each block being characterized by a particular value of $(k - l_s)$. In addition to the (3 x 3) blocks there will be two (2 x 2) blocks for which $(k-l_s) = \pm J$; and two (1 x 1) blocks (unperturbed states) for which $(k-l_s) = \pm (J + 1)$. A typical (3 x 3) block of the Hamiltonian has the form

$$
\begin{array}{ccc}
|0, 1^{+1};\ J, k+1\rangle & |1,0\ ;\ J,k\rangle & |0,1^{-1};\ J,k-1\rangle \\
\left[\begin{array}{ccc}
\left[\nu_s + F'(J,k+1) - 2A'\xi_s^z(k+1)\right] & + 2^{\frac{1}{2}} B' \mathcal{R}_{rs} \xi_{rs}^y [J,k]^{\frac{1}{2}} & \\
 & \nu_r + F'(J,k) & -2^{\frac{1}{2}} B' \mathcal{R}_{rs} \xi_{rs}^y [J,k-1]^{\frac{1}{2}} \\
 & & \left[\nu_s + F'(J,k-1) + 2A'\xi_s^z (k-1)\right]
\end{array}\right] & \\
\text{Hermitian} &
\end{array}
$$

where $F'(J,k) = B'J(J+1) + (A'-B')k^2$

$$\mathcal{R}_{rs} = \tfrac{1}{2}[(\nu_r/\nu_s)^{\frac{1}{2}} + (\nu_s/\nu_r)^{\frac{1}{2}}]$$

and $(J,k)^{\frac{1}{2}} = +[J(J+1) - k(k+1)]^{\frac{1}{2}}$

The rovibrational line strength of a transition is given by

$$S(\psi' \leftarrow \psi'') = 3g \sum_m [aM_s M_k^{k+1} + bM_r M_k^{k} + cM_s M_k^{k-1}]^2$$

where $\psi' = a\psi'_{+} + b\psi'_{o} + C\psi'_{-}$

M_k are the Hönl-London factors and M_r and M_s are the vibrational transition moments of the A_1 and E states. The rovibrational line strengths will show interference effects which will enhance or deplete the intensities of particular lines depending on whether the cross terms in the expansion of the square appear with a positive or negative sign, and thus will depend on the relative signs of M_r and M_s, and on the relative signs of the elements of the eigenvector (a,b,c). The relative signs of (a,b,c) depend on the sign of ξ^{y}_{rs}.

It is well known that the $\upsilon_5 = 1$ state of methyl iodide is coupled with the $\upsilon_3 = 1$, $\upsilon_6 = 1$ state through Fermi resonance[140]. Matsuura and Overend[141], using .03 cm^{-1} resolution found that in addition to the Fermi resonance, there is a further perturbation due to an X-Y type Coriolis interaction between the E states. The perturbation is large and the mixing of the two states is considerable. However the effect is highly localized, therefore we decided that the problem of band fitting to the remainder of the ν_5 band contour would be considerably simplified if we were to ignore the effect. Matsuura and Overend[148] also considered that there was an X-Y type Coriolis interaction between the ν_5 and ν_2 fundamentals. They concluded that the band centres are far enough apart for the interaction to be a second order effect. A more likely pair of fundamentals, for which there could be a first

order X-Y Coriolis effect, are the ν_4 at 3060 cm^{-1} and ν_1 at 2970 cm^{-1}. The two bands were observed to overlap considerably, much of the intensity of the low frequency side of the ν_4 band being 'lost' in the structure of the much more intense ν_1 band. Using an interaction Coriolis constant ξ^y_{14a} (.1134) we were able to obtain the positive and negative contours. There was a hardly noticeable difference between the two contours. Comparison of these calculated X-Y Coriolis spectra with a spectrum obtained by adding the calculated A_1 band to the calculated E band, showed that there was little difference in the methods. As the latter method (i.e. adding on A band to an E band) seemed the simplest to perform we used this and obtained satisfactory fits to the spectra. We shall discuss this last point more fully in the following sections.

The interaction Coriolis constants for the fundamentals of CH_3I were calculated from the theory using a program developed by D. Steele. Actual values for ξ^y_{rs} are given in Table 17.

Table 17 Non zero ξ^y_{rs} Coriolis constants for CH_3I (calculated using the force constants and equilibrium geometry of refs. [120] and [124])

	Q_1	Q_2	Q_3	Q_{4a}	Q_{5a}	Q_{6a}
Q_{4a}	-.1134	.7139	-.0545	0	.2606	-.4216
Q_{5a}	-.0393	.6372	-.0344	-.2606	0	.4920
Q_{6a}	-.7363	.0799	-.1718	.4216	-.4920	0

7.3.2. Observed Band Areas for the Methyl iodide fundamentals

The problem of separating the intensity contributions from a pair of overlapping bands arises in a number of cases for the methyl halide molecules, particularly with the pairs of parallel and perpendicular vibrations, characteristic of the methyl group, which occur at around 3000 cm^{-1} and around 1400 cm^{-1}. As these bands usually show a well defined symmetry; Dickson et al[116] used this fact in applying methods of graphical separation. When only one half of a perpendicular band was overlapped the contour was drawn into make the band symmetrical about its centre, Dickson assigned an error of 20% to the separation of the overlapped area, for each overlapping pair of bands. We used a slight variation of this method which will now be explained.

The overlap of the ν_2 and ν_5 was assumed to be very small (of the order of 5% of the ν_5 band). However as we have already noted in section 7.3.1 the ν_1 and ν_4 bands (around 3000 cm^{-1}) overlap considerably. The contour of the ν_4 (E) fundamental band was calculated using the theory of section 7.1. The calculated band was fitted as best as possible to the observed. (There are many problems with this procedure . We shall discuss the most important of these in section 7.3.3). We assigned an error of 25% to the separation of the overlapped area. The portion of the overlapped E band can therefore be determined. This procedure seems reasonably justified as we managed to obtain values for the band areas which were comparable with those of Dickson et al., see Table 16.

In methyl iodide there is also a resonance interaction between the symmetrical hydrogen stretching vibration, and the overtone $2\nu_5$. This results in the two band centres being pushed apart, and in the

Table 16 Observed band areas for CH_3I (units are dm^2mol^{-1}) (a)

Band (cm^{-1}) centre	Assignment	Barrow & McKean[161]	Dickson et al[116]		This work	
		Γ	Γ	$\sigma(\Gamma)$(b)	Γ	$\sigma(\Gamma)$(c)
3000 region		5.39	4.962	.280	4.882	
3060	ν_4 E	.66	.704	.042	.671	.080
2971	ν_1 A_1	4.03	3.714	.300	3.810	.360
2861	$2\nu_5$ A_1	.70	.544		.401	
1435	ν_5 E	5.72	7.377	.114	7.250	.190
1251	ν_2 A_1	19.13	16.513	.400	17.750	.510
883	ν_6 E	9.09	10.124	.140	10.105	.135
533	ν_3 A_1	3.65	3.623	.006	3.718	.030

(a) Band areas were calculated using equation 6.8a.

(b) $\sigma(\Gamma)$ for Dickson et al were calculated from the standard errors of Beer's Law plots.

(c) $\sigma(\Gamma)$ for this work were calculated from standard errors of Beer's Law plots of selected Q branches of each fundamental band.

weaker band "borrowing" intensity from the stronger. Dickson et al showed that the quantity Γ, integrated over the pair of resonating bands, is independent of the degree of perturbation. Thus in this work, it was assumed that the unperturbed intensity of $2\nu_5$ could be neglected, so the intensity of ν_1 was taken to be the total value of Γ over the pair of bands.

7.3.3 Band fitting results for the E class fundamentals

It was found that in order to obtain the best fit to the observed spectra, a temperature of 70°C (343°K) had to be assumed in computing the theoretical band. An increase in the theoretical temperature leads to a redistribution of the line intensities, such that the intensity in the wings is increased relative to the band centre. The means of fitting, was to sum the intensity in each Q sub-band in both the experimental and theoretical spectra. The frequency interval, over which the summation was carried out, was obviously the same in both cases. The observed and the theoretical spectra are then compared, by considering the ratio $\frac{\text{theoretical intensity}}{\text{experimental intensity}}$, with respect to the $^{R}Q_3$ sub-band.

As an example of the temperature behaviour we show the theoretical/experimental ratios (of the Q sub-bands), at different temperatures, for the ν_6 band, (see Table 18). The cell temperature (and thus the sample temperature) was found to be 33°C (306° K). This was measured simply, by attaching a thermocouple to the cell plate. We can offer no explanation of the large difference between the theoretical temperature and the observed temperature.

Table 18 The temperature behaviour of the ratio $\frac{\text{theoretical intensity}}{\text{experimental intensity}}$ for the ν_6 band of methyl iodide

	306°K	333°K	343°K
R_{Q_1}	.879	.855	.851
R_{Q_2}	.943	.851	.852
R_{Q_3}	1.000	1.000	1.000
R_{Q_4}	.863	.828	.859
R_{Q_5}	.847	.840	.883
R_{Q_6}	.865	.896	.979
R_{Q_7}	.831	.803	.896
R_{Q_8}	.799	.792	.886
R_{Q_9}	.812	.829	1.014

In Table 19 we give the ratios of the theoretical intensities to the experimental intensities of the Q sub-bands, for the three E class fundamentals. The most significant observation is that the theoretical/experimental ratios for the Q sub-bands where K = 0,3,6,9... are larger than those for K = 1,2,4,5.... We might have been able to explain this phenomenon if it had occurred in only one band, in terms of some interaction of the fundamental with another band. However, as there seems to be a consistent redistribution of the intensity of the Q branches, in each of the fundamentals, so that the K = 0,3,6... ratios are some 15% higher than those where K = 1,2,4,5...., we are unable at the present time to provide an explanation.

Table 19 Ratios of theoretical intensities (at 70°C) to experimental intensities (at 33°C), of the Q sub-bands of the E class fundamentals of CH_3I. (a)

	ν_4 (b)	ν_5 (c)	ν_6
$P_{Q_{10}}$			.865
P_{Q_9}			.936
P_{Q_8}			.879
P_{Q_7}			.883
P_{Q_6}			.938
P_{Q_5}			.859
P_{Q_4}			.858
P_{Q_3}	1.060		1.008
P_{Q_2}	.882		.897
P_{Q_1}	.864	.938	.879
R_{Q_0}	1.098	1.036	.983
R_{Q_1}	.873	.932	.851
R_{Q_2}	.891	.909	.852
R_{Q_3}	1.000	1.000	1.000
R_{Q_4}	.845	.919	.859
R_{Q_5}	.818	.905	.883
R_{Q_6}	.936	1.034	.979
R_{Q_7}	.827	.929	.896
R_{Q_8}	.836	.902	.886
R_{Q_9}	.945	1.009	1.014

(a) All ratios are calculated with respect to the R_{Q_3} sub-band.

(b) On the P_{Q_K} side of the ν_4 band many of the Q branches are smothered by the ν_1 band.

(c) For the ν_5 fundamental the P_{Q_K} branches are severely distorted by the fermi resonance and X-Y Coriolis interactions with with the $\nu_3 + \nu_6$ combination band near ν_5 (see p194), therefore no sensible ratios could be obtained.

7.3.4 Band fitting for the A_1 class fundamentals

The means of band fitting was relative simple. Initially the centre of the Q branch of the theoretical spectrum was positioned at the same point as the Q branch in the experimental spectrum. Due to the resolution used in this experiment we could not necessarily identify the particular J multiplets of the P and R branches. Therefore the intensity of the Q branch (for both the experimental and theoretical spectra) was summed over an arbitrary frequency interval. The rest of the band was sectioned into the same frequency interval, and the intensity of each section determined. Values of the ratio theoretical intensity/experimental intensity, are given for the A_1 bands of CH_3I, in Table 20. The temperature used for calculating the theoretical spectrum was $306^{\circ}K$, in each case. All ratios are quoted with respect to the Q branch.

There are obviously some unusual aspects to the results shown in Table 20. For instance, the ratio of theoretical intensity to experimental intensity of the Q branch in the ν_1 band is large compared with the 'ratios' for the rest of the band. This suggests that the experimental intensity in the Q branch is smaller than we would have expected from the theory. The intensity would seem to have dispersed itself evenly between the P and R branches. We can only suggest that on the low frequency side of the band the resonance interaction of ν_1, with $2\nu_5$, causes intensity from the ν_1 band Q branch to be borrowed by the weaker band. Presumably, then, on the high frequency side of the fundamental there is an interaction of similar magnitude. This interaction would be between the ν_1 and ν_4 bands.

Table 20 Ratios of theoretical intensities to experimental intensities, over arbitrary frequency intervals for the A_1 class fundamentals of CH_3I.

ν_1 Frequency interval 5 cm^{-1}

R branch					Q branch	P branch				
.720	.760	.760	.761	.659	1.000	.792	.761	.740	.753	.740

ν_2 Frequency interval 2.5 cm^{-1}

R branch						Q branch	P branch				
1.074	1.034	1.004	.966	.941	.888	1.000	.803	1.038	1.172	1.120	1.077 1.042

ν_3 Frequency interval 4.0 cm^{-1}

R branch					Q branch	P branch				
1.196	1.247	1.258	1.183	1.054	1.000	.953	1.032	1.043	.981	.992

For the ν_2 fundamental the 'ratios' become larger as we move away from the band centre. This suggests that in the experimental spectrum the intensity is shifted nearer to the band centre than in the theoretical spectrum, and therefore the experimental Q branch is stronger than expected. Any X-Y Coriolis interaction with the ν_5 fundamental was not considered to be responsible, as the band centres are some 200 cm^{-1} apart, and we calculate (see section 7.3.1) that the effect is small.

The ν_3 band was somewhat more unusual, in that there is a visible hot band in the experimental band envelope. However, despite the fact that, our theoretical spectrum contains the hot band in its correct position, we were unable to obtain a good fit between the theoretical and experimental spectra.

At the present time we can offer no explanations for these differences between the theoretical and experimental intensity distributions in the A_1 fundamentals of methyl iodide. However, we are not alone in observing this phenomenon. Sarangi and Varanasi[160] reported the ratios of theoretical to experimental intensities of the J multiplets in the CH_3D vibration rotation band at 2200 cm^{-1}, relative to the measured intensity of the doublet P(2). They listed the observed 'ratios' at various temperatures. At all temperatures they noted that the theoretical Q branch, was larger than the experimental Q branch by a factor of two (see Table 21). They suggested that the significant "borrowing of intensity" from the Q branch by the R branch (in the experimental band) could be due to a mixing of the wave functions between the $2\nu_4$ and ν_3 bands due to fermi resonance. However they considered that this would not completely explain the observed phenomenon.

Table 21 Ratio of the theoretical to experimental intensity of J multiplets in the 2200 cm^{-1} A_1 fundamental of CH_3D at 298°K, from reference [160].

R(4)	R(3)	R(2)	R(1)	R(0)	Q	P(1)	P(2)	P(3)	P(4)	P(5)	P(6)	P(7)
.806	.847	.870	.855	1.024	2.208	-	1.00	.909	.907	.946	.945	.956

Chapter 8 THREE METHODS FOR OBTAINING BOND PARAMETER INFORMATION FROM THE INFRA-RED GAS PHASE INTENSITY DATA OF METHYL IODIDE

8.1 Introduction

As seen from section 6.2 the fundamental vibrational intensities of polyatomic molecules lead to values of $\left| \frac{\partial P}{\partial Q_i} \right|$. The values of $\left| \partial P / \partial Q_i \right|$ for methyl iodide are given in Table 22. To proceed further it is necessary to determine the derivative of the dipole moment with respect to a defined molecular coordinate, which is usually taken as the symmetry coordinate S (see Table 12). The transformation relating normal coordinates to symmetry coordinates is

$$S_j = \sum \mathcal{L}_i^j Q_i \qquad 8.1$$

where $\mathcal{L}$ is the symmetrised L matrix (see section 6.5). The elements of $\mathcal{L}$ for methyl iodide are given in Table 23. From equations 8.1 and 6.20 it follows that

$$P_j \equiv \frac{\partial P}{\partial S_j} = \sum_i \frac{\partial P}{\partial Q_i} (\mathcal{L}^{-1})_j^i \qquad 8.2a$$

and similarly $$\frac{\partial P}{\partial Q_i} = \sum_j (\mathcal{L})_j^i \frac{\partial P}{\partial S_j} \qquad 8.2b$$

The calculation of any particular $\partial P / \partial S_j$ requires a knowledge of all $\partial P / \partial Q_i$ values for the particular symmetry species. The $(\mathcal{L}^{-1})_j^i$ matrix coefficients are calculated by inversion of the matrix. The elements of the $\mathcal{L}$ matrix are given by l^s.

The derivatives of the dipole moment with respect to defined coordinates depends (in the Born-Oppenheimer approximation) on the charge distributions, but not on the nuclear masses. Therefore the

Table 22 Harmonic vibration frequencies , and dipole moment derivatives $|\partial P/\partial Q_i|$ for the normal vibrations of methyl iodide, ω is in cm^{-1}; $|\partial P/\partial Q_i|$ in D/Å.

	Dickson, Mills and Crawford[116]				This work[+]	
	CD_3I		CH_3I		CH_3I	
	ω	$\lvert\partial P/\partial Q_i\rvert$	ω	$\lvert\partial P/\partial Q_i\rvert$	ω	$\lvert\partial P/\partial Q_i\rvert$
Q_1	2210.0	.425 ± .010	3060.0	.555 ± .030	3089.3	.554 ± .038
Q_2	975.0	.578 ± .024	1288.3	.709 ± .017	1296.2	.738 ± .024
Q_3	501.7	.153 ± .003	533.1	.214 ± .002	538.2	.218 ± .009
Q_4	2400.0	.092 ± .005	3229.2	.164 ± .005	3201.3	.159 ± .008
Q_5	1082.6	.276 ± .027	1504.4	.362 ± .005	1460.7	.354 ± .016
Q_6	675.8	.197 ± .010	905.8	.329 ± .005	896.6	.327 ± .006

+ Using our experimental band areas and force constant data from reference 124.

Table 23 Elements of the L matrix for methyl iodide.* Units are $amu^{\frac{1}{2}}$

CH_3I

A Species				E Species			
S_1	1.0074	.0126	-.0044	S_{4ab}	+1.0505	+.0362	-.0321
S_2	-.1077	1.3782	-.1295	S_{5ab}	+.0976	+1.5299	+.1492
S_3	-.0457	.0954	-.2829	S_{6ab}	-.1220	+.2734	-.9087

CD_3I

A Species				E Species			
S_1	.7203	.0204	-.0069	S_{4ab}	+.7805	+.0089	-.0304
S_2	-.1560	1.0573	-.0433	S_{5ab}	+.1859	+1.1188	+.0629
S_3	-.0671	.1432	-.2573	S_{6ab}	-.1419	+.1292	-.6763

* calculated using data from reference 124.

values of $\partial p/\partial S_j$ are the same for isotopically substituted molecules, if the symmetry coordinate S_j is defined in the same way. The normal coordinates and the vibrational frequencies, do however, depend on the atomic masses, and in general $\partial p/\partial Q_i$ will change under isotopic substitution.

The fact that the sign of each $\partial p/\partial Q_i$ is indeterminate, as is the sign of each component of $(\mathcal{L}^{-1})^i_j$, means that equation 8.2 does not lead to a unique value of $|P_j|$, but in general gives $2^{(n-1)}$ different solutions, where n is the number of normal vibrations in the particular symmetry species. For methyl iodide the isotopic intensity data were available from reference 116, and thus a second set of $2^{(n-1)}$ values of $|P_j|$ may be obtained. The correct solution must necessarily have the same values for corresponding P_j's calculated from both isotopic molecules. In this way a unique set of P_j's can be determined. However, it should be noted that a unique set of P_j's cannot always be chosen, as the calculated values from the different isotopes do not agree exactly, being subject to uncertainties in the experimental intensities, the harmonic approximation, and the normal coordinates. There is, of course, no necessity for the relative signs of $\partial p/\partial Q_i$ to be the same for isotopic molecules.

Having obtained what is hoped are meaningful dipole moment derivatives in terms of a set of symmetry coordinates the next stage is to reduce the results to a set of bond parameters. Dickson, Mills and Crawford (see the next section (8.2)) used the bond moment hypothesis which requires

i) That stretching a bond by dr produces a change of dipole moment along the bond of $(\partial\mu/\partial r)\,dr$.

ii) The deformation of a bond through an angle $d\phi$ produces a dipole change $\mu d\phi$ perpendicular to the bond and in the plane of movement, μ is the bond dipole.

iii) Changes in the bond do not result in changes in other bonds except when this is geometrically necessary.

Relaxing these constraints while continuing to require a bond parameter formulation results in the introduction of terms of the type $\partial\mu_i/\partial R_j$. The number of such terms will usually far exceed the number of observables. For this reason formulations have been developed by Gribov (see section 8.3), and Crawford, Barrow and McKean (see section 8.4), which are chemically reasonable and which constrain the parameterisation to a level intermediate between the bond moment hypothesis and the general formulation.

The principle object of the work detailed in this chapter, is to compare the three methods of determining bond parameters stated above. It is not the object of this study to compare trends in the parameters for the methyl halides, as this has been done by a number of authors [162-163,116].

8.2 The Method of Dickson, Mills and Crawford[116]

8.2.1 Values of P_j for the A_1 class vibrations

The values of $|\partial P/\partial Q_i|$ were determined from the band areas for each normal coordinate using equation 6.18; they have already been listed in Table 22. The dependence of the dipole moment on a set of symmetry coordinates was then determined using equation 8.2. The elements of the L matrix are given in Table 23, using the symmetry coordinates of Aldous and Mills[118]. It is

particularly important to observe the signs defined for the various symmetry coordinates, since these affect the signs of the p_j vectors discussed later. We have written the dipole moment vectors p^x, etc., to be positive when the positive charge is displaced in the positive x direction. In the case of methyl iodide p_j and $(\partial p/\partial Q_i)$ are always parallel vectors for a given symmetry species, so equation 8.2 reduces to a simple algebraic equation that may readily be solved to give values of p_j; however the unknown relative signs of $(\partial p/\partial Q_i)$ terms leave the usual choice of alternative sets of p_j values. These are distinguished by the notation (++−) etc., indicating the relative signs taken for $(\partial p/\partial Q_i)$ in the successive terms of equation 8.2b.

Several authors have discussed the estimation of statistical errors in the dipole moment derivatives[123,116]. We shall not discuss this point further, other than to say that account is generally taken of contributions from random errors in the experimental intensity data, the intramolecular force constants, the molecular geometry and the harmonic frequencies. The first two contributions are of similar importance, and the latter two are negligible[123]. The errors listed in Table 22 are those of Dickson et al[116] and they are intended to represent the limits within which the true band areas almost certainly lie. They were derived in the following way. For CH_3I the error listed in Table 22 corresponds to the largest of the following three quantities, (a) 2% of the band area, (b) twice the standard error of Table 16, and (c) the separation error of Table 16, where this is dominant. For the CD_3I molecule a similar procedure was followed, except that condition (a) was raised to 5% of the band area, in order to cover errors resulting from impurity in the deuterated samples.

For the three A_1 species of CH_3I, and CD_3I, values for all possible sign combination are given in Table 24.

Table 24 Values of p_j^z for the A_1 class of methyl iodide in D/Å

CH_3I	p_1^z	p_2^z	p_3^z
+++	.5675	.6033	-1.0557
+—	.5328	-.6125	1.0428
++-	.6279	.4927	.5355
+-+	.4724	-.5019	-.5485
CD_3I			
+++	.6598	.6312	-.7184
+—	.5135	-.6501	.6902
++-	.7370	.4652	.4968
+-+	.4363	-.4840	-.5250
Mean, (+-+)	.4543	-.4929	-.5367

As we stated in section 8.1, for a given symmetry coordinate, p_j^z should be the same for different isotopic molecules. Using this as a basis for choosing between the alternative sign combinations, it is seen that the (+-+) sets of $(\partial\rho/\partial S_j)$ give the best agreement in this case.

8.2.2 The E class vibrations

The E class vibrations contain two infra-red active molecular rotations, and because of this it is not possible to make a direct comparison of p_j values between the isotopic molecules.

In order to conserve the overall angular momentum of the molecule during a symmetry distortion S_j, some compensating rotation of the molecule is required. The compensating rotation accompanying a vibration occurs with the same frequency as the vibration and contributes intensity to the vibrational spectrum. This contribution must be subtracted from the value of p_j, determined by equation 8.2b, before this quantity may be treated as an intramolecular parameter; that is to say, before p_j's from two isotopic molecules may be compared. Crawford[164] has given a method of calculating this rotational correction, which is somewhat awkward to follow. Van Straten and Smit[165] have since developed and described this method in a clearer form. Despite being straightforward, the method produces some rather complicated calculations. Before proceeding further we shall describe Van Straten and Smit's method, and its application to methyl iodide.

8.2.2 (i) Van Straten and Smit's formulation for the Rotational Corrections

In this formulation the dipole moment derivatives obtained from equation 8.2a will be denoted by $(\partial p/\partial S)_A$, where subscript A refers to the molecule being considered. The theoretical quantity needed will be denoted by $(\partial p/\partial S)_R$, where R stands for the reference molecule. The determination of the rotational corrections are only made possible if a reference molecule is defined which possesses rotation free internal coordinates. The only rotation free molecule known in the literature is a molecule in which isotopes of zero mass are introduced for atoms which are not situated on the

molecular symmetry axis. Thus for CH_3I and CD_3I, the reference molecule assumes that H and D are of zero mass. In this case the C–I bond will maintain a fixed direction during vibration, and there is no compensating rotational motion. Now we have that

$$(\partial p/\partial S)_R = (\partial p/\partial S)_A - V_{AR} \qquad 8.3a$$

$$\text{or} \quad (p_R) = (p_A) - V_{AR} \qquad 8.3b$$

where, obviously, V_{AR} is the rotational correction. The column vector V_{AR} can be evaluated with the help of two additional coordinate sets:

X : the vector of the 3N cartesian coordinates

$\mathcal{P}$: the external coordinates (six translations and rotations).

The transformation matrices between $\mathcal{P}$, R, S and X are summarised as follows:

$$\begin{array}{lll} R = BX & B = \partial R/\partial X & A = (\partial X/\partial R) \\ S = UBX & UB = \partial S/\partial X & A\,U^t = (\partial X/\partial S) \\ \mathcal{P} = \beta X & \beta = \partial \mathcal{P}/\partial X & \alpha = (\partial X/\partial \mathcal{P}) \end{array} \qquad 8.4$$

(superscript t means 'transpose' of the matrix).

The properties of these transformation matrices for a given isotope are

$$\begin{array}{lll} B\alpha = 0 & \beta A = 0 & BA = E_{3N-6} \\ \beta\alpha = E_6 & \alpha^t = \beta M^{-1} & AB + \alpha\beta = E_{3N} \end{array} \qquad 8.5$$

Crawford[164] derived a relation between the A matrices of two different isotopes. For the A matrix of the reference molecule this relation reads

$$A_R = A_A - \alpha_R \beta_R A_A \qquad 8.6$$

(the subscripts have the meanings given above).

From equation 8.6 we can deduce that

$$UA_R^t \, (\partial \rho \, / \, \partial X) = UA_A^t \, (\partial \rho / \partial X) - UA_A^t \, \beta_R^t \, \alpha_R^t \, (\partial \rho / \partial X) \qquad 8.7$$

This is equivalent to equation 8.3. So the rotational corrections can be written as

$$V_{AR} = \left\{ UA_A^t \, \beta_R^t \right\} \left\{ \alpha_R^t \, (\partial \rho / \partial X) \right\} \qquad 8.8$$

Since the translational motions do not change p, we may rewrite the second part of V_{AR} , giving

$$\alpha_R^t \left(\frac{\partial \rho}{\partial X} \right) = \begin{bmatrix} 0 \\ 0 \\ 0 \\ (p_o^y)k - (p_o^z)j \\ (p_o^z)i - (p_o^x)k \\ (p_o^x)j - (p_o^y)i \end{bmatrix} \qquad 8.9$$

where p_o^x denotes the x component of the permanent dipole moment and i, j and k are the Cartesian unit direction vectors, weighted by (moment of inertia)$^{-\frac{1}{2}}$. For the reference molecule, there is only a non zero component of the permanent moment along the main axis of symmetry, (the z axis).

The A_A matrix is defined as

$$A_A = M_A^{-1} \, B^t \, G_A^{-1} \qquad 8.10$$

8.2.2 (ii) Calculation of the Rotational Contribution V_{AR} for Methyl Iodide for $M_H = 0$

We shall now consider the calculation of V_{AR} in detail. The initial procedure is to calculate $UA_A^t \, \beta_R^t$. From

equations 8.8 and 8.10 we can rearrange the matrices to obtain

$$UA_A^t \beta_R^t = \mathcal{G}_A^{-1} (S_j^n)_A M_A^{-1} \beta_R^t \qquad 8.11$$

where $\mathcal{G}_A$ is the symmetrised G matrix. The (S_j^n) terms are the S_j^n vectors of Meister and Cleveland see section 6.4. The β_R^t matrix for methyl iodide, with $M_H = 0$ reduces to the form:

	Translations t			Rotations r		
	ρ_{tx}	ρ_{ty}	ρ_{tz}	ρ_{rx}	ρ_{ry}	ρ_{rz}
X_1						
Y_1						
Z_1						
X_2		○			○	
Y_2						
Z_2						
X_3						
Y_3						
Z_3						
X_4	$M_4/M^{\frac{1}{2}}$			0	$-M_4Z_4/I_Y^{\frac{1}{2}}$	0
Y_4		$M_4/M^{\frac{1}{2}}$		$-M_4Z_4/I_X^{\frac{1}{2}}$	0	0
Z_4			$M_4/M^{\frac{1}{2}}$	$-M_4Y_4/I_X^{\frac{1}{2}}$	$-M_4Y_4/I_Y^{\frac{1}{2}}$	0
X_5	$M_5/M^{\frac{1}{2}}$			0	$-M_5Z_5/I_Y^{\frac{1}{2}}$	0
Y_5		$M_5/M^{\frac{1}{2}}$		$-M_5Z_5/I_X^{\frac{1}{2}}$	0	0
Z_3			$M_5/M^{\frac{1}{2}}$	$-M_5Y_5/I_X^{\frac{1}{2}}$	$-M_5Y_5/I_Y^{\frac{1}{2}}$	0

where the subscript numbers refer to the atoms as numbered in figure 35 . M is the mass of a particular atom, $M^{\frac{1}{2}}$ is the square root of the total atomic mass, and I is the moment of inertia.

For the reference molecule the moment of inertia about the z axis is zero thus all ζ_{rz} elements have been put as zero. As all translational elements will eventually be multiplied by zero (see equation 8.9), we shall simplify the matrix formulation by ignoring the ζ_t column. Therefore $M_A^{-1}\ \beta_R^t$ can be expressed as

	rotations r		
	ζ_{rx}	ζ_{ry}	ζ_{rz}
$X_{1,2,3}$ $Y_{1,2,3}$ $Z_{1,2,3}$		○	
X_4	0	$-Z_4/I_Y^{\frac{1}{2}}$	0
Y_4	$-Z_4/I_X^{\frac{1}{2}}$	0	0
Z_4	$-Y_4/I_X^{\frac{1}{2}}$	$-X_4/I_Y^{\frac{1}{2}}$	0
X_5	0	$-Z_5/I_Y^{\frac{1}{2}}$	0
Y_5	$-Z_5/I_X^{\frac{1}{2}}$	0	0
Z_5	$-Y_5/I_X^{\frac{1}{2}}$	$-X_5/I_Y^{\frac{1}{2}}$	0

In the reference molecule it is assumed that the only non zero component of the dipole moment is along the z axis (see equation 8.9), therefore all x and y coordinates go to zero.

In section 7.1.1 we stated that for a prolate symmetric top $I_y = I_x$. Thus if we know the centre of mass of the reference molecule we can determine I_y $(=I_x)$. As $M_H = 0$, then the centre of mass lies along the C–I bond, at a point X.

The distance $C - X = R_{CI} \frac{M_C}{M_I} - R_{CI}$

$= -1.9313\text{Å} = Z_5$

$I-X = .2017\text{Å} = Z_4$

As $I = Mr^2$ then

$$I_y = 12 \times (-1.9313)^2 + 126.9 \times (.2017)^2$$

$$= 49.92 \text{ a.m.u. } (\text{Å})^2$$

The coefficients of the $(S_j^n)_A$ matrix for the C and I atoms, in the E species were calculated as:

	X_4	Y_4	Z_4	X_5	Y_5	Z_5
S_{4a}	0	0	0	1.141	0	0
S_{5a}	.625	0	0	1.586	0	0
S_{6a}	0	0	0	.985	0	0

Hence the matrix $(s_j^n)_A M^{-1} \beta_R^t$ is of the form

	ϱ_{r_x}	ϱ_{r_y}	ϱ_{r_z}
S_{4a}	0	$Z_S \, 1.141/I_y^{\frac{1}{2}}$	0
S_{5a}	0	$Z_5 \, 1.586/I_y^{\frac{1}{2}}$	0
S_6	0	$\dfrac{(Z_4 \, 0.625 - .985 \, Z_S)}{I_y^{\frac{1}{2}}}$	0

The $\mathcal{G}$ and $\mathcal{G}^{-1}$ matrices are given in Table 25 for CH_3I and CD_3I. Thus $\mathcal{G}_A^{-1} (S_j^n)_A M_A^{-1} \beta_R^t$ gives the following elements in the ϱ_{ry} column; the other elements being zeros.

	ζ_{r_y}
S_{4a}	$-1.623/I_y^{\frac{1}{2}}$
S_{5a}	$-1.2405/I_y^{\frac{1}{2}}$
S_{6a}	$+2.1028/I_y^{\frac{1}{2}}$

As already shown in equation 8.9 $\alpha_A^t (\partial\rho/\partial X)$ is expressed in terms of dipole moment contributions along the x, y and z axes. For the reference molecule the only non zero component is that along the z axis, p_o^z. Thus $(p_o^z)_i = (p_o^z)/I_y^{\frac{1}{2}}$ (see equation 8.9).

If we adopt Whiffen's definition of dipole moment[166], then for methyl iodide the permanent dipole moment is directed from the halogen atom (negative) to the methyl group (positive), this corresponds to assuming p_o^z to be negative. If this assumption is made about the direction of the permanent dipole moment, then the sign of V_{AR} is determined unambiguously. Thus we shall quote p_o^z as -1.62[116]

The values of the rotational corrections for methyl iodide, using the symmetry coordinates of Table 12, and with a reference molecule in which $M_H = 0$, are therefore given by:

$$V_4 = \frac{-1.623 \times (-1.62)}{I_y} \qquad V_5 = \frac{1.2405 \times (-1.62)}{I_y} \qquad V_6 = \frac{2.1028 \times (-1.62)}{I_y}$$

Table 25a The $\mathcal{G}$ matrix for the CH_3I(and CD_3I) molecule, exact geometry.

	A class		E class
1-1	$M + 3M_1 C\beta^2$	4-4	$M + M_1(1-C\beta)$
1-2	$3M_1\sqrt{(K^2+1)}S\beta C\beta$	4-5	$M_1(1-C\alpha)^2/S\alpha$
1-3	$M_1\sqrt{(3)}\ C\beta$	4-6	$M_1 3S\beta(C\beta-\lambda)/2$
2-2	$(K^2+1)(M + 3M_1 S\beta^2)$	5-5	$M(3-K^2/2) + M_1(1-C\alpha)^3/S\alpha^2$
2-3	$M_1\sqrt{(3)}\ \sqrt{(K^2+1)}S\beta$	5-6	$K/2[M-M_1(C\beta-\lambda)(1-C\alpha)/C\beta]$
3-3	$M_1 + I$	6-6	$M+3M_1(C\beta-\lambda)^2/2 + 3I\lambda^2/2$

M, M_1 and I are the reciprocal masses of H, C and I respectively.

$C\alpha = \cos\alpha$ etc; $\lambda = r_e(CH)/r_{e(CI)}$; $K = -3S\beta C\beta/S\alpha$;

$\alpha = \hat{HCH}$ and $\beta = \hat{HCI}$ in the equilibrium configuration.

Table 25b

$\mathcal{G}^{-1}$ for the E class.

CH_3I	4-4	.923	CD_3I	4-4	1.769
	4-5	-.067		4-5	-.214
	4-6	.103		4-6	.329
	5-5	.375		5-5	.697
	5-6	-.117		5-6	-.140
	6-6	.972		6-6	1.815

Table 26 Rotational Corrections in methyl iodide

	P_o(D)	Reference molecule with $M_X = 0$			Reference molecule with M_C, M_Y x 1000		
		V_{4X}	V_{5X}	V_{6X}	V_{4X}	V_{5X}	V_{6X}
H_3CI	-1.62	.0527	.0403	-.0682	.0525	.0403	-.0680
D_3CI	-1.62	.0836	.0632	-.1098	.0835	.0630	-.1097

Van Straten and Smit also proposed another reference molecule model. This was used to overcome the problems of having pyramidal X_3Y molecules, in which the introduction of an X isotope with zero mass leads to indefinite elements in the β_R^t matrix, thus prohibiting the calculation of the rotational corrections. In this reference molecule the atoms of the actual molecule, which are situated on the main symmetry axis, are replaced by isotopes that are a factor of a thousand or more heavier than the original atoms. In such a reference molecule the compensating rotational motions are negligible because of the large masses of the substituted isotopes. Using this other reference molecule we concluded (as did Van Straten and Smit) that the results agree to within 1% of those obtained using a reference molecule with zero H masses (see Table 26).

8.2.2 (iii) Values of P_j for the E species

In Table 27 values of $(P_H)_j$ and $(P_D)_j$ are given for all sign combinations (reversing the signs of a combination, merely reverses the signs of $(P_H)_j$ and $(P_D)_j$).

Table 27 Methyl iodide E class values of $(P_H)_j$ and $(P_D)_j$ in D/Å.

CH_3I		S_4	S_5	S_6
(P_H)	(+++)	.0881	.2858	−.3161
	(++−)	.1806	.1593	.3796
	(+−+)	.1212	−.1644	−.3912
	(+−−)	.2137	−.2903	.3046
CD_3I				
(P_D)	(+++)	.0035	.2733	−.2556
	(++−)	.1233	.2105	.3053
	(+−+)	.1107	−.2111	−.3159
	(+−−)	.2305	−.2780	.2551

The rotational corrections V_{HR} and V_{DR} are now subtracted from (P_H) and (P_D), for all sign combinations, in accord with equation 8.3 to give (P_R) (see Table 28).

Table 28 Calculated $(\rho_R)_j$ values for various sign choices.

		$(\rho_R)_4$	$(\rho_R)_5$	$(\rho_R)_5$	
CH_3I	(+++)	.0354	.2455	−.2479	Rejected
CD_3I		−.0801	.2141	−.1558	
H	(−−−)	−.1408	−.3261	.3843	Rejected
D		−.0871	−.3405	.3754	
H	(++−)	.1279	.1190	.4478	Rejected
D		.0397	.1473	.4151	
H	(−−+)	−.2333	−.1996	−.3114	Rejected
D		−.2069	−.2737	−.1955	
H	(+−+)	.0685	−.2047	−.3230	Rejected
D		.0271	−.2743	−.2061	
H	(−+−)	−.1739	.1241	.4594	Choice B
		−.1943	.1478	.4257	
H	(+−−)	.1610	−.3312	.3728	
D		.1469	−.3412	.3649	Choice A
H	(−++)	−.2664	.2506	−.2364	Rejected
D		−.3141	.2148	−.1453	

The examination of all the possible sign combinations given in Table 28 can be carried out systematically, by comparing the values for each isotope. For each sign combination the values for each isotope should agree within limits of error. It can be seen that most of the choices can be rejected out of hand, because of too large

a discrepancy in the isotopic values of (P_R). We consider that there are only two choices for which the isotopic values agree relatively well, these are labelled A and B in Table 28. The errors in B are marginally larger than those in A. To obtain final values of $(P_R)_j$ we average the data for each species.

In Table 29 we summarise the final values of $(P_R)_j$ for the E and A classes, obtained in this study. We compare our results with those of Russell et al[123]. In the A class only the relative signs are determined whereas in the E class the signs have been absolutely determined.

Table 29 Values of $(P_R)_j$ in methyl iodide from the preferred sign combinations in Debye/Å; averaged data from CH_3I and CD_3I molecules.

	This work			Russell et al			
A class (+−+)		E class (+−−)		A class		E class	
P_1^z	.4543	P_4^{xy}	.1540	P_1^z	.4648	P_4^{xy}	.1448
P_2^z	−.4929	P_5^{xy}	−.3362	P_2^z	−.4555	P_5^{xy}	−.3435
P_3^z	−.5367	P_6^{xy}	.3689	P_3^z	−.5597	P_6^{xy}	.4056

We believe that the minor differences in the values of the P_j's from the two studies listed in Table 29, are due only to differences in the normal coordinate coefficients, that were used.

8.2.3 Bond Effective Moments

As previously stated, Dickson et. al. discussed the dipole moment changes in a molecule in terms of small effective moments and charges attached rigidly to the bonds of the molecule. The former giving rise to dipole moment changes when the bond bends and the latter when it stretches. Dickson et al related the observed Γ_j values to these bond effective moments by simple geometrical relations[167].

$$
\begin{aligned}
P_1^z &= \sqrt{3}\cos\beta\,\epsilon_{CH} \\
P_2^z &= \frac{\sqrt{3}}{\sqrt{2}}(P+Q)\sin\beta\,\frac{\mu_{CH}}{r_e} \\
P_3^z &= \epsilon_{CI} \\
P_4^{xy} &= +\frac{\sqrt{3}}{\sqrt{2}}\sin\beta\,\epsilon_{CH} \\
P_5^{xy} &= -\sqrt{2}\cos\left(\frac{\alpha}{2}\right)\frac{\mu_{CH}}{r_e} \\
P_6^{xy} &= -\sqrt{6}\cos\beta\,\frac{\mu_{CH}}{r_e}
\end{aligned}
\qquad 8.12
$$

where μ_{CH} is the effective moment in the CH bond, defined to be positive in the sense $C^- - H^+$; r_e is the equilibrium and CH bond distance and $\epsilon_{CH} = (\partial\mu_{CH}/\partial r)$; also $\epsilon_{CI} = (\partial\mu_{CI}/\partial R_{CI})$, where R_{CI} is the carbon-iodine bond distance, and μ_{CI} is the carbon-iodine bond moment defined positive in the sense $C^- - I^+$. P and Q are the redundancy factors in the A_1 class of symmetry coordinates (see Table 12).

In Table 30 the bond effective moments are listed, calculated by applying equation 8.12 to the p_j values of Table 29. In the E class the signs are absolutely determined on the assumption that ρ_o^z is negative $(CH_3^+ - X^-)$.

Table 30 Final bond effective moments for CH_3I derived from the preferred sign combinations, in D/Å. Averaged data from the CH_3I and CD_3I molecules.

A_1	$S_1 \epsilon_{CH}$	$= -.8678$
	$S_2 \mu_{CH}$	$= -.4418$
	$S_3 \epsilon_{CI}$	$= -.5367$
	$S_4 \epsilon_{CH}$	$= +.1319$
	$S_5 \mu_{CH}$	$= .4570$
	$S_6 \mu_{CH}$	$= .5410$

At this point we shall merely comment that the various values of μ_{CH} from the different symmetry species should be the same, and so should the values of ϵ_{CH}. Thus it would appear that this picture is a rather oversimplified one. We shall discuss this further in section 8.5.

8.3 The Gribov Formulation[162,168]

8.3.1 Introduction

The initial step is to calculate the first derivatives of the dipole moment with respect to the normal coordinates from the experimental data. These values have already been given in Table 22. The fact that the dipole moment p and the normal coordinates characterise the state of the molecule as a whole, makes it necessary to describe the behaviour of the various component parts of the molecule before information concerning the structure and intramolecular processes can be obtained from the intensities.

In the Gribov formulation the total molecular dipole is formally resolved into components along the bonds. These components are the sum of dipole moments localised on and along the bonds, with the components of the residual dipole contributions due to off axis moments and lone pair electrons. The resolution of the latter contributions is rather arbitrary, and generally the resolved components will not be centred on the bonds.

8.3.2 The Theory

Considering p as the sum of vector parameters μ_K along each bond, then on vibration the magnitude and direction of these μ_K vectors can alter. These contributions are written as $\mu_K e_K$, where e_K is a unit vector along the bond.

Thus

$$p = \sum_k \mu_k e_k \qquad 8.13$$

If we now consider changes of the dipole moment, represented in terms of $\partial p/\partial Q$, then it is found that there are, not only the μ_K terms, but also derivatives of μ_K with respect to the internal coordinates; these derivatives and the μ_K terms forming the so-

called valence parameters of the molecule. These parameters enter as variables in a system of linear equations. They are independent of the mechanical properties of the molecule, and reflect only the nature of the electron cloud. If the set of bond extension coordinates is designated by r, and the remaining bending coordinates by ϕ then (in matrix form) we have[169]

$$\left(\frac{\partial p}{\partial Q_i}\right) = \left[(e)\left(\frac{\partial \mu}{\partial r} \,\vdots\, \frac{\partial \mu}{\partial \phi}\right) + (\mu)\left(\frac{\partial e}{\partial r} \,\vdots\, \frac{\partial e}{\partial \phi}\right)\right]\left(\begin{matrix} l r_i \\ \hline l \phi_i \end{matrix}\right) \qquad 8.14$$

where $(e) = (e_1, e_2 \ldots e_k)$ is a row matrix whose elements are the unit vectors along the bonds, (μ) is a row matrix with the kth effective bond dipole μ_k as elements. $\left(\frac{\partial \mu}{\partial r} \,\vdots\, \frac{\partial \mu}{\partial \phi}\right)$ is a rectangular array of derivatives of the bond dipole moments with respect to the internal coordinates $\left(\begin{matrix} l r_i \\ \hline l \phi_i \end{matrix}\right)$ is a column vector of the appropriate normal coordinate terms defining Q in terms of r and ϕ. The matrix $\left(\frac{\partial e}{\partial r} \,\vdots\, \frac{\partial e}{\partial \phi}\right)$ determines the change in direction of the bond moments resulting from vibration induced bond rotation (i.e. the rotational correction). The most laborious part of the calculations is the development of the $\left(\frac{\partial e}{\partial r} \,\vdots\, \frac{\partial e}{\partial \phi}\right)$ matrix. This has been treated in detail by Gribov[162], the result being that the bond reorientation terms $\frac{\partial e}{\partial r}$, $\frac{\partial e}{\partial \phi}$ can be written by

$$\left(\frac{\partial e}{\partial r} \,\vdots\, \frac{\partial e}{\partial \phi}\right) = \mathcal{R}^{-1}\left(\Delta M^{-1} B^t G^{-1} - [E \,\vdots\, 0]\right) \qquad 8.15$$

B and G have been defined in equations 6.24 and 6.25. M^{-1} is the diagonal matrix of the nuclear masses. Δ is a matrix in which the number of rows is equal to the number of bonds, and the number of columns is equal to the number of Cartesian coordinates (or number

of atoms if entries are considered as vectors). The row corresponding to a given bond shows the value of +1 in the columns for the terminal atom, and −1 in the columns referring to the coordinates of the initial atom. $\mathfrak{R}^{-1}$ is the diagonal matrix of the reciporcal bond lengths. E is a diagonal square matrix of bond direction vectors, and O is the null matrix of dimensions, of the number of bonds by the number of deformation coordinates less the number of bonds. Substitution of equation 8.15 into 8.14 therefore gives

$$\frac{\partial p}{\partial Q_i} = \left[e \left(\frac{\partial \mu}{\partial r} \vdots \frac{\partial \mu}{\partial \phi} \right) + \mu \mathfrak{R}^{-1} \left(\Delta M^{-1} B^t G^{-1} - [E \vdots O] \right) \right] l_i \qquad 8.16$$

The main limitation to this formulation, is that it involves the computation of G^{-1}. If the chosen basis set of internal valence coordinates involves a redundancy then G will be singular. To overcome this limitation the problem can be transformed at the outset to a molecule fixed cartesian axis system. Defining the relation between internal and nuclear centred cartesian displacement coordinates as R = Bq, then as the reverse relationship cannot be directly derived as B is not square, the reverse transformation is given as

$$q = AR \qquad 8.17$$

Substitution of R = Bq gives q = ABq and therefore AB = E. From equation 6.24 and premultiplying by A we have

$$AG = AB M^{-1} B^t \qquad 8.18$$

$$\text{or} \quad A = M^{-1} B^t G^{-1} \qquad 8.19$$

Use of equation 8.17 gives

$$q = M^{-1} B^t G^{-1} R$$
$$= M^{-1} B^t G^{-1} L Q \qquad 8.20$$

$L = DY$, where Y represents the eigenvectors of D^tFD (D is the diagonal matrix of the reciprocal square roots of the atomic masses). Q is considered to be a normalising constant (see reference 1). Now making the appropriate substitutions into equation 8.15 we have

$$\left(\frac{\partial e}{\partial r} \vdots \frac{\partial e}{\partial \phi}\right)\begin{pmatrix} l_{r_i} \\ l_{\phi_i} \end{pmatrix} = \mathcal{R}^{-1}\,(\Delta - [E \vdots 0]D)\,Y \qquad 8.21$$

The transformation of 8.18 into terms arising from a basis set of symmetry coordinates is straightforward.

$$\frac{\partial p}{\partial Q_i} = \left[e^s \left(\frac{\partial \mu}{\partial S_r} \frac{\partial \mu}{\partial S_\phi}\right)_{eq} + \mu_{eq}\ \mathcal{R}_{eq}^{-1}(\Delta_{eq}M^{-1}(S_j^n)^t\ \mathcal{G}^{-1} - [E^s_{eq} \vdots 0])\right]\begin{pmatrix} l^s_{r_i} \\ l^s_{\phi_i} \end{pmatrix} \qquad 8.22$$

where e^s is a row of non normalised symmetry direction vectors, these being obtained by combining the unit direction vectors of equivalent bonds in the ratio as defined in the appropriate symmetry coordinates S_r. The S_r and S_ϕ are the symmetry coordinates for stretching and bending deformations respectively. $\left(\frac{\partial \mu}{\partial S_r} \vdots \frac{\partial \mu}{\partial S_\phi}\right)_{eq}$ is obtained from $\left(\frac{\partial \mu}{\partial S_r} \vdots \frac{\partial \mu}{\partial S_\phi}\right)$ by striking out all the rows corresponding to equivalent bonds with the exception of the first of each set. Similarly μ_{eq} and $\mathcal{R}^{-1}_{eq}$ are formed by striking out from μ and $\mathcal{R}^{-1}$ all rows except one, corresponding to each equivalent set of bonds. $(S_j^n)^t$ is the transpose of the (S_j^n) matrix, where S_j^n are vectors defined in section 6.4. E^s_{eq} is a diagonalised matrix of normalized symmetry direction vectors.

In the zero order approximation of this theory, all bond moments are assumed to depend only on the variation of their own lengths. On this basis several calculations have been carried out for the bond moments, and their derivatives, with respect to the stretching of their bonds, using the experimental results of the band intensities. However, with this approximation different sets of values are obtained for bond moments and bond derivatives from the sets of the band intensities belonging to different symmetry species, (as happened using the bond moment hypothesis in section 8.2 (see Table 30)). Also the vector sum of the bond moments is not equal to the total dipole moment of the molecule. This fact suggests that this approximation is too rough to explain the observed intensities well. This problem can, however, be well resolved by considering the first order approximation of this valence optical theory. This was the approach used by Gribov.

8.3.3 Expressions for $\partial p/\partial Q_i$ of methyl iodide

After taking into account the symmetry and supplementary relations between the angular coordinates Gribov deduced expressions for the $\partial p/\partial Q_i$ values of methyl iodide. For A type vibrations

$$\frac{\partial p}{\partial Q_i} = \sqrt{3}\left[\frac{1}{3}\left(\frac{\partial \mu}{\partial r} + 2\frac{\partial \mu}{\partial r'}\right) - \frac{\partial \mu_{CI}}{\partial r}\right] r_i^s - \left[\frac{\partial \mu_{CI}}{\partial R_{CI}} - \frac{\partial \mu}{\partial R_{CI}}\right] R_i$$
$$+ \sqrt{3}\left\{\frac{1}{3}\left[\left(\frac{\partial \mu}{\partial \beta} + 2\frac{\partial \mu}{\partial \beta'}\right) - \left(2\frac{\partial \mu}{\partial \alpha} + \frac{\partial \mu}{\partial \alpha'}\right)\right] - \left(\frac{\partial \mu_{CI}}{\partial \beta} - \frac{\partial \mu_{CI}}{\partial \alpha}\right) + \frac{1}{S_{CH}}\mu \sin\theta\right\} \beta_i^s \qquad 8.23$$

For E type vibrations

$$\left(\frac{\partial p}{\partial Q_i}\right) = \sqrt{2}\sin\frac{\theta}{2}\left[\left(\frac{\partial\mu}{\partial r} - \frac{\partial\mu}{\partial r'}\right)r_i^s + \left(\frac{\partial\mu}{\partial\alpha'} - \frac{\partial\mu}{\partial\alpha}\right)\alpha_i^s + \left(\frac{\partial\mu}{\partial\beta} - \frac{\partial\mu}{\partial\beta'}\right)\beta_i^s\right] + \mu_{CI}\,\delta e_{CI}^{(i)} + \mu\sum_k^3 \delta e_k^{(i)} \qquad 8.24$$

Where θ is the tetrahedral angle, α_i^s, β_i^s, r_i^s and R_i are the normalised symmetry coordinates for the ith vibration, they are given by the elements of the $\mathcal{L}$ matrix (see Table 23). The system of vibration coordinates is given in figure 34. The dipole moment of the C-H bond is designated by μ and that of the C-I bond by μ_{CI}. Primed coordinates are used to represent the derivatives of the bond dipole moments with respect to changes in the opposing bonds and angles. $\delta e^{(i)}$ is the total differential of the e (bond rotation) vector for a given mode of vibration.

8.3.4 The A_1 species

The intensities of the A type vibrations are characterised by three combinations of the valence optical parameters. These combinations are:

$$\left[\frac{1}{3}\left(\frac{\partial\mu}{\partial r} + 2\frac{\partial\mu}{\partial r'}\right) - \frac{\partial\mu_{CI}}{\partial r}\right] \quad , \quad \left[\frac{\partial\mu_{CI}}{\partial R_{CI}} - \frac{\partial\mu}{\partial R_{CI}}\right] ,$$

and $$\left\{\frac{1}{3}\left[\left(\frac{\partial\mu}{\partial\beta} + 2\frac{\partial\mu}{\partial\beta'}\right) - \left(2\frac{\partial\mu}{\partial\alpha} + \frac{\partial\mu}{\partial\alpha'}\right)\right] - \left(\frac{\partial\mu_{CI}}{\partial\beta} - \frac{\partial\mu_{CI}}{\partial\alpha}\right) + \frac{1}{S_{CH}}\mu\sin\theta\right\}$$

Six equations for the determination of these combinations can be set up for methyl iodide by using the intensity data for the completely deuterated molecule CD_3I, (Mills intensity data is used for CD_3I and my data for CH_3I).

As for the method of Dickson et al (section 8.2) the unknown relative signs of the $\partial p/\partial Q_i$ terms require that we consider all sign combinations. These are given in Table 31.

Table 31(a) Values of the valence optical parameters for the A_1 species of methyl iodide, for all sign choices of $\partial p/\partial Q_i$. Units are Debyes/Å.

Parameter	Sign Choices			
	(+−+)	(+++)	(+−−)	(++−)
(1) $\frac{1}{3}\left(\frac{\partial\mu}{\partial r}+2\frac{\partial\mu}{\partial r'}\right)-\frac{\partial\mu_{CI}}{\partial r}$	.266	.345	.304	.382
(2) $\left(\frac{\partial\mu_{CI}}{\partial R_{CI}}-\frac{\partial\mu}{\partial R_{CI}}\right)$	.528	.828	−.798	−.540
(3) $\frac{1}{3}\left[\left(\frac{\partial\mu}{\partial\beta}+2\frac{\partial\mu}{\partial\beta'}\right)-\left(2\frac{\partial\mu}{\partial\alpha}+\frac{\partial\mu}{\partial\alpha'}\right)\right]$				
$-\left(\frac{\partial\mu_{CI}}{\partial\beta}-\frac{\partial\mu_{CI}}{\partial\alpha}\right)+\frac{1}{S_{CH}}\mu\sin\theta$	−.286	.351	−.358	.276
	Choice A	Rejected	Rejected	Choice B

Table 31(b) Recalculated values of $\partial p/\partial Q$, obtained by substitution of choices A and B (in Table 31a) into equation 8.23. Percentage deviations from the observed values of $\partial p/\partial Q$ are also quoted.

	Choice A (+−+)		Choice B (++−)	
	$\partial p/\partial Q$	% deviation	$\partial p/\partial Q$	% deviation
CH_3I				
Q_1	.541	2.5	.591	6.5
Q_2	−.728	1.4	+.710	3.7
Q_3	.212	2.8	−.217	0.6
CD_3I				
Q_1	.444	4.5	.368	13.4
Q_2	−.590	2.0	+.590	2.0
Q_3	.154	0.7	−.164	7.2

By reversing all the sign choices in Table 31a we obtain the same parameter values except that they have opposite signs. When the values of $\partial p/\partial Q$ are recalculated using the parameter values of Table 31a and equation 8.23 then we find that only two sets of sign choice (given by A and B) give small percentage deviations from the observed $\partial p/\partial Q$ values. We prefer sign choice A as the percentage deviations are the smallest.

In Table 32 our values of the A class parameters are compared with those obtained by Gribov.

Table 32 A comparison of the values of the parameters for the A_1 class obtained from this work and by Gribov[162]. The numbers (1), (2) and (3) refer to the parameters in Table 31a.

	Parameter		
	(1)	(2)	(3)
This work	.266	.528	-.286
Gribov	.29	.50	-.38

8.3.5 The E species

The six equations (obtained by using the intensity data for CD_3I as well) for the E type vibrations, can be used to separately determine the five quantities

$$\left(\frac{\partial \mu}{\partial r} - \frac{\partial \mu}{\partial r'}\right) \quad ; \left(\frac{\partial \mu}{\partial \alpha'} - \frac{\partial \mu}{\partial \alpha}\right) ; \left(\frac{\partial \mu}{\partial \beta} - \frac{\partial \mu}{\partial \beta'}\right) \quad ; \mu_{CI} \text{ and } \mu$$

The coefficie nts of bond vibration, δe_{CI} and δe_K (which are bond dipole reorientation terms inclusive of rotational correction) can be calculated from Gribov's theory[162], using Duncan et al's force constant data[124] and the equilibrium geometry given in figure 34. The coefficients are listed in Table 33.

Table 33 Coefficients of bond vibration for the E class of methyl iodide (calculated using the force constant data of ref.124; see Table 14).

CH_3I	δe_{CI}	$\sum_K^3 \delta e_K$	CD_3I	δe_{CI}	$\sum_K^3 \delta e_K$
$S_{4_{ab}}$	-.0437	+.1285		-.0600	+.1991
$S_{5_{ab}}$	-.0330	+. 750		-.0421	+.7592
$S_{6_{ab}}$	-.0457	+. 989		-.0515	+.5042

As for the A species we again had to consider all the relative signs of $\partial p/\partial Q$. Values of the parameters, for each of the different sign choices, were obtained by the substitution of the particular L matrix values and coefficients of bond vibration (see Tables 23 and 33) into equation 8.24.

A constraint which it was found necessary to use was that, μ_{CI} be directly related to μ. From the molecular geometry it can be seen that

$$+\mu_{CI} - 3\mu(\sin(\beta-90)) = p_o \qquad 8.25$$

For $\beta = 107.59$ and $p_o = -1.62$ D, then equation 8.25 becomes

$$-.9066\mu + \mu_{CI} = -1.62 \qquad 8.26$$

In obtaining equation 8.26 we assumed that p_o is defined in the sense $(CH_3^+ - I^-)$, as in section 8.2. In Table 34 we show the values

of the E species parameters for the different sign choices. We assume that the $(\partial p/\partial Q)$ sign choices for CD_3I are the same as those for CH_3I as can be deduced from our work on the method of Dickson et al (for instance see Table 29).

In Table 34 most of the sign choices can be rejected on the grounds that either μ_{CI} or μ have values which far exceed the dipole moment of the molecule. We are left with two choices, A and B. By using the same procedure as for the A_1 class, we can determine the percentage discrepancy between the observed and calculated $(\partial p/\partial Q)$'s. The best set of parameters will be that with the smallest total percentage discrepancy (see Table 35a). In Table 35b we compare the parameters of choices A and B, with those quoted by Gribov. Whilst it seems that choice B has the closer agreement with Gribov's values it can be seen that choice A gives the best recalculated $\partial p/\partial Q$'s. There is good agreement in the magnitudes of μ_{CI} and μ.

We shall discuss the relative merits of Gribov's formulation in a later section (8.5); when we shall compare it with both Dickson et al's and McKean's methods. However all that remains at present is to say that the main strength of the Gribov method is to be found when comparing the parameters for a series of simple molecules. For instance Gribov has shown that the relative signs of the parameter combinations which characterise the A_1 and E vibrations can be determined by a study of the parameters (1) and (4) for CH_3Cl and ethane [124]. Similarly it is possible to observe trends in the parameters for the methyl halide series. Gribov noted that parameter (2) increases markedly with bond covalency. This fact was explained in terms of a marked increase in the effect of

Table 34 Values of the valence optical parameters for the E species of methyl iodide, for all sign choices of $\partial p/\partial Q$. Units are Debyes/Å, except for the dipole moments which are in Debyes. Using the constraint $-.9066\mu + \mu_{CI} = -1.62$. Signs of $\partial p/\partial Q$ for CH_3I and CD_3I are the same

Parameters	Sign choices							
	(+++)	(−−−)	(++−)	(−−+)	(+−+)	(−+−)	(+−−)	(−++)
$\left(\frac{\partial\mu}{\partial r} - \frac{\partial\mu}{\partial r'}\right)$	+.127	−.127	+.101	−.101	+.177	−.177	+.151	−.151
$\left(\frac{\partial\mu}{\partial\alpha'} - \frac{\partial\mu}{\partial\alpha}\right)$	−1.138	−.111	−.060	−1.188	−1.535	+.286	−.457	−.791
$\left(\frac{\partial\mu}{\partial\beta} - \frac{\partial\mu}{\partial\beta'}\right)$	.979	.179	.534	.624	.913	.246	.468	.690
μ_{CI}	+.261	−1.883	−1.38	+.235	+.249	−1.870	−1.399	−.222
μ	2.075	−.289	.257	1.528	2.061	−.276	.243	1.542
	Rejected	Rejected	Choice B	Rejected	Rejected	Rejected	Choice A	Rejected

Table 35a Recalculated values of $\partial p/\partial Q$, for the E class of methyl iodide, obtained by substitution of the parameter sets A and B into equation 8.24. Percentage deviations of the calculated $\partial p/\partial Q$ from the observed $\partial p/\partial Q$ (see Table 22) are also quoted

	Choice A (+—)		Choice B (++—)	
CH_3I	$\partial p/\partial Q$	% deviation	$\partial p/\partial Q$	% discrepancy
Q_4	.158	1.5	.134	13.5
Q_5	−.359	1.4	.365	3.1
Q_6	−.322	1.6	−.312	4.7
CD_3I				
Q_4	.094	2.2	.125	35.6
Q_5	−.269	2.4	+.256	7.2
Q_6	−.205	3.9	−.219	11.2

Table 35b A comparison of the parameter sets A and B with the parameter values quoted by Gribov .

	Gribov	A	B
(4) $\left(\frac{\partial\mu}{\partial r} - \frac{\partial\mu}{\partial r'}\right)$	.15	.151	.101
(5) $\left(\frac{\partial\mu}{\partial\alpha'} - \frac{\partial\mu}{\partial\alpha}\right)$	−.05	−.457	−.06
(6) $\left(\frac{\partial\mu}{\partial\beta} - \frac{\partial\mu}{\partial\beta'}\right)$	.27	.468	.534
μ_{CI}	−1.42	−1.399	−1.387
$(.9066)\mu$	(μ =) +.20	+.220	+.235

$\left(\frac{\partial \mu_{CX}}{\partial \beta} - \frac{\partial \mu_{CX}}{\partial \alpha}\right)$ with increasing degree of overlap of the electron clouds of the CX and CH bonds. The parameter $\left(\frac{\partial \mu}{\partial \beta} - \frac{\partial \mu}{\beta'}\right)$ was found to increase at the same time, as it must since it characterised the change in the CX bond dipole resulting from alteration in the angle adjoining the CX bond. Gribov concluded that, while these parameters are highly sensitive instruments for studying effects from various substitutions, their sensitivity reduces the accuracy of spectral intensities calculated for complex molecules on the basis of parameter values for analogous molecules.

8.4 The Barrow, Crawford and McKean treatment[170,171]

Parameters μ_k and $(\partial\mu/\partial r)_k = \epsilon_k$ are assigned to each bond k such that the extension of the bond by an amount δr produces a moment $(\partial\mu/\partial r)_k \delta r$ directed along the bond, while rotation of the bond through an angle α produces a moment, $(\partial\mu/\partial \alpha).\delta\alpha = \mu_k \delta\alpha$, at right angles to the bond. The moments are assumed to add vectorially throughout the molecule. The connection between μ_k and ϵ_k and $\partial p/\partial Q$ is usually made in two stages. First the change of moment with symmetry coordinate, S, is calculated, from experimental data, using equation 8.2a; the results of which are listed in Table 22. Secondly the relations between $\partial p/\partial S$, and μ_k and ϵ_k are calculated. The principles of this second stage have been discussed in section 8.2.

The method of Barrow et al is fundamentally different from that of section 8.2 in that, rather than having to consider a separate rotational correction term, the correction term becomes an integral part of the formulation. Indeed the method is very like that of Gribov's (see section 8.3).

We have seen that the 'bond moment approximation' involves the assumptions that the molecular dipole moment p is given by

$$p = \sum_k \mu_k e_k$$

where e_k is a vector along the bond k, and μ_k are vector parameters along each bond. Thus a change in p is given by

$$\delta p = \sum_k \mu_k \delta e_k + \sum e_k \delta \mu_k \qquad 8.27$$

where δe_k is a vector perpendicular to e_k. The first term represents the contribution from bond rotation, the second to bond stretching. In the latter of course $\delta \mu_k = \epsilon_k \delta r$. δe_k and $\delta \mu_k$ have to be determined from the Cartesian displacements of each of the atoms in the bond k during a change in the symmetry coordinate S_j.

Considering an atom n and defining quantities σ_{kn} such that

$\sigma_{kn} = 0$ if n is not a terminal atom of bond k

$\sigma_{kn} = +1$ if e_k points away from atom n

$\sigma_{kn} = -1$ if e_k points towards atom n.

If the Cartesian displacement vector of atom n is ρ_n then

$$\delta r_k = -\sum_{k\,kn} \sigma_{kn} e_k \rho_k \qquad 8.28a$$

$$\text{and } \delta e_k = -\sum_{k\,kn} \sigma_{kn} \frac{1}{r_k} [\rho_n - e_k (\rho_n \cdot e_k)] \qquad 8.28b$$

Substitution of equations 8.28a and 8.28b, into equation 8.27, we find that the contribution of a particular atom n to the change in dipole

moment δ_p is given by

$$\delta_p = -\sum\left\{ \sigma_{kn} \epsilon_k e_k (e_k \cdot \rho_n) + \sigma_{kn}\left(\frac{\mu_k}{r_k}\right)[\rho_n - e_k(\rho_n \cdot e_k)]\right\} \quad 8.29$$

For all the atoms a further summation over n is added. Thus δ_p can be represented as a sum of terms of the type $(K)(\rho_n)$, where (K) is a row and (ρ_n) is a column vector.

Now the cartesian displacements (ρ_n) are given by[172]

$$(\rho_n) = (M^{-1})(S_j^n)(\mathcal{G}^{-1})(S) \quad 8.30$$

where M^{-1} is the diagonal inverse mass matrix, (S_j^n) is the matrix of S_j^n vectors of Meister and Cleveland (see section 6.4). S is the symmetry coordinate matrix (given by equation 8.1).

We may therefore write,

$$\delta_p = \sum(K)(M^{-1})(S_j^n)(\mathcal{G}^{-1})(S) \quad 8.31$$

The column vector $(\partial p/\partial S)$ is therefore given by a series of terms

$$(\mathcal{G}^{-1})(S_j^n)(M^{-1})\sum(K)^t$$

or $(\mathcal{G}^{-1})(D_j)$ where (D_j) is a column vector.

The direction of $\partial p/\partial S$ is usually known: suppose it is along the z axis.

Then we may write

$$\left(\frac{\partial p_z}{\partial S}\right) = \mathcal{G}^{-1}(D_j \cdot e_z) \quad 8.32$$

$$= \mathcal{G}^{-1} D_j \text{ (where } e_z \text{ is the unit vector along the z axis).}$$

From equation 8.29 it can be shown that the elements of D_j are given as follows:-

$$D_j = \sum_k (\Delta r)_{kj} \epsilon_k e_k e_z + \sum_k (\Delta\beta)_{kj} \mu_k e_z \qquad 8.33$$

where $$(\Delta r)_{kj} = \sum_n \frac{-\sigma_{kn}}{m_n} (e_k . S_j^n) \qquad 8.33a$$

and $$(\Delta\beta)_{kj} = \sum_n \frac{-\sigma_{kn}}{m_n r_k} \left\{ S_j^n - e_k (e_k . S_j^n) \right\} \qquad 8.33b$$

The D matrix for the E species of methyl iodide is given in Table 36a. The constituent parts of each D matrix element are tabulated first according to the respective μ_k or ϵ_k parameter and secondly according to the appropriate reciprocal mass $1/M_n$.
The numerical values of the coefficients of the D matrix for methyl iodide are listed in Table 36b.

Table 36a D matrix* for the E species of methyl iodide+

	ϵ_{CH}		μ_{CH}		μ_{CI}	
	$\frac{1}{M_H}$	$\frac{1}{M_C}$	$\frac{1}{M_H}$	$\frac{1}{M_C}$	$\frac{1}{M_I}$	$\frac{1}{M_C}$
S_{4ab}	$2/\sqrt{3}$	$8\sqrt{3}/9$		$-10\sqrt{3}T/9$		$\frac{-2F}{\sqrt{3}}$
S_{5ab}		$8\sqrt{6}/9$	$-2T\sqrt{6}/3$	$-10T\sqrt{6}/9$		$\frac{-2F\sqrt{6}}{3}$
S_{6ab}		$\frac{-2\sqrt{6}\left(\frac{F}{T}+\frac{1}{3}\right)}{3}$	$+T/\sqrt{6}$	$\frac{+5(F+T/3}{6}$	$\frac{+F^2}{T}\ \frac{\sqrt{6}}{2}$	$\frac{+F(F+T/3)\sqrt{6}}{2T}$

* Assuming tetrahedral angles.

\+ $F = \frac{1}{R_{CI}} = \frac{1}{2.133}$ $\quad T = \frac{1}{r_{CH}} = \frac{1}{1.085}$

Table 36b Numerical values for the coefficients listed above

	ϵ_{CH}		μ_{CH}		μ_{CI}	
	$\frac{1}{M_H}$	$\frac{1}{M_C}$	$\frac{1}{M_H}$	$\frac{1}{M_C}$	$\frac{1}{M_I}$	$\frac{1}{M_C}$
S_{4a}	1.155	1.5396	0	-1.7737	0	-.5414
S_{5a}	0	2.1773	-1.505	-2.508	0	-.7656
S_{6a}	0	-1.375	+.376	+1.584	+.292	+.4835

The numerical values of the coefficients of the final equations relating $\partial p/\partial S$ to the parameters μ_k and ϵ_k for CH_3I and CD_3I, are given in Table 37.

Table 37 Relation between $\partial p/\partial S$ and bond polar properties, for the E species of CH_3I and CD_3I (assuming a tetrahedral molecule).

	$\partial p/\partial S$	ϵ_{CH}	μ_{CH}	μ_{CI}
CH_3I	4a	1.155	+.033	-.033
	5a	0	-.725	-.028
	6a	0	+.707	+.045
CD_3I	4a	1.155	+.051	-.051
	5a	0	-.809	-.043
	6a	0	+.681	+.072

An example of the calculation of the numerical values of the coefficients in Table 37 is shown overleaf:-

contribution of ϵ_{CH} to $\partial p/\partial S_4$ for CH_3I

$$= {}^{E}\mathcal{G}^{-1}_{4-4}\left(1.155 \times \frac{1}{M_H} + 1.5396 \times \frac{1}{M_C}\right) + {}^{E}\mathcal{G}^{-1}_{4-5}\left(2.1773 \times \frac{1}{M_C}\right) + {}^{E}\mathcal{G}^{-1}_{4-6}\left(-1.375 \times \frac{1}{M_C}\right)$$

$$= 1.155$$

(Values of ${}^{E}\mathcal{G}^{-1}$ for tetrahedral angles are calculated from Table 25a, by inversion of the ${}^{E}\mathcal{G}$ matrix).

The equations obtained from Table 37 have a characteristic form which provides a partial check on the accuracy of the coefficients of the various μ_k and ϵ_k terms. Thus for the E species stretching mode of the ZXY_3 group, the coefficient of the term in ϵ_{XY} is $\sqrt{3/2}$. sin β, where β is the ZXY angle. For the same motion the equal and opposite terms in μ_{XZ} and μ_{XY} arise from rotation of the molecular dipole moment $p = \mu_{XY} - \mu_{XZ}$ which must accompany the stretching motion to eliminate angular momentum (exact equality of the terms only occurs for the tetrahedral case (see Table 37)). For the symmetry coordinates S_{5a} and S_{6a} the sum of the μ_{CH} and μ_{CI} terms in Table 37 is $\sqrt{2/3}/r_{CH}$ (for tetrahedral angles).

Using Table 37 we can express the experimentally obtained values of $\partial p/\partial S$ in terms of the bond polar properties. The uncorrected values of $\partial p/\partial S$, known to give the best agreement, are those of the (+—) sign combination, for both CH_3I and CD_3I (see Table 27).

For this calculation the same dipole moment definition as used in the previous sections was needed i.e. $-1.62 = \mu_{CI} - \mu_{CH}$ (for tetrahedral angles). Final values for the bond effective moments of CH_3I and CD_3I, using the Barrow Crawford and McKean method, are given in Table 38.

Table 38 Final bond effective moments for CH_3I and CD_3I derived from the sign combination (+—), in D/Å. The E species* (using tetrahedral angles).

	$S_4 \epsilon_{CH}$	$S_5 \mu_{CH}$	$S_6 \mu_{CH}$
CH_3I	.1387	.446	.502
CD_3I	.1280	.462	.494
Averaged data	.1334	.454	.498

* Compare averaged data with that from Table 30.

8.5 General Discussion

Hornig and McKean[173] presented a large amount of evidence to show that the three assumptions of the bond moment hypothesis (see section 8.2) have only a relative validity. From different bending vibrations in a given molecule values of μ_{CH} were estimated; according to the hypothesis these should be equal; in practice this was found not to be the case. For other molecules totally different values of μ_{CH} were obtained. For example, in ethylene, μ_{CH} was found to be 0.3D or 0.7D depending on the type of vibration considered.

Therefore using the bond moment hypothesis as applied by Dickson et al (see section 8.2), it is no surprise to find that, for methyl iodide, there is little relation between the values of μ_{CH}

derived from the different symmetry species (see Table 30). Similarly the value of ϵ_{CH} in the A_1 class is different to that in the E class. In consideration of this fact, it was suggested that the main theoretical reason for this situation, was that on vibration there are rehybridization changes, due to electron flow from one part of the molecule to another. It was also considered that, during a molecular vibration in which the valence angles at a central atom were changing, it should not be supposed that the hybridization at this atom necessarily followed the directions of the bonds, and always pointed directly towards the bonded atoms; but rather, there might be partial following leading to bonds which, in the displaced situation, could be called 'bent' bonds - to distinguish them from the more conventional straight bonds. Thus it was assumed that changes of interbond angle about the central atom lead to changes of the sp^3 hybridisation (for CH_3I) in the bonding orbitals on the central atom, due to "orbital following" of the bending coordinate. Therefore we would expect that different vibrations of methyl iodide would cause different changes in the interbond angles about the central carbon atom, and thus different changes in the hybridization of the bonding orbitals. Hence it would be reasonable to assume different values for μ_{CH} from the different symmetry species.

As we saw in section 8.3, Gribov resolved the problem by using the first order approximation of the theory. Taking into account the dependence of a bond dipole on the variation of its neighbouring internal coordinates, he pointed out the necessity of introducing the bond moment derivatives with respect to some neighbouring internal coordinates.

Looking at Gribov's formulation in general terms, we consider that the S_2 term (of Dickson's formulation, Table 30) is not merely μ_{CH} but rather contains a complex sum of cross derivative terms as well, some of which could be large (and which could have opposite signs to μ_{CH}). Thus it is probably purely accidental that the magnitudes of the $S_2\,\mu_{CH}$ and $S_5\,\mu_{CH}$ terms in Table 30 are about the same. Similarly we suggest that the $S_1 \in_{CH}$ term has an entirely different combination of terms compared with $S_4 \in_{CH}$.

While Gribov's formulation is reasonable, from the viewpoint of the necessary variation in electron distribution with the displacement of atoms on vibration, the principle disadvantage of this first order approximation to the theory is that the parameters cannot be obtained individually. Only the linear combinations of the parameters can be determined from the intensity calculation (see Tables 31 and 35). Some of the individual parameters can be estimated by considering a whole series of molecules.

McKean's method of formulating the rotational correction is very similar to that of Gribov. The method has the same starting point as that of Dickson et al (i.e. the uncorrected $\partial p/\partial S$ values of Table 27); but rather than having to follow the rather tedious procedure of determining a separate rotational correction, the rotational correction is inherent in the method. McKean's method is easy to formulate for tetrahedral angles; however for non-tetrahedral angles it becomes extremely complex. The other difficulty could arise from the determination of G^{-1} (as in Gribov's method). The method gives the same bond effective moments as the Dickson method (although there is better agreement between the values from $S_5\mu_{CH}$ and $S_6\,\mu_{CH}$) and thus suffers from the same difficulties in interpretation

of the parameters. It should be noted that the values of the parameters obtained from CH_3I and CD_3I are in very good agreement (see Table 38).

In conclusion it seems clear from our assembled data that no rigorous division of p into fixed bond contributions is really acceptable using the form of bond moment hypothesis favoured by Dickson et al, though it does succeed in giving an approximate interpretation of the observed intensities. We therefore suggest that Gribov's formulation provides the best general picture of the effects of vibrations in the methyl iodide molecule, with respect to the two isotopic species CH_3I and CD_3I.

With regard to the sign combination of the experimental $\partial p/\partial Q$ values, we have shown that the E class signs are absolutely determined if p is given by

$$p = \mu_{CI} - \mu_{CH} \quad \text{where } p = -1.62D.$$

However only the relative signs of the A_1 class have been determined. Perhaps when m.o. theory is more developed these could be determined absolutely. Using the basis of familiar ideas about the changes in atomic hybridization on the bending or stretching of bonds the magnitudes and signs of $\partial p/\partial S$ for molecules composed of 1st row elements and hydrogen have been calculated[174]. However it is obviously a much more complex situation to calculate the magnitudes and signs of $\partial p/\partial S$ for CH_3I by this method, as Iodine is a fourth row element.

APPENDIX 1

A listing of program VANSA, used for the processing of data from infra-red spectra. The computations perfomed are:

(a) Input of I_o and I, using a sampling interval of $\Delta\nu$

(b) I_o and I are corrected for slit width distortion, using the Hill-Steele method, (subroutine SLT).

(c) Calculation of $\frac{1}{cl}\int \ln (I_o/I)_\nu \, d\ln\nu$

(d) Determination of the true band maximum, using subroutine MAXIM.

(e) Calculation of the normalised Fourier transform of the band profile, with frequency as the independent variable, (subroutine SECSUM).

(f) Calculation of the natural log (ln) of the real part of C(t), and the natural log of the modulus of C(t). Graphs of ln C(t) against time are given, (using subroutine PLOT).

```
      PROGRAM VANSA (INPUT,OUTPUT)
      DIMENSION AINT(200),BINT(200),RATS(8),RATF(8),CFM(5,4),DESCR(20),
     ZALN(200),CPR(3,3),CTA(3,1),CI(3,3),A(3),CT(80,1),CTNR(80,1),
     ZCTNI(80,1),CTMOD(80,1),DM(300),DP(300)
      COMMON SAMP,A,SFR
      COMMON/BLOCKCT/CTNR,CTNI,CTMOD
      COMMON/BLOCKCT/CT
      READ 100,DESCR
      PRINT 100,DESCR
C     FREQS IS THE STARTING FREQUENCY;FREQM IS FREQUENCY FOR MAXIMUM
C     ABSORPTION;SAMP IS SAMPLING INTERVAL;NP IS NO. OF PTS.;SLIT IS
C     SLIT WIDTH IN CM-1;AINT IS SPECTRAL TRANSMISSION;BINT IS
C     REFERENCE TRANSMISSION;BASE IS BASELINE (NIL TRANSMITTANCE)
      READ 101,FREQS,FREQM,SAMP,NP,SLIT
      PRINT 12,FREQS,FREQM,SAMP,SLIT,NP
      READ 103,BASE
      READ 102,(AINT(I),I=1,NP)
      IF (AINT(NP).LT.0.0)  GO TO 199
      READ 102,(BINT(I),I=1,NP)
      IF (BINT(NP).LT.0.0)  GO TO 199
C     CORRECT IO AND I FOR ZERO PER CENT
      DO 8 J=1,NP
    8 AINT(J)=AINT(J)+BASE
      DO 9 J=1,NP
    9 BINT(J)=BINT(J)+BASE
      ACCS=0.0
      ACCF=0.0
      J=NP
C     CHECK INTENSITY IN WINGS IS V.SMALL,IF NOT ZERO
      DO 10 I=1,6
      RATS(I)=AINT(I)/BINT(I)
      ACCS=ACCS+RATS(I)
      RATF(I)=AINT(J)/BINT(J)
      ACCF=ACCF+RATF(I)
      J=J-1
   10 CONTINUE
      IF (ABS((ACCS-ACCF)/ACCS).LT.0.01)  GO TO 11
      IF (ACCS.GT.ACCF)  GO TO 13
      SCALE=ACCF/6.0
      GO TO 14
   13 SCALE=ACCS/6.0
      GO TO 14
   11 SCALE=(ACCS+ACCF)/12.0
   14 CONTINUE
      DO 15 I=1,NP
   15 AINT(I)=AINT(I)/(BINT(I)*SCALE)
      PRINT 200,(AINT(I),I=1,NP)
      SAMPM=ABS(SAMP)
C     SLIT CORRECTION
      CALL SLT (NP,SLIT,AINT,SAMPM)
      PRINT 200 ,(AINT(I),I=1,NP)
      FREQ=FREQS
      DO 16 I=1,NP
      IF (AINT(I).GT.1.0)  AINT(I)=1.0
      ALN(I)=-ALOG(AINT(I))/FREQ
   16 FREQ=FREQ+SAMP
      PRINT 209,(ALN(I),1,NP)
      SUMX=0.0
```

```
      CALL INTEGRA (SUMX,ALN,NP,SAMPM)
      READ 105,C,PL
      PRINT 104,C,PL
      CINT=SUMX/(C*PL*1.00)
      PRINT 201,CINT
      Y=(FREQM-FREQS)/SAMP
      MAX=IFIX(Y+1.005)
      F1=FREQM
      JFR=IFIX(F1/10.0)
      SFR=10.0*JFR
      SFR=SFR-10.0
      PRINT 520,MAX,SFR
C     SET UP LINEAR EQNS. TO SOLVE FOR FREQ. MAXIMUM. MATRIX IN CFM.
C     FREQUENCIES ARE REDUCED BY 100*SFR.
      FJS=F1-SFR
      ICT=MAX-2
      DO 17 I=1,5
      DO 18 J=1,2
      FJ=FJS**J
   18 CFM(I,J)=FJ
      CFM(I,3)=1.0
      CFM(I,4)=AINT(ICT)
      ICT=ICT+1
   17 FJS=FJS+SAMP
      DO 24 I=1,3
      DO 24 K=1,3
      CPR(I,K)=0.0
      CI(I,K)=0.0
      DO 24 J=1,5
   24 CPR(I,K)=CFM(J,I)*CFM(J,K)+CPR(I,K)
      DO 25 J=1,3
      CTA(J)=0.0
      DO 25 I=1,5
   25 CTA(J)=CTA(J)+CFM(I,J)*CFM(I,4)
      DET=0.0
      CALL MATRIX (10,3,3,0,CPR,DET)
      PRINT 208,DET
C     MATRIX IS LIBRARY ROUTINE ,PUTS  INVERSE OF CPR INTO CPR
C     NOW DO INVERSE TEST
      DO 26 J=1,3
      A(J)=0.0
      DO 26 I=1,3
   26 A(J)=A(J)+CPR(J,I)*CTA(I)
      PRINT 207,(A(J),J=1,3)
      TRMX=0.0
      CALL MAXIM (AINT(MAX),F1,TRMX)
      PRINT 202,TRMX
      K=MAX-1
      L=NP-MAX
      CALL FIND (ALN,DP,DM,MAX,NP,K,L)
      Q=1
      FO=ALN(MAX)
      CALL SECSUM (DM,DP,FO,SUMX,K,L,Q,SAMPM)
      CALL PLOT
  199 STOP
   12 FORMAT (10X,'BAND CENTRE IS',F10.4,//,10X,'STARTING FREQUENCY IS'
     Z,F10.4,//,10X,'SLIT WIDTH=',F10.4,'SAMPLING FREQUENCY=',F10.5,//,
     Z10X,'NO. OF POINTS=',I4)
```

```
100 FORMAT (20A4)
101 FORMAT (3F8.3,I4,F6.3)
102 FORMAT (16F5.0)
103 FORMAT (F6.0)
104 FORMAT (10X,'CONCENTRATION=',E12.5,//,10X,'PATH LENGTH=',E12.5)
105 FORMAT (2E12.5)
200 FORMAT (1H ,10X,'CORRECTED TRANSMITTANCE',/,(10(2X,F6.4),/))
201 FORMAT (1H ,6X,'INTEGRATED INTENSITY=',E12.5,' M2/MOL',/)
202 FORMAT (1H ,10X,'TRUE MAXIMUM',E12.5,//)
207 FORMAT (1H ,3E12.5)
208 FORMAT (10X,'DET=',E12.5,/)
209 FORMAT (1H ,10X,'ABSORBANCES',/,(10(2X,F8.5),/))
520 FORMAT (10X,'MAX=',I4,//,10X,'SFR=',F9.5,/)
    END


    SUBROUTINE SLT (K,S,G,DIFF)
    DIMENSION G(200),D2I(200)
    PX=8.*DIFF**2
    I=K-7
    X=S**2/12.
    DO 101 M=1,I
    M1=M+1
    M3=M+3
    M4=M+4
    M5=M+5
    M7=M+7
101 D2I(M4)=(G(M1)-G(M3)-G(M5)+G(M7))/PX
    DO 102 M=1,I
    M4=M+4
102 G(M4)=G(M4)-X*D2I(M4)
    RETURN
    END

    SUBROUTINE INTEGRA (SUMX,G,N,DNU)
    DIMENSION G(200)
    SUMT=0.0
    DO 1 JC=1,N
  1 SUMT=SUMT+G(JC)
    SUMX=(2.*SUMT-G(1)-G(N))*DNU/2.
    RETURN
    END

    SUBROUTINE FIND (D,DP,DM,O,M,K,L)
    DIMENSION D(200),DP(300),DM(300)
    INTEGER O
    K=O+1
    DO 1 J=K,M
    I=J-K+1
  1 DP(I)=D(J)
    K=I
    L=O-1
    DO 2 J=1,L
    I=L-J+1
  2 DM(I)=D(J)
    RETURN
    END
```

```
      SUBROUTINE MAXIM (AY1,F1,TRMX)
      DIMENSION A(3)
      COMMON SAMP,A,SFR
      F2=F1-SFR+(0.1*SAMP)
      A1=A(1)  £  A2=A(2)  £  A3=A(3)
   19 ATEST=A3+F2*(A2+F2*A1)
      PRINT 205,AY1,ATEST
      IF (AY1-ATEST)  20,20,21
   20 AY1=ATEST
      F2=F2+0.1*SAMP
      GO TO 19
   21 F2=F2-0.1*SAMP
      ATEST=A3+F2*(A2+F2*A1)
      IF (AY1-ATEST)  22,22,23
   22 AY1=ATEST
      GO TO 21
   23 TRMX=F2+0.1*SAMP+SFR
  205 FORMAT (1H ,2E12.5)
      RETURN
      END
```

```
      SUBROUTINE SECSUM (DM,DP,FO,TT,K,L,Q,SAMP)
      DIMENSION CTNR(80,1),CTNI(80,1),CTMOD(80,1),DM(300),DP(300)
      INTEGER Q,R
      COMPLEX SP,SM,EP,EM,S
      COMMON/BLOCKCT/CTNR,CTNI,CTMOD
      DATA PI/3.1417/
      TIME=0.
      CON=2.99776*2.*PI
      DO 711 R=1,70
      CONST=TIME*CON
      SP=(0.,0.)
      SM=(0.,0.)
      D=SAMP*CONST
      EM=CMPLX(COS(D),SIN(D))
      EP=CONJG(EM)
      DP(K)=DP(K)/2.
      DM(L)=DM(L)/2.
      DO 1 J=1,K
      I=K-J+1
    1 SP=DP(I)+SP*EP
      SP=SP*EP*SAMP
      DO2 J=1,L
      I=L-J+1
    2 SM=SM*EM+DM(I)
      SM=SM*EM*SAMP
      S=SP+SM+FO*SAMP
      RE=REAL(S)
      AIM=AIMAG(S)
      Q=1
      CTNR(R,Q)=RE/TT
      CTNI(R,Q)=AIM/TT
      CTMOD(R,Q)=SQRT(CTNR(R,Q)**2+CTNI(R,Q)**2)
  711 TIME=TIME+0.0005
      PRINT 836
      PRINT 835,(CTNR(R,Q),R=1,70)
      PRINT 837
      PRINT 835,(CTNI(R,Q),R=1,70)
      PRINT 838
      PRINT 835,(CTMOD(R,Q),R=1,70)
  835 FORMAT (8(21X,5(E12.5,1X),/),/)
  836 FORMAT (1H ,'REAL PART OF TRANSFORM',/)
  837 FORMAT (1H ,'IMAGINARY PART OF TRANSFORM',/)
  838 FORMAT (1H ,'MODULUS OF TRANSFORM',/)
      RETURN
      END

      SUBROUTINE PLOT
      DIMENSION CTLOG(80,1),CT(80,1),CTNI(80,1),CTMOD(80,1)
      REAL LINE(101)
      INTEGER Q,R
      COMMON/BLOCKCT/CT,CTNI,CTMOD
      DATA STAR,DOT,BLANK,PLUS,ZERO/1H*,1H.,1H ,1H+,1H0/
      Q=1
      PRINT 729
      FAC=80.
      TIME=0.
      LRN=70
      DO 423 R=1,70
```

```
      IF (CT(R,Q).LE.0.0)  GO TO 424
      IF (CTMOD(R,Q).LE.0.0)  GO TO 424
  423 CONTINUE
      GO TO 425
  424 LRN=R-1
  425 DO 426 R=1,LRN
      CTLOG(R,Q)=ALOG(CT(R,Q))
  426 CONTINUE
      DO 427 L=1.101
      LINE(L)=BLANK
  427 CONTINUE
      PRINT 730
      DO 428 R=1,70
      LINE(21)=DOT
      L=IFIX(CT(R,Q)*FAC+21.5)
      LINE(L)=STAR
      IJ=IFIX(CTNI(R,Q)*FAC+21.5)
      LINE(IJ)=PLUS
      IK=IFIX(CTMOD(R,Q)*FAC+21.5)
      LINE(IK)=ZERO
      PRINT 731,LINE,TIME
      LINE(L)=BLANK
      LINE(IJ)=BLANK
      LINE(IK)=BLANK
  428 TIME=TIME+0.05
      LINE(21)=BLANK
      TIME=0.
      PRINT 732
      PRINT 733,(CTLOG(R,Q),R=1,LRN)
      TFAC=-100.0/CTLOG(LRN,Q)
      DO 429 R=1,LRN
      L=IFIX(CTLOG(R,Q)*TFAC+101.5)
      LINE(L)=STAR
      CTLOG(R,Q)=ALOG(CTMOD(R,Q))
      IK=IFIX(CTLOG(R,Q)*TFAC+101.5)
      LINE(IK)=ZERO
      PRINT 734,LINE,TIME
      LINE(L)=BLANK
      LINE(IK)=BLANK
      LINE(101)=DOT
  429 TIME=TIME+0.05
      PRINT 733,(CTLOG(R,Q),R=1,LRN)
  729 FORMAT (20X,'NORMALIZED FOURIER TRANSFORM OF BAND PROFILE WITH
     ZFREQUENCY AS INDEPENDENT VARIABLE')
  730 FORMAT (1H ,20X,////)
  731 FORMAT (1H ,1X,101A1,1X,'T=',F4.2,1X,'PICOSEC')
  732 FORMAT (1H ,40X,27H NATURAL LOG(C(T)) VS. TIME,/,41X,'**********
     Z**********',/,'1ST. ALOG(REAL C(T)) , 2ND. ALOG(MOD C(T))',/)
  733 FORMAT (4(21X,5(E12.5,1X),/),/)
  734 FORMAT (1H ,6X,101A1,1X,3H T=,F4.2,1X,8H PICOSEC)
      RETURN
      END
```

References

1. D. Steele, "Theory of Vibrational Spectroscopy", W.B. Saunders, London 1971.

2. I.R. Hill and D. Steele, J.C.S. Faraday II 1974, 70, 1233.

3. H.A. Zymanski ed., "Raman Spectroscopy", Plenum Press, Volume 1, 1967.

4. L.A. Woodward, "Introduction to the theory of Molecular vibrations and Vibrational Spectroscopy", Oxford, 1972.

5. T.C. Damen, S.P.S. Porto and B. Tell, Phys. Rev. 1966, 142, 570.

6. S. Bratos and E. Marechal, Phys. Rev. 1971, A4 , 1078.

7. D.R. Jones, H.C. Anderson and R. P ecora, Chem. Phys. 1975, 9, 339.

8. I.R. Hill, Ph. D. Thesis, University of London, 1975.

9. R. Bracewell, "The Fourier Transform and its Applications" McGraw Hill 1965.

10. R.G. Gordon, J. Chem. Phys. 1965, 43, 1307.

11. R. Kubo, Lectures in Theoretical Physics, Interscience, New York, 1961, Vol. 1 p.120.

12. R.G. Gordon, Adv. in Magnetic Resonance, 1968, 3, 1.

13. H. Morawitz and K.B. Eisenthal, J. Chem. Phys. 1971, 55, 887.

14. P. van Konynenburg and W.A. Steele, J. Chem.Phys. 1972, 56, 4776.

15. J.A. Bucaro and T.A. Litovitz, J. Chem. Phys. 1971, 54, 3846.

16. H.S. Goldberg and P.S. Pershan, J. Chem. Phys., 1973, 58, 3816.

17. I.R. Hill and D. Steele, to be published.

18. L.A. Nafie and W.L. Peticolas, J. Chem. Phys. 1972, 57, 3145.

19. F.J. Bartoli and T.A. Litovitz, J. Chem. Phys., 1972, 56, 413.

20. W.G. Rothschild, J. Chem. Phys., 1972, 57, 991.

21. J.P. Perchard, W.F. Murphy and H.J. Bernstein, Mol. Phys. 1972, 23, 499.

22. W.A. Steele a) J. Chem. Phys. 1963, 38, 2404.
b) J. Chem. Phys. 1963, 38, 2411.

23. J. Dezwann, D.W. Hess and C.S. Johnson Jr., J. Chem. Phys. 1975, 63, 422.

24. T. Fujiyama and B. Crawford Jr., J. Phys. Chem. 1968, 72, 2174.

25. R.T. Bailey in Specialist Periodical Report, Molecular Spectroscopy Vol. 2, Chem. Soc. London, 1974.

26. P. Debye, "Polar Molecules", Rheinhold New York, 1929.

27. D. Kivelson, M.G. Kivelson and I. Oppenheimer, J. Chem. Phys. 1970, 52, 1811.

28. R.D. McClung and D. Kivelson, J. Chem. Phys., 1968, 49, 3880.

29. G.R. Alms, D.R. Bauer, J.I. Brauman and R. Pecora
a) J. Chem. Phys. 1973, 58, 5570.
b) J. Chem. Phys. 1974, 61, 2255.

30. R.G. Gordon, J. Chem. Phys. 1966, 44, 1830.

31. H.A. Benesi and J.H. Hildebrand, J. Amer. Chem. Soc. 1949, 71, 2703.

32. R.S. Mulliken, J. Amer. Chem. Soc. 1952, 74, 811.

33. J. Yarwood ed., "The Spectroscopy and structure of Molecular Complexes", Plenum Press, London, 1973.

34. R.S. Mulliken and W.B. Person, "Molecular Complexes", Interscience, New York, 1969.

35. M.J.S. Dewar and C.C. Thompson, Tetrahedron Suppl. 1966, 7, 97.

36. R.J.W. LeFevre, D.V. Radford, G.J.D. Ritchie and P.J. Stiles, Chem. Comm., 1967, 1221.

37. M.W. Hanna, J. Amer. Chem. Soc. 1968, 90, 285.

38. M.W. Hanna and D.E. Williams, J. Amer. Chem. Soc., 1968, 90, 5358.

39. C.R. Patrick and G.S. Prosser, Nature, 1960, 187, 1021.

40. M.E. Baur, D.A. Horsma, C.M. Knobler and P. Perez, J. Phys. Chem. 1969, 73, 641.

41. D.V. Fenby and R.L. Scott, Ann. Rev. Phys. Chem. 1969, 20, 111.

42. R. Ferri, Ph.D. Thesis, University of Strathclyde, 1974.

43. R.J. Powell, F.L. Swinton and C.L. Young, J. Chem. Thermodynamics, 1970, 2, 105.

44. R.J. Powell and F.L. Swinton, J. Chem. Thermodynamics, 1970, 2, 87.

45. E.M. Dantzler and C.M. Knobler, J. Phys. Chem. 1969, 73, 1602.

46. D.R. Bauer, J.I. Brauman and R. Pecora, J. Chem. Phys. 1975, 63, 53.

47. T. Ledaal, Tetrahedron Letters, 1968, 14, 1687.

48. R.J.W. LeFevre, D.S.N. Murthy and P.J. Stiles, Aust. J. Chem. 1969, 22, 1421.

49. L. Delbouille, Bull. Classe. Sci. Acad. Roy. Belg. 1958, 44, 971.

50. D. Steele and D.H. Whiffen, Trans. Faraday Soc. 1959, 55, 369.

51. D. Steele and W. Wheatley, J. Mol. Spectr. 1969, 32, 265.

52. R.A.R. Pearce, D. Steele and K. Radcliffe, J. Mol. Structure, 1973, 15, 409.

53. V.J. Eaton and D. Steele, J. Mol. Spectroscopy, 1973, 48, 446.

54. a) G. Jalsovsky and W. Orville Thomas, Trans. Faraday Soc., 1971, 67, 1894.

b) R.E. Bruns and W.B. Person, J. Chem. Phys. 1972, 57, 324.

55. R.M. Barrett, Ph. D. Thesis, University of London, 1973.

56. D.A. Chisholm and H.L. Welsh, Can. J. Phys. 1954, 32, 291.

57. C.E. Favelukes, A.A. Clifford and B.L. Crawford Jr. J. Phys. Chem. 1968, 72, 962.

58. J. Yarwood, Spectroscopy Letters, 1972, 5, 193.

59. C. Lalau, Proc. Conf. Mol. Spectroscopy 1958, ed. E. Thornton and H.W. Thompson, Pergamon, 1959.

60. H. Spedding and D.H. Whiffen, Proc. Roy. Soc. A. 1956, 238, 245.

61. D.N. Hague, "Fast Reactions", Wiley Interscience, New York, 1971, p.12.

62. R. Foster, "Organic Charge Transfer Complexes", Academic Press, London, 1969.

63. L.J. Andrews and R.M. Keefer, J. Amer. Chem. Soc., 1951, 73, 462.

64. J. Collin and L. D'Or, J. Chem. Phys. 1955, 23, 397.

65. L. D'Or and J. Collin, Rec. Trav. Chim. 1956, 75862.

66. H. Stammreich, R. Forneris and Y. Tavares, Spec. Acta. 1961, 17, 1173.

67. W.B. Person, R.E. Buckles and R.E. Erickson, J. Amer. Chem. Soc., 1960, 82, 29.

68. W.B. Person, R.E. Humphreys and A.I. Popov, J. Amer. Chem. Soc. 1959, 81, 273.

69. H.B. Friedrich and W.B. Person, J. Chem. Phys. 1966, 44, 2161.

70 D. Atack and O.K. Rice, J. Phys. Chem. 1954, 58, 1017.

71. J. van Kranendonk a) Physica, 1957, 23, 825.

b) Physica, 1958, 24, 347.

72. T.C. Jao, Ph. D. Thesis, University of Florida, 1974.

73. P. Klaeboe, J. Amer. Chem. Soc., 1967, 89, 3667.

74. Y.R. Shen, H. Rosen and F. Stenman, Chem. Phys. Lett. 1968, 1, 671.

75. H. Rosen, Y.R. Shen and F. Stenman, Mol. Phys. 1971, 22, 33.

76. W. Holzer, W.F. Murphy and H.J. Bernstein, J. Chem. Phys. 1970, 52, 399.

77. J.C. Barral, O. Hartmanshenn and F. Perrin, C.R. Acad. Sci. Paris, 1972, 274B, 981.

78. H. Stammreich and R. Forneris, Spec. Acta, 1961, 17, 775.

79. G. Hochenbleicher and H. Schrotter, Appl. Spectr., 1971, 25, 360.

80. F. Wallart, Can. J. Spectroscopy, 1972, 17, 128.

81. a) O. Redlich, Z. Phys. Chem. 1935, 28, 371.

b) E. Teller, J. Chem. Soc. 1936, 971.

82. D.A. Bahnick and W.B. Person, J. Chem. Phys. 1968, 48, 1251.

83. G.W. Chantry, H.A. Gebbie and H.N. Mirsa, Spec. Acta, 1967, 23A, 2749.

84. R.S. Mulliken, J. Chem. Phys. 1955, 23, 397.

85. E.E. Ferguson, J. Chem. Phys. 1956, 25, 577.

86. O. Hassel, Mol. Phys. 1958, 1, 241.

87. O. Hassel and K. Stomme, Acta. Chem. Scand. a) 1958, 12, 1146.
b) 1959, 13, 1781.

88. W.B. Person, C.F. Cook and H.B. Friedrich, J. Chem. Phys. 1967, 46, 2521.

89. E.E. Ferguson and F.A. Matsen, J. Chem. Phys. 1958, 29, 105.

90. J.D. Childs, Ph. D. Dissertation, University of Oklahoma, 1971.

91. S.D. Christian, J.D. Childs and J. Grundnes, J. Amer. Chem. Soc. 1972, 94, 5657.

92. S.D. Christian, J.D. Childs and E.H. Lane, J. Amer. Chem. Soc. 1972, 94, 6861.

93. G. Kortüm and M.Z. Kortüm-Seiler, Z. Naturforch, 1955, 5A, 544.

94. G. Kortüm and W.M. Vogel, Z. Electrochem. 1955, 59, 16.

95. J.H. Hildebrand and R.L. Scott, "The Stability of Nonelectrolytes" Van Nostrand-Rheinhold, 1970.

96. D.A. Deranleau, J. Amer. Chem. Soc. 1969, 91, 4050.

97. M. Schwartz and C.H. Wang, Chem. Phys. Lett. 1974, 25, 26.

98. I.R. Hill and D. Steele, unpublished data.

99. R.G. Gordon, J. Chem. Phys. 1963, 39, 2788.

100. A. Gierer and K. Wirtz, Z. Naturforsch, 1953, A8, 532.

101. C. Hall, D.W. Kydon, R.E. Richards and R.E. Sharp, Mol. Phys. 1970, 18, 711.

102. R.T. Obermyer, Bull. Am. Phys. Soc. 1970, 15, 127.

103. R.T. Obermyer and E.P. Jones, J.C.P. 1973, 58, 1677.

104. T.C. Farrar and E.D. Becker, "Pulse and Fourier Transform N.M.R.", Academic Press, London, 1971, (p.56).

105. D.E. Woessner, J. Chem. Phys., 1962, 37, 647.

106. H. Shimizu, J. Chem. Phys., 1962, 37, 765.

107. E.R. Steachie and F.M.G. Johnson, J. Amer. Chem. Soc., 1925, 47, 756.

108. R.G. Gordon, J. Chem. Phys. 1964, 41, 1819.

109. R.L. Armstrong, S.M. Blumenfeld and C.G. Gray, Can. J. Phys. 1968, 46, 1331.

110. J.A. Bucaro and T.A. Litovitz, J. Chem. Phys. 1971, 55, 3846.

111. H.D. Dardy, V. Volterra and T.A. Litovitz, J. Chem. Phys. 1973, 59, 4491.

112. P. van Konynenburg and W.A. Steele, J. Chem. Phys. 1975, 62, 2301.

113. J.F. Dill, T.A. Litovitz and J. Bucaro, J. Chem. Phys., 1975, 62, 3839.

114. I.R. Hill and D. Steele, to be published, Chem. Phys. Lett.

115. J. Overend, "Infrared Spectroscopy and Molecular Structure", ed. M. Davies, Elsevier, 1963, Ch. 10.

116. A.D. Dickson, I.M. Mills and B.L. Crawford Jr., J. Chem. Phys. 1957, 27, 445.

117. J.A. Aldous and I.M. Mills, Spec. Acta., 1962, 18, 1073.

118. J.A. Aldous and I.M. Mills, Spec. Acta., 1963, 19, 1567.

119. A.G. Meister and F.F. Cleveland, Amer. J. Phys. 1946, 14, 13.

120. J.L. Duncan, J. Mol. Structure, 1970, 6, 448.

121. E.B. Wilson Jr., J. Chem. Phys. 1939, 7, 1047, and 1941, 9, 76.

122. D.M. Dennison, Rev. Mod. Phys. 1940, 12, 175.

123. J.W. Russell, C.D. Needham and J. Overend, J. Chem. Phys. 1966, 45, 3383.

124. J.L. Duncan, A. Allan and D.C. McKean, Mol. Phys. 1970, 18, 289.

125. I.M. Mills, Spec. Acta. 1963, 19, 1585.

126. P.D. Mallinson, J. Mol. Spectroscopy, 1975, 55, 94.

127. G. Herzberg, "Molecular Spectra and Molecular Structure", Volume II, Van Nostrand, New York, 1960.

128. W.J. Orville-Thomas, J.T. Cox and W.J. Gordy, J. Chem. Phys. 1954, 22, 1718.

129. J.H. Meal and S.R. Polo, J. Chem. Phys. 1956, 24, 1126.

130. Y. Morino and J. Nakamura, Int. Symp. Spectroscopy, Tokyo, 1962, Paper C.206.

131. E.W. Jones and H.W. Thompson, Proc. Roy. Soc. 1965, A288, 50.

132. E.W. Jones, R.J.L. Popplewell and H.W. Thompson, Spec. Acta. 1966, **22, 669.**

133. T.L. Barnett and T.H. Edwards, J. Mol. Spectroscopy, 1966, 20, 347.

134. Y. Morino, J. Nakamura and S. Yamamoto, J. Mol. Spectroscopy, 1967, 22, 34.

135. Y. Morino and C. Hirose, J. Mol. Spectroscopy, 1967, 22, 99.

136. T.L. Barnett and T.H. Edwards, J. Mol. Spectroscopy, 1967, 23, 302.

137. S. Reichmann and J. Overend, J. Chem. Phys., 1968, 48, 3095.

138. R.J. Popplewell and H.W. Thompson, Spec. Acta., 1969, 25A, 287.

139. A. Maki and T. Hexter, J. Chem. Phys., 1970, 53, 453.

140. H. Matsuura, T. Nakagawa and J. Overend, J. Chem. Phys. 1970, 53, 2540.

141. H. Matsuura and J. Overend, J. Chem. Phys., 1971, 55, 1787.

142. T.E. Sullivan and L. Frenkel, J. Mol. Spectroscopy, 1971, 39, 185.

143. H. Matsuura and J. Overend, Spec. Acta, 1971, 27A, 2165.

144. H. Matsuura and J. Overend, J. Chem. Phys., 1972, 56, 5725.

145. P. Connes, J. Pinard and J.P. Maillard, J. de Phys., 1972, 33, 77.

146. H. Matsuura and J. Overend, Bull. Chem. Soc. Japan, 1973, 46, 1102.

147. Y. Kawashima and C. Hirose, Bull. Chem. Soc. Japan, 1973, 46, 2969.

148. H. Matsuura, T. Nakagawa and J. Overend, J. Chem. Phys., 1973, 59, 1449.

149. H. Matsuura, Y. Kawashima and C. Hirose, J. Mol. Structure, 1974, 20, 205.

150. A. Butcher, private communication, 1974.

151. H. Hönl and F. London a) Z. Physik, 1925, 33, 803.
b) Ann. Phys., 1926, 79, 273.

152. D.M. Dennison, Phys. Rev., 1926, 28, 318.

153. F. Reiche and H. Rademaker, Z. Physik, 1926, 39, 444; and 1927, 41, 453.

154. D. Steele and W. Wheatley, J. Mol. Spectroscopy, 1966, 21, 386.

155. D.M. Dennison, Rev. Mod. Phys., 1931, 3, 280.

156. S. Penner and D. Weber, J. Chem. Phys., 1951, 19, 807.

157. D.G. Bourgin, Phys. Rev., 1927, 29, 794.

158. E.B. Wilson and A.J. Wells, J. Chem. Phys., 1946, 14, 578.

159. C. DiLauro and I.M. Mills, J. Mol. Spectroscopy, 1966, 21, 386.

160. S. Sarangi and P. Varnasi, J. Quant. Spec. and Radiation Transfer, 1975, 15, 291.

161. G.M. Barrow and D.C. McKean, Proc. Roy. Soc. (London)., 1952, A213, 27.

162. L.A. Gribov, "Intensity Theory for Infra-red Spectra of Polyatomic Molecules", G.M. Consultants Bureau, 1964.

163. a) L.M. Svedlov, Opt i Spektr., 1959, 6, 729.

b) L.M. Sverdlov and V.M. Mokhnatkin, Zh. Prickl. Spektrosk, 1969, 10, 192.

164. B.L. Crawford, J. Chem. Phys., 1952, 20, 977.

165. A.J. van Straten and W.M.A. Smit, J. Mol. Spectroscopy, 1975, 56, 484.

166. D.H. Whiffen, Phil. Trans. Roy. Soc. London, Ser A, 1955, 248, 131.

167. W. King, I.M. Mills and B. Crawford, J. Chem. Phys., 1957, 27, 455.

168. L.A. Gribov and E.M. Popov, Opt. Spectr. , 1962, 12, 304.

169. Using the nomenclature of S. Saeki and K. Tanabe, Spec. Acta. 1969, 25A, 1325.

170. G.M. Barrow and B.L. Crawford, unpublished material.

171. D.C. McKean, private communication.

172. B.L. Crawford and W.H. Fletcher, J. Chem. Phys. 1951, 19, 141.

173. A. Hornig and D.C. McKean, J. Phys. Chem. 1955, 59, 1133.

174. G.A. Segal and M.L. Klein, J. Chem. Phys. 1967, 47, 4236.

175. W.B. Person and D. Steele, "Molecular Spectroscopy Vol. 2, Specialist Periodical Reports" Chem. Soc. 1974, Ch.3.

176. D. Steele, Quarterly Rev. 1964, 18, 21.

Offprinted from the *Journal of The Chemical Society, Faraday Transactions II,* 1975, vol. 71.

VIBRATIONAL BAND CONTOURS

PART 1.—THE HEXAFLUOROBENZENE–BENZENE SYSTEM

Vibrational Band Contours

Part 1.—The Hexafluorobenzene–Benzene System

BY R. M. BARRETT,† E. B. GILL AND DEREK STEELE*

Department of Chemistry, Royal Holloway College (University of London), Egham, Surrey TW20 OEX

Received 18*th March*, 1974

Interactions between benzene and hexafluorobenzene lead to a frequency shift and a broadening of the band arising from the out-of-plane CF bending vibration (a_{2u} species). It is deduced that the intermolecular interactions are short lived, stochastic, are not simple polar interactions and that the resulting forces are directed perpendicular to the ring plane. This is based on symmetry considerations and on the concentration dependence and magnitudes of the frequency shifts and of the Fourier transforms of the absorption band contours. Assuming that vibrational relaxation occurs through dissociation of the complex with 100% efficiency, leads to lower limits for the rate constants for complex formation and dissociation. There are still a number of outstanding problems of interpretation.

Any absorption band is characterised by three parameters, its frequency, its intensity and its band contour. For vibrational absorption bands in the liquid or solution state, the latter parameter was neglected as a source of molecular information until ten years ago. A probable cause of this neglect was the use of the Schrödinger picture of stationary energy states. Viewed from this angle, the transition frequency and intensity of a band are both well defined molecular parameters, but the band contour is determined by entirely separate considerations, such as Doppler broadening and collisional interactions. Translation of the problem into the Heisenberg formulation shows that the Fourier transform of intensity with respect to the frequency shift from the band centre leads to the autocorrelation function of the transition moment.[1,2] If the transition moment at a time t is written as $m(t)\boldsymbol{u}(t)$ where $m(t)$ is the magnitude and $\boldsymbol{u}(t)$ is a unit vector defining the direction of the moment, then

$$\frac{\langle m(t)\boldsymbol{u}(t) \cdot m(0)\boldsymbol{u}(0)\rangle}{m(0)^2} = \frac{\int \Gamma(\nu) \exp[\mathrm{i}2\pi(\nu-\nu_0)t]\,\mathrm{d}\nu}{\int \Gamma(\nu)\,\mathrm{d}\nu} = G_1(t). \quad (1)$$

ν_0 is the frequency of the band centre; $\Gamma(\nu)$ is $\ln(I_0/I)_\nu$ where $(I_0/I)_\nu$ is the fractional transmission at a frequency ν; the integrations are over the entire band and $m(t)\boldsymbol{u}(t) = \langle\psi'|\mu|\psi''\rangle$.

If $m(t)$ is independent of time and if the motions of different molecules are uncorrelated, then the Fourier transform of the absorption intensity simplifies to the

† present address: Dearborn Chemicals Limited, Water Treatment Division, Foundry Lane, Ditton, Widnes, Lancs.

autocorrelation function of the unit vector defining the direction of the transition moment:

$$\langle \boldsymbol{u}_i(0) \cdot \boldsymbol{u}_i(t) \rangle = \frac{\int \Gamma(\nu) \exp[i2\pi(\nu-\nu_0)t]\, d\nu}{\int \Gamma(\nu)\, d\nu} = G_{1R}(t).$$

Until recently it has been assumed that $G_1(t)$ is governed solely by the reorientation of the transition dipole with time. However, it is now clear (see below) that vibrational relaxation, vibrational frequency shifts and vibrational rotation interaction all frequently contribute to a significant degree. We shall show in a future publication that vibration rotation interaction produces predictable changes in the expansion of correlation functions in terms of time.[3] For our present purposes this may be neglected. In a low viscosity fluid, it appears that separation of the total autocorrelation function into rotational and vibrational parts leads to the identification of two quite different situations. If vibrational relaxation (or, more generally isotropic relaxation) and vibrational frequency shifts are independent of rotational relaxation, the $G_1(t)$ can be expressed as the simple product of the rotational and vibrational contributions.[4] Thus:

$$G_1(t) = G_V(t) \cdot G_{1R}(t).$$

The stochastic behaviour of the intermolecular interactions in this case leads to the result that at times, which are long compared with the average time between collisions, both $G_V(t)$ and $G_{1R}(t)$ show an exponential decay with time. This is shown to be the situation for the a_{2u} band of hexafluorobenzene in the solvent system benzene+cyclohexane.

If on the other hand there is significant coupling between translation and vibrations, a non exponential decay of $G(t)$ results. An example of this behaviour is probably shown by the out-of-plane CH bending modes of benzene in polar solvents.[5] The increase in rate of decay of $G_1(t)$ for these vibrations over the corresponding values in cyclohexane is a Lorentzian function in t. Also, broadening is proportional to the dipole moment of the solute.

When hexafluorobenzene (HFB) and benzene are mixed in equimolar quantities, the system has a melting point 20°C higher than that of either component.[6] It was inferred that HFB and benzene complex, and a considerable number of experimental studies have now been made on the system. The observed effects of the interactions have been disappointingly weak. The dipole moment for the postulated complex was shown to be less than 0.1 debye.[7] No charge transfer bands have been identified and as recently as 1970 it could reasonably be stated that "spectroscopic evidence for complexing has been conspicuous by its absence".[8] Thermodynamic properties of the mixtures clearly show interactions do exist in the liquid state, but the interaction forces seem to be quite weak [see ref. (8) and earlier references therein]. It has been suggested that the interaction is purely electrostatic and is probably of a dipole–quadrupole type.[9] Powell, Swinton and Young applied the statistical theory of Rowlinson and Sutton to measurements of gas–liquid critical temperatures and deduced that there is an angle dependent force, but were of the opinion that the interaction is short lived and could probably be explained without invoking specific covalent bonding forces.[10]

In the following it is shown that subtle changes in the spectrum of HFB resulting from interactions with benzene give new insight into the molecular dynamics and forces obtaining in the system.

EXPERIMENTAL

Hexafluorobenzene was a spectroscopically pure sample from Bristol Organics Ltd. Acetonitrile and cyclohexane were of spectroscopic quality from B.D.A. Spectra in the region of the a_{2u} mode of hexafluorobenzene were recorded both on an RIIC FS 720 interferometer and on a Perkin Elmer 325 double beam spectrometer at resolutions of about 2.0 cm^{-1}. The transmission linearity of the PE 325 was verified as being within 0.5 % by the use of calibrated choppers. Good agreement was obtained from the different runs on frequencies and band widths. The interferometric studies suggested that the a_{2u} band increased in intensity by about 30 % in going from cyclohexane solution to benzene solution. However, the PE 325 measurements showed that no increase occurred on addition of benzene to cyclohexane up to at least a 1 : 1 mixture. A small increase of 10 % occurred in going to HFB in pure benzene. All these measurements were made at an HFB concentration of about 0.08 mol dm^{-3} and in a caesium iodide or polythene cell with a 2 mm path length. The discrepancies in intensities arose because of difficulties in locating the background on the interferometer trace. It would appear that the extended but shallow wings of the band in cyclohexane were not noted in the spectral noise. The error decreased in the much broader band in benzene. The interferometer results were previously reported to lead to an equilibrium constant for the HFB–benzene association of 1.0 dm^3 mol^{-1} and a broadening proportional to the complex concentration.[11] These results were in error and serve to show the difficulties which can occur when seeking to derive equilibrium constants from bands which change in contour.

Data were processed on a CDC 6600 using programs developed in our laboratories. All data were corrected for slit width distortion using the formula:

$$I(\nu) = T(\nu) - \frac{s^2}{12}\frac{\partial^2 T}{\partial \nu^2}(\nu)$$

where $I(\nu)$ and $T(\nu)$ are the true and apparent transmitted intensities and s is the spectral slit width.[12] This method has an advantage over full spectral deconvolution in that it can be applied even when the absorption does not decrease to zero at the spectral limits and also in that it is simple and rapid to apply. Corrections due to refractive index and field distortions were so low as to be negligible.

RESULTS AND DISCUSSION

The most significant observation is that no e_{1u} band is affected in any way by change of solvent whereas the a_{2u} umbrella mode suffers both an increase in wavenumber of 5 cm^{-1} in going from cyclohexane or CS_2 to benzene solution and a drastic change in band contour (see fig. 1). This suggests that benzene and HFB are interacting on collision in such a way as to perturb those orbitals which are symmetric with respect to the C_6 axis. Such an interaction would arise from π–π complexing. The lack of any significant intensity change in the a_{2u} mode does not exclude the possibility of long lived complexing of the π–π type but suggests that it is not very probable. The bands are reasonably symmetric in all solutions. Since the band centre moves by about one half band width this excludes the possibility that such broadening arises from overlapping of bands due to molecules in different long lived states of aggregation. By long lived in this context, we mean existing for longer than the reciprocal of the radial frequency separation between the bands in the two pure solvents ($\sim 1 \times 10^{-12}$ s).

On this basis we can expect the changes in the Fourier transforms of the bands in the solutions to give information on the relaxation mechanisms for the vibration in its various environments. The lack of any second isotope of fluorine simplifies the procedure. We have made no effort to account for the shift of band centre resulting from the natural ^{13}C content on the grounds that the effect will be small and that it

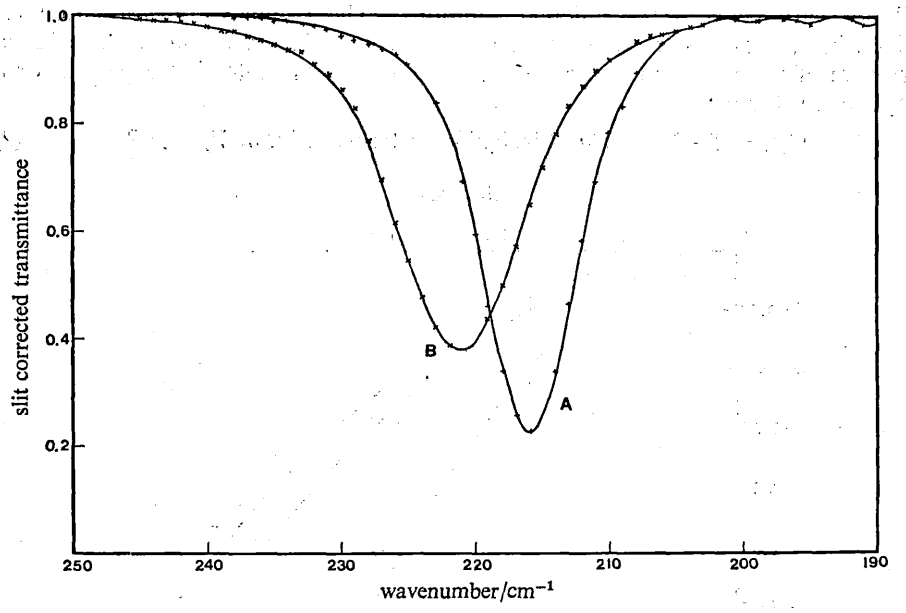

FIG. 1.—The a_{2u} absorption band of hexafluorobenzene (A) in cyclohexane solution and (B) in benzene solution (2 cm path length and 0.08 mol dm^{-3}).

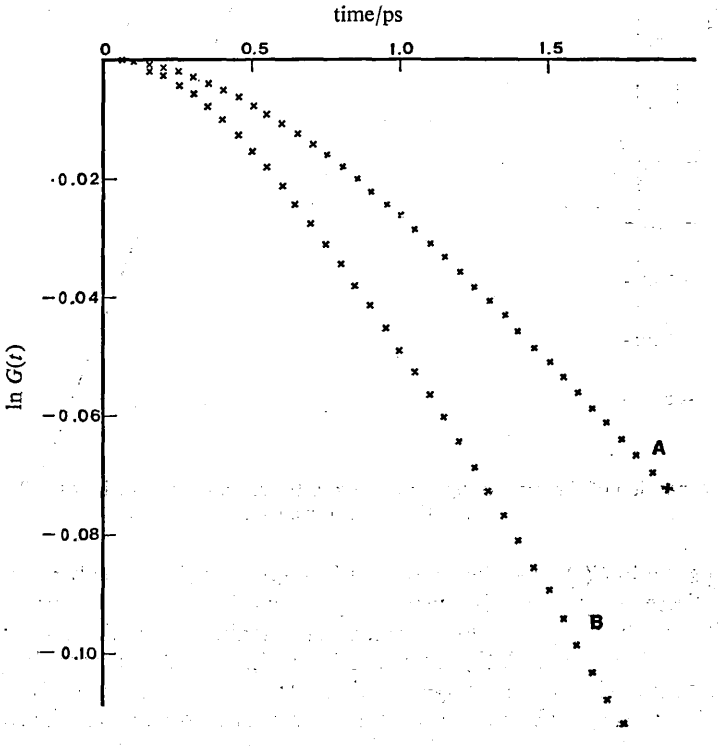

FIG. 2.—The ln[$G(t)$] against time plot for the a_{2u} vibration of hexafluorobenzene in benzene solution (B) and in cyclohexane solution (A).

will not vary between the different solutions. The complex transformation (1) yielded $\ln[G(t)]$ against t graphs such as those shown in fig. 2 and 3. The initial curvature of the plot for the cyclohexane solution is similar to that expected for a simple free rotor [13]:

$$G(t) = 1-2(kT/h)Bt^2+\text{insignificant terms in } (kT/hc)^n,\ n \geqslant 2. \qquad (2)$$

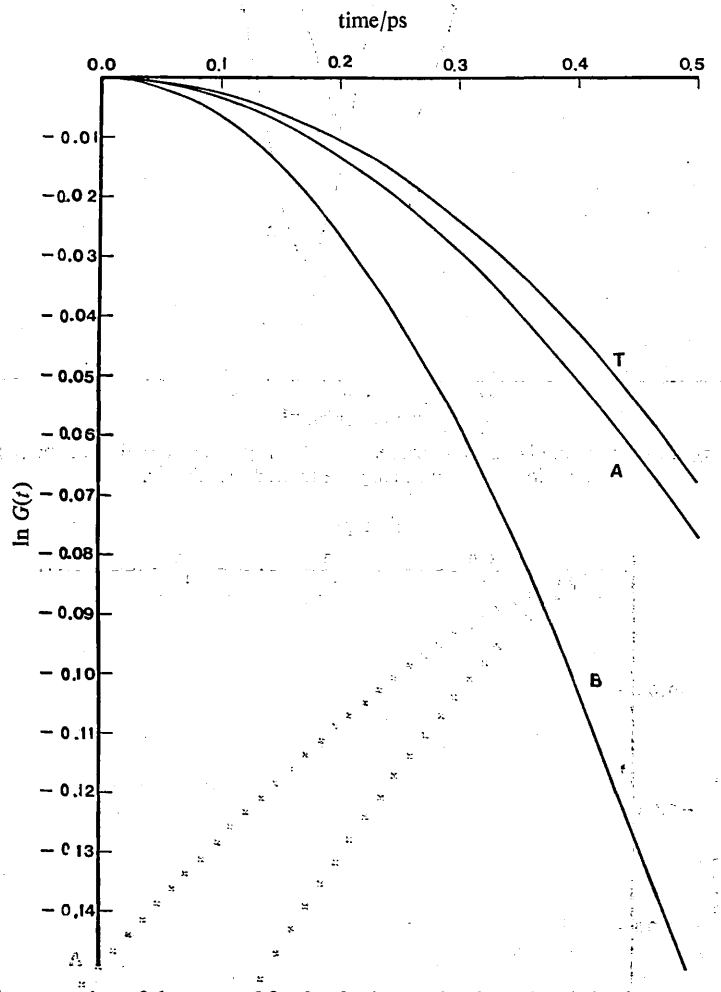

FIG. 3.—An expansion of that part of fig. 2 referring to the short time behaviour ($< 0.5 \times 10^{-12}$ s). T is the free rotor curve.

Up to 0.5 ps the ln $G(t)$ curve lies about 20 % below the theoretical free rotor curve. The initial discrepancy at least is due possibly to experimental difficulties in measuring the intensities in the wings. Two alternative broadening mechanisms seem plausible. If the a_{2u} vibration of the C_6F_6 molecules is sensitive to the surrounding solvation sheath and if the environment changes within a time scale of the order of the reciprocal of the radial frequency difference between the transition frequencies in the two environments ($\tau_e \approx 1/\Delta\omega$), then exchange broadening will occur. In the event of very fast exchange ($\tau_e \ll 1/\Delta\omega$) then coalescence to a single sharp band will occur, whereas if the

exchange time can be reduced so that $\tau_e \gg 1/\Delta\omega$ separate bands from the different solvated species will appear. The alternative explanation for the broadening is that it arises from an induced vibrational relaxation of the a_{2u} vibration. The origin of the relaxation may be due again to the solvation exchange, but the principle difference from the kinetic effect is that an increase in the exchange rate can never lead to a narrowing of the band. Our present data does not allow us to distinguish between these two processes. We favour the vibrational relaxation mechanism and will continue the discussion in this light. This discussion is not significantly affected by which of the two processes is responsible.

For the benzene solution the entire curve lies below the $G(t)$ curve for cyclohexane solution. No adequate explanation for the short time behaviour can be advanced. Extrapolation backwards of the longer time behaviour suggests a relaxation, in addition to that arising from free rotation, peculiar to the short times. Since our overall interpretation indicates that association is a short lived affair, the short time behaviour ought to represent free movement of HFB in the cavity fields. Indeed the changes in e_{1u} band intensities from gas to pure liquid are adequately explained by simple dielectric field theory.[14]

At times longer than 0.5 ps, there is a good linear relationship between $\ln[G(t)]$ and t for all solutions. Two important deductions can be made. First, it indicates that experimental errors in the measured intensities within at least 30 cm^{-1} of the band centre are very small as far as the correlation functions are concerned. It would be more than fortuitous if errors converted a non-linear relationship into a linear one. Secondly we see that all the relaxation processes involved at these times are random. Coupling between translations and vibrations would lead to a Lorentzian contribution to $G(t)$.[5, 15] It is possible that the observed reduction in β at high benzene concentrations is due to exchange narrowing. This would be in accord with the continuing increase in $\Delta\nu$. However, we failed to see a change in band widths on varying the temperature by 50°C. We would have expected the exchange rate to vary significantly over this temperature if only as a result of variation in the molecular velocities. If we further assume that the rotational correlation function is given by β for the cyclohexane solution and is unaltered by addition of benzene then we can write:

$$G(t) = \text{constant} + G(0) \exp -(\beta_v + \beta_r)t$$

where β_v and β_r are the reciprocal relaxation times for vibration and rotation respectively. Extraction of β_v for the various solutions and plotting this against the concentration of benzene yields the curves in fig. 4. All $(\beta_v + \beta_r)$ values were derived by a least squares fitting of some 50 points in the linear portions of the $\ln G(t)$ against t graphs. It appears that $\beta_v + \beta_r$ increases linearly with benzene concentration almost up to its asymptotic value. If β_v was proportional to the extent of complexing and β_r was constant, the variation of $\beta_v + \beta_r$ would have been such as shown for curve (B). It is probably unrealistic to expect such behaviour on account of solvent cage effects alone. The asymptotic behaviour of β is reached at about 35 % benzene. At this concentration the HFB molecules are probably embedded in a cage of benzene molecules. It follows that well before this point relaxation and pairing is going to be enhanced above and beyond the expectations for a simple bimolecular reaction. Some support for the above interpretation comes from the observed vibrational frequency shifts of the a_{2u} mode, which accompany the addition of benzene. These shifts are considerable, being up to 5 cm^{-1} in 210 cm^{-1}. There is an excellent linear relationship between the shift and β up to the maximum value of the relaxation constant. Thereafter, while β changes only very slightly, the frequency shift continues to increase at its previous rate.

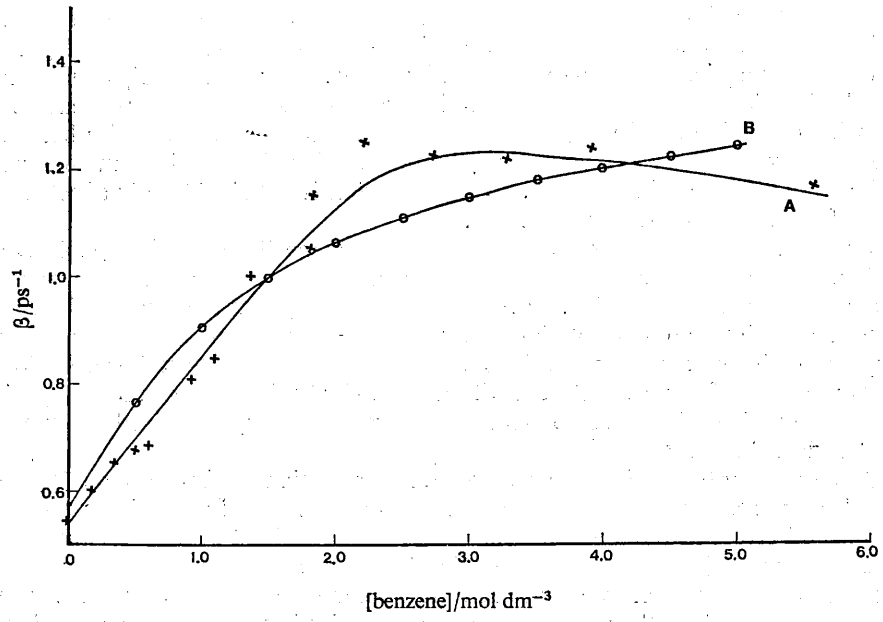

FIG. 4.—A plot of the reciprocal relaxation time ($\beta = \beta_V + \beta_T$) against concentration of benzene. The concentration of hexafluorobenzene is 0.8 mol dm^{-3} in cyclohexane + benzene mixtures [curve (A)]. Curve B is as expected for a property arising from a HFB + benzene complex with an equilibrium constant of 0.625 dm^3 mol^{-1} and assumes $\beta(0) = 0.545\ s^{-1}$ and $\beta(max) = 1.445\ s^{-1}$.

The out-of-plane γ_H vibrations of aromatic systems increase in frequency on addition of polar solvents, and the bands are broadened. LaLau proposed [16] that these effects were due to polar interactions of the type

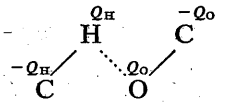

where O represents a terminal atom of any polar bond. If r is the distance between the polar group terminal atom and the hydrogen nucleus then the increment to the force constant for movement of the hydrogen towards the C—O axis is $Q_H Q_O / 4\pi\varepsilon_0 r^3$. Substitution of accepted values for these parameters gives excellent agreement between calculated and observed shifts for systems such as acetone + benzene and acetonitrile + benzene. There are difficulties with the model which are discussed below. However, the predicted magnitude of the shift for the benzene + HFB case is far too small to account for the observations. Taking the CH and CF bond dipoles as 0.3 D and 0.6 D (1×10^{-30} and 2×10^{-30} C m) [17, 18] and taking the average distance of approach, r, as about 2.3 Å then the extra dipolar restoring force is 0.0010 mdyn $Å^{-1}$ (0.10 N m^{-1}) which is to be compared with the actual force constant for movement of the fluorine out of the plane of 0.2 mdyn $Å^{-1}$ (20 N m^{-1}). This would explain only a 0.5 cm^{-1} shift. In fact there are other difficulties with the model. If we accept a model in which the interacting bonds are collinear, it is difficult to see why only the out-of-plane CH vibrations are affected. It might be expected that the in-plane β_H modes are affected equally. No shifts or band broadening are observed for the in-

plane modes. A more favourable configuration than that suggested above might be one in which the two dipoles were opposed in the manner

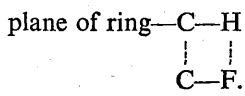

In this configuration only the γ modes would be affected, but now the modification to the restoring forces through electrostatic interactions must be much reduced since during the γ distortion one pair of interacting poles will approach while the other recedes. It appears then that, at least for the case being investigated, electrostatic interactions are an inadequate explanation of the observed phenomena. We postulate that the observed frequency shifts arise from π–π interactions which modify the restoring forces. This seems reasonable, but the relation between the frequency shift and the reciprocal relaxation time shown in fig. 5 must be rationalised. It should be noted that the observed sharp change in gradient in the β against $\Delta\nu$ curve occurs at a very high benzene concentration (35 %). This indicates that at an attainable concentration all excited molecules have achieved their maximum relaxation rate, but that the HFB molecules have not yet been surrounded by the maximum density of benzene molecules. A continued increase in the number of benzene molecules in the HFB environment leads to further increases in the restoring force.

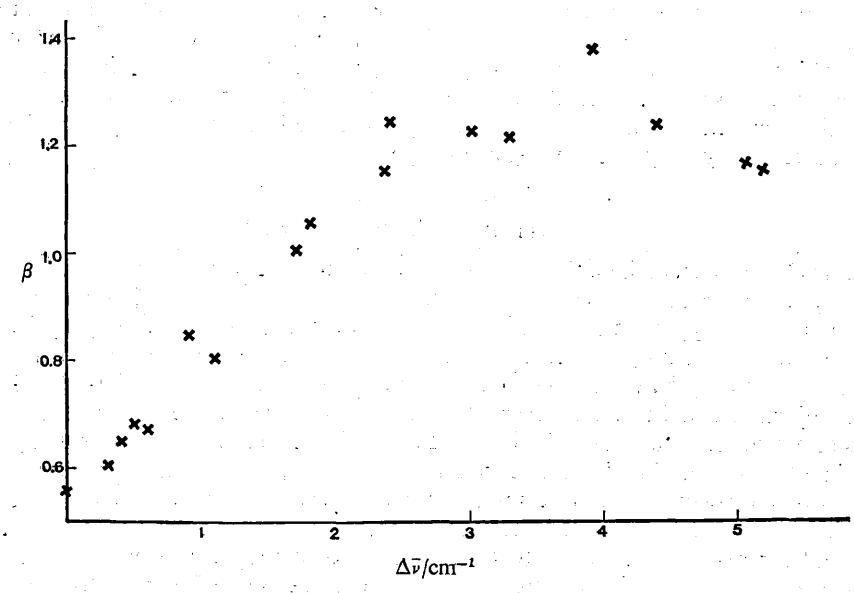

FIG. 5.—A plot of reciprocal relaxation time against frequency shift for the HFB + benzene + cyclohexane system.

Indeed the continued increase in $\Delta\nu$ up to 100 % benzene solvent is in accord with the thermodynamic evidence that the association energy between HFB and benzene is very small. Some studies of the temperature dependence have been made. Experimental difficulties have resulted in the results being of low accuracy, but any temperature effects on bands widths over a 50°C temperature range are clearly very small. Small frequency shifts of 0.03 cm^{-1} $°C^{-1}$ were observable. If the kinetic exchange, rather than the vibrational relaxation, mechanism is responsible for the band width

effects we would have expected to have seen some sign of further band narrowing in the benzene+C_6F_6 solution on increasing the temperature. This is based on the assumption that the observed fall off in $\Delta\nu_{\frac{1}{2}}$ as compared with the frequency shift, is due in this interpretation, to exchange narrowing.

While it is easy to visualise the manner in which interactions (charge transfer for example) can lead to an increase in the γ restoring force, the mechanism of vibrational relaxation is less obvious. In the time intervals involved, vibrational energy transfer seems most unlikely. It may be significant however that the vibrational quantum is very close to kT ($\sim$210 cm^{-1}). Differences between the effective bond dipoles as derived from intensity measurements of in-plane and out-of-plane fundamentals of benzene and HFB [17-19] have been interpreted as showing that there is an electronic rehybridisation moment resulting from movement of the H or F atoms out of the plane of the ring. It follows that any π–π interactions will be modified to some extent by γ type motions. It could well be then that in a dissociation process the vibrational quantum has a significant probability of being degraded into thermal energy. This process will be rendered much more likely by the similarity in magnitude of kT and $h\nu$. The implications of such a process will now be explored. If every dissociation of a molecular pair involving a vibrationally excited HFB molecule led to vibrational relaxation, then from the data in fig. 4 we can deduce that the equilibrium constant for complex formation is about 0.8 mol dm^{-3}. Taking the reciprocal lifetime of the complex as the asymptotic value of β_v we deduce the dissociation rate constant to be 0.70×10^{12} s^{-1}. The bimolecular association constant is then 0.5×10^{12} dm^3 mol^{-1} s^{-1}. This value is about 100 times larger than predicted for a dissociation controlled reaction with an efficiency factor of unity.[20] In fact cage effects may well explain this enhancement. In view of the extremely short lifetime a very high rate of interaction events may occur within a solvent cage.

SPECTROSCOPIC PROBLEMS

It has been assumed here that the band of hexafluorobenzene near 210 cm^{-1} arises from the a_{2u} vibration. The first assignment [21] of the vibrational fundamentals of HFB placed the a_{2u} mode at 315 cm^{-1} and the lowest e_{1u} mode near 210 cm^{-1}. On the basis of a more complete study these assignments were reversed,[22] and this was given some support by the band contours as measured in the vapour phase.[18] However, Fujiyama and Crawford reverted to the original Delbouille assignment on the basis of molecular rotation studies in liquid HFB.[14b] The basis of this was that β_r can be related to the rotational diffusion coefficients about specific axes. Whereas the a_{2u} vibration is affected only by rotation about axes perpendicular to the C_6 axis, all e_{1u} transition moments are rotated through space by molecular rotation about the C_6 axis and the axes perpendicular to this. The β constants derived by Fujiyama and Crawford (actually $\beta_v+\beta_r$ for pure liquid) were 0.83, 0.84 and 0.44 ps^{-1} for the 1534, 1010 and 315 cm^{-1} bands respectively. Since the low frequency value was so much smaller it was proposed that it arises from a different species to the two high frequency bands. These deductions are valid only in the absence of important vibration rotation interactions. All e_{1u} modes must exhibit first order Coriolis coupling between the degenerate components. While molecular rotation undergoes frequent interruptions in the condensed state, the coupling must still exist during rotation. The necessary theory has not yet been developed to account for the dependence of the long time behaviour of $G(t)$ on the Coriolis coupling constants. We note however that the $\beta_v+\beta_r$ value for the 210 cm^{-1} band in cyclohexane is 0.55 ps^{-1}, which is only slightly higher than that for the 315 cm^{-1} band. A comprehensive study of the out-of-plane

and in-plane vibrations and force fields of all substituted benzenes has yielded confirmation of the assignments used in the present work.[23, 24]

Baur, Horsma, Knobler and Perez [7] have shown how atomic polarisabilities can be deduced from polarisation and refraction data for systems containing two weakly interacting compounds. Applying their method to benzene and HFB they found a non linear dependence of the atomic polarisation on the fractional composition of the benzene+hexafluorobenzene mixtures. The deviation from linearity is up to 20 %. Now atomic polarisation P_a is related [25] to infra-red band intensities through

$$P_a = \frac{Nc}{3\pi^2}\sum_i \frac{\Gamma_i}{\nu_i}.$$

The above result implies that intensities of either the benzene bands or the HFB bands should change in a non linear fashion on mixing. We have measured the intensities of two lowest e_{1u} bands of HFB in benzene and cyclohexane and found no significant changes. Because of band overlapping between the 1500 cm^{-1} bands of benzene and of HFB, we were unable to carry out such studies for these bands. At the present time we can only say that the intensity changes implied by the atomic polarisation data are surprising and that we have not observed them in the vibrational absorption bands studied.

CONCLUSIONS

The observed broadening and frequency shifts of the a_{2u} vibrational band of hexafluorobenzene on addition of benzene shows that the presence of significant interactions directed perpendicular to the ring plane. Purely polar interactions are insufficient to explain the observations. It would appear that interactions between benzene and HFB directly perturb those orbitals which determine the restoring force on a substituent moved out of the plane of the ring. This leads to a mechanism by which the frequency can be perturbed and also by which the vibrational energy may degrade to thermal energy.

Problems in interpretation of details of the available data still exist. For example, the initial curvature of the $G(t)$ curve of the a_{2u} band of HFB in benzene is much greater than expected for a free rotor, and identification of the relaxation process with the " dissociation " of a collision complex leads to a rather high value for the bimolecular association constant.

R. M. B. and E. B. G. gratefully acknowledge the awards of S.R.C. studentships. We are also grateful to the S.R.C. for grants towards the cost of the Perkin Elmer 325 spectrometer and for technical assistance in a study of weak intermolecular interactions. Some of the earliest measurements on the HFB benzene system were made by Dr. W. Wheatley, now at B.P. Chemicals, Sunbury, Middlesex.

[1] R. Kubo, *Lectures in Theoretical Physics* (Interscience, New York, 1961), vol. 1, p. 120.
[2] R. G. Gordon, *Adv. Magnetic Resonance*, 1968, **3**, 1.
[3] I. R. Hill and D. Steele, *J. C. S. Faraday II*, 1975, **71**, 555.
[4] (*a*) H. Morawitz and K. B. Eisenthal, *J. Chem. Phys.*, 1971, **55**, 887; (*b*) H. S. Goldberg and P. S. Pershan, *J. Chem. Phys.*, 1973, **58**, 3816.
[5] I. R. Hill and D. Steele, to be published.
[6] C. R. Patrick and G. S. Prosser, *Nature*, 1960, **187**, 1021.
[7] M. E. Baur, D. A. Horsma, C. M. Knobler and P. Perez, *J. Phys. Chem.*, 1969, **73**, 641.
[8] R. J. Powell and F. L. Swinton, *J. Chem. Thermodynamics*, 1970, **2**, 87.
[9] M. W. Hanna, footnote on page 4108 of D. V. Fenby and R. L. Scott, *J. Phys. Chem.*, 1967, **71**, 4103.

[10] R. J. Powell, F. L. Swinton and C. L. Young, *J. Chem. Thermodynamics*, 1970, **2**, 105.
[11] D. Steele, *Theory of Vibration Spectroscopy* (Saunders, Philadelphia, 1971), p. 203.
[12] I. R. Hill and D. Steele, *J.C.S. Faraday II*, 1974, **70**, 1233.
[13] R. G. Gordon, *J. Chem. Phys.*, 1963, **39**, 2788.
[14] (*a*) W. Wheatley, *Ph. D. Thesis* (University of London, 1968); (*b*) T. Fujiyama and B. Crawford Jr., *J. Phys. Chem.*, 1968, **72**, 2174.
[15] D. A. Chisholm and H. L. Welsh, *Canad. J. Phys.* 1954, **32**, 291.
[16] C. La Lau, *Proc. Conf. Molecular Spectroscopy*, 1958, ed. E. Thornton and H. W. Thompson (Pergamon, 1959), p. 205.
[17] H. Spedding and D. H. Whiffen, *Proc. Roy. Soc. A*, 1956, **238**, 245.
[18] D. Steele and W. Wheatley, *J. Mol. Spectr.*, 1969, **32**, 265.
[19] (*a*) G. Jalsovszky and W. J. Orville Thomas, *Trans. Faraday Soc.*, 1971, **67**, 1894; (*b*) R. E. Bruns and W. B. Person *J. Chem. Phys.*, 1972, **57**, 324.
[20] see for example, D. N. Hague, *Fast Reactions* (Wiley-Interscience, New York, 1971), p. 12.
[21] L. Delbouille, *J. Chem. Phys.*, 1956, **25**, 182.
[22] D. Steele and D. H. Whiffen, *Trans. Faraday Soc.*, 1959, **55**, 369.
[23] R. A. R. Pearce, D. Steele and K. Radcliffe, *J. Mol. Structure*, 1973, **15**, 409.
[24] V. J. Eaton and D. Steele, *J. Mol. Spectr.*, 1973, **48**, 446.
[25] D. H. Whiffen, *Trans. Faraday Soc.*, 1958, **54**, 327.

PRINTED IN GREAT BRITAIN AT
THE UNIVERSITY PRESS
ABERDEEN